SF 298 MASTER COPY KEEP THIS COPY FOR REPRODUCTION PURPOSES

REPORT DOCUMENTATION PAGE

Form Approved
OMB NO. 0704-0188

1. AGENCY USE ONLY *(Leave blank)*	2. REPORT DATE	3. REPORT TYPE AND DATES COVERED
	May 1996	Final 18 Jan 93 - 17 May 96

4. TITLE AND SUBTITLE

Phonon Interactions in Novel Semiconductor Nanostructures

5. FUNDING NUMBERS

DAAH04-93-D-0003

6. AUTHOR(S)

Michael A. Stroscio (Principal Investigator)

7. PERFORMING ORGANIZATION NAMES(S) AND ADDRESS(ES)

North Carolina State University
Department of Electrical and Computer Engineering
North Carolina State University
Raleigh, NC 27607

8. PERFORMING ORGANIZATION REPORT NUMBER

9. SPONSORING / MONITORING AGENCY NAME(S) AND ADDRESS(ES)

U.S. Army Research Office
P.O. Box 12211
Research Triangle Park, NC 27709-2211

10. SPONSORING / MONITORING AGENCY REPORT NUMBER

ARO 30905.1-EL

11. SUPPLEMENTARY NOTES

The views, opinions and/or findings contained in this report are those of the author(s) and should not be construed as an official Department of the Army position, policy or decision, unless so designated by other documentation.

12a. DISTRIBUTION / AVAILABILITY STATEMENT

Approved for public release; distribution unlimited.

12 b. DISTRIBUTION CODE

13. ABSTRACT *(Maximum 200 words)*

During this research effort, numerous interactions of confined phonons in nanostructures have been modelled theoretically; these include: piezoelectric scattering in cylindrical quantum wires; generalized piezoelectric scattering rate for elections in a two-dimensional election gas; Gamma-X transitions driven by interface phonons; interface optical modes in cylindrical quantum wires; microscopic model for election-optical-phonon interactions in quantum wells; optical phonons in quantum dots; electron-acoustic-phonon scattering in both rectangular and cylindrical quantum wires; and acoustic modes in quantum wires and dots.

14. SUBJECT TERMS

Confined optical phonons; confined acoustic phonons; electron-phonon interactions

15. NUMBER IF PAGES

16. PRICE CODE

17. SECURITY CLASSIFICATION OR REPORT	18. SECURITY CLASSIFICATION OF THIS PAGE	19. SECURITY CLASSIFICATION OF ABSTRACT	20. LIMITATION OF ABSTRACT
UNCLASSIFIED	UNCLASSIFIED	UNCLASSIFIED	UL

DISCLAIMER NOTICE

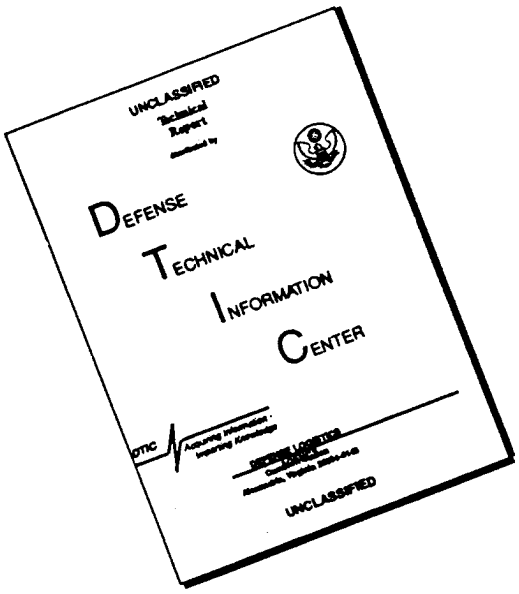

THIS DOCUMENT IS BEST QUALITY AVAILABLE. THE COPY FURNISHED TO DTIC CONTAINED A SIGNIFICANT NUMBER OF PAGES WHICH DO NOT REPRODUCE LEGIBLY.

PHONON INTERACTIONS IN NOVEL SEMICONDUCTOR NANOSTRUCTURES

FINAL REPORT

MICHAEL A. STROSCIO

17 MAY 1996

U.S. ARMY RESEARCH OFFICE

NORTH CAROLINA STATE UNIVERSITY

1A. STATEMENT OF PROBLEM STUDIED.

Research on nanoscale and mesoscopic electronic and optoelectronic structures has focused extensively on carrier-phonon interactions. However, until recently this research has been based on the assumption that both optical and acoustic phonons may be treated as bulk phonons without regard to dimensional confinement effects. In the past few years, this situation has been improved as a result of numerous investigations of the properties and interactions of optical phonons in nanoscale electronic and optoelectronic structures confined in one or more spatial dimensions.[1] In spite of considerable experimental evidence on the importance of dimensional confinement in determining the properties of acoustic phonons, [2-9] there have been very few attempts to model confined acoustic phonons in electronic and optoelectronic structures having nanometer characteristic dimensions (i.e., nanoscale) and wavelike electron (i.e., mesoscopic) properties. In particular, selected acoustic phonons in nanoscale structures have been analyzed for the cases of superlattices, free-standing slabs, free-standing cylinders, and quantum wires with rectangular cross sections. In this research we have modeled numerous interactions of confined phonons in nanostructures. These include: piezoelectric scattering in cylindrical quantum wires; generalized piezoelectric scattering rate for elections in a two-dimensional election gas; Gamma-X transitions driven by interface phonons; interface optical modes in cylindrical quantum wires; microscopic model for election-optical-phonon interactions in quantum wells; optical phonons in quantum dots; electron-acoustic-phonon scattering in both rectangular and cylindrical quantum wires; and acoustic modes in quantum wires and

1B. SUMMARY OF MOST IMPORTANT RESULTS

In this research effort we have achieved a number of results that provide for the subsequent design of ultrafast nanoelectronic and opt-electronic devices. Among these results are: piezoelectric scattering rates for carriers in a cylindrical quantum wire; the design of metal-encapsulated quantum wires for enhanced charge transport; the generalized piezoelectric scattering rate for elections in a two-dimensional election gas; direct-indirect transition rates in short-period superlattices due to phonon-assisted transitions; the normalization of interface optical phonon modes in cylindrical quantum wires with semiconductor-semiconductor and metal-semiconductor boundary conditions; a microscopic model for election-optical-phonon interactions in quantum wells; characteristics of bottleneck effects due to confined phonons in quantum dots; a model for deformation potential interactions in rectangular quantum wires;

a model for election-acoustic-phonon scattering rates in rectangular quantum wires; quantized acoustic phonon modes in quantum wires and quantum dots; election-acoustic-phonon scattering rates in cylindrical quantum wires; methods for tailoring acoustic phonon modes in mesoscopic devices; a model for optical-phonon lifetimes in gallium arsenide; a model for elastic vibrations of microtubules in a fluid; a model for interface phonons in spherical gallium-arsenide--aluminum-gallium-arsenide quantum dots; and a general prescription for and derivation of acoustic phonon quantization in buried waveguides and resonators.

These results are essential results needed for an understanding of deformation potential, piezoelectric and Frohlich scattering in nanoscale electronic and optoelectronic devices. These results are of special significance since the identified phonon-driven interactions are derived with both election and phonon confinement taken into account. In summary, our results containing many of the pioneering findings on carrier-phonon interactions for device geometries where phonon confinement modifies the phonons from the usual bulk phonons.

1C. LIST OF ALL PUBLICATIONS AND TECHNICAL REPORTS.

Michael A. Stroscio and K.W. Kim, "Piezoelectric Scattering of Carriers from Confined Acoustic Modes in Cylindrical Quantum Wires," Phys. Rev. B, 48, 1936 (1993).

R.M. de la Cruz, S.W. Teitsworth and M.A. Stroscio, "Phonon Bottleneck Effects for Confined Longitudinal Optical Phonons in Quantum Boxes," Superlattices and Microstructures, 13, 481 (1993).

M.U. Erdogan, V. Sankaran, K.W. Kim, M.A. Stroscio, and G.J. Iafrate, "Real-Space Transfer of Photoexcited Electrons in Type-II Superlattices via Optical-Phonon Emission," Proceedings of the SPIE, Vol. 2146, 34-41 (1994).

K.W. Kim, SeGi Yu, M.U. Erdogan, Michael A. Stroscio, and Gerald J. Iafrate, "Acoustic Phonons in Rectangular Quantum Wires: Approximate Compressional Modes and the Corresponding Deformation Potential Interactions," Proceedings of the SPIE, Vol. 2142, 77-86 (1994).

SeGi Yu, K.W. Kim, Michael A. Stroscio, Gerald J. Iafrate and Arthur Ballato, "Electron--Acoustic-Phonon Scattering Rates in Rectangular Quantum Wires," Phys. Rev., B50, 1733 (1994).

Michael A. Stroscio, K.W. Kim, SeGi Yu, and Arthur Ballato,

"Quantized Acoustic Phonons in Quantum Wires and Quantum Dots," J. Appl. Phys., 76, 4670 (1994).

M.U. Erdogan, V. Sankaran, K.W. Kim, M.A. Stroscio and Gerald J. Iafrate, "Phonon-Assisted Gamma-X Transition Rates in Type-II Superlattices," Phys. Rev., B50, 2485 (1994)

A.R. Bhatt, K.W. Kim and M.A. Stroscio, "Theoretical Calculation of the Longitudinal-Optical Lifetime in GaAs," J. Appl. Phys., 76, 3905 (1994).

SeGi Yu, K.W. Kim, M.A. Stroscio and G.J. Iafrate, "Electron--Acoustic-Phonon Scattering Rates in Cylindrical Quantum Wires," Phys. Rev., B51, 4695 (1995).

R.M. de la Cruz, S.W. Teitsworth, and M.A. Stroscio, "Interface Phonons in Spherical GaAs/A1(x)Ga(1-x)As Quantum Dots," Phys. Rev. B, 52, 1489 (1995).

Yuri M. Sirenko, Michael A. Stroscio, K.W. Kim, and Vladimir Mitin, "Ballistic Propagation of Interface Optical Photons," Phys. Rev., B51, 9863 (1995).

Yuri M. Sirenko, Michael A. Stroscio, and K.W. Kim, "Elastic Vibrations of Microtubules in a Fluid," Phys. Rev., E53, 1003 (1996).

Yuri M. Sirenko, J.-B. Jeon, K.W. Kim, M.A. Littlejohn, and M.A. Stroscio, "Envelope Function Formalism for Valence Bands in Wurtzite Quantum Wells," Phys. Rev., B53, 3467 (1996).

M.A. Stroscio, Yu. M. Sirenko, S. Yu, and K.W. Kim, "Acoustic Phonon Quantization in Buried Waveguides and Resonators," Journal of Physics: Condensed Matter, 8, 2143 (1996).

N.S. Mansour, Yu. M. Sirenko, K.W. Kim, M.A. Littlejohn, and M.A. Stroscio, "Carrier Capture in Quantum Well Embedded Quantum Wire Structures," submitted to Appl. Phys. Lett., February 1996.

N.S. Mansour, Yu. M. Sirenko, K.W. Kim, M.A. Littlejohn, and M.A. Stroscio, "Carrier Capture in Quantum Well Embedded Quantum Wire Structures," submitted to Appl. Phys. Lett.

Book Chapters

Michael A. Stroscio, Gerald J. Iafrate, Ki Wook Kim, M.A. Littlejohn, Amit Bhatt and Mitra Dutta, "Confined and Interface Optical Phonons in Quantum Wells and Quantum Wires," in Critical Reviews of Optical Science and Technology, SPIE Publication CR45 (1993).

Michael A. Stroscio, Gerald J. Iafrate, Henry Everitt, Ki Wook Kim, Yuri Sirenko, SeGi Yu, M.A. Littlejohn, and Mitra Dutta, "Confined and Interface Optical and Acoustic Phonons in Quantum Wells, Superlattices and Quantum Wires," to appear in Properties of III-V Superlattices and Quantum Wells, INSPEC Vol. published by the Institution of Electrical Engineers, London, United Kingdom, ed. by Pallab Bhattacharya (1995).

2. REPORT OF INVENTION

Metal-Encapsulated Quantum Wire for Enhanced Charge Transport, Mitra Dutta, Harold L. Grubin, Gerald J. Iafrate, Ki Wook Kim and Michael A. Stroscio, U.S. Patent No. 5,264,711 dated November 23, 1993.

3. BIBLIOGRAPHY

[1]See, for example, M.A. Stroscio, G.J. Iafrate, K.W. Kim, M.A. Littlejohn, A. Bhatt, and M. Dutta, in *Integrated Optics and Optoelectronics*, edited by K.-K. Wong and M. Razeghi (SPIE, Bellingham, WA, 1993), Vol. CR-45, p. 341.

[2]J. Seyler and M.N. Wybourne, Phys. Rev. Lett. **69**, 1427 (1992); A. Tanaka, S. Onari, and T. Arai, Phys. Rev. B **47**, 1237 (1993).

[3]Z.V. Popovic, J. Spitzer, T. Ruf, M. Cardona, R. Notzel, and K. Ploog, Phys. Rev. B **48**, 1659 (1993).

[4]P.V. Santos, A.K. Sood, M. Cardona, K. Ploog, Y. Ohmori, and H. Okamoto, Phys. Rev. B **37**, 6381 (1988).

[5]Y.F. Chen, J.L. Shen, L.Y. Lin, and Y.S. Huang, J. Appl. Phys. **73**, 4555 (1993).

[6]A. Pots, M.J. Kelly, C.G. Smith, D.G. Hasko, J.R.A. Cleaver, H. Ahmed, D.C. Peacock, D.A. Ritchie, J.E.F. Frost, and G.A.C. Jones, J. Phys: Condens. Matter **2**, 1817 (1990).

[7]C. Colvard, T.A. Gant, M.V. Klein, R. Merlin, R. Fisher, H. Morkoc, and A.C. Gossard, Phys. Rev. B **31**, 2080 (1985).

[8]R. Bhadra, M. Grimsditch, I.K. Schuller, and F. Nizzoli, Phys. Rev. B **39**, 12456 (1989).

[9]M. Grimsditch, R. Bhadra, and I.K. Schuller, Phys. Rev. Lett. **58**, 1216 (1987).

4. APPENDIX OF SELECTED PAGES OF KEY PUBLICATIONS UNDER THIS GRANT.

Piezoelectric scattering of carriers from confined acoustic modes in cylindrical quantum wires

Michael A. Stroscio
U.S. Army Research Office, P.O. Box 12211, Research Triangle Park, North Carolina 27709-2211

K. W. Kim
Department of Electrical and Computer Engineering, North Carolina State University, Raleigh, North Carolina 27695-7911
(Received 16 February 1993)

Confined acoustic modes are derived for a free-standing nanometer-scale cylindrical polar semiconductor quantum wire. The piezoelectric scattering Hamiltonian is calculated for the interaction of charge carriers with the lowest-order azimuthally symmetric torsional modes in such nanometer-scale quantum wires.

Many proposed applications of mesoscopic electronic structures involve carrier transport at low temperatures and low carrier energies; frequently, the regime of interest is one where dimensional confinement modifies the phase space substantially. In this low-temperature, low-energy regime,[1-6] acoustic phonons play an enhanced role in carrier scattering and may dominate over the scattering of carriers by optical phonons. Furthermore, in nanometer-scale structures it is possible that phase-space restrictions may weaken or forbid optical-phonon scattering processes that would normally dominate in bulk structures. In recent years, there has been extensive literature on the role of dimensional confinement in modifying optical-phonon modes and their interactions with charge carriers (see, for example, Refs. 7–11 and the numerous references therein). However, there are relatively few treatments dealing with the role of dimensional confinement in modifying acoustic-phonon modes and their interactions with charge carriers.[2-4] While there is extensive literature on the theory of acoustic modes in conventional waveguides, resonators and related structures,[5] no efforts have been reported to formulate a theory of acoustic phonons in nanometer-scale structures where both phonon confinement and a quantum-mechanical treatment of phonon normalization are both essential; Constantinou has, however, discussed the unnormalized acoustic-phonon modes in cylindrical polar semiconductor quantum wires.[12]

In this paper, the general piezoelectric polarization vector is derived in terms of the acoustic-phonon mode displacements in free-standing cylindrical quantum wires fabricated of zinc-blende polar semiconductors. By taking an approach analogous to the dielectric continuum theory of confined optical phonons, the proper quantum-mechanical technique of normalizing such acoustic-phonon modes is illustrated and the piezoelectric scattering Hamiltonian is calculated for the interaction of charge carriers with the lowest-order azimuthally symmetric torsional modes in nanometer-scale quantum wires of both infinite and finite length (i.e., quantum dots or boxes).

The piezoelectric tensor relating the piezoelectric polarization vector and the acoustic strain tensor may be expressed in matrix notation[5] for the case of a zinc-blende crystal in rectangular coordinates as

$$\tilde{e}=\begin{bmatrix} 0 & 0 & 0 & e_{x4} & 0 & 0 \\ 0 & 0 & 0 & 0 & e_{x4} & 0 \\ 0 & 0 & 0 & 0 & 0 & e_{x4} \end{bmatrix}.$$

The piezoelectrically induced electric polarization vector $\mathbf{P}$ is given in terms of $\tilde{e}$ by the matrix equation,

$$\mathbf{P}=\tilde{e}S\ ,$$

where $\mathbf{P}$ is a three-component vector,

$$\mathbf{P}=\begin{bmatrix} P_1 \\ P_2 \\ P_3 \end{bmatrix},$$

and S is the six-component strain vector with components,[5]

$$S_1=S_{rr}=\frac{1}{i\omega}\frac{\partial v_r}{\partial r}\ ,$$

$$S_2=S_{\phi\phi}=\frac{1}{i\omega}\left[\frac{v_r}{r}+\frac{1}{r}\frac{\partial v_\phi}{\partial\phi}\right],$$

$$S_3=S_{zz}=\frac{1}{i\omega}\frac{\partial v_z}{\partial z}\ ,$$

$$S_4=2S_{z\phi}=\frac{1}{i\omega}\left[\frac{\partial v_\phi}{\partial z}+\frac{1}{r}\frac{\partial v_z}{\partial\phi}\right]=2S_{\phi z}\ ,$$

$$S_5=2S_{rz}=\frac{1}{i\omega}\left[\frac{\partial v_r}{\partial z}+\frac{\partial v_z}{\partial r}\right]=2S_{zr}\ ,$$

$$S_6=2S_{r\phi}=\frac{1}{i\omega}\left[\frac{1}{r}\frac{\partial v_r}{\partial\phi}+\frac{\partial v_\phi}{\partial r}-\frac{v_\phi}{r}\right]=2S_{\phi r}\ ,$$

where $\mathbf{v}$ is the velocity associated with the acoustic-phonon displacement $\mathbf{u}$ and ω is the harmonic frequency assumed for the phonon field; that is, $\mathbf{v}=i\omega\mathbf{u}$. To cast $\tilde{e}$ into a form suitable for a cylindrical quantum wire, it is necessary to express $\tilde{e}$ in a more general form where the coordinate axes are rotated with respect to the principal axes of the crystal. Upon applying the rotation transformation matrices of Auld[5] to the case of rotation by an angle ϕ about the z axis ([100] axis),

$$\tilde{e}'=\begin{bmatrix} 0 & 0 & 0 & e_{x4}(\cos^2\phi-\sin^2\phi) & 2e_{x4}\cos\phi\sin\phi & 0 \\ 0 & 0 & 0 & -2e_{x4}\cos\phi\sin\phi & e_{x4}(\cos^2\phi-\sin^2\phi) & 0 \\ 2e_{x4}\cos\phi\sin\phi & -2e_{x4}\cos\phi\sin\phi & 0 & 0 & 0 & e_{x4}(\cos^2\phi-\sin^2\phi) \end{bmatrix}.$$

With the generalized piezoelectric matrix, it follows that

$$P_1=2e_{x4}(\cos^2\phi-\sin^2\phi)S_{z\phi}+4e_{x4}\cos\phi\sin\phi S_{rz}\ ,$$

$$P_2=-4e_{x4}\cos\phi\sin\phi S_{z\phi}+2e_{x4}(\cos^2\phi-\sin^2\phi)S_{rz}\ ,$$

$$P_3=2e_{x4}\cos\phi\sin\phi S_{rr}-2e_{x4}\cos\phi\sin\phi S_{\phi\phi}+2e_{x4}(\cos^2\phi-\sin^2\phi)S_{r\phi}\ .$$

As discussed by Vogl,[13] the $\mathbf{k}$ component of the piezoelectric potential may be simplified for a cubic material as

$$\delta V_{\mathbf{k}}(\mathbf{r})=\frac{-i4\pi}{k^2\epsilon_0}\mathbf{k}\cdot\mathbf{P}_{\mathbf{k}}(\mathbf{r})\ ,$$

where $\mathbf{k}$ is the acoustic-phonon wave vector and ϵ_0 is the dielectric constant. The piezoelectrically induced electric polarization vector $\mathbf{P}_{\mathbf{k}}$ is given directly by $\tilde{e}'S$ for the $\mathbf{k}$ mode as discussed previously. Then, the interaction Hamiltonian for piezoelectric scattering may be written as

$$H_{ep}=\frac{1}{\sqrt{N}}\sum_{\mathbf{k}}(e\delta V_{\mathbf{k}}(\mathbf{r})[a_{\mathbf{k}}+a^{\dagger}_{-\mathbf{k}}]+\text{c.c.})\ ,$$

where N is the number of unit cells, e is the unit charge, and $a_{\mathbf{k}}$ ($a^{\dagger}_{-\mathbf{k}}$) is the annihilation (creation) operator.

The characteristic modes for acoustic phonons in an infinitely long free-standing cylinder have been obtained previously[5] by imposing the boundary conditions of vanishing stress components on the free surface of the cylinder at $r=a$. The general solutions with these boundary conditions are given in terms of Bessel functions and the phonon wave vector in the confining direction is discretized by a dispersion relation. In this work, we will concentrate on the lowest-order azimuthally symmetric torsional mode since its simple analytical solution permits us to develop a quantization prescription that has general applicability to acoustic-phonon modes. The characteristic velocity field of this mode is given as

$$v_{\phi}=\gamma r e^{-i\omega z/V_s}\ ,$$

where $V_s=(c_{44}/\rho)^{1/2}$ and γ is a normalization constant to be determined. For this mode, v_r and v_z vanish along with k_r and k_{ϕ} (i.e., $k_z=k=\omega/V_s$). For the case of a cylinder of finite length (i.e., quantum dot), the velocity field of the corresponding mode may be obtained by requiring the $z\phi$ component of the stress to vanish at the ends of the cylinder at $z=0$ and $z=L$. Hence, the velocity field of the lowest-order azimuthally symmetric torsional mode for a cylinder of length L may be written as

$$v_{\phi}^{(\text{dot})}=\gamma' r\cos\left[\frac{\nu\pi}{L}z\right]\ ,$$

where $\nu\pi/L=\omega/V_s$ and γ' is a normalization constant.

The normalization of the acoustic-phonon modes can be obtained by considering the average displacement energy of the phonon field. Since the acoustic-phonon displacement is written in this work as

$$\mathbf{u}(\mathbf{r})=\frac{1}{\sqrt{N}}\sum_{\mathbf{k}}(\mathbf{u}_{\mathbf{k}}(\mathbf{r})[a_{\mathbf{k}'}+a^{\dagger}_{-\mathbf{k}}]+\text{c.c.})\ ,$$

the quantity $\mathbf{u}_{\mathbf{k}}(\mathbf{r})$ must be normalized to $\hbar/2M\omega$, where M is the mass for a unit cell. For a free-standing quantum dot where the acoustic mode vanishes outside of the quantum dot, this normalization condition becomes

$$\frac{1}{\pi a^2 L}\int_0^L dz\int_0^{2\pi}d\phi\int_0^a r\,dr\,\mathbf{u}_k^*\cdot\mathbf{u}_k=\frac{\hbar}{2M\omega}\ .$$

Here, a and L are the radius and the length of the quantum dot, respectively, as mentioned before. For the lowest-order azimuthally symmetric torsional mode, it then follows that the characteristic mode for displacement is given as

$$u_{\phi}^{(\text{dot})}=\left[\frac{\hbar}{2M\omega}\right]^{1/2}\frac{2}{a}r\cos\left[\frac{\nu\pi}{L}z\right]\ .$$

For the quantum wire of infinite length, k_z is a good quantum number. Accordingly, the normalization condition is

$$\frac{1}{\pi a^2}\int_0^{2\pi}d\phi\int_0^a r\,dr\,\mathbf{u}_k^*\cdot\mathbf{u}_k=\frac{\hbar}{2M\omega}\ ;$$

hence,

$$u_{\phi}^{(\text{wire})}=\left[\frac{\hbar}{2M\omega}\right]^{1/2}\frac{\sqrt{2}}{a}re^{-i\omega z/V_s}\ .$$

These examples demonstrate the general method for normalizing the acoustic-phonon modes, i.e., $\mathbf{u}_{\mathbf{k}}(\mathbf{r})$ times its complex conjugate when integrated over all space and divided by the volume is equal to $\hbar/2M\omega$. This approach is analogous to the dielectric continuum theory of confined optical phonons,[7] and may be used to normalize other acoustic-phonon modes in semiconductor nanostructures. In particular, all of the acoustic field solutions known in the literature of classical acoustic fields may be normalized by this relation to obtain the quantum-mechanical modes and the interaction Hamiltonians for piezoelectric scattering in nanostructures.

In conclusion, the general piezoelectrically induced electric polarization vector has been derived in terms of the acoustic-phonon mode displacement amplitude. The procedure for normalizing the acoustic modes has been demonstrated by normalizing the lowest-order azimuthally symmetric torsional modes in cylindrical quantum wires and quantum dots. These normalized modes are

used to develop an interaction Hamiltonian for piezoelectric scattering when the acoustic-phonon modes are confined dimensionally.

The authors gratefully acknowledge helpful discussions with Dr. G. J. Iafrate and Professor M. A. Littlejohn. The authors would also like to thank Professor M. N. Wybourne for information on recent experimental evidence on acoustic-phonon confinement. This work was supported, in part, by the Office of Naval Research and the U.S. Army Research Office.

[1]T. Kawamura and S. Das Sarma, Phys. Rev. B 45, 3612 (1992).
[2]B. Hillebrands, S. Lee, G. I. Stegeman, H. Cheng, J. E. Potts, and F. Nizzoli, Phys. Rev. Lett. 60, 832 (1988).
[3]J. Seyler and M. N. Wybourne, Phys. Rev. Lett. 69, 1427 (1992).
[4]H. Benistry, C. M. Sotomayor-Torres, and C. Weisbuch, Phys. Rev. B 44, 10945 (1991).
[5]B. A. Auld, *Acoustic Fields and Waves* (Wiley, New York, 1973).
[6]P. J. Price, Ann. Phys. 133, 217 (1981).
[7]N. Mori and T. Ando, Phys. Rev. B 40, 6175 (1989).
[8]M. A. Stroscio, Phys. Rev. B 40, 6428 (1989).
[9]K. W. Kim and M. A. Stroscio, J. Appl. Phys. 68, 6289 (1990).
[10]K. W. Kim, M. A. Stroscio, A. Bhatt, V. V. Mitin, and R. Mickevicius, J. Appl. Phys. 70, 319 (1991).
[11]M. A. Stroscio, K. W. Kim, G. J. Iafrate, M. Dutta, and H. L. Grubin, Philos. Mag. Lett. 65, 173 (1992).
[12]N. C. Constantinou, in Phonons in Semiconductor Nanostructures, edited by Jean-Pierre Leburton, Clivia M. Sotomayer Torres, and Jordi Pascual (Kluwer, Boston, in press).
[13]P. Vogl, in *Physics of Transport in Semiconductors*, edited by D. K. Ferry, J. R. Barker, and C. Jacoboni (Plenum, New York, 1980), pp. 75–115.

US005264711A

United States Patent [19]

Dutta et al.

[11] Patent Number: 5,264,711

[45] Date of Patent: Nov. 23, 1993

[54] METAL-ENCAPSULATED QUANTUM WIRE FOR ENHANCED CHARGE TRANSPORT

[75] Inventors: Mitra Dutta, Matawan, N.J.; Harold L. Grubin, West Hartford, Conn.; Gerald J. Iafrate, Raleigh, N.C.; Ki Wook Kim; Michael A. Stroscio, both of Durham, N.C.

[73] Assignee: The United States of America as represented by the Secretary of the Army, Washington, D.C.

[21] Appl. No.: 945,040

[22] Filed: Sep. 15, 1992

[51] Int. Cl.[5] H01L 29/02

[52] U.S. Cl. 257/14; 257/17; 257/22; 257/27; 257/774; 257/771

[58] Field of Search 257/21, 17, 15, 14, 257/774, 775, 773, 20, 22, 27, 771

[56] References Cited

U.S. PATENT DOCUMENTS

4,503,447	3/1985	Iafrate et al.	257/15
4,591,889	5/1986	Gossard et al.	257/15
4,733,282	3/1988	Chang et al.	257/14 X
4,751,194	6/1988	Cibert et al.	257/14 X
4,769,683	9/1988	Goronkin et al.	257/20
4,899,201	2/1990	Xu et al.	257/20
5,119,151	6/1992	Onda	257/14

OTHER PUBLICATIONS

Hong et al., "MBE Growth and Properties of Fe, (AlSi) on GaAs (100)", *Journal of Crystal Growth*, vol. 111, 1991, pp. 984–988.

Ralston et al., "Overgrowth and Strain in MBE-Grown GaAs/ErAs/GaAs Structures," *Journal of Crystal Growth*, vol. 111, 1991, pp. 989–995.

Kuo et al. "Rheed Studies of Epitaxial Growth of CoGa on GaAs by MBE Determination of Epitaxial Phases and Orientations," *Journal of Crystal Growth*, vol. 111, 1991, pp. 996–1002.

H. Sakaki, Japanese Journal of Applied Physics, "Superlattices and Coupled Quantum Box Arrays: A Novel Method to Suppress Optical Phonon Scattering in Semiconductors", 28, L314, 1989.

S. Luryi and F. Capasso, "Resonant Tunneling of Two-Dimensional Electrons though a Quantum Wire: A Negative Transconductance Device", Applied Physics Letters, 47, 1347, 1985.

M. Tsuchiya et al, "Optical Anisotropy in a Quantum-Well-Wire Array with Two-Dimensional Quantum Confinement", Physical Review Letters, 62, 466, 1989.

M. A. Reed et al, "Observation of Discrete Electronic States in a Zero-Dimensional Semiconductor Nanostructure", Physical Review Letters, 60, 535, 1988.

Michael A. Stroscio, "Interaction between longitudinal-optical phonon modes of a rectangular quantum wire and charge carriers of a one-dimensional electron gas", Physical Review, B, 40, 6428, 1989.

N. Mori et al, "Electron-optical-phonon interaction in single and double heterostructures", Physical Review B, 40, 6175, 1989.

K. W. Kim et al, "Electron-optical-phonon scattering rates in a rectangular semiconductor quantum wire", Journal of Applied Physics, 70, 319, 1991.

M. A. Stroscio et al, "Transition from longitudinal-optical phonon scattering to sruface-optical phonon scattering in polar semiconductor superlattices", Applied Physics Letters, 59, 1093, 1991.

J. P. Harbison et al, "MBE growth of ferromagnetic metastable epitaxial MnAl thin films on AlAs/GaAs heterostructures", *Journal of Crystal Growth*, vol. 111, 1991, pp. 978–981.

Primary Examiner—William Mintel

Attorney, Agent, or Firm—Michael Zelenka; William H. Anderson

[57] ABSTRACT

A polar semiconductor quantum wire for use in electronic and opto-electronic devices. The polar semiconductor quantum wire is either completely or partially encapsulated in metal to reduce the strength of the scattering potential associated with interface optical phonons normally established at the lateral boundaries of polar semiconductor quantum wires. Metal alone or metal employed in conjunction with modulation doping enhances the transport of charge carriers within the polar semiconductor quantum wire.

17 Claims, 3 Drawing Sheets

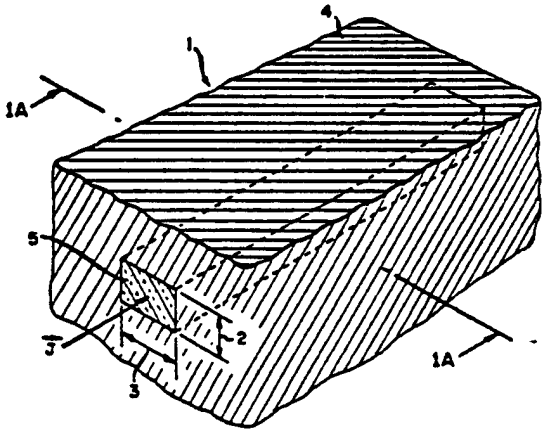

FIG. 1

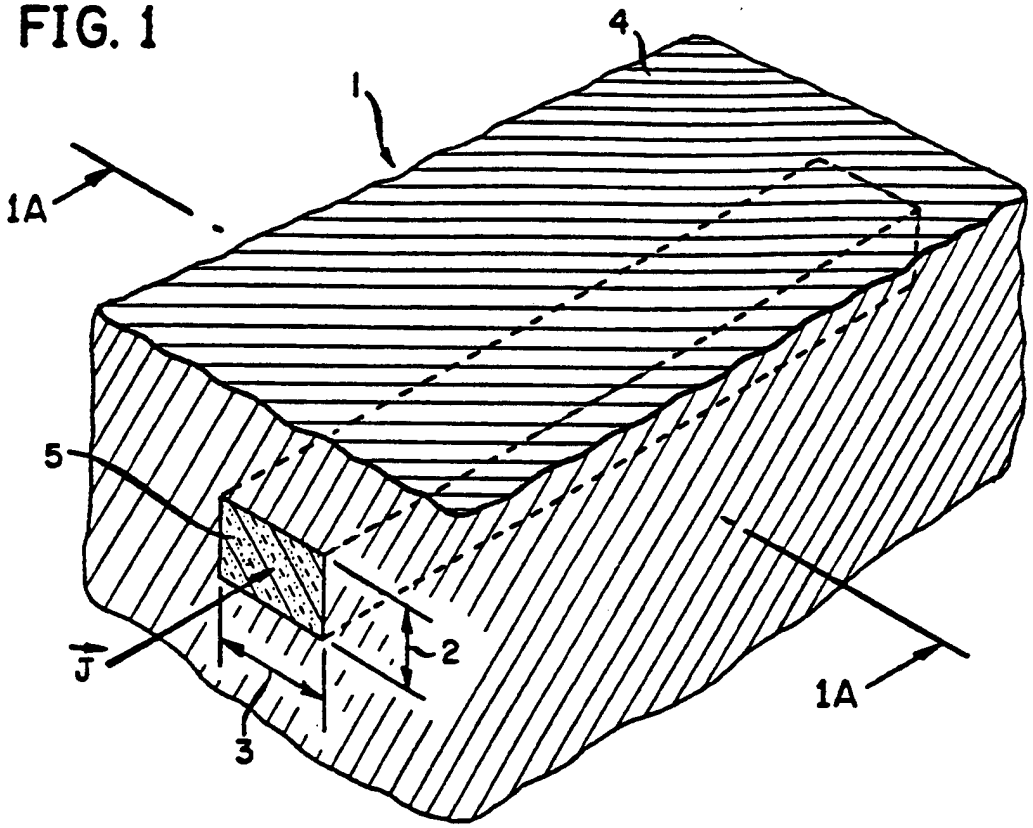

FIG. 2

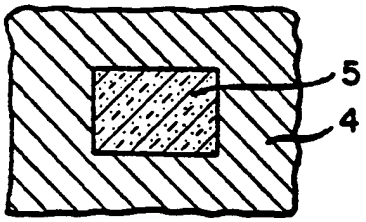

FIG. 3

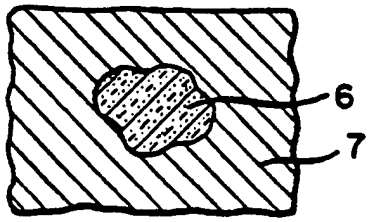

FIG. 4

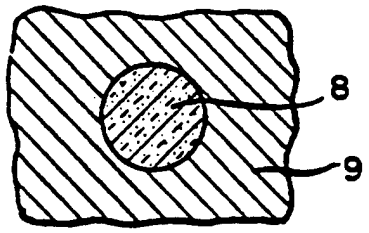

FIG. 5a

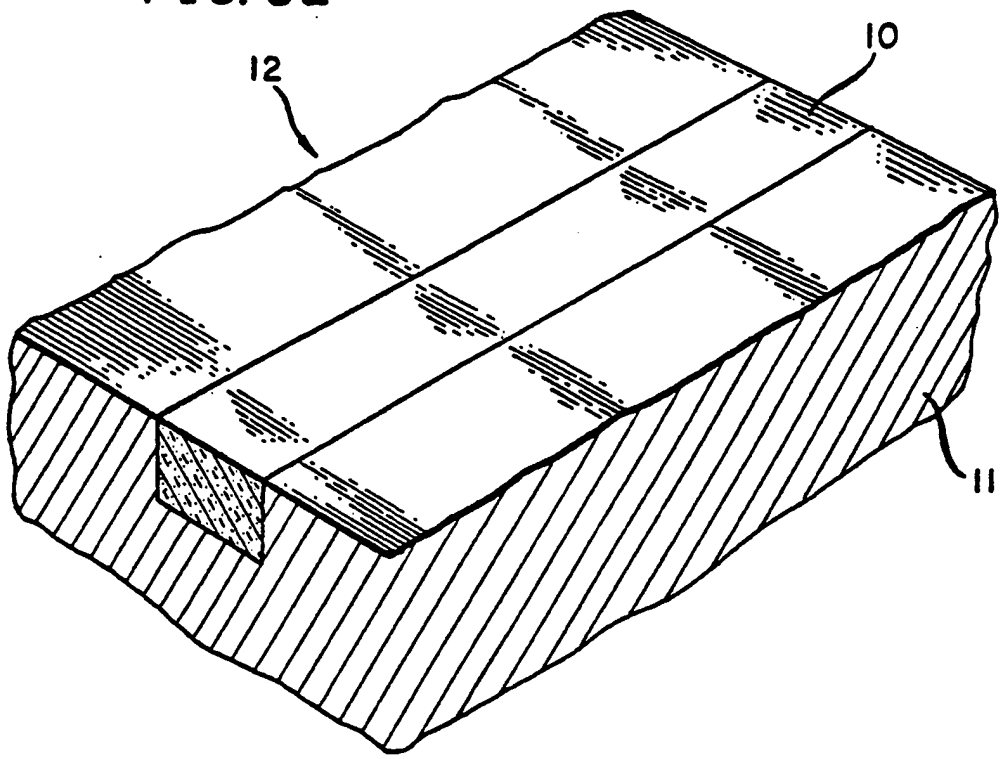

FIG. 5b

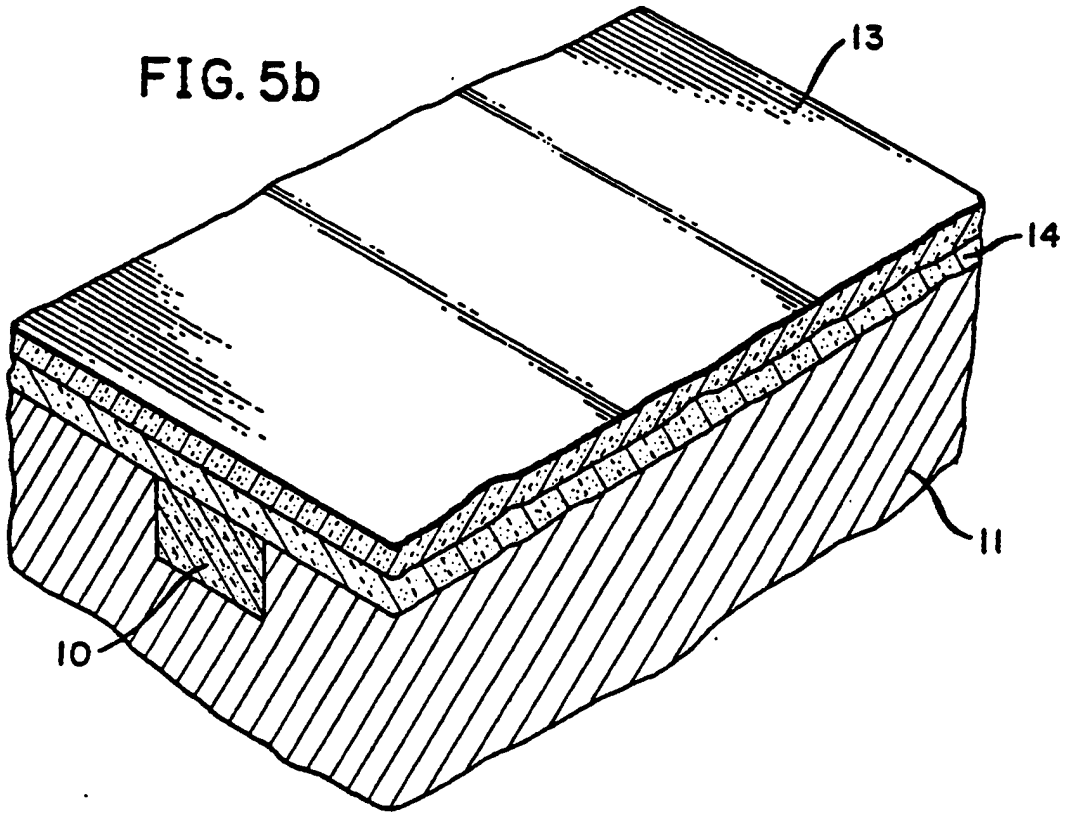

FIG. 6a

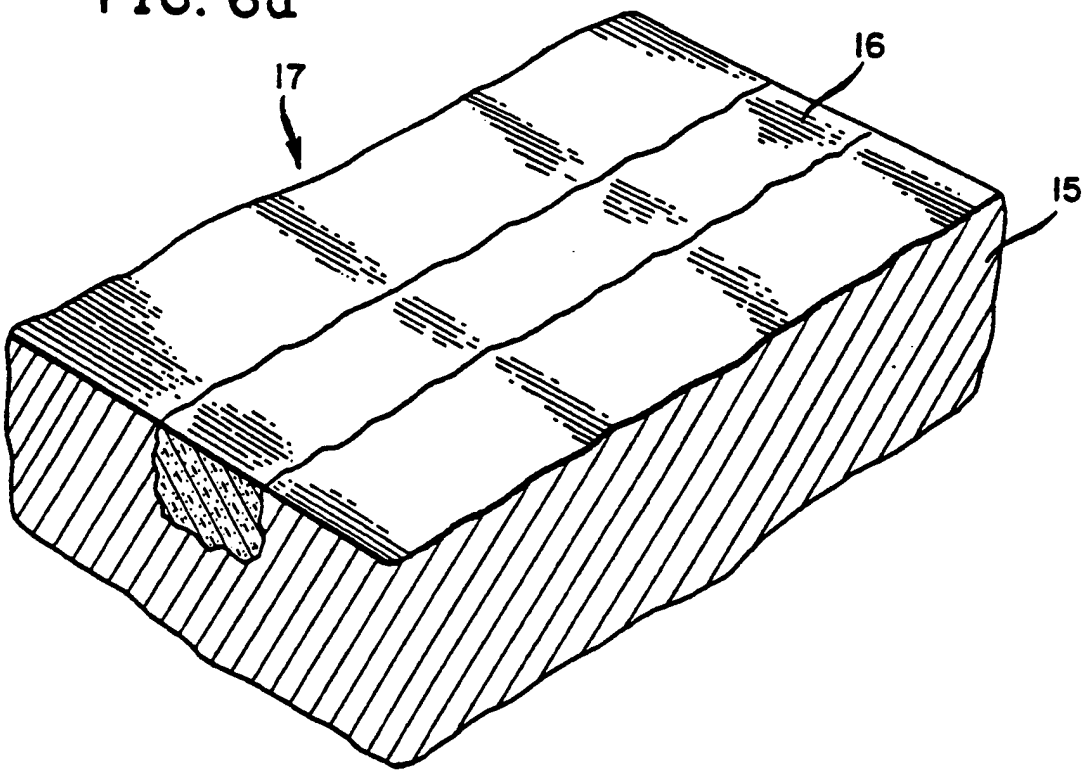

FIG. 6b

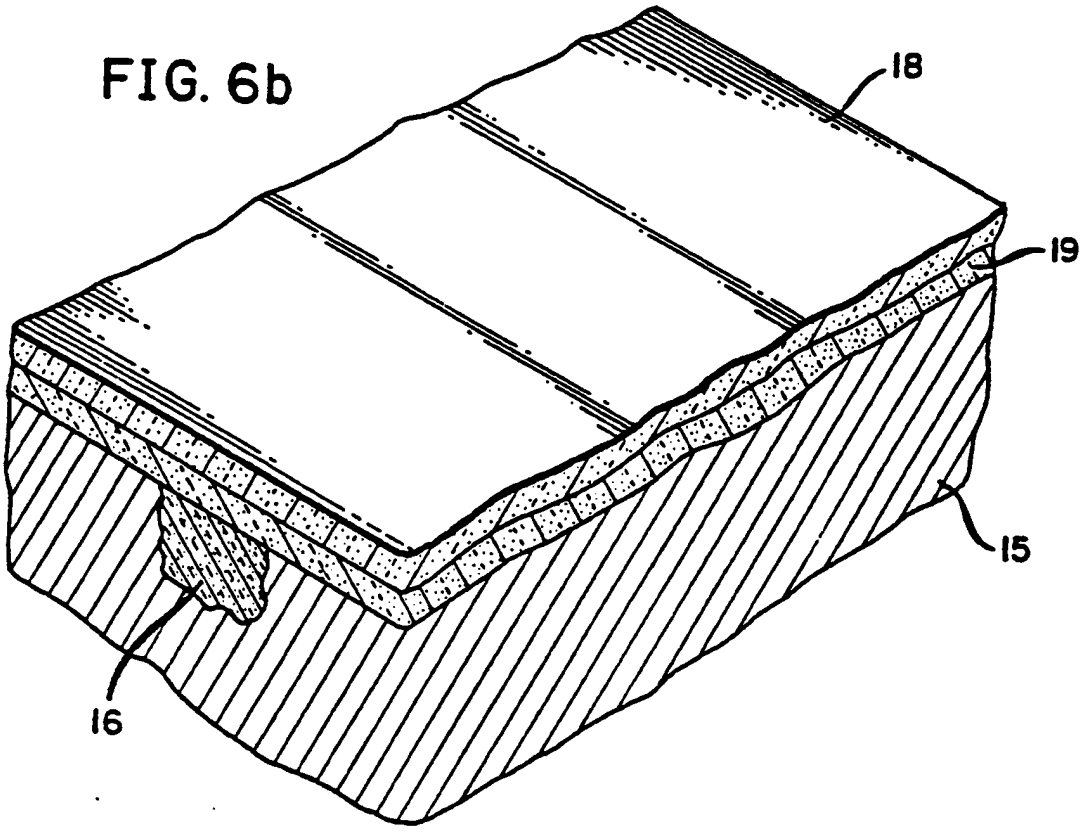

METAL-ENCAPSULATED QUANTUM WIRE FOR ENHANCED CHARGE TRANSPORT

GOVERNMENT INTEREST

The invention described herein may be manufactured, used, and licensed by or for the Government of the United States of America for governmental purposes without the payment to us of any royalty thereon.

BACKGROUND OF THE INVENTION

1. Field of the Invention

This invention relates to the field of electronic and opto-electronic devices that rely upon quantum-wire structures for charge transport between device components as well as for charge transport within active wire-like elements of device components.

2. Description of the Prior Art

As originally proposed by H. Sakaki in the *Japanese Journal of Applied Physics*, 19, L735, 1980, the predicted high mobilities of quasi-one-dimensional wire-like regions of semiconducting material underlie many proposed quantum-wire system concepts. Such a system concept is the quantum-wire array described by H. Sakaki in the *Japanese Journal of Applied Physics*, 28, L314, 1989. Enhanced carrier mobility is achieved in the subject quantum-wire array by engineering the minibands of the array so that longitudinal-optical (LO) phonon transitions are forbidden. As a second example of the utility of the semiconductor quantum wire is found in S. Luryi and F. Capasso, *Applied Physics Letters*, 47, 1347, 1985, in which a novel three-terminal resonant-tunneling structure is based on resonant tunneling of a two-dimensional electron gas into a gated one-dimensional quantum wire to produce a negative transconductance. The experimental realization of such a device would portend applications for low-power logic circuits. Quantum wire arrays have also been considered as potential low-current-threshold semiconductor lasers; in fact, there have been indications of strong optical anisotropy in such quantum-wire arrays as reported by M. Tsuchiya, J. M. Gaines, R. H. Yan, R. J. Simes, P. O. Holtz, L. A., Coldren, and P. M. Petroff, *Physical Review Letters*, 62, 466, 1989. Other efforts on the fabrication and characterization of quantum-wire structures have been reported by M. A. Reed, J. N. Randall, R. J. Aggarwal, R. J. Matyi, T. M. Moore, and A. E. Wetsel, *Physical Review Letters*, 60, 535, 1988 in connection with quantum-coupled electron device architectures and by M. Watt, C. M. Sotomayer Torres, H. E. G. Arnot, and S. P. Beaumont, *Semiconductor Science and Technology*, 285, 1990.

Recently, however, theoretical studies of the interaction between LO phonons and carriers in polar-semiconductor quantum wires, such as M. A. Stroscio, *Physical Review*, B40, 6428, 1989, have revealed the presence of discrete LO phonon modes similar to those identified earlier for polar-semiconductor quantum wells as discussed recently by N. Mori and T. Ando in *Physical Review*, B40, 6175, 1989. As for quantum wells, interface LO phonons are established at the semiconductor-semiconductor boundaries of quantum wires as described by K. W. Kim, M. A. Stroscio, A. Bhatt, R. Mickevicius and V. V. Mitin in the *Journal of Applied Physics*, 70, 319, 1991 where interface-phonon scattering effects are demonstrated to be a major source of scattering for electrons confined in the extreme quantum limit for wires with lateral dimensions less than about 40 Angstroms. As recently demonstrated by M. A. Stroscio, G. J. Iafrate, K. W. Kim, M. A. Littlejohn, H. Goronkin and G. N. Maracas in *Applied Physics Letters*, 59, 1093, 1991, interface-phonon scattering is a major contributor to carrier scattering in superlattices with structure dimensions of about 150 Angstroms or less. Experimental evidence for the enhancement of carrier-interface-phonon scattering as quantum well dimensions are reduced has been reported by K. T. Tsen, D. S. Smith, S. C. Y. Tsen, N. S. Kumar, and H. Morkoc in the *Journal of Applied Physics*, 70, 418, 1991. This enhanced inelastic carrier-interface-phonon scattering for confinement dimensions of less than roughly 100 Angstroms is undesirable since it reduces carrier mobility. Recent progress in the area of epitaxially-matched, metal to semiconductor interfaces in quantum-well devices has been made. J. P. Harbison, T. Sands, N. Tabatabaie, W. K. Chan, L. T. Florez, and V. G. Kermidas have reported on structures containing such metal-semiconductor interfaces in *Applied Physics Letters*, 53, 1717, 1988 and in the *Journal of Crustal Growth*, 95, 425, 1989. Additional papers reporting such results are A. Givarclh, J. Caulet, B. Guernais, Y. Ballini, R. Guerin, A. Poudoulec and A. Regreny in the *Journal of Crustal Growth*, 95, 427, 1989 and N. Tabatabaie, T. Sands, J. P. Harbison, H. L. Gilchrist and V. G. Kermidas in *Applied Physics Letters*, 53, 2528, 1988.

SUMMARY OF THE INVENTION

One object of the invention is to provide a means to improve carrier transport in quantum wires. A second object of the invention is to eliminate o reduce interface phonon modes in quantum wires through the introduction of metal-semiconductor heterojunctions at the lateral boundaries of the quantum wire. A third object of the invention is to eliminate or reduce interface phonon modes in quantum wires by combining partial encapsulation of the quantum wire in metal with modulation doping of the quantum wire. Another object of the invention is to provide quantum-wire cross sections of varying shapes, i.e., rectangular, circular, or arbitrary shapes. A still further object of the invention is to provide quantum-wire cross sections that vary along the length of the quantum wire.

BRIEF DESCRIPTION OF DRAWINGS

FIG. 1 is a pictorial view of a rectangular quantum wire encapsulated in metal.

FIG. 2 depicts a cross section of the quantum wire depicted in FIG. 1 along line IA—IA.

FIG. 3 is a pictorial view of a cross section of an arbitrarily-dimensioned quantum wire.

FIG. 4 is a pictorial view of a cross section of a circular quantum wire.

FIG. 5(*a*) is a pictorial view of a rectangular quantum wire encapsulated with metal on three sides and with a vacuum on its upper lateral surface.

FIG. 5*b*) is a pictorial view of a rectangular quantum wire encapsulated with metal on three sides and with a layered semiconductor structure on its upper lateral surface;

FIG. 6(*a*) is a pictorial view of the structure of FIG. 5(*a*) where the rectangular quantum wire is replaced with a quantum wire of arbitrary cross section;

FIG. 6(*b*) is a pictorial view of illustrates the structure of FIG. 5(*b*) where the rectangular quantum wire is replaced with a quantum wire of arbitrary cross section.

DETAILED DESCRIPTION OF THE PREFERRED EMBODIMENT

According to the invention there is further provided a region of metal encapsulation around the lateral surfaces of the charge transporting quantum wire. Such regions of metal encapsulation are shown in FIGS. 1 through 4. To enhance high-mobility transport in the quantum wire it is desirable to have uniform and smooth metal-semiconductor interfaces. In FIG. 1, a rectangular quantum wire 5 is encapsulated on all lateral surfaces by a metal 4. The ends of the quantum wire would be free of metal to a degree sufficient to allow entry and exit points for current J. The rectangular quantum wire has a fixed length 1, height 2, and width 3. In FIG. 1 the current J is depicted traveling along the x axis of the quantum wire.

FIG. 2 depicts a cross section of the quantum wire in FIG. 1 along line 1A—1A, showing graphically that each lateral surface of the quantum wire 5 is in contact with metal 4. FIG. 3 depicts a cross section of quantum wire having an arbitrary cross section 6 with each lateral surface of the quantum wire 6 in contact with metal 7. Similarly, FIG. 4 depicts a cross section of quantum wire having a circular cross section 8 with each lateral surface of the quantum wire 8 in contact with metal 9. It is understood that a single quantum wire may possess variable cross sections, i.e., at any point along its length it may vary from circular, to rectangular, to arbitrary, depending on its function within a device or design constraints imposed upon the device.

To facilitate the growth of uniform and smooth metal-semiconductor interfaces it may be advisable to select metal-semiconductor combinations such as Fe-GaAs which have lattice constants differing approximately by a multiple of an integer. Similar metal-semiconductor combinations include NiAl-AlAs, MnAl-AlAs, and CoAl-AlAs. Selecting metals with lattice constants less than that of the semiconductor enhances the possibility of recovering the electronic properties of the bulk metal in the minimum distance into the metal from the metal-semiconductor interface. Fe has a lattice constant about one-half that of GaAs so the Fe-GaAs system satisfies the condition of having lattice constants differing by an integral multiple as well as the condition of having the lattice constant of the metal being less than that of the semiconductor. Finally, as will be explained in the next paragraph, it may be desirable to select a metal with a large magnetic permeability since the classical penetration distance of the LO phonon field into a metal may be reduced as the magnetic permeability is increased.

It has been demonstrated recently by Michael A. Stroscio, K. W. Kim, Gerald J. Iafrate, Mitra Dutta and Harold L. Grubin in the *Proceedings of the* 1991 *International Semiconductor Device Research Symposium*, pages 87-91, 1991 Engineering Academic Outreach Publication, School of Engineering and Applied Science, University of Virginia, (ISBN Number: 1-880920-00-X), Dec. 4–6, 1991, that the interface LO phonon potential vanishes as the interface phonon attempts to penetrate from a polar semiconductor into a metal. This vanishing of the interface LO phonon mode coupled with the fact that the interface phonon modes are long-range Coulomb modes, as discussed in S. Baroni, P. Giannozzi and E. Molinari, *Physical Review*, B41, 3870, 1991, implies that encapsulating a substantial fraction of the quantum-wire lateral surfaces with metal will eliminate or greatly reduce the strength of the interface LO phonon potential. Consequently unwanted inelastic scattering due to the interface LO modes, which dominates for small (<100 Angstroms) dimensional scales, is reduced or eliminated by the metal encapsulation depicted in FIGS. 1 through 4.

Enhanced carrier mobility can be realized with less than complete encapsulation of the quantum wire. The long-range interface LO phonon potential will also be reduced significantly by partial metal encapsulation of quantum wires as depicted in FIGS. 5 and 6. In FIG. 5, a polar semiconductor quantum wire 10 is shown encapsulated in metal 11 on three of its lateral surfaces. The remaining lateral surface of the quantum wire 10 is exposed to a vacuum 12.

In all of the embodiments discussed above, carriers may be depleted from the semiconductor near the metal-semiconductor interface. The extent of depletion of minority and majority carriers will depend upon the properties of the bulk metal and semiconductor as well as on the equilibrium established at the metal-semiconductor interface. To enhance the carrier confinement density in the quantum wires of FIG. 5(*a*), the vacuum region bounding the top lateral surface of the quantum wires may be replaced by a layered semiconductor structure. In FIG. 5(*b*) the polar semiconductor quantum wire 10 is again shown encapsulated in metal 11. In this instance, however, the remaining lateral surface of the quantum wire 10 is bounded by a semiconductor lattice layer 14 which is matched to the polar semiconductor quantum wire 10. The semiconductor lattice layer 14 is in turn bounded by a polar or non-polar semiconductor 13. Through modulation doping of the semiconductor lattice layer 14 bounding the quantum wire 10 the carrier confinement density in the quantum wire 10 may be increased.

In FIG. 6(*a*), a polar semiconductor quantum wire 16 with an arbitrary cross section is shown encapsulated in metal 15 on approximately 75% of its lateral surface. The remaining lateral surface of the quantum wire 16 is exposed to a vacuum 17. FIG. 6(*b*) depicts the polar semiconductor quantum wire of FIG. 6(*a*) 16 again encapsulated in metal 15 with the remaining lateral surface of the quantum wire 15 bounded by a semiconductor lattice layer 19 which is matched to the polar semiconductor quantum wire 15. The semiconductor lattice layer 19 is in turn bounded by a polar or non-polar semiconductor 18. Through modulation doping of the semiconductor lattice layer 19 bounding the quantum wire 16, the carrier confinement density in the quantum wire 16 may be increased.

Because of the practical difficulties in achieving consistently uniform and smooth metal-semiconductor interfaces, it is envisioned that FIGS. 5(*b*) and 6(*b*) represent the best mode of practicing the invention.

Alternate embodiments of the structures depicted in FIGS. 5(*a*), 5(*b*), 6(*a*) and 6(*b*) include structures where arrays of parallel quantum wires replace the single quantum wire as well as structures where the quantum wires are bounded by multiple regions of metal and other materials such as insulators, semiconductors and vacuum.

The embodiments of FIGS. 5(*b*) and 6(*b*) are preferred when carrier densities must be enhanced above the level remaining after depletion of the semiconductor near the metal-semiconductor interface. Other embodiments may be used when the remaining density of either majority or minority carriers is adequate after depletion.

What is claimed is:

1. A partially metal-encapsulated quantum wire for enhanced charge transport comprising:

a polar semiconductor quantum wire having a lateral exterior surface and having a lattice constant of predetermined value; and

a metal encapsulation abutting at least a fifty percent portion of the lateral exterior surface of said polar semiconducting quantum wire thereby leaving an exposed surface of said polar quantum wire, said metal encapsulation having a lattice constant of predetermined value.

2. The partially metal-encapsulated quantum wire of claim 1 wherein said metal is magnetic.

3. The partially metal-encapsulated quantum wire of claim 1 wherein the lattice constant of said polar semiconductor quantum wire is an integral multiple of the lattice constant of said metal.

4. The partially metal-encapsulated quantum wire of claim 1 wherein a cross-section of said polar semiconductor quantum wire is rectangular.

5. The partially metal-encapsulated quantum wire of claim 1 wherein a cross-section of said polar semiconductor quantum wire is circular.

6. A completely metal-encapsulated quantum wire for enhanced charge transport comprising:

a polar semiconductor wire having a lateral exterior surface and having a lattice constant of predetermined value; and

a layer of metal completely encapsulating the lateral exterior surface of said polar semiconducting quantum wire, said layer of metal having a lattice constant of predetermined value.

7. The completely metal-encapsulated quantum wire of claim 6 wherein said metal is magnetic.

8. The completely metal-encapsulated quantum wire of claim 6 wherein the lattice constant of said polar semiconductor quantum wire is an integral multiple of the lattice constant of said metal.

9. The completely metal-encapsulated quantum wire of claim 6 wherein a cross-section of said polar semiconductor quantum wire is rectangular.

10. The completely metal-encapsulated quantum wire of claim 6 wherein a cross-section of said polar semiconductor quantum wire is circular.

11. The completely metal-encapsulated quantum wire of claim 1 wherein said polar semiconductor quantum wire is AlAs and said metal is selected from the group including NiAl, MnAl, and CoAl.

12. The partially metal-encapsulated quantum wire of claim 6 wherein said polar semiconductor quantum wire is AlAs and said metal is selected from the group including NiAl, MaAl, and CoAl.

13. The completely metal-encapsulated quantum wire of claim 1 wherein said polar semiconductor quantum wire is GaAs and said metal is Fe.

14. The partially metal-encapsulated quantum wire of claim 6 wherein said polar semiconductor quantum wire is GaAs and said metal is Fe.

15. The partially metal-encapsulated quantum wire of claim 1 wherein the metal encapsulation abuts at least a seventy five percent portion of said polar quantum wire.

16. The partially metal-encapsulated quantum wire of claim 1 further comprising a semiconductor lattice abutting the exposed surface of the polar quantum wire, the semiconductor lattice being comprised of at least two different semiconductor materials.

17. The partially metal-encapsulated quantum wire of claim 16 wherein one of the semiconductor materials comprising the semiconductor lattice is modulation doped.

* * * * *

Solid-State Electronics Vol. 37, No. 1, pp. 181–182, 1994
Printed in Great Britain.

0038-1101/94 $6.00 + 0.00

NOTE

GENERALIZED PIEZOELECTRIC SCATTERING RATE FOR ELECTRONS IN A TWO-DIMENSIONAL ELECTRON GAS

(Received 21 May 1993; in revised form 19 June 1993)

INTRODUCTION

Many envisioned applications of mesoscopic semiconductor structures are based on the transport of charge carriers at low temperatures and at low carrier energies. At such low temperatures and low carrier energies, the scattering of carriers from acoustic phonons may dominate over carrier scattering from optical phonons[1–4]. Transport of carriers in a two-dimensional electron gas is of special importance within the field of carrier transport in semiconductors. In this connection, Price[1] has given an excellent comprehensive treatment of the role of phonon scattering in two-dimensional electron transport in polar semiconductor layers; specifically, for the case of a two-dimensional electron gas, Price has given a detailed account of electron scattering by the Frohlich, deformation and piezoelectric potentials. In the case of piezoelectric scattering of electrons from acoustic phonons, Price has used the piezoelectric constants given by Zook[2] in the form summarized by Hearmon[3]. As discussed by Price, the piezoelectric constants given by Zook were derived under the assumption that the elastic anisotropy of the crystal is small. Price has made the additional approximation of averaging Zook's piezoelectric constants over the azimuthal directions in the plane of the two-dimensional electron gas. In this work, Price's treatment of piezoelectric scattering is generalized by not taking such an average over these azimuthal directions.

DISCUSSION

As discussed previously[1], the piezoelectric scattering rate function, $W(1,2)$, for electrons in a two-dimensional electron gas interacting with the acoustic phonon in a zincblende crystal may be written as:

$$W(1,2)=\frac{2\pi}{\hbar}\frac{S}{(2\pi)^3}2\delta[E(1)-E(2)], \tag{1}$$

where:

$$S=\frac{kT(eh_{14})^2}{2}\frac{\pi}{Q}\left(\frac{B_l}{\rho s_l^2}+\frac{2B_t}{\rho s_t^2}\right), \tag{2}$$

with:

$$B_l=\frac{Q}{\pi}\int_{-\infty}^{+\infty}\frac{A_l}{Q^2+q^2}\,dq, \tag{3a}$$

$$B_t=\frac{Q}{\pi}\int_{-\infty}^{+\infty}\frac{A_t}{Q^2+q^2}\,dq, \tag{3b}$$

$$A_l=36\frac{q^2Q_y^2Q_z^2}{(q^2+Q^2)^3}, \tag{4a}$$

and

$$2A_t+A_l=\frac{4}{(q^2+Q^2)}(q^2Q_y^2+Q_y^2Q_z^2+Q_z^2q^2); \tag{4b}$$

in these results $W(1,2)$ equals the rate of transitions from initial state, 1, to final state, 2, per unit volume of k space, q is the acoustic phonon wavevector normal to a two-dimensional electron gas in the (100) plane, Q_y and Q_z are the phonon wavevectors in the (100) plane, $Q^2=Q_y^2+Q_z^2$, k is Boltzmann's constant, T is the temperature of the lattice, e is the charge on an electron, h_{14} is the piezoelectric constant which has a value of roughly 1.57×10^9 V/m for GaAs, ρ is the mass density, and $s_l(s_t)$ is the longitudinal (transverse) velocity of sound in the lattice. The limitations of eqns (1)–(4b) have been discussed previously in Ref. [1] where it is noted that a linear proportionality between phonon frequency and phonon wavevector has been assumed. Upon performing the indicated integrations over q:

$$\frac{\pi}{Q}B_l=\frac{9}{4}\pi\frac{Q_y^2Q_z^2}{(Q_y^2+Q_z^2)^{5/2}}, \tag{5a}$$

and

$$\frac{\pi}{Q}B_t=\frac{\pi}{2}\frac{1}{(Q_y^2+Q_z^2)^{1/2}}-\frac{3\pi}{4}\frac{Q_y^2Q_z^2}{(Q_y^2+Q_z^2)^{5/2}}. \tag{5b}$$

Thus:

$$S=\frac{kT(eh_{14})^2}{2}\left[\left(\frac{9}{4}\pi\frac{Q_y^2Q_z^2}{(Q_y^2+Q_z^2)^{5/2}}\right)\frac{1}{\rho s_l^2}+\left(\frac{\pi}{2}\frac{1}{(Q_y^2+Q_z^2)^{1/2}}-\frac{3\pi}{4}\frac{Q_y^2Q_z^2}{(Q_y^2+Q_z^2)^{5/2}}\right)\frac{1}{\rho s_t^2}\right]. \tag{6}$$

As in Refs [1–3], the effects of screening have not been considered in deriving eqn (6).

In the limit where the average is taken over azimuthal directions[1]:

$$Q_y^2Q_z^2\to Q^4/8, \tag{7a}$$

and

$$Q_y^2=Q_z^2\to Q^2/2, \tag{7b}$$

with the result that:

$$S=\frac{kT(eh_{14})^2}{2}\frac{\pi}{Q}\left(\frac{9}{32}\frac{1}{\rho s_l^2}+\frac{13}{32}\frac{1}{\rho s_t^2}\right), \tag{8}$$

as originally derived by Price.

In deriving the generalized piezoelectric scattering rate for a two-dimensional electron gas, it has been assumed that the stiffness constants for the zincblende crystal are isotropic. Indeed, for each of GaAs, GaP, InSb, InAs and InP the three independent experimentally-determined stiffness constants differ in magnitude by less than 35% from stiffness constants consistent with an isotropic medium. On the other hand, the generalized expression for $\pi B_l/Q$ may vary from zero to twice its azimuthally averaged value, $9\pi/32Q$ depending upon the relative magnitudes of Q_y and Q_z. While applications such as calculations of mobility were not considered in this work, the fact that the generalized expression for $\pi B_l/Q$ may vanish as Q_y or Q_z goes to zero may be of special significance of the frequently-discussed cases where the dominant charge carrier momentum in the two-dimensional electron gas or the phonon momentum is highly anisotropic; in particular, mobilities for such systems may be enhanced since the longitudinal scattering terms may be suppressed as a result of the anisotropic form of eqn (5a). The variation in $\pi B_t/Q$ is much less pronounced having a range from $10\pi/32Q$ to $16\pi/32Q$ depending upon the relative magnitudes of Q_y and Q_z.

CONCLUSION

A generalized piezoelectric scattering rate for electrons in a two-dimensional electron gas has been derived by relaxing the previous constraint of averaging over azimuthal directions in the two-dimensional electron gas. The generalized scattering rate is found to deviate little from the azimuthally averaged rate for terms depending on the transverse acoustic phonon velocity but the corrections to the terms containing the longitudinal acoustic phonon velocity may be substantial.

[1]*U.S. Army Research Office*
P.O. Box 12211
Research Triangle Park
NC 27709-2211
U.S.A.

MICHAEL A. STROSCIO[1]
K. W. KIM[2]

[2]*Department of Electrical and Computer Engineering*
North Carolina State University
Raleigh
NC 27695-7911
U.S.A.

Acknowledgement—The authors gratefully acknowledge helpful conversations with Dr Gerald J. Iafrate and Professor M. A. Littlejohn. This research was supported, in part, by the Office of Naval Research and the U.S. Army Research Office.

REFERENCES

1. P. J. Price, *Ann. Phys.* **133**, 217 (1981).
2. J. David Zook, *Phys. Rev.* **136**, A869 (1964).
3. R. F. S. Hearmon, *Acta crystallogr.* **10**, 121 (1957).
4. T. Kawamura and S. Das Sarma, *Phys. Rev. B*, **45**, 2612 (1992).
5. H. Sakaki, *Jap. J. Appl. Phys.* **19**, L 175 (1980).

Transitions between Γ and X states of short-period superlattices driven by antisymmetric interface phonons

Michael A. Stroscio
U.S. Army Research Office, P.O. Box 12211, Research Triangle Park, North Carolina 27709-2211

Mitra Dutta
Electronics and Power Sources Directorate, U.S. Army Research Laboratory, Ft. Monmouth, New Jersey 07703-5601

Xiao-qiang Zhang
Department of Electrical Engineering, Duke University, Durham, North Carolina 27708-2901

(Received 19 July 1993; accepted for publication 1 November 1993)

Relative transition probability amplitudes for antisymmetric-interface-phonon-assisted Γ-*X* transitions in selected short-period superlattices are estimated by using the dielectric continuum model for antisymmetric interface optical phonons in conjunction with a Kronig–Penney model of the superlattice electronic properties.

I. INTRODUCTION

Approximate expressions for the phonon dispersion relation for each of the confined and interface (IF) longitudinal-optical (LO) phonon modes as well as for the carrier-LO-phonon interaction Hamiltonian are provided by the dielectric continuum model of confined and interface longitudinal-optical phonons.[1–5] Furthermore, this model predicts an enhancement of carrier-interface-phonon scattering relative to carrier-confined-phonon scattering in polar semiconductor heterostructures as heterojunction-to-heterojunction separations are reduced.[5,6] Recently, measured Raman spectra[7] have provided evidence in support of the predicted enhancement[5] in carrier-interface-phonon scattering in short-period GaAs-AlAs superlattices. In addition, related evidence confirming the importance of interface-LO-phonon modes has come from two separate observations: interface-phonon-assisted Γ-*X* transitions[8] in GaAs/AlAs quantum wells and interface-phonon-assisted tunneling[9] in double-barrier GaAs/AlAs quantum well structures. In related measurements, exciton delocalization and electron conduction via the *X* valley have been observed in GaAs-AlAs quantum wells.[10,11]

Motivated by predicted enhancements in carrier-interface-phonon scattering[5] in short-period superlattices as well as by recent Raman spectra[7] involving interface phonons, this paper presents the first theoretical treatment of interface-phonon-assisted Γ-*X* transitions for antisymmetric phonons; symmetric IF phonons are not considered herein since the relative Γ-*X* transition amplitudes for symmetric IF phonons have been derived previously.[11] The Kronig–Penney formalism of Cho and Prucnal[12] is used in conjunction with the antisymmetric interface phonon energies and the IF phonon mode symmetries determined by the dielectric continuum model[3–5] to specify the dimensional parameters of a number of GaAs-AlAs and GaAs-GaP superlattices which are expected to exhibit interface-phonon-assisted Γ-*X* transitions for particular Γ and *X* minibands. Furthermore, the envelope wave function approach is used to estimate the relative magnitudes of antisymmetric interface-phonon-assisted Γ-*X* transitions in polar semiconductor superlattices.

Typical interface phonon wave vectors[13] are in the range of 0.01–0.02 Å^{-1}. Since these interface phonon potentials fall off exponentially,[3,5] in tens of angstroms[13] to e^{-1} of the value of the phonon potential at the interface, the relative magnitudes of the interface-phonon-assisted Γ-*X* transition probabilities for these short-period superlattices are estimated by approximating the interface-phonon potential in the small-wave vector limit by using the envelope wave functions to evaluate the Γ-*X* overlap integral.[14]

II. RELATIVE PROBABILITY AMPLITUDES FOR Γ-X TRANSITIONS ASSISTED BY ANTISYMMETRIC INTERFACE LO PHONONS

A portion of the GaAs-AlAs and GaAs-GaP superlattices of interest in this work is shown in Fig. 1. Figure 1(a) defines the Γ-valley discontinuity V_Γ, the effective masses in the barrier m_I, and the well m_{II}, as well as the barrier and well thicknesses, b and a, respectively. Figure 1(b) defines the corresponding quantities for the *X*-valley parameters of the two semiconductor layers.

For the GaAs-AlAs superlattice, $m_I=0.15m_0$, $m_{II}=0.067m_0$, and $V=V_\Gamma=1$ eV specify the Γ-valley properties; the corresponding parameters for the *X*-valley properties are $m_b^l=1.3m_0$, $m_w^l=1.1m_0$, and $V=V_x=170$ meV for the longitudinal *X* valley and $m_b^t=0.23m_0$, $m_w^t=0.19m_0$, and $V=V_x=170$ meV for the transverse *X* valley. The numerical value of V_x is subject to large experimental uncertainty; however, it has been demonstrated previously[11] that a 100 meV variation in V_x changes the energies of the *X* minibands by less than 2 meV. For the GaAs-GaP superlattice, $m_I=0.13m_0$, $m_{II}=0.067m_0$, and $V=V_\Gamma=400$ meV have been taken to specify the Γ-valley properties; the corresponding parameters for the *X*-valley properties have been approximated by $m_b^l=1.3m_0$, $m_w^l=0.91m_0$, and $V=V_x=660$ meV for the longitudinal *X* valley and by $m_b^t=0.23m_0$, $m_w^t=0.25m_0$, and $V=V_x=660$ meV for the transverse *X* valley.

 0021-8979/94/75(4)/1977/5/$6.00

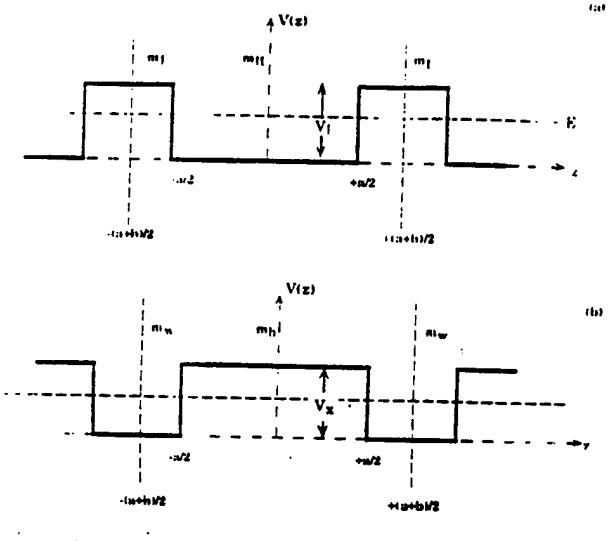

FIG. 1. (a) This figure depicts a representative portion of the Γ valley conduction band minimum in a superlattice of period $a+b$; V_Γ is the Γ valley discontinuity and the effective masses m_I and m_{II} are assigned to the indicated layers. E is the energy measured relative to the lower value of the Γ valley conduction band minimum. (b) This figure depicts a representative portion of the X valley conduction band minimum in a superlattice of period $a+b$; V_X is the X valley discontinuity and the effective masses m_b and m_w are assigned to the indicated layers. E is the energy measured relative to the lower value of the X valley conduction band minimum.

In the GaAs/AlAs double-barrier quantum-well heterostructures, the two antisymmetric interface phonon modes have potential envelopes, $f_{A\pm}(Q,z)$, of the form[3,5]

$$f_{A\pm}(Q,z)=\begin{cases} -e^{Q(z+\frac{1}{2}a)}, & z<-\frac{1}{2}a, \quad (1a)\\ \sinh(Qz)/\sinh(\frac{1}{2}Qa), & \frac{1}{2}a<z<\frac{1}{2}a, \quad (1b)\\ +e^{-Q(z-\frac{1}{2}a)}, & z>\frac{1}{2}a, \quad (1c)\end{cases}$$

where the low-wave vector limits of the $A^\pm$ modes approach the AlAs TO and the GaAs LO frequencies denoted by ω_{A+} and ω_{A-}, respectively. For the AlAs-GaAs system, the zone-center values for $\hbar\omega_{S+}$, $\hbar\omega_{A+}$, $\hbar\omega_{A-}$, and $\hbar\omega_{S-}$ are $\sim$50, 45, 36, and 33 meV, respectively. Thus, for the antisymmetric modes, as $Q\to 0$, the frequency of the A^+ mode, ω_{A+}, approaches the AlAs transverse-optical (TO) frequency; the frequency of the A^- mode, ω_{A-}, approaches the GaAs longitudinal-optical (LO) frequency. Likewise, for the GaP-GaAs system, the zone-center values for $\hbar\omega_{S+}$, $\hbar\omega_{A+}$, $\hbar\omega_{A-}$, and $\hbar\omega_{S-}$ are $\sim$50, 45, 36, and 33 meV, respectively. In these results, z is directed normal to the heterointerfaces located at $z=\pm a/2$ and Q is the wave vector of the interface optic phonon.

The relative magnitudes of the antisymmetric-interface-phonon-assisted Γ-X transition probability amplitudes are given herein for the special case where superlattice layer dimensions are small compared with the scales characterizing the exponential decay distances for interface phonons; these results follow immediately upon calculating the overlap between the antisymmetric interface phonon envelopes and the miniband states of Cho and Prucnal.[11,12] Since the IF phonon potential times the charge of the carrier is identically equal to[5] the carrier-IF-LO-phonon perturbation Hamiltonian and since the Γ components of the X-like and Γ-like wave functions are proportional to the mixing potential for nondegenerate miniband minima,[15] the relative probability amplitudes for interface-phonon-assisted Γ-X transitions are approximated accurately by the overlapping integral of the envelope function of the Γ valley, that of the X valley, and the potential of the interface phonon. Accordingly, for transitions between the lowest X miniband and a Γ miniband with even index i, the probability amplitude of a Γ-X transition assisted by an antisymmetric interface phonon of a given wave vector, Q, is proportional to

$$I^{(1,i)}=2\int_0^{a/2}(-a_1^{(i)}a_2')\frac{\sinh(Qz)}{\sinh(\frac{1}{2}Qa)}\sin(\beta^{(i)}z)\cosh(\alpha' z)dz$$
$$+2\int_0^{b/2}(-a_1'a_2^{(i)})\frac{\sinh(Qz)}{\sinh(\frac{1}{2}Qb)}\cos(\beta' z)$$
$$\times\cosh(\alpha^{(i)}z)dz, \quad (2)$$

where the envelope wavefunctions for the even-index Γ bands at energy minimum have been taken as[11,12,16]

$$\psi_{a(\Gamma)}^{(i)}=-a_1^{(i)}\sin(\beta^{(i)}z), \quad -\frac{a}{2}<z<\frac{a}{2}, \quad (3a)$$

$$\psi_{b(\Gamma)}^{(i)}=a_2^{(i)}\cosh\left\{\alpha^{(i)}\left[z+\left(\frac{a+b}{2}\right)\right]\right\}, \quad -\frac{a}{2}-b<z<-\frac{a}{2}, \quad (3b)$$

$$\psi_{b(\Gamma)}^{(i)}=a_2^{(i)}\cosh\left\{\alpha^{(i)}\left[z-\left(\frac{a+b}{2}\right)\right]\right\}, \quad \frac{a}{2}<z<\frac{a}{2}+b; \quad (3c)$$

in Eqs. (3a)–(3c),

$$\alpha^{(i)}=\sqrt{2m_{II}(V-E^{(i)})/\hbar^2}, \quad (4a)$$

$$\beta^{(i)}=\sqrt{2m_I E^{(i)}/\hbar^2}, \quad (4b)$$

$$a_1^{(i)}=\cosh\left(\frac{\alpha^{(i)}b}{2}\right)a_2^{(i)}/\sin\left(\beta^{(i)}\frac{a}{2}\right), \quad (4c)$$

and

$$a_2^{(i)}=1\Big/\left(\frac{1}{2\alpha^{(i)}}[\alpha^{(i)}b+\sinh(\alpha^{(i)}b)]\right.$$
$$\left.+\frac{\cosh^2(\alpha^{(i)}b/2)}{\sin^2(\beta^{(i)}a/2)}\frac{1}{2\beta^{(i)}}[\beta^{(i)}a-\sin(\beta^{(i)}a)]\right)^{1/2}. \quad (4d)$$

The envelope wavefunctions for the lowest X miniband are defined by

$$\psi_{a(X)}^{(1)}=a_2'\cosh(\alpha' z), \quad -\frac{a}{2}<z<\frac{a}{2}, \quad (5a)$$

$$\psi^{(1)}_{b(X)}=a'_1\cos\left\{\beta'\left[z+\left(\frac{a+b}{2}\right)\right]\right\},\quad -\frac{a}{2}-b<z<-\frac{a}{2},\tag{5b}$$

$$\psi^{(1)}_{b(X)}=a'_1\cos\left\{\beta'\left[z-\left(\frac{a+b}{2}\right)\right]\right\},\quad \frac{a}{2}<z<\frac{a}{2}+b.\tag{5c}$$

For transitions between the second X miniband and a Γ miniband with even index i, the transition probability amplitude for the case of antisymmetric interface phonons is proportional to

$$I^{\{2,i\}}=2\int_0^{a/2}(-a_1^{(i)}a_2'^{(2)})\frac{\sinh(Qz)}{\sinh(\frac{1}{2}Qa)}\sin(\beta^{(i)}z)\times\cosh(\alpha'^{(2)}z)dz+2\int_0^{b/2}(a_1'^{(2)}a_2^{(i)})\times\frac{\sinh(Qz)}{\sinh(\frac{1}{2}Qb)}\sin(\beta'^{(2)}z)\cosh(\alpha^{(i)}z)dz,\tag{6}$$

where

$$\psi^{(2)}_{a(X)}=a_2'^{(2)}\cosh(\alpha'^{(2)}z),\quad -\frac{a}{2}<z<\frac{a}{2},\tag{7a}$$

$$\psi^{(2)}_{b(X)}=a_1'^{(2)}\sin\left\{\beta'^{(2)}\left[z+\left(\frac{a+b}{2}\right)\right]\right\},\quad -\frac{a}{2}-b<z<-\frac{a}{2},\tag{7b}$$

$$\psi^{(2)}_{b(X)}=a_1'^{(2)}\sin\left\{\beta'^{(2)}\left[z-\left(\frac{a+b}{2}\right)\right]\right\},\quad \frac{a}{2}<z<\frac{a}{2}+b\tag{7c}$$

define the envelope wavefunction for the second X miniband. In Eqs. (5a)–(5c) and Eqs. (7a)–(7c),

$$\alpha'^{(i)}=\sqrt{2m_b^{\perp,t}(V-E^{(i)})/\hbar^2}\tag{8a}$$

and

$$\beta'^{(i)}=\sqrt{2m_w^{\perp,t}E^{(i)}/\hbar^2};\tag{8b}$$

in the case where $i=1$, $\alpha'^{(1)}$ and $\beta'^{(1)}$ are denoted simply by α' and β'. In Eqs. (5a)–(5c)

$$a'_1=\cosh(\alpha' a/2)a'_2/\cos(\beta' b/2)\tag{8c}$$

and

$$a'_2=1\Big/\left(\frac{\cosh^2(\alpha' a/2)}{\cos^2(\beta' b/2)}\frac{[\beta' b+\sin(\beta' b)]}{2\beta'}+\frac{[\alpha' a+\sinh(\alpha' a)]}{2\alpha'}\right)^{1/2}.\tag{8d}$$

In Eqs. (7a)–(7c), additional quantities are

$$a_1'^{(2)}=-\cosh(\alpha'^{(2)}a/2)a_2'^{(2)}/\sin(\beta'^{(2)}b/2)\tag{8e}$$

and

$$a_2'^{(2)}=1\Big/\left(\frac{1}{2\alpha'^{(2)}}[\alpha'^{(2)}a+\sinh(\alpha'^{(2)}a)]+\frac{\cosh^2(\alpha'^{(2)}a/2)}{\sin^2(\beta'^{(2)}b/2)}\frac{1}{2\beta'^{(2)}}[\beta'^{(2)}b-\sin(\beta'^{(2)}b)]\right)^{1/2}.\tag{8f}$$

The integral $I^{\{1,i\}}$ may be performed to yield

$$\begin{aligned}I^{\{1,i\}}=&-\frac{2a_1^{(i)}a'_2}{2\sinh(\frac{1}{2}Qa)}\left[\frac{(Q+\alpha')\cosh[(Q+\alpha')a/2]\sin(\beta^{(i)}a/2)}{[(Q+\alpha')^2+(\beta^{(i)})^2]}-\frac{\beta^{(i)}\sinh[(Q+\alpha')a/2]\cos(\beta^{(i)}a/2)}{[(Q+\alpha')^2+(\beta^{(i)})^2]}\right.\\&\left.+\frac{(Q-\alpha')\cosh[(Q-\alpha')a/2]\sin(\beta^{(i)}a/2)}{[(Q-\alpha')^2+(\beta^{(i)})^2]}-\frac{\beta^{(i)}\sinh[(Q-\alpha')a/2]\cos(\beta^{(i)}a/2)}{[(Q-\alpha')^2+(\beta^{(i)})]^2}\right]\\&-\frac{2a'_1a_2^{(i)}}{2\sinh(\frac{1}{2}Qb)}\left[\frac{(Q+\alpha^{(i)})\cosh[(Q+\alpha^{(i)})b/2]\cos(\beta' b/2)}{[(Q+\alpha^{(i)})^2+(\beta')^2]}+\frac{\beta'\sinh[(Q+\alpha^{(i)})b/2]\sin(\beta' b/2)}{[(Q+\alpha^{(i)})^2+(\beta')^2]}\right.\\&\left.+\frac{(Q-\alpha^{(i)})\cosh((Q-\alpha')b/2)\cos(\beta' b/2)}{[(Q-\alpha^{(i)})^2+(\beta')^2]}+\frac{\beta'\sinh[(Q-\alpha^{(i)})b/2]\sin(\beta' b/2)}{[(Q-\alpha^{(i)})^2+(\beta')^2]}\right]\\&+\frac{2a'_1a_2^{(i)}}{2\sinh(\frac{1}{2}Qb)}\left[\frac{(Q+\alpha^{(i)})}{[(Q+\alpha^{(i)})^2+(\beta')^2]}+\frac{(Q-\alpha^{(i)})}{[(Q-\alpha^{(i)})^2+(\beta')^2]}\right].\end{aligned}\tag{9}$$

Likewise, the integral $I^{\{2,i\}}$ may be evaluated as

$$I^{\{2,i\}}=\frac{-2a_1^{(i)}a_2'^{(2)}}{2\sinh(\frac{1}{2}Qa)}\left[\frac{(Q+\alpha'^{(2)})\cosh[(Q+\alpha'^{(2)})a/2]\sin(\beta^{(i)}a/2)}{[(Q+\alpha'^{(2)})^2+(\beta^{(i)})^2]}-\frac{\beta^{(i)}\sinh[(Q+\alpha'^{(2)})a/2]\cos(\beta^{(i)}a/2)}{[(Q+\alpha'^{(2)})^2+(\beta^{(i)})^2]}\right.$$

$$\left.+\frac{(Q-\alpha'^{(2)})\cosh[(Q-\alpha'^{(2)})a/2]\sin(\beta^{(i)}a/2)}{[(Q-\alpha'^{(2)})^2+(\beta^{(i)})^2]}-\frac{\beta^{(i)}\sinh[(Q-\alpha'^{(2)})a/2]\cos(\beta^{(i)}a/2)}{[(Q-\alpha'^{(2)})^2+(\beta^{(i)})^2]}\right]$$

$$+\frac{2a_1'^{(2)}a_2^{(i)}}{2\sinh(\frac{1}{2}Qb)}\left[\frac{(Q+\alpha^{(i)})\cosh[(Q+\alpha^{(i)})b/2]\sin(\beta'^{(2)}b/2)}{[(Q+\alpha^{(i)})^2+(\beta'^{(2)})^2]}-\frac{\beta'^{(2)}\sinh((Q+\alpha^{(i)})b/2)\cos(\beta'^{(2)}b/2)}{[(Q+\alpha^{(i)})^2+(\beta'^{(2)})^2]}\right.$$

$$\left.+\frac{(Q-\alpha^{(i)})\cosh((Q-\alpha^{(i)})b/2)\sin(\beta'^{(2)}b/2)}{[(Q-\alpha^{(i)})^2+(\beta'^{(2)})^2]}-\frac{\beta'^{(2)}\sinh((Q-\alpha^{(i)})b/2)\cos(\beta'^{(2)}b/2)}{[(Q-\alpha^{(i)})^2+(\beta'^{(2)})^2]}\right]. \quad (10)$$

The relative antisymmetric-interface-phonon-assisted transition probability amplitudes for transitions between the second Γ miniband Γ_2 and various X minibands as given by $I^{\{1,i\}}$ and $I^{\{2,i\}}$ are summarized in Table I. In each case, the amplitude corresponding to the smaller dimensional parameter applies to the situation where the Γ miniband minimum is 45 meV greater than the X miniband minimum; the amplitude given for the larger dimensional parameter is for the situation where the Γ miniband minimum is 45 meV less than the X miniband minimum. In these calculations a single value for the higher-frequency antisymmetric interface phonon mode has been assumed; this assumption is accurate since both the AlAs and the GaP TO frequencies at zone center are about 45 meV.

TABLE I. Interface-phonon-assisted transition probability amplitudes are given in this table for transitions between the second lowest-energy Γ miniband and the two lowest energy X^l and X^t minibands for a variety of GaAs-AlAs and GaAs-GaP superlattices. As explained in the text, the amplitude corresponding to the smaller dimensional parameter applies to the case where the Γ miniband minimum is 45 meV greater than the X miniband minimum and the amplitude given for the larger dimensional parameter is for the case where the Γ miniband minimum is 45 meV less than the X miniband minimum. The accuracies of the approximate probability amplitudes in this table increase as both a and b are decreased; in addition, the standard degeneracy factors for the X^l and X^t bands have not been included in these approximate probability amplitudes.

	ΔE=45 meV			
	Γ_2–X_1^l	Γ_2–X_1^t	Γ_2–X_2^l	Γ_2–X_2^t
GaAs-AlAs	0.06	0.19	0.35	0.35
$a=b$	a=75 Å	a=72 Å	a=72 Å	a=62 Å
	0.05	0.08	0.27	0.31
	a=101 Å	a=97.5 Å	a=97 Å	a=81 Å
GaAs-AlAs	0.21	0.33	0.24	0.75
$b=a$+37.5 Å	a=26 Å	a=24 Å	a=24.5	a=20 Å
	0.17	0.16	0.16	0.60
	a=40 Å	a=37 Å	a=37 Å	a=28.5 Å
GaAs-GaP			0.39	0.31
$a=b$+45 Å	b<5 Å	b<5 Å	b=11 Å	b=20 Å
			0.31	0.40
	b<5 Å	b<5 Å	b=12 Å	b=25 Å
GaAs-GaP			0.25	0.30
$a=b$+37.5 Å	b<5 Å	b<5 Å	b=9 Å	b=19 Å
			0.31	0.43
	b<5 Å	b<5 Å	b=11 Å	b=24 Å

III. CONCLUSION

The dimensional parameters of Table I are based on the requirements that the GaAs layers in the GaAs-AlAs structures be thin enough for confinement effects to elevate the Γ_1 miniband to energies near those of the X miniband and that the GaP layers in the GaAs-GaP structures be thin enough for confinement effects to elevate the X miniband to energies near the Γ minibands.[17–20] For the dimensional parameters considered in this paper the constraints imposed by these confinement effects, as well as those imposed by the finite energy ranges associated with V_Γ and V_X, the Γ_3 miniband energies are raised to values too high to obtain miniband-to-miniband transitions involving the allowed Γ_3-$X_2^{l,t}$ couplings. For this reason, only Γ_2-$X_2^{l,t}$ transition probability amplitudes are given in Table I. Transitions involving Γ_2 minibands are not allowed for symmetric interface phonon potentials when miniband to miniband transitions occur between miniband minima; however, it is clear the transitions involving the Γ_2 bands are allowed for the case of antisymmetric interface phonons considered in this paper.

In summary, this paper provides the first theory of antisymmetric-interface-phonon-assisted Γ-X transitions in short-period superlattices.

ACKNOWLEDGMENTS

The authors gratefully acknowledge the many fruitful discussions with Professor A. Petrou of SUNY Buffalo, Professor W. Poetz of the University of Illinois at Chicago, Dr. Gerald J. Iafrate, Director of the U.S. Army Research Office, Professor K. W. Kim of the North Carolina State University, and M. U. Erdogan of the North Carolina State University. The authors are also grateful to Patricia Lassiter for the excellent preparation of the manuscript.

[1] R. Fuchs and K. L. Kliewer, Phys. Rev. 140, A2076 (1965).
[2] J. J. Licari and R. Evrard, Phys. Rev. B 15, 2254 (1977).
[3] N. Mori and T. Ando, Phys. Rev. B 40, 6175 (1989).
[4] R. Chen, D. L. Lin, and T. F. George, Phys. Rev. B 41, 1435 (1990).
[5] K. W. Kim and M. A. Stroscio, J. Appl. Phys. 68, 6289 (1990).
[6] M. A. Stroscio, G. J. Iafrate, K. W. Kim, M. A. Littlejohn, H. Goronkin, and G. N. Maracas, Appl. Phys. Lett. 59, 1093 (1991); K. W. Kim, M. A. Littlejohn, M. A. Strocio, and G. J. Iafrate, Semicond. Sci. Technol. B 7, 49 (1992).

[7]K. T. Tsen, K. R. Wald, T. Ruf, P. Y. Yu, and H. Morkoc, Phys. Rev. Lett. 67, 2557 (1991).
[8]L. P. Fu, T. Schmiedel, A. Petrou, M. Dutta, P. G. Newman, and M. A. Stroscio, Phys. Rev. B 46, 7196 (1992).
[9]S. Teitsworth and P. Turley, Phys. Rev. B 55, 8181 (1991); P. J. Turley, C. R. Wallis, S. W. Teitsworth, W. Li, and P. K. Bhattacharya, *ibid.* 47, 12640 (1993).
[10]M. Dutta, D. D. Smith, P. G. Newman, X. C. Lin, and A. Petrou, Phys. Rev. B 42, 1474 (1990).
[11]M. Dutta and M. A. Stroscio, J. Appl. Phys. 73, 1693 (1993).
[12]H.-S. Cho and P. R. Prucnal, Phys. Rev. B 36, 3237 (1987).
[13]N. J. Pulsford, R. J. Nicholas, P. Dawson, K. J. Moore, G. Duggan, and C. T. B. Foxon, Phys. Rev. Lett. 63, 2284 (1989); H. Rucker, E. Molinari, and P. Lugli, Phys. Rev. B 44, 3463 (1991).
[14]T. Ando, S. Wakahara, and H. Akera, Phys. Rev. B 40, 11609 (1989); T. Ando and H. Akera, *ibid.* 40, 11619 (1989).
[15]M. U. Erdogan, K. W. Kim, and M. A. Stroscio, J. Appl. Phys. 74, 4777 (1993).
[16]G. Bastard, Phys. Rev. B 24, 5693 (1981).
[17]M.-H. Meynadier, R. E. Nahory, J. M. Worlock, N. C. Tamargo, J. L. de Migues, and M. D. Sturge, Phys. Rev. Lett. 60, 1338 (1988).
[18]N. J. Pulsford, R. J. Nicholas, P. Dawson, K. J. Moore, G. Duggan, and C. T. Foxon, Surf. Sci. 228, 62 (1990).
[19]H. P. Zhou and C. M. Sotomayer Torres, Proc. SPIE 1675, 186 (1992).
[20]M. Reico, G. Armelles, J. Melendez, and F. Briones, J. Appl. Phys. 67, 2044 (1990).

NORMALIZATION OF INTERFACE OPTICAL PHONON MODES IN CYLINDRICAL QUANTUM WIRES WITH SEMICONDUCTOR-SEMICONDUCTOR AND METAL-SEMICONDUCTOR BOUNDARY CONDITIONS

Chui-Jih Chiu

Department of Electrical Engineering, Duke University
Durham, NC 27708-0291

and

Michael A. Stroscio

U. S. Army Research Office, P.O. Box 12211
Research Triangle Park, NC 27709-2211

(Received 11 February 1993)

In this work, analytical solutions for the interface longitudinal-optical (LO) phonons in cylindrical polar-semiconductor quantum wires are normalized by the standard quantization condition. Two cases are considered: polar-semiconductor quantum wires encapsulated in another polar-semiconductor and polar-semiconductor quantum wires encapsulated in metal. For the case of metal encapsulation it is demonstrated that unwanted inelastic interface LO phonon scattering is eliminated since the interface modes do not satisfy the appropriate boundary conditions.

1 Introduction

In many embodiments of novel quantum-effect polar-semiconductor structures, charges are transported in quasi-one-dimensional quantum wires [1,2] which must support the transport of charges at high mobilities. It has recently been demonstrated that the LO phonons established at quantum-wire interfaces lead to dramatic enhancements in carrier-phonon interactions and concomitant degradation in carrier mobility [3-6]. It was recently demonstrated [7] that phonon modes may be tailored through the judicious use of metal-semiconductor interfaces in such a way as to dramatically reduce unwanted emission of interface LO phonons and, consequently, to lead to the achievement of high quantum-wire mobility.

Theoretical studies of the interaction between LO phonons and carriers in a polar-semiconductor quantum wire [8] have revealed the presence of discrete LO phonon modes similar to those identified for polar-semiconductor quantum wells [3,9,10,11]. As for the case of quantum wells, interface LO phonons are established at the boundaries of quantum wires [4]. Furthermore, it has been shown that, for carrier energies in excess of the interface LO-phonon energy, the inelastic scattering caused by carrier-interface-phonon interactions dominates over other scattering mechanisms when confinement occurs on a scale for about 40 $\AA$ or less [5].

The technology for the epitaxial growth of metals in intimate contact with polar semiconductors [12,13] provides an impetus for applying the dielectric continuum model of interface-phonon modes to determine the carrier-interface-phonon interaction Hamiltonian near a semi-infinite metal-polar-semiconductor interface [6,7].

0749-6036/93/040401+04 $08.00/0

The validity of using such a continuum approach in describing interface modes is supported by recent detailed microscopic calculations of interface modes in polar semiconductors [14] which indicated that the dielectric continuum model provides an accurate formalism for modelling carrier-interface-phonon interactions.

In this paper, the application of metal-semiconductor boundary conditions to the interface phonon modes in polar-semiconductor quantum wires encapsulated in metal reveals that no interface modes are allowed in such as structure.

2 The case of LO phonon modes in a cylindrical quantum wire

In this section, the polarization eigenvectors and dispersion relations of LO phonon modes in a cylindrical quantum wire are derived in the continuum approximation. A cylindrical quantum wire with dielectric function $\epsilon_1(\omega)$ is assumed to be surrounded by a material with dielectric function $\epsilon_2(\omega)$. Since the system is translationally invariant in the z direction, the potential describing the optical-phonon modes may be taken as

$$\phi(r,\theta,z) = \Phi(r,\theta)exp(ikz), \tag{1}$$

where k_z, the phonon wave vector in the z direction, has been denoted by k; we shall use this notation throughout this paper. In the absence of any free charge, the potential ϕ(r,θ,z) of the phonon modes must satisfy

$$\nabla^2\Phi - k^2\Phi = 0. \tag{2}$$

Given Eq.(1) , the solution for Eq.(2) has two forms. Inside the cylindrical quantum wire. the solution is,

$$\phi_1(r,\theta,z) = AI_\nu(kr)exp(i\nu\theta)exp(ikz). \tag{3}$$

Outside the cylindrical quantum wire, the solution takes the form,

$$\phi_2(r,\theta,z) = BK_\nu(kr)exp(i\nu\theta)exp(ikz), \tag{4}$$

where A and B are constant, and $I_\nu(kr)$ and $K_\nu(kr)$ are modified Bessel functions. The potential ϕ is kept continuous through the space and the normal component of ϵ_nE is kept continuous at the quantum-wire boundaries. The following two conditions have to be satisfied at the boundaries: $\phi_1 = \phi_2$ and $\epsilon_1 E_1 = \epsilon_2 E_2$. From the continuity conditions, A and B satisfy,

$$\frac{A}{B} = \frac{K_\nu(k\rho)}{I_\nu(k\rho)}, \tag{5}$$

and the dispersion relation is,

$$\frac{\epsilon_1}{\epsilon_2} = \frac{I_\nu(k\rho)K'_\nu(k\rho)}{K_\nu(k\rho)I'_\nu(k\rho)}, \tag{6}$$

where ρ is the radius of the cylindrical quantum wire and the prime denotes the derivative with respect to ρ. The microscopic relations [4,10] which govern the equation of ionic motion yield the following expression for the polarization field P(r):

$$\begin{aligned} P(r) &= n_n e_n^* \Theta_n^{-\frac{1}{2}} u(r) \\ &= n_n e_n^* \Theta_n^{-\frac{1}{2}} \sum_k u(r,\theta,k)exp(ikz), \end{aligned} \tag{7}$$

where $u(r)$ is the relative displacement of an ion pair, the subscript n labels the material region, e_n^* is the effective charge of an ion pair, and n_n is the number of ion pairs per unit volume. In addition, $\Theta_n^{-\frac{1}{2}} = 1 + \mu_n a_n(\omega^2 - \omega_{on}^2)/e_n^{*2}$ where μ_n is the reduced mass of the ion pair, a_n is the electronic polarizability per ion pair, and ω_{on} is the frequency associated with the short-range force between ions. To ensure proper quantization of the phonon field [10, 16], each mode must satisfy,

$$\int_0^{2\pi}\int_0^R [(\mu_n n_n L)^{\frac{1}{2}}u]^*[(\mu_n n_n L)^{\frac{1}{2}}u]rdrd\theta = 1, \tag{8}$$

where R extends over all values where the relative displacement has a nonzero value, and L is the length of the cylindrical quantum wire; in this result, u has been normalized by dividing the displacement by $\sqrt{\hbar/2\omega}$. Using the relation

$$\begin{aligned} \frac{\epsilon_0^2\chi_n^2}{n_n^2 e_n^{*2}\Theta_n^{-1}} n_n\mu_n &= \epsilon_0\epsilon_n(\infty)\frac{(\omega_{in}^2 - \omega_{in}^2)}{(\omega^2 - \omega_{in}^2)^2} \\ &= \epsilon_0\frac{1}{2\omega}\frac{\partial\epsilon_n(\omega)}{\partial\omega}, \end{aligned} \tag{9}$$

as in Ref. [16], it evidently follows from Eqs. (3), (4), (7) and (8) that the normalization constant, A, satisfies,

$$\begin{aligned} &\frac{C_1}{2\pi}\int_0^{2\pi}\int_0^\rho A^2[\nabla(I_\nu(kr)exp(i\nu\theta))]^* \\ &\quad\cdot[\nabla(I_\nu(kr)exp(i\nu\theta))]rdrd\theta \\ &+\frac{C_2}{2\pi}\int_0^{2\pi}\int_\rho^R \frac{(AI_\nu(k\rho))^2}{K_\nu^2(k\rho)}[\nabla(K_\nu(kr)exp(i\nu\theta))]^* \\ &\quad\cdot[\nabla(K_\nu(kr)exp(i\nu\theta))]rdrd\theta \\ &= 1, \end{aligned} \tag{10}$$

where the subscripts l and t label the longititudinal-optical (LO) and the transverse-optical (TO) modes, respectively. In these results C_1 and C_2 are defined by $C_1 = 2\pi L\epsilon_0\epsilon_1(\infty)(\omega_{l1}^2 - \omega_{t1}^2)/(\omega^2 - \omega_{t1}^2)^2$ and $C_2 = 2\pi L\epsilon_0\epsilon_2(\infty)(\omega_{l2}^2 - \omega_{t2}^2)/(\omega^2 - \omega_{t2}^2)^2$.

For initial electron energies in the range from 0 to 250 meV, the phonon wavevector, k, varies from $0.01\AA^{-1}$ to $0.15\AA^{-1}$ in GaAs and has typical values of about $0.02\AA^{-1}$. Since the interface phonon potentials fall off roughly as $exp(-kr)$ near heterointerfaces, the transition from weak to strong interface-phonon effects should occur in the neighborhood of $kr = k\rho = 1$. Taking $k = 0.02\AA^{-1}$, the integrals in Eq. (10) have been performed for values of ρ such that $k\rho = 0.5$, 1.0, 2.0 and 3.0. With $\nu = 0$, the integrals in Eq. (10) may be performed numerically and the normalization constant, A, may be written in the form $A = 1/\sqrt{x_1C_1 + x_2C_2}$, where the pair (x_1, x_2) has the values (0.0040723, 0.700749) for $k\rho = 0.5$, (0.737697, 1.45499) for $k\rho = 1.0$, (1.91922, 7.48258) for $k\rho = 2.0$, and (21.0182, 46.5724) for $k\rho = 3.0$. When the radius of wire, ρ, decreases, the constant, A, increases. This implies that interface modes are important when the radius of the cylindrical quantum wire assumes smaller values. This conclusion is in agreement with Ref. [4] where it is demonstrated that the potential of interface phonons with $k = 0.02\AA^{-1}$ begins to dominate over the potential of confined phonons when the lateral dimensions of rectangular quantum wire are less than 50 $\AA^{-1}$.

3 Demonstration that no interface modes exist for quantum wires encapsulated in metal

In this section, the interface LO-phonon is discussed for the semiconductor-metal structure. Recently, it has been argued that the confined and interface LO phonons in mesoscopic devices may be tailored through the judicious use of metal-semiconductor interfaces in such a way as to dramatically reduce unwanted interface LO phonon scattering. It is demonstrated that [7] only those confined and interface modes having odd potentials about the metal-semiconductor interfaces satisfy the boundary conditions at the metal-semiconductor interface.

In an ideal metal, no potential or electric field can exist. When a cylindrical quantum wire with dielectric constant, ϵ_1, is encapsulated in an ideal metal, the potential outside the cylindrical quantum wire is equal to zero, $\phi_2 = 0$. Based on the continuum model, ϕ_1 must go to zero at the boundaries. $\phi_1(\rho, \theta) = AI_\nu(k\rho)exp(i\nu\theta) = 0$ has a solution if $I_\nu(k\rho) = 0$ or if $exp(i\nu\theta) = 0$. $I_\nu(k\rho)$ is equal to zero only if $\nu \neq 0$ and $\rho = 0$. For the real case $k\rho > 0$; thus, $I_\nu(k\rho)$ cannot vanish and it follows that there is no solution for ϕ_1 satisfying the boundary condition. Hence, if $\nu = 0$, no interface modes exist in a quantum wire encapulated in metal. If $\nu \neq 0$ and $I_\nu(k\rho)$ is nonzero, then it is impossible for $\phi_1(\rho, \theta)$ to be zero for all values θ; hence the only physical solution corresponds to $I_\nu(k\rho) = 0$. This is similar to the result of Ref. [7] where it was demonstrated that only the antisymmetric interface phonon modes survive at a metal-semiconductor interface. In the case of a cylinder, however, no interface phonon modes survive.

4 Conclusion

Based on the dielectric continuum model, we have derived the potential of the cylindrical quantum wire. We have presented arguments indicating that inelastic scattering caused by the carrier interface-phonon interactions becomes increasingly important as the cylindrical quantum wire radius is reduced. We have considered the special cases of a GaAs cylinder embedded in AlAs and a GaAs cylinder embedded in metal. We have illustrated why the judicious use of metal-semiconductor interfaces allows the dramatic reduction or elimination of unwanted carrier energy loss caused by carrier interactions with interface LO phonon modes. In the case of a rectangular quantum wire [7,17] the imposition of a metal-semiconductor boundary condition eliminates only a subset of the interface LO phonon modes; however, all of the interface LO phonon modes are eliminated for a polar-semiconductor cylinder embedded in a perfectly conducting metal. The reduction of carrier-interface-phonon interactions may be achieved by embedding polar-semiconductor quantum wires in metal. For metal-semiconductor combinations where the semiconductor is inverted, such as for Al on InAs, this technique provides a way to maintain high mobility transport in wire-like polar-semiconductor nanostructures.

Acknowledgement- This research was supported, in part, by the U.S. Army Research Office. One of us (M. A. S.) thanks Dr. Gerald J. Iafrate, Prof. Ki Wook Kim and Dr. Mitra Dutta for many stimulating conversations.

References

[1] M. Tsuchiya, J. M. Gaines, R. H. Yan, R. J. Simes, P. O. Holtz, L. A. Coldren, and P. M. Petroff, Physical Review Letters 62, 466 (1989).

[2] M. Watt, C. M. Sotomayor Torres, H. E. G. Arnot, and S. P. Beaumont, Semiconductor Science and Technology 5, 285 (1990).

[3] K. W. Kim and M. A. Stroscio, Journal of Applied Physics 68, 6289 (1990).
[4] K. W. Kim, M. A. Stroscio, A. Bhatt, R. Mickevicius, and V. V. Mitin, Journal of Applied Physics 70, 319 (1991).
[5] M. A. Stroscio, G. J. Iafrate, K. W. Kim, M. A. Littlejohn, H. Goronkin, and G. N. Maracas, Applied Physics Letters 59, 1093 (1991).
[6] M. A. Stroscio, G. J. Iafrate, K. W. Kim, M. A. Littlejohn, H. L. Grubin, V. V. Mitin, and R. Mickevicius, in *Nanostructures and Mesoscopic Systems*, edited by M. A. Reed and W. P. Kirk (Boston: Academic Press), 379 (1992).
[7] M. A. Stroscio, K. W. Kim, G. J. Iafrate, M. Dutta and H. L. Grubin, Philosophical Magazine Letters 65, 176 (1992).
[8] M. A. Stroscio, Physical Review B 40, 6428 (1989).
[9] J. J. Licari and R. Evrard, Physical Review B 47, 1347 (1977).
[10] N. Mori and T. Ando, Physical Review B 40, 6175 (1989).
[11] K. L. Kliewer and R. Fuchs, Physical Review 150, 573 (1966).
[12] J. P. Harbison, T. Sands, N. Tabatabaie, W. K. Chan, L. T. Florez, and V. G. Keramidas, Applied Physics Letters 53, 1717 (1988).
[13] A. Guivarc'h, J. Caulet, B. Guenais, Y. Ballini, R. Guérin, A. Poudoulec, and A. Regreny, Journal of Crystal Growth 95, 427 (1989).
[14] H. Rücker, E. Molinari, and P. Lugli, Physical Review B 44, 3463 (1991).
[15] K. T. Tsen, D. S. Smith, S.-C. Y. Tsen, N. S. Kumar, and H. Morkoc, Journal of Applied Physics 70, 418 (1991).
[16] L. Wendler, Physica Status Solidi B 129, 513 (1985).
[17] A. R. Bhatt, K. W. Kim, M. A. Stroscio, G. J. Iafrate, M. Dutta, H. L. Grubin, R. Haque, and X. T. Zhu, Journal of Applied Physics 73, in press (1993).

PHYSICAL REVIEW B VOLUME 48, NUMBER 19 15 NOVEMBER 1993-I

Simplified microscopic model for electron–optical-phonon interactions in quantum wells

A. R. Bhatt and K. W. Kim
Department of Electrical and Computer Engineering, North Carolina State University, Raleigh, North Carolina 27695-7911

M. A. Stroscio
U.S. Army Research Office, P.O. Box 12211, Research Triangle Park, North Carolina 27709-2211

J. M. Higman*
Beckman Institute, University of Illinois, Urbana, Illinois 61801

(Received 17 May 1993)

A simplified microscopic model of optical phonons in dimensionally confined structures is formulated and applied to calculate electron–optical-phonon scattering rates in GaAs/AlAs quantum wells. For this simplified model which circumvents performing a complicated *ab initio* calculation of the force constants at the interface, it is demonstrated that the resulting dispersion relation and scattering rates for electron–optical-phonon interactions agree very well with those obtained from detailed *ab initio* studies. It is also shown that for GaAs/AlAs structures, the macroscopic dielectric continuum model provides a good approximation to the scattering rate predicted by the microscopic models.

The electronic and optical properties of semiconductor superlattices (SL's) and quantum wells (QW's) have been investigated extensively. A principal advantage of using such heterostructures results from the ability to tailor the electronic and optical properties of the structures for realizing a potentially vast array of high-performance electronic and optoelectronic devices. To fully understand and utilize the properties of these nanometer-scale heterostructures, it is necessary to develop formalisms for studying confinement effects as well as picosecond and subpicosecond processes. It has been known for many years that the scattering by polar–optical-phonon modes is an important energy-loss mechanism for electrons in a wide variety of III-V semiconductor devices. However, effects of confinement on these phonon modes have been investigated extensively only in the past several years.

In recent years, a number of models has been put forward to explain electron–optical-phonon interactions in reduced dimensional systems. They can be broadly classified in two categories: macroscopic[1–9] and microscopic.[10–12] Macroscopic models ignore the effect of individual layers of atoms but they have the considerable advantage of making the interaction calculation very simple. Among these macroscopic models are the dielectric continuum model[1–5] (slab model, which uses purely electrostatic boundary conditions), hydrodynamic model,[7] hybrid model,[8] and a recent dispersive continuum treatment of Nash.[9] In some parameter regimes, these models are fairly accurate and provide good estimates of energy-loss rates. However, scaling of the electron–optical-phonon interaction with diminishing device length presents a serious challenge to the accurate use of such models. As a result, there has recently been an increasing need for more rigorous analysis and detailed knowledge of electron–optical-phonon interactions in reduced dimensional systems. This has been the main motivation for the emergence of *ab initio* microscopic models.[12] Though such models provide the most accurate analysis of the structure, they have not been used extensively. This can be attributed to the fact that the *ab initio* microscopic analysis involves very arduous and time consuming first-principle calculations of lattice dynamics[13,14] rather than employing adjustable parameters.[15–17]

Precise *ab initio* calculations of force constants at the interface may not be essential for most of the heterostructures except those involving extremely thin layers. It is well known that even a simple linear-chain model with nearest-neighbor force constants can predict the zone-center LO-phonon frequencies in a SL with a reasonable accuracy except in the cases where layers are single monolayer thick. Such an approximate model is based on the assumption that atomic-force constants at heterojunction interfaces are identical to those of the bulk or of uniform pseudomorphic layers. In a qualitative analysis of the effect of varying force constants at the heterojunction interfaces of a strained layer, short-period, GaAs/GaP SL with two monolayers per SL layer, it was also found that frequencies of the confined phonon modes are only weakly dependent on the variations in the interfacial force constants.[18] The variation in interfacial force constants by values as extreme as 10% results in less than about a 2% change in the frequencies of confined phonon modes. It should be noted that as a practical matter, changes in the frequencies of the confined LO-phonon modes will be considerably less than 2%, since in most SL's and QW's the ratio of the number of bonds at the interfaces to the number of bonds one or more monolayers away from the interfaces is less than that for the case where each layer is two monolayers thick.

Based on the results of Ref. 18, as well as on supporting observations from other investigators,[19] we have formulated a simplified microscopic model which facilitates the accurate modeling of confined and interface phonons without *ab initio* calculations of force constants. The valence-shell model developed by Kunc and Nielson for bulk[20] has been extended for the SL/QW structures. In-

0163-1829/93/48(19)/14671(4)/$06.00

terpolation of the force constants at the heterointerfaces and a periodic-boundary condition have been applied as suggested by Yip and Chang.[15] The calculated phonon dispersion and atomic displacements have been used to derive the interaction Hamiltonian and the electron–optical-phonon scattering rates in SL/QW heterostructures. As will be demonstrated below, this simplified model provides an excellent approximation to the fully microscopic model. As a specific example in this study, we consider GaAs/AlAs SL/QW structures grown in the (001) direction.

The dispersion relation can be obtained from the dynamical matrix constructed using our modified shell model. Three types of interactions are included: the core-to-core (Φ^R) potential, the shell-to-core (Φ^T) potential, and the shell-to-shell (Φ^S) potential. The corresponding dynamical matrices are[20]

$$R_{\alpha\beta}(j,j',\mathbf{q})=\sum_{l-l'}\Phi^R_{\alpha\beta}(l-l',j,j')e^{i\mathbf{q}\cdot[\mathbf{z}(l,j)-\mathbf{z}(l',j')]}, \quad (1)$$

$$S_{\alpha\beta}(j,j',\mathbf{q})=\sum_{l-l'}\Phi^S_{\alpha\beta}(l-l',j,j')e^{i\mathbf{q}\cdot[\mathbf{z}(l,j)-\mathbf{z}(l',j')]}, \quad (2)$$

$$T_{\alpha\beta}(j,j',\mathbf{q})=\sum_{l-l'}\Phi^T_{\alpha\beta}(l-l',j,j')e^{i\mathbf{q}\cdot[\mathbf{z}(l,j)-\mathbf{z}(l',j')]}, \quad (3)$$

where j (j') denotes the atom in the cell and its type, l (l') represents the unit cell, $\mathbf{z}(l,j)$ [$\mathbf{z}(l',j')$] is the position of the jth (j'th) atom in the lth (l'th) cell, and α,β denote the direction. Along with these matrices, we also need to use "effective" shell-shell interactions as,[20]

$$\Delta_{\alpha\beta}(j,j',\mathbf{q})=S_{\alpha\beta}(j,j',\mathbf{q})+\delta_{\alpha\beta}\delta_{jj'}[K_j+T_{\alpha\alpha}(j,j,0)-S_{\alpha\alpha}(j,j,0)], \quad (4)$$

where K_j represents the internal core-shell spring. The equation of motion can be found using the following matrix equations:[20]

$$\omega^2 M\mathbf{u}=(R-ZBZ)\mathbf{u}+(T-ZBY)\mathbf{w}, \quad (5)$$

and

$$0=(T^+-YBZ)\mathbf{u}+(\Delta-YBY)\mathbf{w}, \quad (6)$$

where M, Z, Y, and B are matrices of masses, ionic charges, shell charges, and the real part of Coulomb interaction, respectively, as specified in Ref. 20. Here $\mathbf{u}$ and $\mathbf{w}$ stand for the amplitudes $\mathbf{u}(\mathbf{q})$ and $\mathbf{w}(\mathbf{q})$ of the core and relative-shell displacement, respectively, which may given as

$$u^\nu_\alpha(lj)=u^\nu_\alpha(j,\mathbf{q})\exp[-i\omega_\nu(\mathbf{q})t+i\mathbf{q}\cdot\mathbf{z}(lj)], \quad (7)$$

and

$$w^\nu_\alpha(lj)=w^\nu_\alpha(j,\mathbf{q})\exp[-i\omega_\nu(\mathbf{q})t+i\mathbf{q}\cdot\mathbf{z}(lj)], \quad (8)$$

where ν represents the phonon mode index. From Eqs. (5) and (6), it is clear that the eigenvalue problem reduces to

$$[C(\mathbf{q})-\omega^2 I]\mathbf{e}=0, \quad (9)$$

with

$$C(q)=M^{-1/2}[(R-ZBZ)-(T-ZBY)\times(\Delta-YBY)^{-1}\times(T^+-YBZ)]M^{-1/2}. \quad (10)$$

In a bulk zinc-blende structure, this equation results in six eigenvalues, ω_ν, and six eigenvectors, $\mathbf{e}_\nu$, for a given $\mathbf{q}$. The corresponding phonon-dispersion relations and displacements are obtained directly from the expressions given above. The results are essentially the same as those calculated in a simple linear-chain model with nearest-neighbor force constants. The long-range Coulomb interaction turns out to be less important because its force range is effectively reduced and its effect is only to slightly modify the nearest-neighbor and next-nearest-neighbor force constants.[16] The parameters used in this study for three types of interaction [i.e., R, S, and T in Eqs. (1)–(3)] are as listed in Table I; these parameters yield an excellent description of bulk-phonon characteristics for both GaAs and AlAs. All the other required parameters can be found in the literature.[11,15,16,20] Extension of this approach to a SL is rather straightforward. In a SL grown in the (001) direction, the symmetry consideration along the x-y plane is maintained, while the translational period in the z direction needs to be modified. We define a SL unit cell L along the z direction which consists of n unit cells of each material and a SL wave vector $\mathbf{q}_z$. Hence, along z direction all summations need to be performed over all unit cells of the SL cell. Interactions up to the second nearest neighbors are taken into account. As mentioned before, the bulk parameters are used in each layer except at the heterointerfaces where the interpolated force constants are adopted. The resulting dynamical matrices provide all of the SL eigenfrequencies and eigenvectors for phonon modes.

Figure 1 shows the phonon-dispersion relation for a (001) oriented $(GaAs)_{20}/(AlAs)_{20}$ SL along the in-plane (100) direction and also as a function of angle θ between the direction of wave vector $\mathbf{q}$ and the in-plane direction for vanishingly small q; θ ranges from 0 to $\pi/2$. Two clearly defined GaAs-like and AlAs-like frequency ranges are apparent in Fig. 1. Along with LO and TO modes, it

TABLE I. Converted parameters used in this study for the three types of interaction [i.e., R, S, and T in Eqs. (1)–(3)]. A, B, $C1$, $D1$, $E1$, $F1$, $C2$, $D2$, $E2$, and $F2$ are as defined in Ref. 19 and determined by fitting the bulk GaAs and AlAs phonon-dispersion relations.

	Converted parameters					
	GaAs			AlAs		
	R	S	T	R	S	T
A	−19.67	−24.92	−19.67	−20.13	−23.87	−20.13
B	−4.44	3.31	−0.847	−4.31	3.39	−0.892
$C1$	0.817	1.034	0.817	0.799	1.011	0.799
$D1$	−0.736	0.933	−0.736	−0.801	0.933	0.801
$E1$	−0.550	−0.697	−0.550	−0.610	−0.701	−0.610
$F1$	1.942	2.461	1.942	2.42	3.643	2.42
$C2$	0.817	1.034	0.817	−0.799	1.011	0.799
$D2$	0.736	−0.933	−0.736	0.801	−0.933	−0.801
$E2$	0.550	−0.697	−0.550	0.610	−0.701	−0.610
$F2$	1.942	2.461	1.942	2.42	3.643	2.42

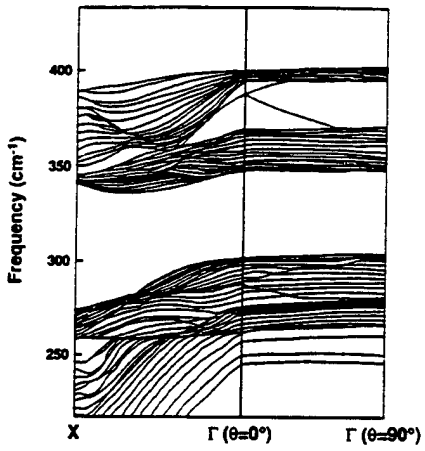

FIG. 1. Phonon dispersion of a (001)-oriented $(GaAs)_{20}/(AlAS)_{20}$ SL along the in-plane direction and as a function of angle θ between the direction of wave vector q and the in-plane direction for vanishing small q.

should be noted that the two "AlAs-like" principal modes and two "GaAs-like" principal modes take the limit of the well known "interface modes" of the dielectric continuum model over a portion of the domain of Fig. 1. Another feature of interest is the anticrossing of the modes in the right-hand panel (i.e., angular dependence).[15] (Similar anticrossing characteristics of the modes have been observed in Refs. 8 and 9 as well.) Compared to the results from the *ab initio* approach,[12] it is clear that our simple microscopic model can describe detailed characteristics of phonon dynamics accurately at the current dimension. As the layer thickness decreases, however, the accuracy of our model may suffer due to the assumptions made for the interface force constants. As an indication for validity of our model, the LO-phonon frequencies have been calculated for the $(GaAs)_m/(AlAs)_n$ SL's with $m=n$ ranging from 1 to 4. In this comparison, our results match well with the observed LO-phonon frequencies[21] for $m=n\geq 2$ (within 3 cm^{-1}). For the monolayer case, the agreement between the experimental data and our microscopic model is not as good, but it is considerably better than those calculated by using the simple linear-chain model.[21] To study this case accurately, one will have to employ first-principle calculations using *ab initio* calculations at the heterostructure interface. Nevertheless, our model should provide excellent results for the great majority of device applications since layer thicknesses generally exceed one monolayer.

The Hamiltonian for the polar electron–optical-phonon interaction in a single QW can be found from the potential given as[12]

$$\phi(z)=\sum_{n,\nu,q_\parallel} U^\nu e_n^* \left[\frac{iq_\parallel u_{nz}^\nu(q_\parallel)}{|q_\parallel|}-u_{nz}^\nu(q_\parallel)\mathrm{sgn}(z-z_n)\right] \times e^{-(q_\parallel|z-z_n|)} \tag{11}$$

with

$$U^\nu=\frac{1}{2\Omega_\parallel\epsilon_\infty}\left[\frac{\hbar}{2N_0\omega_\nu(q_\parallel)}\right]^{1/2}, \tag{12}$$

where e_n^* is effective charge ($2.07|e|$ for GaAs and $2.17|e|$ for AlAs), n ranges all the N_0 lattice points in the normalization volume, and $\Omega_\parallel$ is the area of two-dimensional unit cell. Based on the Fermi golden rule, the scattering rate for the electron–optical-phonon interaction can be obtained as

$$\Gamma(i,j)=(2\pi/\hbar)|\langle f|H|i\rangle|^2\delta(E_f-E_i)\,, \tag{13}$$

where i and f denote the initial and final states of the crystal, respectively, and H is the interaction Hamiltonian given by $-e\phi$, where e is the electron charge and ϕ is the electrostatic potential associated with the lattice vibration as given above. Accordingly,

$$\Gamma_{ij}(k_\parallel)=\frac{2\pi e^2}{\hbar}\sum_{k'_\parallel,\nu}|G_{ij}(q_\parallel,\nu)|^2(N+\tfrac{1}{2}\pm\tfrac{1}{2}) \times\delta\left[\frac{\hbar^2k_\parallel^2}{2m^*}-\frac{\hbar^2k'^2_\parallel}{2m^*}\mp\hbar\omega^*\right], \tag{14}$$

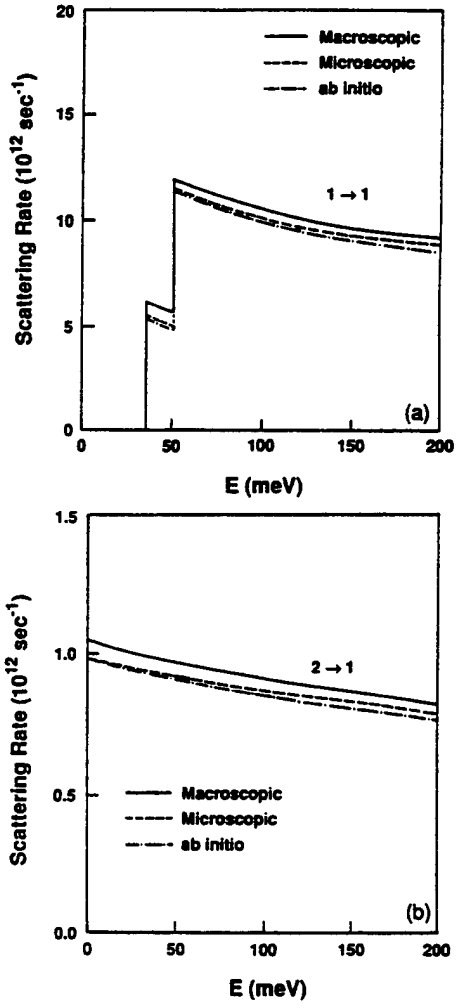

FIG. 2. Scattering rates by electron–optical-phonon interaction as a function of electron energy in a GaAs/AlAs single QW structure with a 20-monolayer GaAs well at 300 K. The results in (a) present the intrasubband transition rates of the lowest subband (1→1), while the data in (b) show the intersubband transition rates from the second lowest to the lowest subband (2→1).

where $\hbar\omega^* = \hbar\omega_\nu(q_\parallel) \pm (E_j - E_i)$ and $k_\parallel = k'_\parallel \pm q_\parallel$. Also, the form factor G_{ij} is given by

$$G_{ij}(q_\parallel, \nu) = \int \zeta_i^*(z)\zeta_j(z)\phi(z)dz \ , \tag{15}$$

where ζ_i and ζ_j are the electronic envelope functions for subbands i and j, respectively. ϕ is the potential associated with the quantized phonon modes. For intrasubband ($i=j$) scattering, G_{ij} is nonzero only for phonons with symmetric potentials and modes of opposite parity do not contribute. For the intersubband scattering, G_{ij} is nonzero for only the modes having opposite parity.

Figure 2 shows the calculation of the scattering rates for the polar electron–optical-phonon interaction based on our method. A GaAs/AlAs single QW structure with a 20-monolayer GaAs well is considered for the $1 \rightarrow 1$ (intrasubband) and $2 \rightarrow 1$ (intersubband) transitions by phonon emission at 300 K. Electronic envelope functions are obtained from the solutions of the Schrödinger equation within the effective-mass approximation. For purposes of comparison, Fig. 2 also depicts the corresponding rates as obtained using the *ab initio* calculation[12] and the dielectric continuum model. It is observed in our calculation that for intrasubband scattering, the lowest-order and highest frequency, ω_{LO1}, confined mode is the most dominant mode and will dominate over all higher-order modes; similarly, for the case of intersubband scattering, ω_{LO2} is the mode which provides the maximum contribution to the scattering strength. Interface modes also provide sizable contributions. These observations and the scattering rates by our microscopic model are in excellent agreement with the results from the *ab initio* calculation. It is also evident from the figure that the dielectric continuum model overestimates the scattering rate only slightly in this structure (i.e., 20-monolayer QW), as compared to our model.

In Fig. 3 we have studied the $1 \rightarrow 1$ and $2 \rightarrow 1$ scattering rates for different QW widths. The general trend in both intrasubband and intersubband scattering is an increase in the scattering rate with diminishing well width d; however, the rate of increase for the intrasubband scattering case is much higher than that for the intersubband case. The intersubband scattering rate increases by only 10% for the whole range of well widths. Surprisingly, the

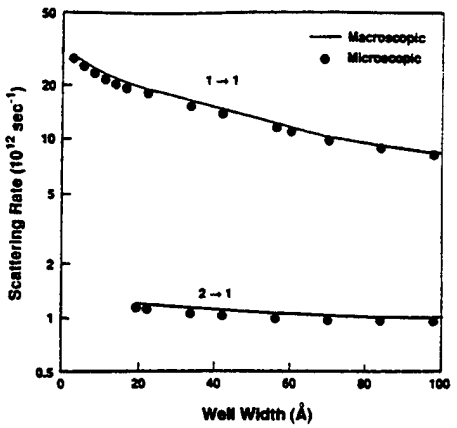

FIG. 3. $1 \rightarrow 1$ and $2 \rightarrow 1$ scattering rates as a function of QW width at 300 K. The electron energy is fixed at 50 meV.

macroscopic approach shows an excellent agreement with the microscopic treatment for well widths as small as 25 Å. As the width of the well is reduced further beyond the range of validity of continuum approximations, the agreement suffers slightly, but still it is well within the acceptable range. We have plotted the intersubband scattering rate for well widths as small as 19 Å. For smaller well widths, the well has only one bound state. There will be a quasibound state outside the well which will contribute to the scattering rate. Though not explicitly shown, the intersubband scattering rate will drop off when the well width becomes smaller than required to maintain at least two bound states. As shown in Ref. 8, the intrasubband and intersubband scattering rates calculated using the hybrid model are also close to those predicted by the dielectric continuum model. Hence we expect that the scattering rate calculations from our microscopic model should form a good agreement with the corresponding results obtained using the hybrid model.

The authors gratefully acknowledge helpful discussions with Dr. G. J. Iafrate and Professor M. A. Littlejohn. This work was supported, in part, by the Office of Naval Research and the U.S. Army Research Office.

*Present address: Advanced Products Research and Development Laboratory, Motorola Inc., Austin, TX 78721.

[1]R. Fuchs and K. L. Kliewer, Phys. Rev. **140**, A2076 (1965); K. L. Kliewer and R. Fuchs, *ibid.* **150**, 573 (1966).
[2]J. J. Licari and R. Evrard, Phys. Rev. B **15**, 2254 (1977).
[3]L. Wendler, Phys. Status Solidi B **129**, 513 (1985).
[4]N. Mori and T. Ando, Phys. Rev. B **40**, 6175 (1989).
[5]K. W. Kim and M. A. Stroscio, J. Appl. Phys. **68**, 6289 (1990).
[6]S. Rudin and T. L. Reinecke, Phys. Rev. B **41**, 7713 (1990).
[7]B. K. Ridley and M. Babiker, Phys. Rev. B **43**, 9096 (1991).
[8]B. K. Ridley, Phys. Rev. B **47**, 4592 (1993); N. C. Constantinou *et al.*, Solid State Commun. **86**, 191 (1993).
[9]K. J. Nash, Phys. Rev. B **46**, 7723 (1992).
[10]K. Huang and B. Zhu, Phys. Rev. B **38**, 377 (1988).
[11]Takuma Tsuchiya, Ph.D. thesis, University of Tokyo, 1990.
[12]E. Molinari *et al.*, Semicond. Sci. Technol. **7**, B67 (1992); H. Rücker *et al.*, Phys. Rev. B **45**, 6747 (1992).
[13]K. Kunc and R. M. Martin, Phys. Rev. Lett **48**, 406 (1982).
[14]S. Baroni *et al.*, Phys. Rev. B **41**, 3870 (1990).
[15]S. K. Yip and Y. C. Chang, Phys. Rev. B **30**, 7037 (1984).
[16]S.-F. Ren *et al.*, Phys. Rev. Lett. **59**, 1841 (1987).
[17]E. Richter and D. Strauch, Solid State Commun. **64**, 867 (1987).
[18]M. A. Stroscio *et al.*, Superlatt. Microstruct. **7**, 115 (1990).
[19]E. Molinari (private communication).
[20]K. Kunc and O. H. Nielson, Comp. Phys. Commun. **17**, 413 (1979): **16**, 181 (1979).
[21]M. Nakayama *et al.*, Solid State Commun. **53**, 493 (1985).

BOTTLENECK EFFECTS DUE TO CONFINED PHONONS IN QUANTUM DOTS

R. M. de la Cruz * and S. W. Teitsworth
Department of Physics, Duke University, Box 90305, Durham, NC 27708-0305, USA

M. A. Stroscio
U.S. Army Research Office, P.O. Box 12211,
Research Triangle Park, NC 27709, USA

(Received 12 July 1993)

A generalization of the three-dimensional Fröhlich hamiltonian for a polar semiconductor is presented which describes the interaction between charge carriers of a zero-dimensional electron gas and longitudinal optical (LO) phonon modes confined in three spatial dimensions. This hamiltonian is used to calculate the scattering rate of electrons by LO phonons in a GaAs quantum box which is free-standing in vacuum. The suppression of scattering through a phonon bottleneck effect is discussed in terms of the selection rules.

1. Introduction

The progress in epitaxial growth and microfabrication techniques in recent years has motivated studies of low dimensional semiconductor structures such as quantum wells, wires and dots.[1-12] As a result of their possible application in microelectronic devices, these structures have been the subject of extensive theoretical and experimental research. An important aspect to take into account is the role of electron-phonon interactions in transport phenomena. In polar semiconductors such as GaAs, the interaction of electrons with longitudinal optical (LO) phonons is a primary energy loss and scattering mechanism which dominates the carrier mobility. To optimize electrical transport properties of devices one generally wants to enhance carrier mobility. Accordingly, several researchers have suggested designs of low dimensional structures which lead to suppression of optical phonon as well as other types (e.g., ionized impurities) of scattering.[6, 13, 14] On the other hand, in proposed quantum wire and quantum dot lasers it is actually desirable to *increase* the effectiveness of optical phonon scattering in order to increase relaxation of electrons to the ground state and improve photoluminescence efficiency.[15]

Studies of electron-LO phonon interactions have been carried out in single and double heterostructures[16] as well as in quantum well, wire and dot structures.[1-5,12] Bockelmann and Bastard[17] have calculated LO and LA phonon scattering in these three types of structures including effects of quantum confinement of electrons as well as broadening in the zero-, one-, or two-dimensional density-of-states. Other researchers have begun to address the effects of dimensional confinement on the phonon modes and the resultant electron-phonon hamiltonian. Shigekawa et al.[18] have pointed out a noticeable difference between the scattering probability of confined and bulk-like modes on electron transport in semiconductor superlattices. Similar results have been found in quantum wires.[19] However, to our knowledge, the effect of longitudinal phonon confinement in quantum dots has not been reported previously.

In this paper, we present a calculation of the zero-dimensional electron-LO phonon scattering rate in a GaAs quantum box which is free-standing in vacuum taking into account the confinement of the carriers as well as the confinement of LO phonons treated within a dielectric continuum framework.[16] The mathematical procedure used to derive the zero-dimensional Fröhlich hamiltonian is based on a treatment used for the quantum wire problem reported previously.[19] In Sec. 2 the expression for the generalized Fröhlich hamiltonian is obtained. In Sec. 3 it is used to calculate the scattering rate of carriers in a zero-dimensional electron gas by confined LO phonons. Discussion of the results is contained in Sec. 4.

2. Frölich Hamiltonian for LO Phonons Confined in a Quantum Box

To obtain the Fröhlich hamiltonian describing the interaction between the confined LO phonons and electrons of a zero-dimensional electron gas, the three-dimensional Fröhlich hamiltonian for scattering in a bulk semiconductor is subjected to the boundary conditions requiring that the LO phonon electrostatic potential vanishes at the heterostructure interfaces.[16] The three-dimensional Fröhlich hamiltonian, $H_{Fr}^{(3D)}$, can be written as

*Permanent address: Dpto. de Física de Materiales, Facultad de C.C. Físicas, U.C.M., 28040 Madrid (Spain).

0749-6036/93/040481 + 06 $08.00/0

$$H_{Fr}^{(3D)} = \sum_{k} \frac{1}{k} \frac{\alpha}{\sqrt{V}} e^{-i\,k.r} \left(a(k) + a^{\dagger}(-k) \right) \tag{2.1}$$

where $a(k)$ and $a^{\dagger}(k)$ are, respectively, the annihilation and creation operators for bulk LO phonons, k is the three-dimensional phonon wave vector, V is the volume of the crystal and α is the Fröhlich coupling constant defined as

$$\alpha = \left[2\pi e^2 \hbar\omega_{LO} \left(\frac{1}{\varepsilon_{\infty}} - \frac{1}{\varepsilon_o} \right) \right]^{1/2} . \tag{2.2}$$

In the above equation, $\hbar\omega_{LO}$ is the LO phonon energy and ε_{∞}, ε_o are, respectively, the high frequency and low frequency dielectric constants. Writing the sum over k in Eq. (2.1) as a sum over the positive values of k_x, k_y and k_z, expanding all the exponentials $e^{\pm ik_x x}$, $e^{\pm ik_y y}$ and $e^{\pm ik_z z}$ and taking $k_x = \pm m\pi/L$, $k_y = \pm n\pi/L$ and $k_z = \pm p\pi/L$ to ensure that the electrostatic potentials associated with the confined modes vanish at $x = \pm L/2$, $y = \pm L/2$ and $z = \pm L/2$, where L is the size of the quantum box, results in

where the factor B(m, n, p) is given by

$$B(m, n, p) = \left\{ \left(\frac{m\pi}{L} \right)^2 + \left(\frac{n\pi}{L} \right)^2 + \left(\frac{p\pi}{L} \right)^2 \right\}^{1/2} \tag{2.3b}$$

and the phonon annihilation operators for the zero-dimensional confined modes are defined as

$$A_{++}(k)_{\pm} = \frac{1}{\sqrt{2}} \left(A_{+}(k_x)_{\pm} + A_{+}(-k_x)_{\pm} \right) \tag{2.4a}$$

$$A_{+-}(k)_{\pm} = \frac{-i}{\sqrt{2}} \left(A_{+}(k_x)_{\pm} - A_{+}(-k_x)_{\pm} \right) \tag{2.4b}$$

$$A_{-+}(k)_{\pm} = \frac{1}{\sqrt{2}} \left(A_{-}(k_x)_{\pm} + A_{-}(-k_x)_{\pm} \right) \tag{2.4c}$$

$$\begin{aligned}
H_{Fr}^{(0D)} = 2\sqrt{2}\,\frac{\alpha}{\sqrt{V}} \Bigg[& \sum_{m=1,3..} \sum_{n=1,3..} \sum_{p=1,3..} \frac{\cos\left(\frac{m\pi x}{L}\right) \cos\left(\frac{n\pi y}{L}\right) \cos\left(\frac{p\pi z}{L}\right)}{B(m, n, p)} \left(A_{++}(k)_{+} + A^{\dagger}_{++}(-k)_{+} \right) \\
& + \sum_{m=2,4..} \sum_{n=1,3..} \sum_{p=1,3..} \frac{\sin\left(\frac{m\pi x}{L}\right) \cos\left(\frac{n\pi y}{L}\right) \cos\left(\frac{p\pi z}{L}\right)}{B(m, n, p)} \left(A_{+-}(k)_{+} + A^{\dagger}_{+-}(-k)_{+} \right) \\
& + \sum_{m=1,3..} \sum_{n=2,4..} \sum_{p=1,3..} \frac{\cos\left(\frac{m\pi x}{L}\right) \sin\left(\frac{n\pi y}{L}\right) \cos\left(\frac{p\pi z}{L}\right)}{B(m, n, p)} \left(A_{-+}(k)_{+} + A^{\dagger}_{-+}(-k)_{+} \right) \\
& + \sum_{m=2,4..} \sum_{n=2,4..} \sum_{p=1,3..} \frac{\sin\left(\frac{m\pi x}{L}\right) \sin\left(\frac{n\pi y}{L}\right) \cos\left(\frac{p\pi z}{L}\right)}{B(m, n, p)} \left(A_{--}(k)_{+} + A^{\dagger}_{--}(-k)_{+} \right) \\
& + \sum_{m=1,3..} \sum_{n=1,3..} \sum_{p=2,4..} \frac{\cos\left(\frac{m\pi x}{L}\right) \cos\left(\frac{n\pi y}{L}\right) \sin\left(\frac{p\pi z}{L}\right)}{B(m, n, p)} \left(A_{++}(k)_{-} + A^{\dagger}_{++}(-k)_{-} \right) \\
& + \sum_{m=2,4..} \sum_{n=1,3..} \sum_{p=2,4..} \frac{\sin\left(\frac{m\pi x}{L}\right) \cos\left(\frac{n\pi y}{L}\right) \sin\left(\frac{p\pi z}{L}\right)}{B(m, n, p)} \left(A_{+-}(k)_{-} + A^{\dagger}_{+-}(-k)_{-} \right) \\
& + \sum_{m=1,3..} \sum_{n=2,4..} \sum_{p=2,4..} \frac{\cos\left(\frac{m\pi x}{L}\right) \sin\left(\frac{n\pi y}{L}\right) \sin\left(\frac{p\pi z}{L}\right)}{B(m, n, p)} \left(A_{-+}(k)_{-} + A^{\dagger}_{-+}(-k)_{-} \right) \\
& + \sum_{m=2,4..} \sum_{n=2,4..} \sum_{p=2,4..} \frac{\sin\left(\frac{m\pi x}{L}\right) \sin\left(\frac{n\pi y}{L}\right) \sin\left(\frac{p\pi z}{L}\right)}{B(m, n, p)} \left(A_{--}(k)_{-} + A^{\dagger}_{--}(-k)_{-} \right) \Bigg]
\end{aligned} \tag{2.3a}$$

$$A_{..}(k)_{\pm} = \frac{-i}{\sqrt{2}}\left(A_{.}(k_x)_{\pm} - A_{.}(-k_x)_{\pm}\right). \tag{2.4d}$$

The operators $A_{\pm}(k_x)_{\pm}$ can be expressed in terms of the original three dimensional phonon annihilation operator a(k) as in Ref. 19,

$$A_{+}(k_x)_{\pm} = \frac{1}{\sqrt{2}}\left[a_{\pm}(k_x, k_y) + a_{\pm}(k_x, -k_y)\right] \tag{2.5a}$$

$$A_{-}(k_x)_{\pm} = \frac{-i}{\sqrt{2}}\left[a_{\pm}(k_x, k_y) - a_{\pm}(k_x, -k_y)\right] \tag{2.5b}$$

where $a_{\pm}(k_x, k_y)$ are given by

$$a_{+}(k_x, k_y) = \frac{1}{\sqrt{2}}\left[a(k_x, k_y, k_z) + a(k_x, k_y, -k_z)\right] \tag{2.6a}$$

$$a_{-}(k_x, k_y) = \frac{-i}{\sqrt{2}}\left[a(k_x, k_y, k_z) - a(k_x, k_y, -k_z)\right]. \tag{2.6b}$$

Taking the hermitian conjugates of Eqs. (2.4)-(2.6) yields analogous expressions for creation operators. The zero-dimensional Fröhlich hamiltonian of Eq. (2.3a) describes the interaction of an electron and the LO phonon modes characterized by standing waves in the three directions x, y and z. Within a microscopic approach, the electrostatic potentials associated with the confined modes are nearly zero at the heterostructure interfaces.[20, 21] Therefore, the approximation used here that electrostatic potentials vanish at the box boundaries $x = \pm L/2$, $y = \pm L/2$ and $z = \pm L/2$ is reasonable.

3. Electron-Confined Phonon Scattering Rates in a GaAs Quantum Box

In the present calculation, it will be assumed that the quantum box forms an infinitely deep potential well, so that the wave function for electrons will be a product of cosine and sine functions. For the case of equal parity in the x, y and z directions, the electronic wave function is only a product of cosine (sine) functions for odd (even) parity; i.e.,

$$|ijl\rangle = \left(\frac{2}{L}\right)^{3/2}\cos\left(\frac{i\pi x}{L}\right)\cos\left(\frac{j\pi y}{L}\right)\cos\left(\frac{l\pi z}{L}\right) \quad \text{for } i, j, l = 1, 3, 5.. \tag{3.1a}$$

and

$$|ijl\rangle = \left(\frac{2}{L}\right)^{3/2}\sin\left(\frac{i\pi x}{L}\right)\sin\left(\frac{j\pi y}{L}\right)\sin\left(\frac{l\pi z}{L}\right) \quad \text{for } i, j, l = 2, 4, 6.. \tag{3.1b}$$

where the factor $(2/L)^{3/2}$ is a normalization constant, L is the size of the quantum box, and $-L/2 \le x, y, z \le +L/2$. The corresponding electron energies for the different states are

$$E(i, j, l) = \frac{\hbar^2}{2m^*}\left\{\left(\frac{i\pi}{L}\right)^2 + \left(\frac{j\pi}{L}\right)^2 + \left(\frac{l\pi}{L}\right)^2\right\}. \tag{3.2}$$

The assumption of an infinitely deep potential well leads to simple scattering matrix elements. A more realistic treatment would employ finite confining potentials; however, this requires the use of extensive numerical evaluation and we have found that including this effect leads to relatively small corrections in the energies (see Sec. IV).

Using the Fermi-Golden rule, the probability of making a transition from initial electronic state |ijl> with energy E(i, j, l) to final electronic state |i'j'l'> with energy E(i', j', l') is

$$W\begin{Bmatrix} e \\ a \end{Bmatrix} = \frac{2\pi}{\hbar}\left|M\begin{Bmatrix} e \\ a \end{Bmatrix}\right|^2 \delta\left(E(i', j', l') - E(i, j, l) \pm \hbar\omega_{LO}\right) \tag{3.3a}$$

where the upper sign denotes phonon emission, the lower sign denotes absorption and the matrix element is given by

$$M\begin{Bmatrix} e \\ a \end{Bmatrix} = \left\langle i', j', l'; N_k + \frac{1}{2} \pm \frac{1}{2}\left|H_{Fr}^{(0D)}\right|i, j, l; N_k + \frac{1}{2} \pm \frac{1}{2}\right\rangle. \tag{3.3b}$$

The phonon occupation number is taken as $N_k + 1$ for emission and as N_k for absorption. As a consequence of the conservation of energy in the scattering process, at least one of the integers of the final electronic state (i', j', l') is smaller (larger) than any of the integers of the initial state (i, j, l) for the process of emission (absorption) of a phonon. Inserting the expressions for $H_{Fr}^{(0D)}$ and the electronic wave functions into Eq. (3.3b) and taking into account the orthogonality of the cosine and sine functions, it is evident that the matrix elements are nonzero only when the initial and final electronic states have the same parity in the x, y and z directions; i.e., only transitions with equal parity between the integers (i, i'), (j, j') and (l, l') are allowed. Rewriting the Eq. (3.3b) for the case in which all integers are odd, we obtain

$$W\begin{Bmatrix} e \\ a \end{Bmatrix} = \frac{2\pi}{\hbar}\frac{8\alpha}{V}^2\left[\sum_{m=1,3..}\sum_{n=1,3..}\sum_{p=1,3..}\frac{P(m, n, p)}{B(m, n, p)}\right]^2 \times\left(N_k + \frac{1}{2} \pm \frac{1}{2}\right)\delta\left(E(i', j', l') - E(i, j, l) \pm \hbar\omega_{LO}\right) \tag{3.4a}$$

where P(m, n, p) is the overlap integral

$$P(m, n, p) = \int_{-L/2}^{L/2} dx \left(\frac{2}{L}\right)\cos\left(\frac{i'\pi x}{L}\right)\cos\left(\frac{m\pi x}{L}\right)\cos\left(\frac{i\pi x}{L}\right)$$

$$\times \int_{-L/2}^{L/2} dy \left(\frac{2}{L}\right) \cos\left(\frac{j'\pi y}{L}\right) \cos\left(\frac{n\pi y}{L}\right) \cos\left(\frac{j\pi y}{L}\right)$$

$$\times \int_{-L/2}^{L/2} dz \left(\frac{2}{L}\right) \cos\left(\frac{l'\pi z}{L}\right) \cos\left(\frac{p\pi z}{L}\right) \cos\left(\frac{l\pi z}{L}\right) \qquad (3.4b)$$

in which the dependence on initial and final electronic states has been suppressed. Similar expressions can be obtained for even integers by replacing the cosine functions by sine functions in Eq. (3.4b) and by expanding the sum with suitable integers in Eq. (3.4a). For a given transition |ijl> ⟶ |i'j'l'>, the phonon modes which give the dominant contribution to the overlap integral are m = i, i', i±2, i'±2; n = j, j', j±2, j'±2 and p = l, l', l±2, l'±2; any other modes yield contributions that tend rapidly to zero with a power law. Therefore, they have not been taken into account in the evaluation of P(m, n, p).

Conservation of energy as imposed by the delta function in Eq. (3.4a), requires that E(i', j', l') - E(i, j, l) ± $\hbar\omega_{LO}$ = 0; i.e.,

$$\left(i'^2 - i^2\right) + \left(j'^2 - j^2\right) + \left(l'^2 - l^2\right) \pm \frac{2m^*L^2}{\hbar\pi^2}\omega_{LO} = 0. \qquad (3.5)$$

This condition implies that each transition |ijl> ⟶ |i'j'l'> is characterized by a specific value of L, the size of the box. Transforming the argument of the delta function as in Eq. (3.5), the scattering rate results in

$$W\begin{Bmatrix} e \\ a \end{Bmatrix} = \frac{32m^*\alpha}{\hbar^3}\left[\frac{\hbar}{2m^*\omega_{LO}}\left\{\left|i'^2-i^2\right| + \left|j'^2-j^2\right| + \left|l'^2-l^2\right|\right\}_f\right]^{1/2}$$

$$\times A^2\left(N_k + \frac{1}{2} \pm \frac{1}{2}\right) \qquad (3.6)$$

where A is a constant arising from the sum. In Table I, the scattering rates for several interband transitions to (from) the bottom band with emission (absorption) of LO phonons in a GaAs quantum box which is free-standing in vacuum is shown with the specific value of L that characterizes each transition. The values of the constants m^*, ω_{LO} and α to calculate W are taken from Ref. 22 and the lattice temperature is assumed to be 300 K.

TABLE I

Emission			Absorption	
		L(Å)		
Transition	W ($\times 10^{13}$ s^{-1})		Transition	W($\times 10^{12}$ s^{-1})
{ |311>} ⟶ |111>	2.51	352	|111> ⟶ { |311>}	5.77
{ |331>} ⟶ |111>	1.71	498	|111> ⟶ { |331>}	3.93
|333> ⟶ |111>	1.02	610	|111> ⟶ |333>	2.33
{ |135>} ⟶ |111>	1.20	704	|111> ⟶ { |135>}	2.76
{ |511>} ⟶ |111>	1.69	610	|111> ⟶ { |511>}	3.88
{ |533>} ⟶ |111>	0.81	787	|111> ⟶ { |533>}	1.86
{ |551>} ⟶ |111>	0.91	863	|111> ⟶ { |551>}	2.09
|555> ⟶ |111>	0.86	1056	|111> ⟶ |555>	1.56

Table 1.- Scattering rates for several interband transitions involving emission (absorption) of LO phonons in a GaAs quantum box. The scattering rate for each transition is calculated for different values of box size L. The expression { |ijl> } refers to all distinct states which correspond to permutations of the quantum numbers i, j and l; for example, { |311> } refers to |311>, |131> and |113>.

4. Discussion

From the above results, two interesting features are predicted in the case where the confining potential for electrons is approximated as being infinitely deep. Firstly, the intraband transitions are forbidden for a box of cubic geometry ($L_x = L_y = L_z = L$) since the initial and final electronic states have the same energy and no emission (absorption) of LO phonons can occur. This process involves the excess (loss) of an amount of energy equal to the energy of the phonon, $\hbar\omega_{LO}$. Conversely for a hexahedral box ($L_x \neq L_y \neq L_z$), the intraband transitions are allowed only if a special condition among L_x, L_y and L_z is imposed by the conservation of energy. This feature has not appeared in quantum wells and wires, where the intrasubband transitions are allowed independent of the lengths of the sides in the confining dimensions. [1,4,5]

Secondly, the interband transitions for a quantum box of cubic geometry (the case studied here) are characterized by a particular value of L; i.e., a given transition is only allowed for those cubic box dimensions satisfying Eq. (3.5); for other box sizes, the transition is forbidden. However, sets of transitions from (to) electronic states of the same band to (from) electronic states of the bottom band are characterized for the same values of L and W as shown in Table 1. These striking features are a consequence of the near energy monochromaticity of the LO phonons and the discrete spacing of the electronic energy levels. This so-called "phonon bottleneck" effect has been used previously to explain the low energy relaxation rate of excited states in a quantum box through phonon emission. It has been pointed out that small variations of the lateral confinement dimensions reduce significantly the relaxation rate.[8] The suppression of scattering by LO phonons due to the above selection rules would limit the photoluminescence efficiency in proposed quantum dot lasers. Recently, multiphonon processes involving LO and LA phonon scattering have been invoked as a possibility to increase the effectiveness of the scattering.[15] We expect that the effects of the confined LO modes derived in this paper could be incorporated into such a multiphonon calculation in a straightforward manner.

On the other hand, for a given transition from (to) the bottom band, the transitions involving upper energy levels are associated with smaller scattering rates and larger box sizes. Comparison between the values in Table 1 and the scattering rates obtained in Ref. 4 for a GaAs quantum wire (extrapolation of the values in Fig. 6) reveals similar strengths for the electron-LO phonon interactions.

Although the results listed in Table 1 should be interpreted as approximate since in this calculation the electronic states are assumed to be confined in three dimensional infinitely deep potential wells, it is expected that the effect of this approach on determining the real energy levels would be small. An estimation of the two first energy levels in a GaAs quantum box with L = 352 Å and embedded in AlAs barriers yields values within 10 % of those obtained for the free-standing case. A value of 0.96 eV corresponding to the conduction-band offset relative to the GaAs band edge[23] was taken for the well potential height in the epitaxial growth direction. Smaller variations will be obtained for boxes with larger dimensions.

Investigations in quantum wells and wires have shown that another important scattering mechanism of electrons is the scattering by interface (IF) phonons.[3-5,16] In quantum wires, it has been pointed out that the scattering rates of IF phonons are comparable in magnitude with those of LO phonons as the dimensions of these structures decrease.[4,5] On the other hand, studies of a GaAs quantum wire have shown the relevant role of the embedding material on the scattering process by IF phonons. Scattering rates are larger when the wire is free-standing in vacuum than when it is embedded in a polar semiconductor (e.g., AlAs).[4] In the light of these results, investigations of a GaAs quantum dot embedded in different materials seem to be crucial for the photoluminescence efficiency problem. Scattering by IF phonons could yield significant contributions along with the multiphonon processes previously reported[15] to enhance the effectiveness of the scattering. Microscopic calculations of IF modes in one-dimensional quantum box arrays indicate very substantial dispersion - which would be expected to reduce size sensitivity of phonon scattering.[21]

Acknowledgements - We thank P. J. Turley for helpful discussions. R.M. de la Cruz would like to acknowledge the financial support by Ministerio de Educación y Ciencia, Spain. S.W. Teitsworth acknowledges support of the National Science Foundation through grant DMR-9157539.

References

1. J. P. Leburton, Journal of Applied Physics **56**, 2850 (1984).
2. G. Fasol, M. Tanaka, H. Sakaki and Y. Horikoshi, Physical Review B **38**, 6056 (1988).
3. P. J. Turley and S.W. Teitsworth, Journal of Applied Physics **72**, 2356 (1992).
4. K.W. Kim, M.A. Stroscio, A. Bhatt, R. Mickevicius and V.V. Mitin, Journal of Applied Physics **70**, 319 (1991).
5. R. Mickevicius, V.V. Mitin, K.W. Kim, M.A. Stroscio and G.J. Iafrate, Journal of Physics: Condensed Matter **4**, 4959 (1992).
6. H. Sakaki, Japanese Journal of Applied Physics **28**, L314 (1989).
7. M.A. Reed, J.N. Randall, R.J. Aggarwal, R.J. Matyi, T.M. Moore and A.E. Wetsel, Physical Review Letters **60**, 535 (1988).
8. H. Benisty, C.M. Sotomayor-Torres and C. Weisbuch, Physical Review B **44**, 10945 (1991).
9. H.-S. Cho and P.R. Prucnal, Physical Review B **39**, 11150 (1989).
10. G.W. Bryant, Physical Review B **39**, 3145 (1989).
11. P.A. Knipp and T.L. Reinecke, Physical Review B **46**, 10310 (1992).
12. M.H. Degani and G.A. Farias, Physical Review B **42**, 11950 (1990).
13. R. Dingle, H.L. Störmer, A.C. Gossard and W. Wiegmann, Applied Physics Letters **33**, 665 (1978).
14. H. Sakaki, Japanese Journal of Applied Physics **19**, L735 (1980).
15. T. Inoshita and H. Sakaki, Physical Review B **46**, 7260 (1992).
16. N. Mori and T. Ando, Physical Review B **40**, 6175 (1989).
17. U. Bockelmann and G. Bastard, Physical Review B **42**, 8947 (1990).
18. N. Shigekawa, T. Mizutani and K. Yokoyama, Journal of Applied Physics **65**, 677 (1989).

19. M.A. Stroscio, Physical Review B 40, 6428 (1989).
20. H. Rücker, E. Molinari and P. Lugli, Physical Review B 44, 3463 (1991).
21. C. Bungaro, P. Lugli, F. Rossi, L. Rota and E. Molinari in "Ultrafast Lasers Probe Phenomena in Semiconductors and Superconductors", edited by R.R. Alfano, Proc. SPIE vol. 1677 (Bellingham, 1992), p. 55.
22. S. Adachi, Journal of Applied Physics 58, R1 (1985).
23. H.C. Casey and M.B. Panish in "Heterostructure Lasers" (Academic, New York, 1978), Pt. A, Chap. 4.

Real-space transfer of photoexcited electrons in type-II superlattices via optical-phonon emission

M. U. Erdoğan, V. Sankaran, and K. W. Kim

Department of Electrical and Computer Engineering
North Carolina State University
Raleigh, North Carolina 27695-7911

M. A. Stroscio and G. J. Iafrate

U.S. Army Research Office
Research Triangle Park, North Carolina 27709-2211

ABSTRACT

The Γ-X scattering rate of electrons in type-II superlattices by optical-phonon emission is calculated. The tight binding method for electronic band structure and the dielectric continuum model for phonons are used. The relative strength of scattering due to different phonon modes is examined for varying superlattice dimensions. The scattering rate is highest when the energy separation between the Γ and X levels is smallest, and decreases quickly as the separation increases. It is found that the strongest scattering rate is due to the emission of AlAs confined modes. Changing of parity with layer thickness and its effect on scattering are discussed.

1. INTRODUCTION

Recently, there has been considerable interest in hot carrier dynamics in heterostructures. One important issue in this area has been the relaxation of photoexcited carriers in heterostructures from higher energy subbands to the lower ones. This process has been studied extensively both experimentally and theoretically because of its fundamental physics and for possible device applications.[1-6] Most of the work up to now has been on type-I heterostructures where the bandgap of one material is entirely nested within the gap of another material. In this structure, electrons and holes are both localized in the same layer. On the other hand, in the so-called type-II superlattices, the holes are localized in one layer, whereas the lowest energy electrons are contained in the other layer.[7] The well studied $Al_xGa_{1-x}As/GaAs$ superlattices can be made type-II by appropriately choosing the layer thicknesses and alloy composition. For example, the GaAs/AlAs superlattices with thick AlAs layers are known to be type-II for GaAs layer thicknesses less than or equal to 35 $\AA$ (12 monolayers).[7] Type-I to type-II transitions can also be achieved by application of external forces such as an electric field or hydrostatic pressure. In the case of type-II structures, the lowest conduction band level is not in the GaAs but in the $Al_xGa_{1-x}As$ layer. In type-I heterostructures, electrons photoexcited from the valence band to the conduction band relax to lower energy levels within the same layer. However, in type-II structures, the electrons excited to a direct-gap energy level (Γ) in one layer then can relax to an indirect-gap energy level (X) in the adjacent layer. This is a very interesting case because electron relaxation happens with real-space transfer. This

0-8194-1441-7/94/$6.00

process, which is normally forbidden, is now possible due to the mixing of Γ and X states by the superlattice potential and relaxation of momentum conservation due to interface disorder (lateral mixing). Several experimental results related to Γ-X transfer are available in the literature.[4-6] In spite of the spatial charge transfer, the relaxation rate can be very high. Experimental evidence has been presented that Γ-X electron transfer occurs by the emission of long-wavelength optical phonons.[6] However, a detailed theoretical analysis for the Γ-X transfer in type-II structures has not yet been given. In this paper, we calculate the Γ-X scattering rate due to optical phonon emission using a realistic band structure model.

2. FORMULATION

It is well known that the electron-phonon interaction in low-dimensional systems is altered strongly due to the confinement of the carriers and the confinement of the phonons. Usually, a single-band, spherical effective-mass is used for the description of the wave functions of confined carriers. It is commonly assumed that each of these confined states is derived from bulk states of a given symmetry (e.g. Γ, X or L) only, and levels derived from different bulk states do not interact with each other. However, in a superlattice, due to broken periodicity in the growth direction (taken as the z-direction in this study), momentum in this direction is not conserved and bulk states of different symmetry can mix, i.e. the confined states are made of more than one bulk state. Due to this mixing of Γ and X states, the electronic band structure is more complicated in type-II superlattices. Therefore, the envelope-function approximation, which works very well in many cases, is not suitable in this case. In type-II superlattices, a model for band structure that can handle the mixing between different valleys is needed. Several such methods have been employed in the literature.[8-12] In this study, an empirical tight-binding method with an sp^3 basis is used for describing the electronic band structure. In the calculation, first and second nearest neighbor interactions are retained. The mixing of the Γ and X valleys is intrinsically included in this model since the complete band-structure is described in the tight-binding method. The parameters used in the tight-binding calculation are taken from Ref. 8. These parameters were optimized to reproduce the highest valence band and lowest conduction band accurately. The parameters across an interface are taken as the average of the values from the two bulk regions. The spin-orbit coupling and camel-back features of the X band are neglected since these will not affect the Γ-X mixing.

In a superlattice, the 6-fold degeneracy of the X valley is removed, with the formation of an X_z doublet having momentum along the growth axis, and an $X_{x,y}$ quadruplet, with momentum in the plane. The $X_{x,y}$ and L minima are not coupled to the Γ valley due to the conservation of lateral momentum. However, momentum in the z-direction is not conserved because of the discontinuities in the superlattice potential. Therefore, only the Γ and X_z valleys are coupled through this potential. Accordingly, out of all the X states, only the X_z states are mixed with the Γ states by the perfect superlattice potential, and, herein, the X-point will be used to mean X_z particularly. The X states in the plane of the interface ($X_{x,y}$) are not coupled to the Γ states by the perfect superlattice potential. However, these X states are mixed with the Γ states by interface disorder.[12] Obviously, this effect will be more important for short period superlattices. Interface disorder effects are not taken into account in this study.

For proper calculation of the electron-phonon scattering rates, the effect of confinement of

phonons should also be taken into account. It is well known that the vibrational modes in low-dimensional structures are different from those in the bulk. Microscopic lattice-dynamical models have been used with great success to model these phonon modes.[13,14] However, using these models in the calculation of electron-phonon interaction requires intensive computation. Therefore, for the description of phonon confinement, the dielectric continuum (slab) model employing electromagnetic boundary conditions is used because of its simplicity and reasonable accuracy.[15–17] This model predicts the existence of LO modes for both layers and several interface modes due to the dielectric discontinuity between the two media. There is no dispersion of confined phonon modes in this model, and the frequency of each mode is taken as identical to its bulk value. In the dielectric continuum model picture, these modes are totally confined within an individual layer, and the phonon potential of one type of layer is identically zero in the adjacent layer. Hence, phonon potentials in each well do not interact with each other, and consequently, confined phonon modes in a superlattice are the same as the ones for a quantum well in this picture.

Figure 1 shows a schematic drawing of the band-edge alignment of a type-II superlattice grown in the z-direction. The thickness and dielectric constant of material I (II) are denoted by d_1 (d_2) and ϵ_1 (ϵ_2), respectively. The Hamiltonian for the electron-confined phonon interaction for the confined modes of material I is given by[15]

$$H_{C_1} = \sum_{\mathbf{q}_{||}} \left(\frac{e^2\hbar\omega_{L_1}}{ANd_1\epsilon_0}\right)^{1/2} \left[\frac{1}{\epsilon_1(\infty)} - \frac{1}{\epsilon_1(0)}\right]^{1/2} e^{i\mathbf{q}_{||}\cdot\rho}(a_{\mathbf{q}_{||}} + a^{\dagger}_{-\mathbf{q}_{||}})$$

$$\times \begin{cases} sin[m\pi(z-nd)/d_1]/\sqrt{q_{||}^2 + (m\pi/d_1)^2}, & nd < z < nd + d_1, \\ 0, & nd + d_1 < z < (n+1)d, \end{cases}$$

$$m = 1, 2, 3, \ldots . \qquad (1)$$

Here, $a^{\dagger}_{-\mathbf{q}_{||}}$ ($a_{\mathbf{q}_{||}}$) is the creation (annihilation) operator, and $\mathbf{q}_{||}$ and ρ stand for the two-dimensional phonon wave vector and position vector in the x-y plane, respectively. Area in the x-y plane is denoted by A, N is the total number of unit cells, and n indexes the unit cells. The confined phonon frequency, ω_{L1} is taken identical to the bulk phonon frequency at zone center. The Hamiltonian for the confined modes of material II is given by a similar expression. The interface phonon modes in a superlattice, on the other hand, are modified due to the periodicity of the structure and the overlapping of potentials.[15,16] In this case, the phonon potential extends over the whole superlattice. The resulting Hamiltonian due to interacting interface modes is very complicated. To simplify the calculations, in this work, we derive the Hamiltonian for interface modes only for the case of q_z=0. The phonon dispersion relations obtained with this condition are as follows:

$$\epsilon_1 tanh\left(\frac{1}{2}q_{||}d_1\right) + \epsilon_2 tanh\left(\frac{1}{2}q_{||}d_2\right) = 0 \qquad (2)$$

for symmetric modes, and

$$\epsilon_1 coth\left(\frac{1}{2}q_{||}d_1\right) + \epsilon_2 coth\left(\frac{1}{2}q_{||}d_2\right) = 0 \qquad (3)$$

for antisymmetric modes. The Hamiltonian for the interface modes (with q_z=0) is,

$$H_{IF} = \sum_{q_{||}} \left(\frac{\hbar e^2}{\epsilon_0 A}\right)^{1/2} \left[\frac{\partial \epsilon_1}{\partial \omega} tanh\left(\frac{1}{2} q_{||} d_1\right) + \frac{\partial \epsilon_2}{\partial \omega} tanh\left(\frac{1}{2} q_{||} d_2\right)\right]^{-1/2} \frac{1}{\sqrt{2q_{||}}} e^{iq_{||}\cdot\rho} (a_{q_{||}} + a^{\dagger}_{-q_{||}})$$

$$\times \begin{cases} cosh[q_{||}(z - (nd + d_1/2))]/cosh(q_{||}d_1/2), & nd < z < nd + d_1, \\ cosh[q_{||}(z - (nd + d_1 + d_2/2))]/cosh(q_{||}d_2/2), & nd + d_1 < z < (n+1)d. \end{cases} \quad (4)$$

The scattering rate due to optical the phonon emission is calculated by using Fermi's Golden Rule. The temperature is taken to be close to 0 K and the phonon occupation number is taken to be very small. The summations within the 2-D Brillouin zone are evaluated numerically.[18] For simplicity, the interface phonon energy is taken as a constant in the energy conservation equation since the dispersion is small. For the calculation of the Hamiltonian, however, phonon frequencies obtained from the above given dispersion relations are used.

3. RESULTS AND DISCUSSION

In this work, a superlattice with M layers of GaAs and N layers of AlAs is studied. The energy levels at the miniband minimum obtained from the tight binding calculation as a function of AlAs layer thickness are shown in Fig. 2. The GaAs layer was kept constant at 8 monolayers. The levels are labeled as Γ and X following the effective mass notation although each level is actually a combination of these two bulk states. Here, the superlattice states are labeled after the dominant one of the two bulk states forming them. As can be seen, the effect of changing the AlAs layer thickness is to make the energy difference, hence, the interaction between the lowest Γ level and the X levels vary. The parity behavior of states needs to be mentioned briefly because of the effect of parity on the overlap. In the superlattice, the electronic wave functions have definite parity only when the electron is at the miniband minimum or miniband maximum. The coefficients of the s (p_z) orbitals have the same (opposite) parity as the level itself.[8] The initial state for the electron is assumed to be the bottom of the miniband, and the following discussion applies for k_z=0. The parity of the Γ_1 state is even, regardless of AlAs layer thickness. The parity of the X levels, on the other hand, depends on the number of AlAs monolayers. The X_i levels (i=1, 2, 3, ...) with odd (even) i have the same (opposite) parity as N. The parity behavior of states is important because the states of opposite parity do not mix for k_z=0. For $k_z \neq 0$, the electron states do not have well defined parity and all states mix. This mixing, however, is much weaker than had their parities been the same.

Scattering rates due to emission of different phonon modes is shown in Fig. 3. The results presented are the sum of contributions by all normal modes for a given type of phonon. In calculating the intersubband scattering rates, the electron is taken to be initially at the bottom of the lowest Γ subband. It then transfers to the lowest X subband by emitting an optical phonon. As is apparent from Figs. 2 and 3, the scattering rate is strongest when the Γ and X levels are closest in energy. Under this condition, the levels interact very strongly with each other and the Γ level has large X character. Therefore, the overlap between the initial and final states is large. This interaction and the resulting large overlap decreases rapidly as the energy separation increases. This is one of the two reasons for strong thickness dependence (other being parity) of the scattering rate as seen in Fig. 3.

As can be seen, for the most part, the AlAs confined modes are strongest, followed by AlAs interface modes. The GaAs modes are weaker, with the GaAs confined modes being the weakest. This is due to the fact that the final state X_1 wave function is strongly confined within the AlAs layers. Consequently, the overlap involving GaAs confined modes is very small. An interesting point to note about Fig. 3 is that the dominant phonon modes alternate between being even and odd. This is because the parity of the X level alternates as the AlAs thickness is changed by one monolayer each time. For even (odd) AlAs layer thickness, parity of the lowest X level is even (odd); hence, the even (odd) phonon modes are strong. The effect of parity can be also be observed at cross-over points where the Γ and X level energies become very close. From Fig. 2, it is seen that the two levels have almost the same energy for N=5, but they do not mix and repel each other. This is because Γ_1 and X_1 have the opposite parity for this thickness. For other thicknesses where the two levels become close, however, they do repel each other because they have the same parity. This is the reason why the scattering rate for N=19 is much stronger than N=20. The energy separation between the Γ_1 and X_4 levels is actually smaller for N=20 than it is for N=19. However, as explained before, the parities are opposite. This results in strong (weak) mixing and scattering rate for the N=19 (N=20) case.

As is evident from Fig. 3 the interface modes become weaker as the AlAs thickness increases. This is similar to the case of type-I superlattices.[3] The results obtained here can be compared with an experiment by de Paula *et al.*,[4] where the Γ to X transition rate via phonon emission was obtained by a time-resolved anti-Stokes measurement. For the case of M=8 and N=14, they found the transfer time to be around 1 ps, which is in agreement with the rate calculated in this study. However, it is very difficult to make an exact comparison due to the nature of the experiment. Another point to note is that it was not possible in their experiment to determine whether intra-subband scattering was also involved. It should also be mentioned that there may be mechanisms other than optical-phonon emission for electron relaxation, e.g. carrier-carrier scattering, non-polar optical-phonon scattering and acoustic phonon scattering. Besides these mechanisms, interface roughness may cause additional scattering as well. In this study, only the transition from Γ_1 to X_1 is considered. Depending on the layer thickness, there may be more than one X level to which the Γ electron may transfer.

4. CONCLUSION

The Γ-X intersubband scattering rate due to phonon emission is calculated by using the tight binding method for electrons and the dielectric continuum model for phonons. As expected, the scattering is strongest when the levels anti-cross. Among various phonon modes, the strongest one is found to be the AlAs confined modes, the weakest being the GaAs confined modes. Scattering rate due to the interface modes are observed to get weaker with increasing AlAs thickness. The parity behavior of electron states and its effect on scattering are examined. The results obtained are in general agreement with the experiment.

5. ACKNOWLEDGEMENT

The authors would like to thank J. M. Higman for useful technical discussions. The authors are also grateful to M. Dutta for providing unpublished data on Γ-X transitions and for stimulating the initiation of the current calculations. This work was, in part, supported by the Office of Naval Research and the U.S. Army Research Office.

6. REFERENCES

1. M. C. Tatham, J. F. Ryan, and C. T. Foxon, "Time-resolved Raman measurements of intersubband relaxation in GaAs quantum wells," Phys. Rev. Lett., vol. 63, pp. 1637-1640, 1989.

2. S. M. Goodnick, J. E. Lary, and P. Lugli, "Intersubband relaxation of hot carriers in quantum well systems," Superlatt. Microstruct., vol. 10, pp. 461-466, 1991.

3. S. Rudin and T. L. Reinecke, "Electron-LO-phonon scattering rates in semiconductor quantum wells," Phys. Rev. B, vol. 41, pp. 7713-7717, 1990.

4. A. M. de Paula, A. C. Maciel, G. Weber, J. F. Ryan, P. Dawson, and C. T. Foxon, "Subpicosecond real-space charge transfer in GaAs/AlAs type II superlattices," Semicond. Sci. Technol., vol. 7, pp. B120-B123, 1992.

5. J. Feldmann, J. Nunnenkamp, G. Peter, E. Gobel, J. Kuhl, K. Ploog, P. Dawson, and C. T. Foxon, "Experimental study of the Γ-X electron transfer in type-II (Al,Ga)As/AlAs superlattices and multiple-quantum-well structures," Phys. Rev. B, vol. 42, pp. 5809-5821, 1990.

6. L. P. Fu, T. Schmiedel, A. Petrou, M. Dutta, P. G. Newman, and M. A. Stroscio, "Raman study of interface phonons in GaAs/AlAs quantum wells: Resonance with the e_2-h_2 exciton," Phys. Rev. B, vol. 46, pp. 7196-7199, 1992.

7. For a review of work on type-II structures, see B. A. Wilson, "Carrier dynamics and recombination mechanisms in staggered-alignment heterostructures," IEEE J. Quantum Electron., vol. QE-24, pp. 1763-1777, 1988.

8. Y.-T. Lu and L. J. Sham, "Valley-mixing effects in short-period superlattices," Phys. Rev. B, vol. 40, pp. 5567-5578, 1989.

9. M. A. Gell and D. C. Herbert, "Zone folding and subband dispersions in GaAs-$Al_xGa_{1-x}As$ (001) superlattices," Phys. Rev. B, vol. 35, pp. 9591-9604, 1987.

10. D. Z.-Y. Ting and Y.-C. Chang, "Γ-X mixing in GaAs/$Al_xGa_{1-x}As$ and $Al_xGa_{1-x}As$/AlAs superlattices," Phys. Rev. B, vol. 36, pp. 4359-4374, 1987.

11. T. Ando and H. Akera, "Connection of envelope functions at semiconductor heterointerfaces: II. Mixings of Γ and X valleys in GaAs/$Al_xGa_{1-x}As$," Phys. Rev. B, vol. 40, pp. 11619-11633, 1989.

12. I. Morrison, L. D. Brown, and M. Jaros, "Valley-mixing effects in $(GaAs)_l(AlAs)_m$ superlattices with microscopically imperfect interfaces," Phys. Rev. B, vol. 42, pp. 11818-11825, 1990.

13. H. Rucker, E. Molinari, and P. Lugli, "Microscopic calculation of the electron-phonon interaction in quantum wells," Phys. Rev. B, vol. 45, pp. 6747-6756, 1992.

14. A. R. Bhatt, K. W. Kim, M. A. Stroscio, and J. M. Higman, "Simplified microscopic model for electron-optical-phonon interactions in quantum wells," Phys. Rev. B, vol. 48, pp. 14671-14674, 1993.

15. L. Wendler and R. Haupt, "Electron-phonon interaction in semiconductor superlattices," Phys. Stat. Sol. (b), vol. 143, pp. 487-510, 1987.

16. R. Enderlein, "Macroscopic theory of optical phonons in superlattices," Phys. Rev. B, vol. 43, pp. 14513-14531, 1991.

17. N. Mori and T. Ando, "Electron-optical phonon interaction in single and double heterostructures," Phys. Rev. B, vol. 40, pp. 6175-6188, 1989.

18. G. Gilat and L. J. Raubenheimer, "Accurate numerical method for calculating frequency-distribution function in solids," Phys. Rev., vol. 144, pp. 390-395, 1966.

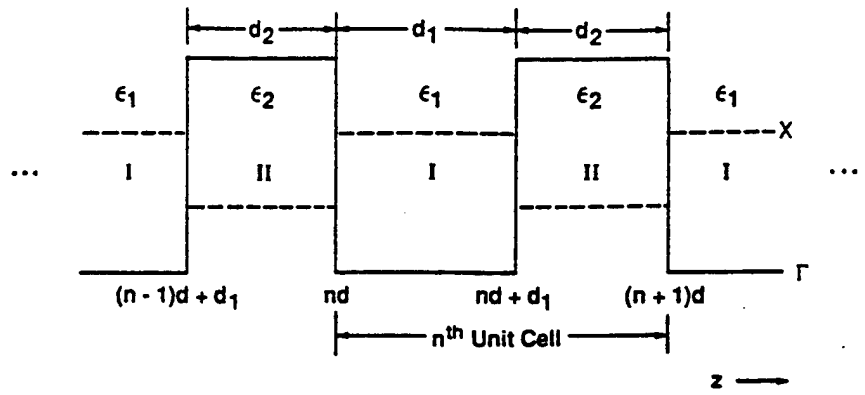

Fig. 1. Schematic drawing of the band-edge alignment of a type-II superlattice grown in the z-direction.

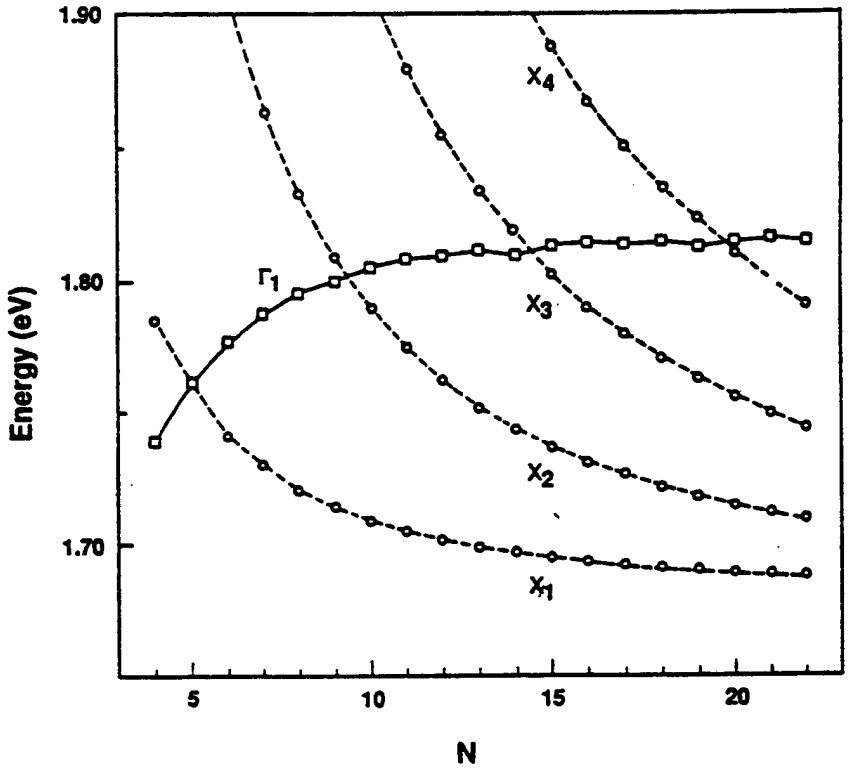

Fig. 2. Energy levels at the miniband minimum obtained from the tight binding calculation as function of AlAs layer thickness in monolayers. The GaAs thickness is constant at 8 monolayers. The discrete energy levels are marked as Γ (squares) and X (circles) to designate the dominant one of the two bulk states making up the confined state.

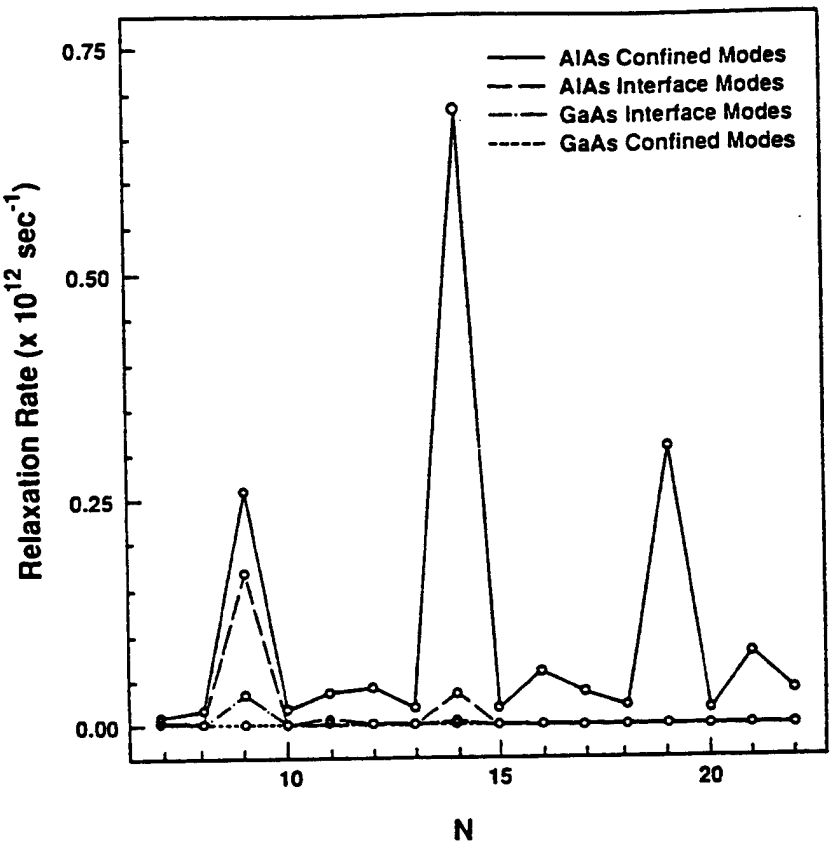

Fig. 3. Γ_1-X_1 relaxation rate due to optical phonon emission as a function of AlAs layer thickness in monolayers. The GaAs thickness is 8 monolayers throughout. Scattering rates due to the GaAs confined phonon modes are very small and hard to distinguish in the figure.

PROCEEDINGS
SPIE—The International Society for Optical Engineering

Ultrafast Phenomena in Semiconductors

David K. Ferry
Henry M. van Driel
Chairs/Editors

27-28 January 1994
Los Angeles, California

Sponsored and Published by
SPIE—The International Society for Optical Engineering

Volume 2142

Acoustic phonons in rectangular quantum wires: approximate compressional modes and the corresponding deformation potential interactions

K. W. Kim, SeGi Yu, and M. U. Erdoğan

Department of Electrical and Computer Engineering
North Carolina State University
Raleigh, North Carolina 27695-7911

Michael A. Stroscio and Gerald J. Iafrate

U.S. Army Research Office
P.O. Box 12211
Research Triangle Park, North Carolina 27709-2211

ABSTRACT

The Hamiltonian describing the deformation potential interaction of confined acoustic phonons with carriers is derived by quantizing the appropriate, experimentally-verified approximate compressional acoustic phonon modes in a rectangular quantum wire. The scattering rate due to the deformation potential interaction is calculated for a range of quantum wire dimensions.

1. INTRODUCTION

Many proposed applications of mesoscopic electronic structures involve carrier transport at low temperatures and low carrier energies; frequently, the regime of interest is one where dimensional confinement modifies the phase space substantially. In this low temperature, low energy regime,[1-6] acoustic phonons play an enhanced role in carrier scattering and may dominate over the scattering of carriers by optical phonons. Furthermore, in nanoscale structures it is possible that phase space restrictions may weaken or forbid optical phonon scattering processes that would normally dominate in bulk structures. In recent years, there has been an extensive literature on the role of dimensional confinement in modifying longitudinal optical (LO) phonon modes and their interactions with charge carriers in nanoscale and mesoscopic semiconductor structures (see, for example, Refs. 7–12 and the numerous papers referenced therein). However, there are relatively few treatments dealing with the role of dimensional confinement in modifying acoustic phonon modes and their interactions with charge carriers.[2-4] While there is an extensive literature on the theory of acoustic modes in conventional waveguides, resonators and related structures, few efforts have been reported to formulate a theory of acoustic phonons in nanoscale structures where both phonon confinement and a quantum mechanical treatment of phonon normalization are essential; Constantinou has, however, discussed the unnormalized acoustic phonon modes in a cylindrical polar semiconductor quantum wire.[13] The need for such theoretical treatments has been underscored recently by experimental studies providing both direct and indirect[3,4] evidence of the importance of acoustic phonon confinement in reduced dimensional electronic structures.

0-8194-1437-9/94/$6.00

In this paper, by appropriately quantizing the acoustic phonon displacements we have obtained the correctly normalised expressions for acoustic phonons confined in a rectangular quantum wire. There are no exact solutions for the complete set of phonon modes for a rectangular quantum wire; however, as for the case of LO phonon modes,[10] the approximate modes presented in this work provide simple and useful expressions which are well suited for modeling the interaction of carriers with acoustic phonons. To investigate the effects of reduced dimensionality on the coupling between acoustic phonons and carriers, we have formulated the interaction Hamiltonian for the deformation potential associated with confined acoustic phonon modes in rectangular quantum wires. The resulting Golden Rule scattering rates are compared with those obtained from the bulk phonon modes. The technique used to quantize the acoustic phonons in a rectangular quantum wire is based on recent results[14] for confined phonon modes in a free-standing nanoscale cylindrical quantum wire. In Ref. 14, the general procedure for quantizing the amplitudes of acoustic phonon modes is also demonstrated for cylindrical quantum dots.

2. QUANTIZATION OF COMPRESSIONAL ACOUSTIC PHONON MODES FOR A RECTANGULAR QUANTUM WIRE

The compressional acoustic phonon modes in free-standing rods of rectangular cross section have been examined both experimentally[15] and theoretically[16,17] by Morse in an extended study. In that research, Morse has derived an approximate set of compressional acoustic phonon modes[16,17] which are found to accurately approximate the experimentally observed modes over a wide range of conditions.[15] In particular, Morse has found that the approximate modes derived by assuming separation of variables[16,17] have simple analytical representations and provide convenient approximations for the rectangular geometry when the cross-sectional dimensions have aspect ratios of approximately 2 or greater. For smaller aspect ratios, it is necessary to turn to numerical solutions since exact analytical solutions for the compressional acoustic phonon modes in a rectangular structure are not expressible analytically. In this account, we shall restrict our analysis to rectangular quantum wires having aspect ratios of cross-sectional dimensions equal to 2.

Following Morse,[16] we consider a free-standing rectangular rod of infinite length in the z-direction having an x-directed height, $2a$, and a y-directed width, $2d$; the origin of coordinates in the x-y plane is placed in the geometric center of the rectangular cross section and the $x-$, $y-$, $z-$directed acoustic mode displacements are represented, respectively, by,

$$u_1 = u(x,y)e^{i\gamma(z-ct)}, \tag{1}$$

$$v_1 = v(x,y)e^{i\gamma(z-ct)}, \tag{2}$$

$$w_1 = w(x,y)e^{i\gamma(z-ct)}, \tag{3}$$

where $\gamma = 2\pi/\lambda$, λ being the wavelength, γ is the z-directed free wavevector, and c is the phase velocity. Assuming Morse's form for the approximate separation-of-variables solution, the compressional waves may be represented by,

$$u = \{Asink_1x + Bsink_2x\}cos(hy), \tag{4}$$

$$v = \{\frac{h}{k_1}Acosk_1x + Ccosk_2x\}sin(hy), \tag{5}$$

$$w = i\{-\frac{\gamma}{k_1}Acosk_1x + \frac{1}{\gamma}(k_2B + hC)cosk_2x\}cos(hy), \quad (6)$$

where

$$k_1^2 + h_1^2 = \gamma^2[(c/c_d)^2 - 1], \quad (7)$$
$$k_2^2 + h_2^2 = \gamma^2[(c/c_s)^2 - 1], \quad (8)$$

and the dilatational, or compressional, sound speed, c_d, as well as the shear, or transverse, sound speed, c_s, are expressed in terms of the Lamé constants λ' and μ:

$$c_d^2 = (\lambda' + 2\mu)/\rho, \quad (9)$$
$$c_s^2 = \mu/\rho, \quad (10)$$

with ρ being the density of the medium. Substitution of Eqs. (4)–(6) into the conditions that the T_{xx}, T_{yx} and T_{zx} stress components vanish at $x = \pm a$ and taking $h = h_1 = h_2$ [16,17] to approximate the stress components as products of functions of x and y separately, yields a set of three simultaneous equations for the amplitudes A, B, and C:

$$2Ahsink_1a + Bhsink_2a + Ck_2sink_2a = 0, \quad (11)$$
$$-A(\gamma^2 + h^2 - k_2^2)cosk_1a + 2Bk_1k_2cosk_2a = 0, \quad (12)$$
$$2A(h^2 + \gamma^2)sink_1a + B(\gamma^2 + h^2 - k_2^2)sink_2a = 0. \quad (13)$$

When $k_2 \neq 0$, the condition that the determinant of coefficients vanishes requires that,

$$\frac{tank_2a}{tank_1a} = -\frac{4k_1k_2(h^2 + \gamma^2)}{(h^2 + \gamma^2 - k_2^2)^2}, \quad (14)$$

which serves as the dispersion relation; Eq. (14) may be recognized as being similar to the corresponding dispersion relation for the case of a slab.[18] Using Eq. (13) to solve for B in terms of A and applying the resultant expression in conjunction with Eq. (11) to solve for C in terms of A, it follows that,

$$u_1 = A\{sink_1x + \alpha sink_2x\}cos(hy)e^{i\gamma(z-ct)}, \quad (15)$$
$$v_1 = A\{\frac{h}{k_1}cosk_1x + \beta cosk_2x\}sin(hy)e^{i\gamma(z-ct)}, \quad (16)$$
$$w_1 = iA\{-\frac{\gamma}{k_1}cosk_1x + \frac{1}{\gamma}(k_2\alpha + h\beta)cosk_2x\}cos(hy)e^{i\gamma(z-ct)}, \quad (17)$$

where α and β are defined by,

$$B = -\frac{sink_1a}{sink_2a}\frac{2(h^2 + \gamma^2)}{(\gamma^2 + h^2 - k_2^2)}A = \alpha A, \quad (18)$$

and

$$C = -\left(\frac{k_2 h}{h^2+\gamma^2}\right) B = \frac{sink_1 a}{sink_2 a}\frac{2k_2 h}{(\gamma^2+h^2-k_2^2)} A = \beta A. \tag{19}$$

As described previously,[14] the normalization constant may be determined by quantizing the phonon modes so that,

$$\frac{1}{4ad}\int_{-a}^{+a} dx \int_{-d}^{+d} dy\{uu^* + vv^* + ww^*\} = \frac{\hbar}{2M\omega_\gamma}, \tag{20}$$

where ω_γ is the radial frequency of the mode with wavevector, γ. Evaluation of Eq. (20) produces the amplitude A in terms of the following equations:

$$\begin{aligned}\frac{A^2}{4ad} \times & \left\{ f_1(h,d)\left[f_2(k_1,a) + 2\alpha g_1(k_1,k_2,a) + \alpha^2 f_2(k_2,a)\right]\right. \\ & -f_1(h,d)\left[\frac{h^2}{k_1^2} f_1(k_1,a) + \frac{2\beta h}{k_1} g_2(k_1,k_2,a) + \beta^2 f_1(k_2,a)\right] \\ & +f_1(h,d)\left[\frac{\gamma^2}{k_1^2} f_1(k_1,a) - \frac{2}{k_1}(k_2\alpha + h\beta) g_2(k_1,k_2,a) + \frac{(k_2\alpha + h\beta)^2)}{\gamma^2} f_1(k_2,a)\right] \\ & \left. +2d\left[\frac{h^2}{k_1^2} f_1(k_1,a) + \frac{2\beta h}{k_1} g_2(k_1,k_2,a) + \beta^2 f_1(k_2,a)\right]\right\} = \frac{\hbar}{2M\omega_\gamma}, \end{aligned} \tag{21}$$

where,

$$f_1(h,d) = d\left(1 + \frac{sin(2hd)}{(2hd)}\right), \tag{22}$$

$$f_2(h,d) = 2d - f_1(h,d), \tag{23}$$

$$g_1(k_1,k_2,a) = \frac{sin(k_1-k_2)a}{(k_1-k_2)} - \frac{sin(k_1+k_2)a}{(k_1+k_2)}, \tag{24}$$

$$g_2(k_1,k_2,a) = \frac{sin(k_1-k_2)a}{(k_1-k_2)} + \frac{sin(k_1+k_2)a}{(k_1+k_2)}. \tag{25}$$

In the remainder of this paper, we shall write A^2 as,

$$A^2 = \frac{2\hbar}{M\omega_\gamma B_\gamma}, \tag{26}$$

where B_γ is defined straightforwardly by Eqs. (21) and (26).

As discussed by Morse,[16] the boundary conditions at $y = \pm d$ determine the value of h; however, the adjustment of h alone is insufficient to satisfy T_{yy}, T_{xy} and T_{zy} at $y = \pm d$. For aspect ratios where the width of the rectangular cross section $(2d)$ is greater than or approximately twice the height $(2a)$, the two shear stresses T_{xy} and T_{zy} become negligible and, accordingly, Morse chooses h so that the extensional stress T_{yy} vanishes; this requires,

$$hd = (n + \tfrac{1}{2})\pi, \qquad n = 0, 1, 2, \ldots . \tag{27}$$

The principal propagation mode is the mode having no nodal surfaces parallel to the length; this is the mode with $n = 0$. Motivated by Morse's experimental observation that the principal mode is dominant[15] as well as by the analysis in section 3, the present paper will present numerical results for only the principal mode of the set of modes defined by Eq. (27). As demonstrated in Refs. 15 and 16, there is another principal mode observed experimentally. This mode corresponds to a "width mode" and is determined as demonstrated previously for the "thickness mode". For the "width mode", however, the approximate solution is based on taking $k_1 = k_2 = k$ and by satisfying the boundary conditions on the stress at $y = \pm d$; for this mode, k is then determined in an analogous manner by approximately satisfying the boundary conditions at $x = \pm a$; for these modes it follows that $2ka = n\pi$ with $n = 0, 1, 2, \ldots$. This paper shall present detailed numerical results only for the principal "width mode" which corresponds to taking $k = 0$. The dispersion relation resulting from the boundary conditions at $y = \pm d$ for the "width modes" is identical in form to Eq. (14). Eq. (14) may be written as,

$$\frac{tan(\pi\sqrt{\chi^2 - \psi^2})}{tan(\pi\sqrt{\epsilon\chi^2 - \psi^2})} = -\frac{4\psi^2\sqrt{\chi^2 - \psi^2}\sqrt{\epsilon\chi^2 - \psi^2}}{(2\psi^2 - \chi^2)^2}, \tag{28}$$

where,

$$\chi^2 = s^2(c/c_s)^2, \tag{29}$$

$$\psi^2 = s^2 + (ah/\pi)^2, \tag{30}$$

$$s = a\gamma/\pi, \tag{31}$$

$$\epsilon = (c_s/c_d)^2 = (1 - 2\sigma)/2(1 - \sigma). \tag{32}$$

In Eq. (32), σ is Poisson's ratio.

3. SCATTERING RATES IN A RECTANGULAR QUANTUM WIRE DUE TO THE DEFORMATION POTENTIAL DRIVEN BY COMPRESSIONAL ACOUSTIC PHONON MODES

The Hamiltonian, H_{def}, for the deformation potential interaction of the "thickness mode" is given by,

$$\begin{aligned} H_{def} &= E_a \nabla \cdot \vec{u}(\vec{r}) \\ &= E_a \sum_{\gamma,n,m} \left[c_{n,m}(\gamma) + c^{\dagger}_{n,m}(-\gamma)\right] \left(\frac{\partial u}{\partial x} + \frac{\partial v}{\partial y} + i\gamma w\right) e^{i\gamma z}, \end{aligned} \tag{33}$$

where $c_{n,m}(\gamma)$ and $c^{\dagger}_{n,m}(-\gamma)$ are the usual annihilation and creation operators; specifically,

$$\vec{u}(\vec{r}) = \sum_{\gamma,n,m} \left[c_{n,m}(\gamma) + c^{\dagger}_{n,m}(-\gamma)\right] \vec{u}(x, y, \gamma) e^{i\gamma z}. \tag{34}$$

The time dependent term, $e^{-i\omega_\gamma t}$, is not included in Eqs. (33) and (34) since it will be included in the energy-conserving delta function in the Golden Rule. In Eqs. (33) and (34), the sum over γ represents the usual integration over wavevector, while the sums over n and m represent the

addition of the various acoustic phonon modes. For the normalized compressional, or longitudinal, modes of section 2, it follows that,

$$H_{def} = \sum_{\gamma,n,m} E_a A \frac{\omega_\gamma^2}{c_d^2 k_1} cosk_1 x cos(hy) \left[c_{n,m}(\gamma) + c_{n,m}^\dagger(-\gamma)\right] e^{i\gamma z}. \tag{35}$$

where $\omega_\gamma^2 = c^2\gamma^2$. In the extreme quantum limit, the ground state effective mass electronic wavefunction is given by,

$$\psi_q(x,y,z) = \frac{1}{\sqrt{ad}} cos\left(\frac{\pi x}{2a}\right) cos\left(\frac{\pi y}{2d}\right) e^{iqz}, \tag{36}$$

and the eigen energy is,

$$E = \frac{\hbar^2}{2m}\left[\left(\frac{\pi^2}{(2a)^2} + \frac{\pi^2}{(2d)^2}\right) + q^2\right]. \tag{37}$$

Accordingly, the matrix element, $< q'|H_{def}|q >$, is given by,

$$< q'|H_{def}|q >= \sum_{\gamma,n,m} E_a A \frac{\omega_\gamma^2}{c_d^2 k_1} \frac{\pi^2 sink_1 a}{k_1 a(\pi^2 - k_1^2 a^2)} \frac{\delta_{q-q'+\gamma}}{\left\{\left(n+\frac{1}{2}\right)\pi\left[1-\left(n+\frac{1}{2}\right)^2\right]\right\}} \left[c_{n,m}(\gamma) + c_{n,m}^\dagger(-\gamma)\right]. \tag{38}$$

An examination of the n-dependent terms in Eq. (38) demonstrates that they contribute to the matrix element squared in such a way that these terms for $n = 1$ are only 1/25 of their magnitude for $n = 0$; a similar reduction occurs in going from $n = 1$ to $n = 2$ and it is concluded that only the principal mode contributes significantly to Eq. (38) which was derived on the assumption that the carriers remain in the ground state of the extreme quantum limit, x-y potential.

The Fermi Golden Rule scattering rate corresponding to the matrix element of Eq. (38) is given by,

$$\frac{1}{\tau} = \sum_{n,m} \int_{-\infty}^{+\infty} d\gamma \frac{L}{2\pi} \frac{2\pi}{\hbar} \left[E_a A_\gamma \frac{\omega_\gamma^2}{c_d^2 k_1}\right]^2 \left[\frac{\pi^2 sink_1 a}{k_1 a(\pi^2 - k_1^2 a^2)}\right]^2 \left[\frac{1}{\left(n+\frac{1}{2}\right)\pi\left[1-\left(n+\frac{1}{2}\right)^2\right]}\right]^2$$
$$\times \left(N + \frac{1}{2} \pm \frac{1}{2}\right) \delta\left(\frac{\hbar^2}{2m}(\gamma^2 \mp 2q\gamma) \pm \hbar\omega_\gamma\right), \tag{39}$$

where A has been written as A_γ to indicate the γ dependence of A_γ, L is the normalization length along the axis of the quantum wire and N is the usual temperature-dependent Bose-Einstein occupation number for the acoustic phonons. Using Eq. (26) and defining factors Z_1 and Z_2, Eq. (39) may be written as,

$$\frac{1}{\tau} = \sum_{n,m} \int_{-\infty}^{+\infty} d\gamma E_a^2 \left(\frac{1}{2\rho ab B_\gamma}\right) \frac{\omega_\gamma^3}{(c_d^2 k_1)^2} Z_1^2 Z_2^2 \left(N + \frac{1}{2} \pm \frac{1}{2}\right) \delta\left(\frac{\hbar^2}{2m}(\gamma^2 \mp 2q\gamma) \pm \hbar\omega_\gamma\right), \tag{40}$$

where

$$Z_1 = \frac{\pi \sin k_1 a}{k_1 a(\pi^2 - k_1^2 a^2)}, \tag{41}$$

$$Z_2 = \frac{1}{\left(n+\frac{1}{2}\right)\pi\left[1-\left(n+\frac{1}{2}\right)^2\right]}. \tag{42}$$

As discussed previously, the "width mode" scattering rate may be readily formulated by interchanging the roles of x and y.

4. NUMERICAL RESULTS

The deformation-potential scattering rates have been calculated for two separate quantum wire dimensions. The quantum wire aspect ratio of width to height is taken as two and the dimensions of the rectangular cross section are taken as 28.3 Å by 56.6 Å, and 100 Å by 200 Å. In these calculations an isotropic cubic medium has been assumed and the compressional, or longitudinal, sound speed has been taken to be that of GaAs; it should be noted that imposing both of these constraints makes it impossible to have a transverse sound speed matching that of GaAs. This is a consequence of the fact that GaAs may be treated as having an isotropic elastic tension only in a very rough approximation. In this paper, Poisson's ratio, σ, is taken to be 1/3; this choice fixes the value of ϵ as given by Eq. (32).

Scattering rates for emission and absorption as functions of electron energy are plotted in Fig. 1 for a quantum wire with a 28.3 Å × 56.6 Å (10 monolayers by 20 monolayers) cross section; these scattering rates are calculated at 77 K for both bulk acoustic modes and for the compressional modes. Three distinct and important features are obvious from Fig. 1 as well as from Fig. 2 which presents related results for different dimensional parameters. First, the scattering rates for the case of the compressional modes are approximately an order of magnitude higher than the corresponding bulk scattering rates. These enhanced scattering rates provide a clear indication that conceptual designs for mesoscopic devices must be evaluated in light of the fact that confined acoustic modes may play a significant role in carrier transport in these devices. As shown in Fig. 2, for the case of a 100 Å × 200 Å cross section we find similar scaling of the scattering rates with energy; however, the rates are approximately an order of magnitude lower than those for the 28.3 Å × 56.6 Å quantum wire. The second important feature of Figs. 1 and 2 is the appearance of structure in the scattering rates which results from the energy threshold for the different mode values, m, of the "thickness" and "width" modes. As is obvious from Figs. 1 and 2, each of these modes makes a notable contribution to the density-of-states and to the scattering rate. The scattering rates in Figs. 1 and 2 have been calculated by including the five lowest-order "thickness" modes as well as the five lowest-order "width" modes. The present calculations demonstrate that it is essential to retain a number of acoustic modes in order to obtain accurate scattering rates. The third important feature of these results is the enhancement in the scattering rate due to emission of compressional modes with energies of a few meV. This pronounced peaking of the scattering rate is due to the dominance of selected compressional modes in the emission process. Thus, the results in this analysis indicate that it is essential to consider carrier-acoustic phonon scattering processes

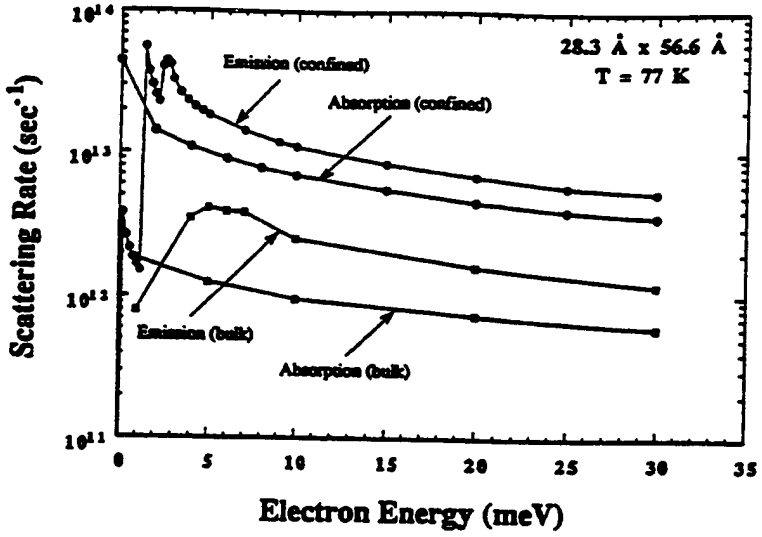

Figure 1. Deformation potential scattering rates by bulk and confined acoustic phonon modes in a free-standing rectangular quantum wire at 77 K. Enhancements in the scattering rates for the case of confined acoustic modes occur at the onset of emission for the various "width" and "thickness" modes. These thresholds occur at 0.03, 1.23, 2.37, 2.48, and 2.50 *meV* for the "width" mode, and 2.04, 2.73, 4.44, 5.45, and 5.85 *meV* for the "thickness" mode. The plotting resolution depicted is not fine enough to fully illustrate the importance of the density-of-states effects in the rectangular quantum wire.

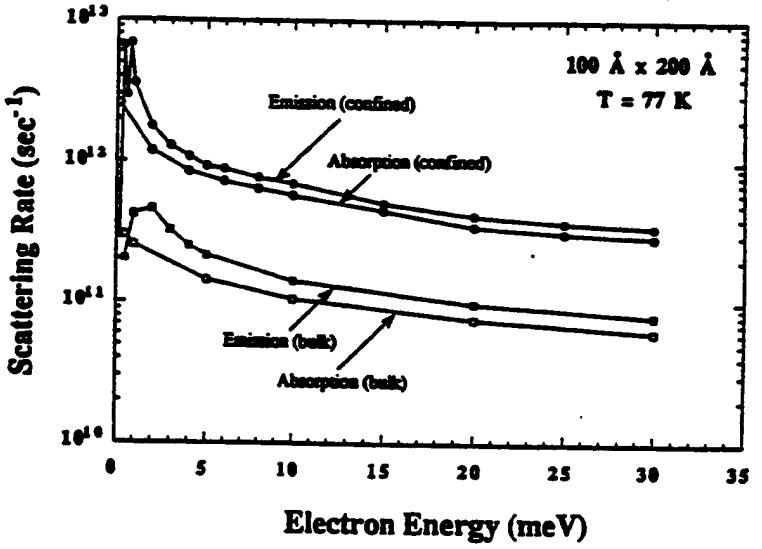

Figure 2. Deformation potential scattering rates by bulk and confined acoustic phonon modes in a free-standing rectangular quantum wire at 77 K. Enhancements in the scattering rates for the case of confined acoustic modes occur at the onset of emission for the various "width" and "thickness" modes. These thresholds occur at 0.01, 0.36, 0.66, 0.72, and 0.75 *meV* for the "width" mode, and 0.60, 0.78, 1.26, 1.57, and 1.69 *meV* for the "thickness" mode. As in Fig. 1, plotting resolution is limited.

when designing mesoscopic devices containing quantum-wire elements. Based on what appears to be the most complete set of approximate compressional modes available for a rectangular quantum wire,[16] it is demonstrated that the details of the modal structure must be taken into account if deformation-potential scattering is to be modeled accurately. Further analysis is necessary to rigorously show that deformation-potential scattering rates by acoustic phonons in quantum wires exceed the corresponding bulk scattering rates; however, these results provide a first indication that acoustic phonon scattering may be significantly enhanced in quantum wires.

5. ACKNOWLEDGMENT

The authors would like to thank Dr. James W. Mink for his support and Dr. Mitra Dutta for making us aware of spectroscopic studies of confined acoustic phonons. The authors would like to thank Prof. M. N. Wybourne for advance information on his recent experimental evidence for acoustic phonon confinement. The authors are also grateul to Prof. V. Mitin, Dr. R. Mickevičius, and Mr. N. Bannov for many interactions on related confined phonon effects in nanostructures. Special thanks are due to Dr. Arthur Ballato for his advice on the theory of acoustic phonons. This work was supported, in part, by the Office of Naval Research and the U.S. Army Research Office.

6. REFERENCES

1. T. Kawamura and S. Das Sarma, "Phonon-scattering-limited electron mobilities in $Al_xGa_{1-x}As/GaAs$ heterojunctions," Phys. Rev. B, vol. 45, pp. 3612-3627, 1992.

2. B. Hillebrands, S. Lee, G. I. Stegeman, H. Cheng, J. E. Potts, and F. Nizzoli, "Evidence for the existence of guided longitudinal acoustic phonons in ZnSe films on GaAs," Phys. Rev. Lett., vol. 60, pp. 832-835, 1988.

3. J. Seyler and M. N. Wybourne, "Acoustic waveguide modes observed in electrically heated metal wires," Phys. Rev. Lett., vol. 69, pp. 1427-1430, 1992; Z. V. Popvic, J. Spitzer, T. Ruf, M. Cardona, R. Notzel, and K. Ploog, "Folded acoustic phonons in GaAs/AlAs corrugated superlattices grown along the [311] direction," Phys. Rev. B, vol. 48, pp. 1659-1664, 1993.

4. H. Benistry, C. M. Sotomayor-Torrés, and C. Weisbuch, "Intrinsic mechanism for the poor luminescence properties of quantum-box system," Phys. Rev. B, vol. 44, pp. 10945-10948, 1991.

5. B. A. Auld, *Acoustic Fields and Waves*, Wiley, New York, 1973.

6. P. J. Price, "Two-dimensional electron transport in semiconductor layer: I. Phonon scattering," Ann. Phys., vol. 133, pp. 217-239, 1981.

7. N. Mori and T. Ando, "Electron-optical-phonon interaction in single and double heterostructures," Phys. Rev. B, vol. 40, pp. 6175-6188, 1989.

8. M. A. Stroscio, "Interaction between longitudinal-optical phonon modes of a rectangular quantum wire and electron gas," Phys. Rev. B, vol. 40, pp. 6428-6431, 1989.

9. K. W. Kim and M. A. Stroscio, "Electron-optical-phonon interaction in binary/ternary heterostructures," J. Appl. Phys., vol. 68, pp. 6289-6295, 1990.

10. K. W. Kim, M. A. Stroscio, A. Bhatt, V. V. Mitin, and R. Mickevičius, "Electron-optical-phonon scattering rates in a rectangular semiconductor quantum wire," J. Appl. Phys., vol. 70, pp. 319-327, 1991.

11. M. A. Stroscio, K. W. Kim, G. J. Iafrate, M. Dutta, and H. L. Grubin, "Dramatic reduction of the longitudinal-optical phonon emission rate in polar-semiconductor quantum wires," Phil. Mag. Lett., vol. 65, pp. 173-176, 1992.

12. M. A. Stroscio, G. J. Iafrate, K. W. Kim, M. A. Littlejohn, A. Bhatt, and M. Dutta, "Confined and interface phonons in polar-semiconductor quantum wells and quantum wires," in *Integrated Optics and Optoelectronic*, edited by K.-K. Wong and M. Razeghi, vol. CR 45, pp. 341-357, SPIE, Bellingham, 1993.

13. N. C. Constantinou, "Optical phonons in superlattices and cylindrical quantum wires," to be published in *Proceedings of NATO Advanced Research Workshop on Phonons in Nanostructures*, Kluwer, Boston, 1993.

14. M. A. Stroscio and K. W. Kim, "Piezoelectric scattering of carriers from confined acoustic modes in cylindrical quantum wires," Phys. Rev. B, vol. 48, pp. 1936-1938, 1993.

15. R. W. Morse, "Dispersion of compressional waves in isotropic rods of rectangular cross section," J. Acous. Soc. Am., vol. 20, pp. 833-837, 1948.

16. R. W. Morse, "The velocity of compressional waves in rods of rectangular cross section," J. Acous. Soc. Am., vol. 22, pp. 219-223, 1950.

17. R. W. Morse, "The dispersion of compressional waves in isotropic rods of rectangular cross section," Ph.D. Thesis, Brown University, Providence, RI, 1949.

18. M. Redwood, *Mechanical Waveguides*, Pergamon, Oxford, 1960.

Electron–acoustic-phonon scattering rates in rectangular quantum wires

SeGi Yu* and K. W. Kim
Department of Electrical and Computer Engineering, North Carolina State University, Raleigh, North Carolina 27695-7911

Michael A. Stroscio and Gerald J. Iafrate
U.S. Army Research Office, P. O. Box 12211, Research Triangle Park, North Carolina 27709-2211

Arthur Ballato
Electronics and Power Sources Directorate, U.S. Army Research Laboratory, Ft. Monmouth, New Jersey 07703-5601
(Received 18 March 1994)

Electron–acoustic-phonon scattering in a rectangular quantum wire is studied. The Hamiltonian describing the deformation-potential interaction of confined acoustic phonons with carriers is derived by quantizing the appropriate, experimentally verified approximate compressional acoustic-phonon modes in a free-standing rectangular quantum wire. The scattering rate due to the deformation-potential interaction is obtained for GaAs quantum wires with a range of cross-sectional dimensions. The results demonstrate that a proper treatment of confined acoustic phonons may be essential to correctly model electron scattering rates at low energies in nanoscale structures.

I. INTRODUCTION

A number of proposed applications of mesoscopic electronic structures involve carrier transport at low temperatures and low carrier energies; frequently, the regime of interest is one where dimensional confinement modifies the phase space substantially. It is well known that in this low-temperature, low-energy regime,[1–6] acoustic phonons play an enhanced role in carrier scattering and may dominate over the scattering of carriers by optical phonons. In addition, in nanoscale structures it is possible that phase-space restrictions may weaken or forbid optical-phonon scattering processes that would normally dominate in bulk structures. Recently, there has been an extensive literature on the role of dimensional confinement in modifying longitudinal-optical (LO) phonon modes and their interactions with charge carriers in nanoscale and mesoscopic semiconductor structures (see, for example, Refs. 7–12 and the numerous papers referenced therein). On the other hand, there are relatively few treatments dealing with the role of dimensional confinement in modifying acoustic-phonon modes and their interactions with charge carriers.[2–4,13,14] In spite of the fact that there is an extensive literature on the theory of acoustic modes in conventional waveguides, resonators, and related structures, few efforts have been reported on formulating a theory of acoustic phonons in nanoscale structures, where both phonon confinement and a quantum-mechanical treatment of phonon normalization are essential. The necessity for such theoretical treatments has been demonstrated recently by experimental studies providing both direct and indirect[3,4] evidence of the importance of acoustic-phonon confinement in reduced dimensional electronic structures.

In this paper, we have obtained the normalized expressions for acoustic phonons confined in a free-standing rectangular quantum wire by appropriately quantizing the acoustic-phonon displacements. As is well known, there are no exact solutions for the complete set of phonon modes for a rectangular quantum wire; nevertheless, as for the case of LO phonon modes,[8] the approximate modes presented in this work provide simple and useful expressions, which are well suited for modeling the interaction of carriers with acoustic phonons. As a basis for investigating the role of reduced dimensionality on the coupling between acoustic phonons and carriers, we have formulated the interaction Hamiltonian for the deformation potential associated with confined acoustic-phonon modes in rectangular quantum wires. The resulting scattering rates (based on the golden rule approximation) are compared with those obtained from the bulk-phonon modes. For numerical calculations, GaAs is used as the material of choice throughout this study.

II. QUANTIZATION OF COMPRESSIONAL ACOUSTIC-PHONON MODES FOR A RECTANGULAR QUANTUM WIRE

The compressional, or dilatational, acoustic-phonon modes in free-standing rods of rectangular cross section have been examined both experimentally[15] and theoretically[16,17] by Morse in an extended study. Morse has derived an approximate set of hybrid compressional, or dilatational, acoustic-phonon modes,[16,17] which are found to accurately approximate the experimentally observed modes over a wide range of conditions.[15] Specifically, Morse has found that the approximate hybrid modes derived by assuming separable boundary conditions[16,17] have simple analytical representations and provide convenient approximations for the rectangular geometry when the cross-sectional dimensions have aspect ratios of approximately 2 or greater. For smaller aspect ratios (i.e., close to 1), Morse has argued correctly that it is necessary to turn to numerical solutions since exact

0163-1829/94/50(3)/1733(6)/$06.00

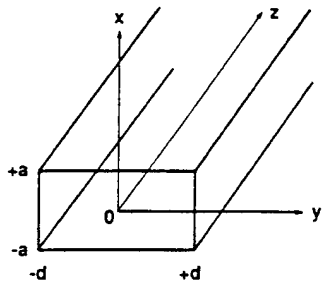

FIG. 1. Schematic drawing of a free-standing rectangular quantum wire considered in the analysis of electron–acoustic-phonon scattering.

analytical solutions for the compressional acoustic-phonon modes in a rectangular structure are not expressible analytically. In this paper, we shall restrict our analysis to rectangular quantum wires with aspect ratios of 2 or greater.

As depicted in Fig. 1, we consider a free-standing rectangular rod of infinite length in the z direction having an x-directed height (or thickness) $2a$, and a y-directed width $2d$; the origin of coordinates in the x-y plane is taken to be at the geometric center of the rectangular cross section, and the x-, y-, and z-directed acoustic-mode displacements are represented, respectively, by

$$u_1 = u(x,y)e^{i\gamma(z-ct)} , \tag{1}$$

$$v_1 = v(x,y)e^{i\gamma(z-ct)} , \tag{2}$$

$$w_1 = w(x,y)e^{i\gamma(z-ct)} , \tag{3}$$

where $\gamma = 2\pi/\lambda$, λ being the wavelength, γ is the z-directed free wave vector, and c is the phase velocity. Adopting Morse's form for the approximate separation-of-variables solution, the compressional waves for the "thickness" modes may be represented by

$$u = \{ A \sin k_1 x + B \sin k_2 x \} \cos(hy) , \tag{4}$$

$$v = \left\{ \frac{h}{k_1} A \cos k_1 x + C \cos k_2 x \right\} \sin(hy) , \tag{5}$$

$$w = i \left\{ -\frac{\gamma}{k_1} A \cos k_1 x + \frac{1}{\gamma}(k_2 B + hC) \cos k_2 x \right\} \cos(hy) , \tag{6}$$

where

$$k_1^2 + h^2 = \gamma^2 [(c/c_d)^2 - 1] , \tag{7}$$

$$k_2^2 + h^2 = \gamma^2 [(c/c_s)^2 - 1] , \tag{8}$$

and the compressional, or dilatational, sound speed c_d, as well as the transverse, or shear, sound speed c_s, are expressed in terms of the Lamé constants λ' and μ:

$$c_d^2 = (\lambda' + 2\mu)/\rho , \tag{9}$$

$$c_s^2 = \mu/\rho , \tag{10}$$

with ρ being the density of the medium. Substituting Eqs. (4)–(6) into the conditions that the T_{xx}, T_{yx}, and T_{zx} stress components vanish at $x = \pm a$, it follows that simultaneous equations for the amplitudes A, B, and C are given by

$$2Ah \sin k_1 a + Bh \sin k_2 a + Ck_2 \sin k_2 a = 0 , \tag{11}$$

$$-A(\gamma^2 + h^2 - k_2^2)\cos k_1 a + 2Bk_1 k_2 \cos k_2 a = 0 , \tag{12}$$

$$2A(h^2 + \gamma^2)\sin k_1 a + B(\gamma^2 + h^2 - k_2^2)\sin k_2 a = 0 . \tag{13}$$

When $k_2 \neq 0$, the condition that the determinant of coefficients vanishes requires that

$$\frac{\tan k_2 a}{\tan k_1 a} = -\frac{4k_1 k_2 (h^2 + \gamma^2)}{(h^2 + \gamma^2 - k_2^2)^2} , \tag{14}$$

which serves as the dispersion relation; this result is similar to the corresponding dispersion relation for the case of a slab.[18] Using Eq. (13) to solve for B in terms of A and applying the resultant expression in conjunction with Eq. (11) to solve for C in terms of A, Eqs. (3)–(6) may be written as

$$u_1 = A \{ \sin k_1 x + \alpha \sin k_2 x \} \cos(hy) e^{i\gamma(z-ct)} , \tag{15}$$

$$v_1 = A \left\{ \frac{h}{k_1} \cos k_1 x + \beta \cos k_2 x \right\} \sin(hy) e^{i\gamma(z-ct)} , \tag{16}$$

$$w_1 = iA \left\{ -\frac{\gamma}{k_1} \cos k_1 x + \frac{1}{\gamma}(k_2 \alpha + h\beta) \cos k_2 x \right\} \times \cos(hy) e^{i\gamma(z-ct)} , \tag{17}$$

where α and β are defined by

$$B = -\frac{\sin k_1 a}{\sin k_2 a} \frac{2(h^2 + \gamma^2)}{(\gamma^2 + h^2 - k_2^2)} A = \alpha A , \tag{18}$$

and

$$C = -\left[\frac{k_2 h}{h^2 + \gamma^2} \right] B = \frac{\sin k_1 a}{\sin k_2 a} \frac{2k_2 h}{(\gamma^2 + h^2 - k_2^2)} A = \beta A . \tag{19}$$

Following the quantization procedure of Ref. 14, the normalization constant may be determined by quantizing the phonon modes so that,

$$\frac{1}{4ad} \int_{-a}^{+a} dx \int_{-d}^{+d} dy \{ uu^* + vv^* + ww^* \} = \frac{\hbar}{2M\omega_\gamma} , \tag{20}$$

where ω_γ is the radial frequency of the mode with wave vector γ. Performing the indicated integration, Eq. (20) yields the amplitude A in terms of the following equations:

$$\frac{A^2}{4ad}\left\{f_1(h,d)[f_2(k_1,a)+2\alpha g_1(k_1,k_2,a)+\alpha^2 f_2(k_2,a)]-f_1(h,d)\left[\frac{h^2}{k_1^2}f_1(k_1,a)+\frac{2\beta h}{k_1}g_2(k_1,k_2,a)+\beta^2 f_1(k_2,a)\right]\right.$$
$$+f_1(h,d)\left[\frac{\gamma^2}{k_1^2}f_1(k_1,a)-\frac{2}{k_1}(k_2\alpha+h\beta)g_2(k_1,k_2,a)+\frac{(k_2\alpha+h\beta)^2}{\gamma^2}f_1(k_2,a)\right]$$
$$\left.+2d\left[\frac{h^2}{k_1^2}f_1(k_1,a)+\frac{2\beta h}{k_1}g_2(k_1,k_2,a)+\beta^2 f_1(k_2,a)\right]\right\}=\frac{\hbar}{2M\omega_\gamma}\ , \tag{21}$$

where

$$f_1(h,d)=d\left[1+\frac{\sin(2hd)}{(2hd)}\right]\ , \tag{22}$$

$$f_2(h,d)=2d-f_1(h,d)\ , \tag{23}$$

$$g_1(k_1,k_2,a)=\frac{\sin(k_1-k_2)a}{(k_1-k_2)}-\frac{\sin(k_1+k_2)a}{(k_1+k_2)}\ , \tag{24}$$

$$g_2(k_1,k_2,a)=\frac{\sin(k_1-k_2)a}{(k_1-k_2)}+\frac{\sin(k_1+k_2)a}{(k_1+k_2)}\ . \tag{25}$$

Henceforth, A^2 is written as

$$A^2=\frac{2\hbar}{M\omega_\gamma B_\gamma}\ , \tag{26}$$

where B_γ is defined straightforwardly by Eqs. (21) and (26).

In accordance with the solutions of Morse,[16] the boundary conditions at $y=\pm d$ determine the value of h; however, the adjustment of h alone is sufficient to make T_{yy}, T_{xy}, and T_{zy} vanish at $y=\pm d$. For aspect ratios where the width of the rectangular cross section ($2d$) is greater than or approximately equal to twice the height ($2a$), this problem can be circumvented since the two shear stresses T_{xy} and T_{zy} become negligible. Accordingly, Morse chooses h so that the extensional stress T_{yy} vanishes; this condition requires

$$hd=(n+\tfrac{1}{2})\pi\ ,\quad n=0,1,2,\ldots\ . \tag{27}$$

The principal propagation mode (i.e., $n=0$ or $h=\pi/2d$) has no nodal surfaces parallel to the length. Motivated by the analysis in Sec. III, as well as by Morse's experimental observation that the principal mode is dominant,[15] the present paper considers the $n=0$ case for the thickness modes in numerical calculations. In addition to the thickness modes, another set of acoustic modes is observed experimentally.[15,16] These modes correspond to "width modes" and are determined in a manner similar to that used to determine the thickness modes. By satisfying the boundary conditions on the stress at $y=\pm d$, the solutions for the width modes show expressions analogous to Eqs. (15)–(17) with the roles of x and y as well as k and h interchanged, respectively. For these modes, k is then determined by approximate boundary conditions at $x=\pm a$.[16] The dispersion relation for the width mode is identical in form to Eq. (14), and the normalization procedure for proper quantization is as described in Eq. (20). As for the thickness modes, only the principal mode with $k=0$ is considered for the width modes.

We have calculated acoustic-phonon frequencies as a function of wave vector γ for the thickness and width modes in GaAs quantum wires. For this purpose, Eq. (14) may be written as

$$\frac{\tan(\pi\sqrt{\chi^2-\psi^2})}{\tan(\pi\sqrt{\epsilon\chi^2-\psi^2})}=-\frac{4\psi^2\sqrt{\chi^2-\psi^2}\sqrt{\epsilon\chi^2-\psi^2}}{(2\psi^2-\chi^2)^2}\ , \tag{28}$$

where

$$\chi^2=s^2(c/c_s)^2\ , \tag{29}$$

$$\psi^2=s^2+(ah/\pi)^2\ , \tag{30}$$

$$s=a\gamma/\pi\ , \tag{31}$$

$$\epsilon=(c_s/c_d)^2=(1-2\sigma)/2(1-\sigma)\ , \tag{32}$$

and σ is Poisson's ratio. Due to the periodic nature of trigonometric functions, the phonon frequency ω_γ ($=c\gamma$) has multiple solutions for a given γ and n (i.e., fixed h or k). Thus, an additional index m is needed to distinguish different modes. Figures 2 and 3 depict dispersion curves of the six lowest thickness modes ($h=\pi/2d$, $m=1,\ldots,6$) and the corresponding width modes ($k=0$, $m=1,\ldots,6$). The quantum wire cross-sectional dimensions are chosen to be 28.3×56.6 Å^2 for Fig. 2 and 50×200 Å^2 for Fig. 3, respectively. As expected, the width modes tend to have lower energies than the thick-

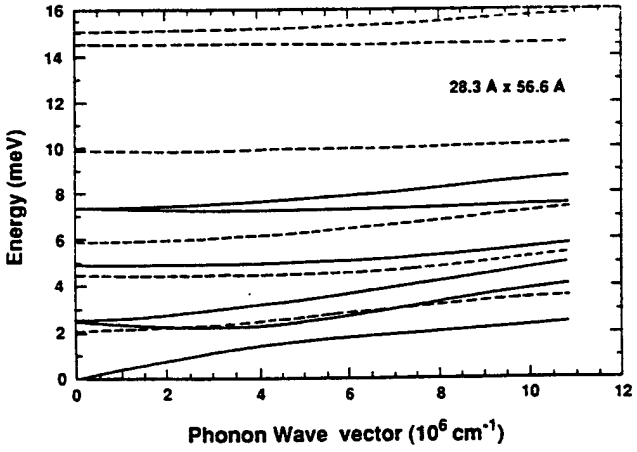

FIG. 2. Dispersion curves for the six lowest width and thickness modes ($m=1,\ldots,6$) of a 28.3×56.6-Å^2 GaAs quantum wire. The solid lines are for the width modes and the dashed lines are for the thickness modes.

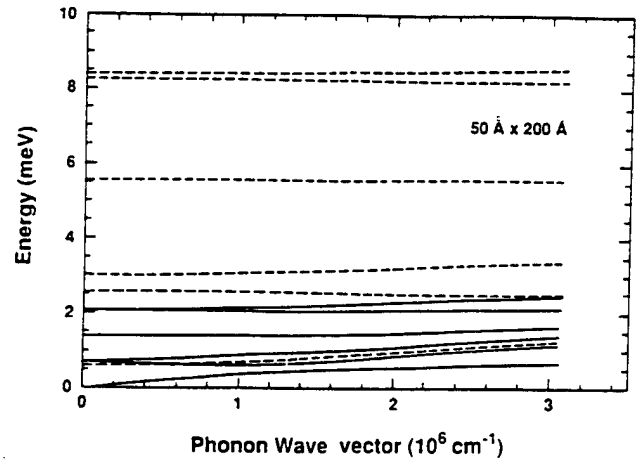

FIG. 3. Dispersion curves for the six lowest width and thickness modes ($m=1,\ldots,6$) of a 50×200-Å^2 GaAs quantum wire. The solid lines are for the width modes and the dashed lines are for the thickness modes.

ness modes, since the width is greater than the thickness for each of the cases represented in these figures.

III. ELECTRON–ACOUSTIC-PHONON SCATTERING RATES IN A RECTANGULAR QUANTUM WIRE

The deformation-potential interaction of the thickness mode is describable in terms of the Hamiltonian $H_{\rm def}$,

$$H_{\rm def}=E_a\nabla\cdot\mathbf{u}(\mathbf{r}) =E_a\sum_{\gamma,n,m}[c_{n,m}(\gamma)+c^{\dagger}_{n,m}(-\gamma)] \times\left[\frac{\partial u}{\partial x}+\frac{\partial v}{\partial y}+i\gamma w\right]e^{i\gamma z}, \tag{33}$$

where $c_{n,m}(\gamma)$ and $c^{\dagger}_{n,m}(-\gamma)$ are the usual annihilation and creation operators and

$$\mathbf{u}(\mathbf{r})=\sum_{\gamma,n,m}[c_{n,m}(\gamma)+c^{\dagger}_{n,m}(-\gamma)]\mathbf{u}(x,y,\gamma)e^{i\gamma z}. \tag{34}$$

The time-dependent factor $e^{-i\omega_\gamma t}$ is not included in Eqs. (33) and (34), since it will be included in the energy-conserving δ function in the golden rule. In Eqs. (33) and (34), the sum over γ represents the usual integration over wave vector, while the sums over n and m represent the addition of the various acoustic-phonon modes. For the normalized compressional, or dilatational, modes of Sec. II, it follows that

$$H_{\rm def}=\sum_{\gamma,n,m}E_a A\frac{\omega_\gamma^2}{c_d^2k_1}\cos(k_1x)\cos(hy) \times[c_{n,m}(\gamma)+c^{\dagger}_{n,m}(-\gamma)]e^{i\gamma z}, \tag{35}$$

where $\omega_\gamma^2=c^2\gamma^2$. Assuming the extreme quantum limit, the ground-state effective-mass electronic wave function is given by

$$\psi_q(x,y,z)=\frac{1}{\sqrt{ad}}\cos\left[\frac{\pi x}{2a}\right]\cos\left[\frac{\pi y}{2d}\right]e^{iqz}, \tag{36}$$

and the eigenenergy is

$$E=\frac{\hbar^2}{2m}\left[\left[\frac{\pi^2}{(2a)^2}+\frac{\pi^2}{(2d)^2}\right]+q^2\right]. \tag{37}$$

Hence, the matrix element $\langle q'|H_{\rm def}|q\rangle$ is given by

$$\langle q'|H_{\rm def}|q\rangle=\sum_{\gamma,n,m}E_a A\frac{\omega_\gamma^2}{c_d^2k_1}\frac{\pi^2\sin k_1a}{k_1a(\pi^2-k_1^2a^2)} \times\frac{\delta_{q-q'+\gamma}}{\{(n+\frac{1}{2})\pi[1-(n+\frac{1}{2})^2]\}} \times[c_{n,m}(\gamma)+c^{\dagger}_{n,m}(-\gamma)]. \tag{38}$$

An examination of the n-dependent terms in Eq. (38) makes it apparent that they contribute to the matrix element squared in such a way that these terms for $n=1$ are only $\frac{1}{25}$ of their magnitude for $n=0$; a similar reduction occurs in going from $n=1$ to $n=2$ and it is clear that only the principal mode contributes significantly to Eq. (38), which was derived on the assumption that the carriers remain in the ground state of the extreme quantum limit, x-y potential.

Hence, the Fermi golden rule scattering rate corresponding to the matrix element of Eq. (38) is given by

$$\frac{1}{\tau}=\sum_{n,m}\int_{-\infty}^{+\infty}d\gamma\frac{L}{2\pi}\frac{2\pi}{\hbar}\left[E_aA_\gamma\frac{\omega_\gamma^2}{c_d^2k_1}\right]^2 \times\left[\frac{\pi^2\sin k_1a}{k_1a(\pi^2-k_1^2a^2)}\right]^2\left[\frac{1}{(n+\frac{1}{2})\pi[1-(n+\frac{1}{2})^2]}\right]^2(N+\tfrac{1}{2}\pm\tfrac{1}{2})\delta\left[\frac{\hbar^2}{2m}(\gamma^2\mp2q\gamma)\pm\hbar\omega_\gamma\right], \tag{39}$$

where A has been written as A_γ to indicate the γ dependence of A_γ, L is the normalization length along the axis of the quantum wire, and N is the usual temperature-dependent Bose-Einstein occupation number for the acoustic phonons. Introducing B_γ through Eq. (26) and defining factors Z_1 and Z_2, Eq. (39) may be written as

$$\frac{1}{\tau}=\sum_{n,m}\int_{-\infty}^{+\infty}d\gamma E_a^2\left[\frac{1}{2\rho abB_\gamma}\right]\frac{\omega_\gamma^3}{(c_d^2k_1)^2}Z_1^2Z_2^2(N+\tfrac{1}{2}\pm\tfrac{1}{2}) \times\delta\left[\frac{\hbar^2}{2m}(\gamma^2\mp2q\gamma)\pm\hbar\omega_\gamma\right], \tag{40}$$

where

$$Z_1 = \frac{\pi \sin k_1 a}{k_1 a(\pi^2 - k_1^2 a^2)} \tag{41}$$

and

$$Z_2 = \frac{1}{(n+\frac{1}{2})\pi[1-(n+\frac{1}{2})^2]} . \tag{42}$$

The "width-mode" scattering rate may be readily formulated by following the procedure described above.

IV. NUMERICAL RESULTS

Deformation-potential scattering rates have been calculated in GaAs for two different quantum-wire aspect ratios. In the first case, the quantum-wire aspect ratio of width to height is taken as 2 and the dimensions of the rectangular cross section are taken as 28.3×56.6 Å^2 (i.e., 10×20 ML) and 100×200 Å^2. In the second case, the corresponding aspect ratio is taken as 4 and the wire dimensions are taken as 50×200 Å^2. In these calculations, an isotropic cubic medium has been assumed and the compressional, or longitudinal, sound speed has been taken to be that of GaAs; it should be noted that imposing both of these constraints makes it impossible to have a transverse sound speed matching that of GaAs. This is a consequence of the fact that GaAs may be treated as having an isotropic elastic tension only in a very rough approximation. In this paper, Poisson's ratio σ is taken to be $\frac{1}{3}$; this choice fixes the value of ϵ as given by Eq. (32).

Scattering rates for emission and absorption as functions of electron energy are plotted in Fig. 4 for a quantum wire with a 28.3×56.6 Å^2 cross section; these scattering rates are calculated at 77 K for both bulk acoustic modes and for the hybrid compressional modes. Figures 5 and 6 present results analogous to those of Fig. 4 but for different cross-sectional dimensions. Two distinct and important features are obvious from Figs. 4–6, which present related results for different dimensional parameters. First, the appearance of structure is prominent in the scattering rates (for confined phonons), which results from the energy threshold for the different mode values m of the thickness and width modes. As can be

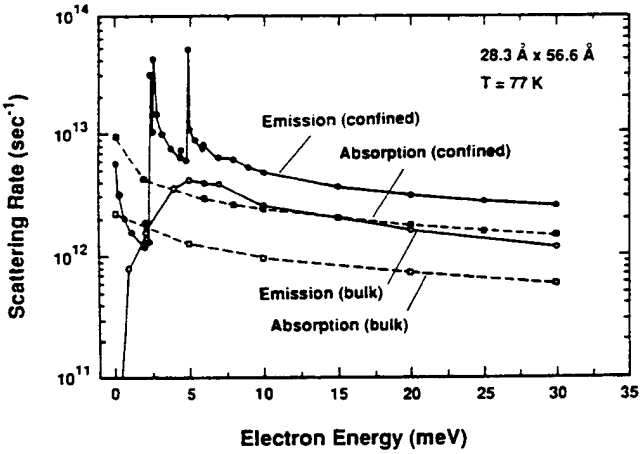

FIG. 4. Deformation-potential scattering rates for bulk and confined acoustic-phonon modes in a 28.3×56.6-Å^2 GaAs quantum wire at 77 K. Enhancements in the scattering rates for the case of confined acoustic modes occur at the onset of emission for the various width and thickness modes. These thresholds are at 0.03, 2.36, 2.55, 4.90, 7.30, and 7.40 meV for the width modes, and at 2.06, 4.44, 5.90, 9.87, 14.5, and 15.1 meV for the thickness modes. The plotting resolution depicted is not fine enough to illustrate fully the importance of the density-of-states effects in the rectangular quantum wire.

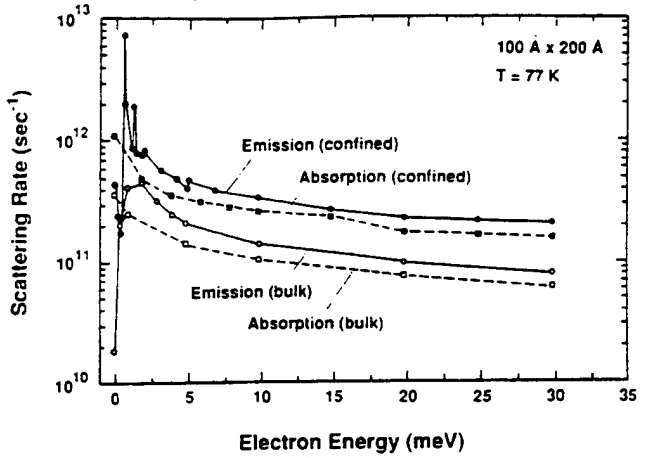

FIG. 5. Deformation-potential scattering rates for bulk and confined acoustic-phonon modes in a 100×200-Å^2 GaAs quantum wire at 77 K. Enhancements in the scattering rates for the case of confined acoustic modes occur at the onset of emission for the various width and thickness modes. These thresholds are at 0.03, 0.65, 0.75, 1.39, 2.06, and 2.12 meV for the width modes, and at 0.59, 1.26, 1.68, 2.80, 4.11, and 4.28 meV for the thickness modes. As in Fig. 4, the plotting resolution is limited.

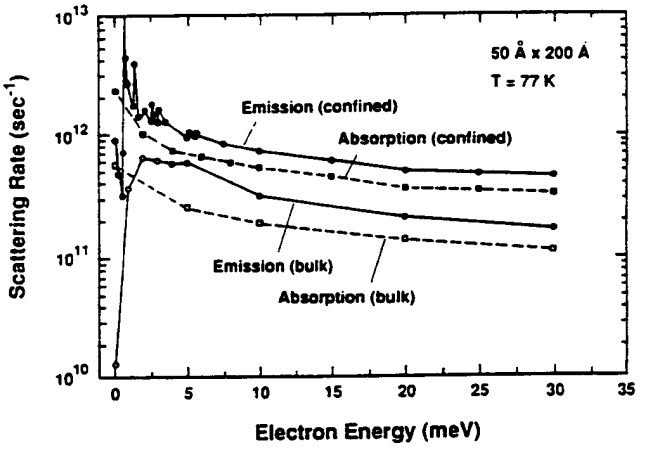

FIG. 6. Deformation-potential scattering rates for bulk and confined acoustic-phonon modes in a 50×200-Å^2 GaAs quantum wire at 77 K. Enhancements in the scattering rates for the case of confined acoustic modes occur at the onset of emission for the various width and thickness modes. These thresholds are at 0.03, 0.65, 0.75, 1.39, 2.06, and 2.12 meV for the width modes, and at 0.61, 2.58, 3.05, 5.56, 8.24, and 8.43 meV for the thickness modes. As in Figs. 4 and 5, the plotting resolution is limited.

seen from Figs. 4–6, each of these modes makes a notable contribution to the density of states and to the scattering rate. In particular, the scattering rates at low energies show pronounced peaks and are strongly enhanced due to the dominance of selected compressional modes in the emission process. Thus, it is essential to retain a number of acoustic modes for an accurate estimation of scattering rates. The results shown in Figs. 4–6 have been obtained by including the six lowest-order thickness modes as well as the six lowest-order width modes. Due to the limited resolution in plotting, the details of one-dimensional nature (such as the number of peaks and their heights) are not illustrated fully in these figures. The second important feature of Figs. 4–6 is that the scattering rates for the case of the hybrid compressional modes are higher than the corresponding bulk scattering rates. These enhanced scattering rates provided an indication that conceptual designs for mesoscopic devices need to be based on an awareness of the fact that confined acoustic modes may play a significant role in carrier transport in these devices. As shown in Fig. 5, for the case of a 100×200-Å^2 cross section we find similar scaling of the scattering rates with energy as for the case of Fig. 4; however, the rates are approximately an order of magnitude lower than those for the 28.3×56.6-Å^2 quantum wire of Fig. 4.

The hybrid modes considered in this paper contain both longitudinal and transverse components as is evident from Eqs. (15)–(18); as expected, only the longitudinal components contribute to the deformation potential of Eq. (35). The appearance of a hybrid-mode dispersion relation, Eq. (14), similar to that for the dilatational modes of a slab[18] is entirely reasonable, since the flexural modes are similar to the shear modes.[19] Such modes have strong transverse components and they make little contribution to electron–acoustic-phonon interaction through the deformation potential.

V. CONCLUSION

The results in this analysis suggest that it may be important to consider carrier–acoustic-phonon scattering processes when designing mesoscopic devices containing quantum-wire elements. Based on what appears to be the most complete set of approximate compressional modes available for a free-standing rectangular quantum wire,[16] it is demonstrated that the details of the modal structure need to be taken into account if deformation-potential scattering is to be modeled accurately. Further analysis is necessary to rigorously show that deformation-potential scattering rates by confined acoustic phonons exceed the corresponding rates obtained from bulk phonons in quantum wires; however, these results provide an indication that acoustic-phonon scattering may be enhanced considerably in some nanoscale structures.

ACKNOWLEDGMENTS

The authors would like to thank Dr. James W. Mink for his support and Professor M. N. Wybourne for advance information on his recent experimental evidence for acoustic-phonon confinement. The authors are also grateful to Professor V. Mitin, Dr. R. Mickevičius, and N. Bannov for many interactions on related confined-phonon effects in nanostructures. This work was supported, in part, by the Office of Naval Research and the U.S. Army Research Office.

*Also with Department of Physics, North Carolina State University, Raleigh, NC 27695.

[1]T. Kawamura and S. Das Sarma, Phys. Rev. B **45**, 3612 (1992).
[2]B. Hillebrands, S. Lee, G. I. Stegeman, H. Cheng, J. E. Potts, and F. Nizzoli, Phys. Rev. Lett. **60**, 832 (1988).
[3]J. Seyler and M. N. Wybourne, Phys. Rev. Lett. **69**, 1427 (1992); Z. V. Popvic, J. Spitzer, T. Ruf, M. Cardona, R. Notzel, and K. Ploog, Phys. Rev. B **48**, 1659 (1993).
[4]H. Benistry, C. M. Sotomayor-Torrés, and C. Weisbuch, Phys. Rev. B **44**, 10 945 (1991).
[5]B. A. Auld, *Acoustic Fields and Waves* (Wiley, New York, 1973).
[6]P. J. Price, Ann. Phys. (N.Y.) **133**, 217 (1981).
[7]N. Mori and T. Ando, Phys. Rev. B **40**, 6175 (1989).
[8]M. A. Stroscio, Phys. Rev. B **40**, 6428 (1989); K. W. Kim, M. A. Stroscio, A. Bhatt, V. V. Mitin, and R. Mickevičius, J. Appl. Phys. **70**, 319 (1991).
[9]K. W. Kim and M. A. Stroscio, J. Appl. Phys. **68**, 6289 (1990).
[10]R. Rücker, E. Molinari, and P. Lugli, Phys. Rev. B **45**, 6747 (1992).
[11]K. J. Nash, Phys. Rev. B **46**, 7723 (1992).
[12]M. A. Stroscio, G. J. Iafrate, K. W. Kim, M. A. Littlejohn, A. R. Bhatt, and M. Dutta, in *Integrated Optics and Optoelectronics*, edited by K.-K. Wong and M. Razeghi (SPIE, Bellingham, WA, 1993), Vol. CR45, p. 341.
[13]N. C. Constantinou, *Proceedings of NATO Advanced Research Workshop on Phonons in Nanostructures* (Kluwer, Boston, 1993), pp. 113–119.
[14]M. A. Stroscio and K. W. Kim, Phys. Rev. B **48**, 1936 (1993).
[15]R. W. Morse, J. Acoust. Soc. Am. **20**, 833 (1948).
[16]R. W. Morse, J. Acoust. Soc. Am. **22**, 219 (1950).
[17]R. W. Morse, Ph.D. thesis, Brown University, 1949.
[18]M. Redwood, *Mechanical Waveguides* (Pergamon, Oxford, 1960).
[19]R. A. Sykes, in *Quartz Crystals for Electrical Circuits*, edited by R. A. Heising (Van Nostrand, Toronto, 1946), p. 205.

Quantized acoustic phonon modes in quantum wires and quantum dots

Michael A. Stroscio
U.S. Army Research Office, P.O. Box 12211, Research Triangle Park, North Carolina 27709-2211

K. W. Kim and SeGi Yu[a)]
Department of Electrical and Computer Engineering, North Carolina State University, Raleigh, North Carolina 27695-7911

Arthur Ballato
Electronics and Power Sources Directorate, U.S. Army Research Laboratory, Fort Monmouth, New Jersey 07703-5601

(Received 6 April 1994; accepted for publication 30 June 1994)

Acoustic phonon modes in isotropic cubic media are derived for a number of quantum-wire and quantum-dot geometries of significant interest in nanoelectronics and optoelectronics. In each case, the mode amplitude is determined by requiring that the mode energy be given by that of the properly quantized phonon. For the case of cylindrical quantum wires and quantum dots with rectangular faces, the Hamiltonians for the deformation potential interactions are derived. These quantized acoustic modes and the associated deformation potential Hamiltonians provide a basis for modeling carrier-acoustic-phonon interactions in a variety of mesoscopic devices. Our new results supplement previous treatments of related piezoelectric effects in cylindrical quantum wires.

I. INTRODUCTION

Research on nanoscale and mesoscopic electronic and optoelectronic structures has focused extensively on carrier-phonon interactions. However, until recently this research has been based on the assumption that both optical and acoustic phonons may be treated as bulk phonons without regard to dimensional confinement effects. In the past few years, this situation has been improved as a result of numerous investigations of the properties and interactions of optical phonons in nanoscale electronic and optoelectronic structures confined in one or more spatial dimensions.[1] In spite of considerable experimental evidence on the importance of dimensional confinement in determining the properties of acoustic phonons,[2–9] there have been very few attempts to model confined acoustic phonons in electronic and optoelectronic structures having nanometer characteristic dimensions (i.e., nanoscale) and wavelike electron (i.e., mesoscopic) properties. In particular, selected acoustic phonons in nanoscale structures have been analyzed for the cases of superlattices,[10] free-standing slabs,[11] free-standing cylinders,[12] and quantum wires with rectangular cross sections.[13] In addition, confined acoustic phonons in spherical quantum dots have been analyzed in the context of excitonic dephasing.[14] In the case of the free-standing slabs,[11] the dilatational, flexural, and shear modes have all been properly quantized and appropriate deformation potential and piezoelectric interaction Hamiltonians have been derived. However, for the free-standing cylinder,[12] only the lowest-order transverse torsional mode has been considered in deriving the piezoelectric interaction Hamiltonian. In the case of a quantum wire with a rectangular cross section,[13] only approximate compressional modes (also known as dilatational modes) have been considered; as for the case of optical phonons, it is impossible to exactly satisfy all boundary conditions for the rectangular geometry.[1]

In this article, the quantized acoustic phonon modes are derived for a number of quantum-wire and quantum-dot geometries of significant interest in nanoelectronics and optoelectronics. In particular, the classical solution for the longitudinal mode of a free-standing cylinder[15–17] is quantized for a nanoscale free-standing cylinder under the assumption of a cubic, isotropic medium. (In the literature on classical acoustics, these longitudinal modes are frequently designated by the terms compressional modes or dilatational modes; they are equivalent.) This longitudinal mode is of special interest since it provides the dominant contribution to the acoustic-phonon deformation potential interaction for carriers in the radial ground state of a free-standing cylindrical quantum wire. Indeed, since the well-known deformation potential is proportional to the divergence of the acoustic phonon displacement, it follows that transverse modes make no contribution to the deformation potential. Furthermore, this article presents derivations of the normalized lowest-order breathing mode[16] (i.e., lowest-order radial compressional mode) and the normalized lowest-order torsional mode[16] (i.e., lowest-order transverse mode with shear normal to the radial direction) for a free-standing, isotropic spherical quantum dot. These modes are important for deformation potential scattering and piezoelectric scattering, respectively. Our results clearly illustrate that acoustic-phonon-assisted processes in spherical crystallites have selection rules that are sensitive to the spherical confinement geometry. Finally, this article presents the quantization procedure for approximate acoustic phonon modes for free-standing quantum dots with rectangular faces. As is well-known, such modes may be required to properly model phonon bottleneck effects in nanoscale quantum-dot structures.[18–20]

[a)]Also with Department of Physics, North Carolina State University, Raleigh, NC 27695.

 0021-8979/94/76(8)/4670/6/$6.00

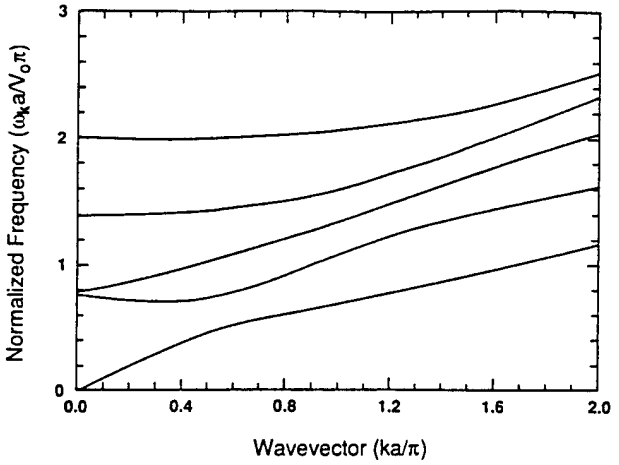

FIG. 1. Dispersion curves for the five lowest longitudinal modes of an isotropic cylinder with $\sigma=0.30$. V_0 represents the sound speed of the Young's module mode, $V_0=\sqrt{E/\rho}$.

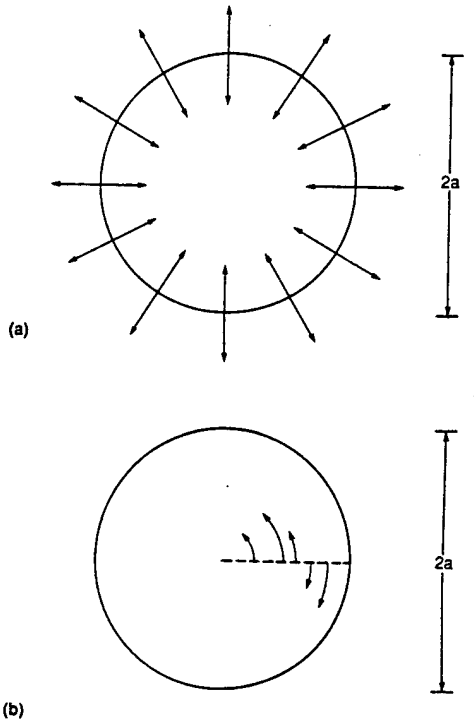

FIG. 2. Schematic lattice displacement patterns for (a) the radially directed breathing mode and (b) the azimuthally directed torsional mode in a spherical quantum dot of radius a.

II. PRESCRIPTION FOR QUANTIZING CONFINED ACOUSTIC PHONONS IN QUANTUM WIRES AND QUANTUM DOTS

The normalization of acoustic-phonon modes in quantum wires and quantum dots can be obtained by considering the average displacement energy of the phonon field.[12] By taking the acoustic-phonon displacement $\mathbf{u}(\mathbf{r})$ to be

$$\mathbf{u}(\mathbf{r})=\frac{1}{\sqrt{N}}\sum_{\mathbf{k}}[\mathbf{u}(\mathbf{k},\mathbf{r})a_{\mathbf{k}}+\text{c.c.}], \tag{1}$$

the amplitude for the $\mathbf{k}$th component of the displacement must be normalized to $\hbar/2M\omega_{\mathbf{k}}$ [i.e., $1/V\int d^3r|\mathbf{u}(\mathbf{k},\mathbf{r})|^2=\hbar/2M\omega_{\mathbf{k}}$], where M is the mass of the ions in a unit cell, $a_{\mathbf{k}}$ is the phonon annihilation operator for phonons in mode $\mathbf{k}$, $\omega_{\mathbf{k}}$ is the angular frequency, $\mathbf{r}$ is the position vector, N is the number of unit cells in the normalization volume V, and c.c. represents the complex conjugate of the first term. Throughout this article, the vector notation $\mathbf{k}$ is used to denote the phonon states (or modes), i.e., $\mathbf{k}$ represents collectively the phonon wave vector and/or discrete mode indices to specify a phonon state (which correspond to the wave vector and/or subband indices of electronic states). This provides a convenient convention since the dimension of the phonon wave vector and the number of necessary indices change with differing degrees of confinement and geometry considered in our study. For a free-standing quantum wire of infinite length and radius a, this normalization condition thus requires that

$$\frac{1}{\pi a^2}\int_0^{2\pi}d\phi\int_0^a drr\mathbf{u}^*(\mathbf{k},r,\phi,z)\cdot\mathbf{u}(\mathbf{k},r,\phi,z)=\frac{\hbar}{2M\omega_{\mathbf{k}}}, \tag{2}$$

where r defines radial locations normal to z, and ϕ is the usual azimuthal angle in the cylindrical coordinates. Likewise, for a free-standing spherical quantum dot of radius a, the normalization condition requires

$$\frac{3}{4\pi a^3}\int_0^a drr^2\int_0^{\pi}d\theta\sin\theta\int_0^{2\pi}d\phi\mathbf{u}^*(\mathbf{k},r,\theta,\phi)\cdot\mathbf{u}(\mathbf{k},r,\theta,\phi)=\frac{\hbar}{2M\omega_{\mathbf{k}}}, \tag{3}$$

where r, θ, and ϕ are the usual spherical coordinates. Finally for a free-standing quantum dot with rectangular faces the normalization condition requires

$$\frac{1}{abc}\int_{-a/2}^{a/2}dx\int_{-b/2}^{b/2}dy\int_{-c/2}^{c/2}dz\,\mathbf{u}^*(\mathbf{k},x,y,z)\cdot\mathbf{u}(\mathbf{k},x,y,z)=\frac{\hbar}{2M\omega_{\mathbf{k}}}, \tag{4}$$

where a, b, and c define the dimensions of each of the three sides of the quantum dot and x, y, and z denote the usual Cartesian coordinates. Equations (2)–(4) define the conditions needed to properly normalize the quantum-wire and quantum-dot acoustic-phonon modes discussed in this work.

III. ACOUSTIC-PHONON NORMALIZATION IN A FREE-STANDING CYLINDRICAL QUANTUM WIRE AND THE CORRESPONDING DEFORMATION POTENTIAL HAMILTONIAN

The normalization of the lowest order torsional (i.e., ϕ-independent transverse) acoustic modes in a free-standing cylindrical quantum wire have been considered previously;[12] accordingly, the current derivation focuses on the corresponding longitudinal, ϕ-independent, acoustic modes. It is

well-known that these longitudinal modes in a free-standing isotropic, cubic medium of cylindrical geometry have only radial and axial displacements given by[15–17]

$$u_r(\mathbf{k},r,z)=\left\{\frac{d}{dr}\left[AJ_0(pr)+BJ_0(qr)\right]\right\}e^{ik(z-vt)}, \tag{5}$$

$$u_z(\mathbf{k},r,z)=i\left[\frac{-p^2}{k}AJ_0(pr)+kBJ_0(qr)\right]e^{ik(z-vt)}, \tag{6}$$

where J_0 and J_1 are the ordinary Bessel functions, k is the phonon wave-vector component in the z direction, v is the phonon phase velocity, and A and B are normalization constants. [As defined in Eq. (1), $|\mathbf{k}|\neq k$; $\mathbf{k}$ denotes other indices as well.] In addition, p and q are defined by

$$p^2=k^2\left[\frac{\rho v^2}{\mu}-1\right], \tag{7}$$

$$q^2=k^2\left[\frac{\rho v^2}{\lambda'+2\mu}-1\right], \tag{8}$$

where λ' and μ are the Lamé constants, and ρ is the density of the medium. The proportionality between the normalization constants B and A defines the quantity β through $\beta=B/A$; this relation is specified by Eqs. (5) and (6) coupled with the boundary condition where the tractions across the cylindrical surface vanish at $r=a$. For the general case, this relationship is defined by the following set of equations

$$B\left[2\mu\frac{\partial^2 J_0(qa)}{\partial a^2}-\frac{v^2k^2\rho\lambda'}{\lambda'+2\mu}J_0(qa)\right]-2A\mu p\frac{\partial J_1(pa)}{\partial a}=0, \tag{9}$$

$$2Bk\frac{\partial J_0(qa)}{\partial a}-A\frac{p}{k}\left[2k^2-\frac{v^2k^2\rho}{\mu}\right]J_1(pa)=0. \tag{10}$$

The dispersion relation and the ratio B/A are obtained from these two relations. Figure 1 shows dispersion curves for the five lowest modes as a function of ka, where V_0 represents the sound speed of the Young's module mode, $V_0=\sqrt{E/\rho}=\sqrt{\mu(3\lambda'+2\mu)/(\lambda'+\mu)\rho}$. Due to the oscillatory nature of Bessel functions, Eqs. (9) and (10) give multiple solutions for a given k value. Consequently, additional indices (i.e., other than k) are needed to denote a specific phonon state, which are collectively represented by $\mathbf{k}$ as mentioned previously. Since the longitudinal modes are ϕ-independent, the normalization condition of Eq. (2) then gives

$$\begin{aligned}\frac{\hbar}{2M\omega_{\mathbf{k}}}&=\frac{2}{a^2}\int_0^a drr(u_ru_r^*+u_zu_z^*)\\&=\frac{2A^2}{a^2}\int_0^a drr\left[\frac{p^4}{k^2}J_0^2(pr)-2p^2\beta J_0(pr)J_0(qr)\right.\\&\quad+k^2\beta^2J_0^2(qr)+p^2J_1^2(pr)\\&\quad\left.+2pq\beta J_1(pr)J_1(qr)+q^2\beta^2J_1^2(qr)\right],\end{aligned} \tag{11}$$

and upon performing the integrations it is possible to arrive at the following analytical expression for A

$$A=\frac{a}{2}\sqrt{\frac{\hbar}{M\omega_{\mathbf{k}}}}\Big/\sqrt{\sigma}, \tag{12}$$

where

$$\begin{aligned}\sigma=\left\{\right.&\frac{p^4}{k^2}\frac{a^2}{2}[J_1^2(pa)+J_0^2(pa)]-2p^2\beta\frac{a}{q^2-p^2}[qJ_1(qa)J_0(pa)-pJ_1(pa)J_0(qa)]+k^2\beta^2\frac{a^2}{2}[J_1^2(qa)+J_0^2(qa)]\\&+p^2\frac{a^2}{2}[J_1^2(pa)-J_0(pa)J_2(pa)]+2pq\beta\frac{a}{q^2-p^2}[pJ_0(pa)J_1(qa)\\&\left.-qJ_0(qa)J_1(pa)]+q^2\beta^2\frac{a^2}{2}[J_1^2(qa)-J_0(qa)J_2(qa)]\right\}.\end{aligned} \tag{13}$$

The deformation potential Hamiltonian H_{def} for the case of spherically symmetric constant energy surfaces is given in terms of the deformation potential constant E_a and the dilatation $\Delta(\mathbf{r})=\nabla\cdot\mathbf{u}(\mathbf{r})$ by[21]

$$H_{\text{def}}=E_a\Delta(\mathbf{r})=\frac{E_a}{\sqrt{N}}\sum_{\mathbf{k}}\left\{\left[\frac{1}{r}\frac{\partial(ru_r)}{\partial r}+\frac{\partial u_z}{\partial z}\right]a_{\mathbf{k}}+\text{c.c.}\right\}. \tag{14}$$

Accordingly, with Eqs. (5) and (6),

$$H_{\text{def}}=-\frac{1}{\sqrt{N}}\sum_{\mathbf{k}}[E_aA(q^2+k^2)\beta J_0(qr)e^{ik(z-vt)}a_{\mathbf{k}}+\text{c.c.}], \tag{15}$$

where the normalization constant A is given by Eqs. (12) and (13).

IV. NORMALIZATION OF ACOUSTIC PHONON MODES IN QUANTUM DOTS

The classical solutions of pure compressional modes for a free-standing, isotropic sphere have been analyzed previ-

ously and are given in a convenient form in Ref. 16. For the lowest-order compressional mode, also known as the breathing mode, the acoustic-phonon displacement of a sphere of radius a is given by

$$\mathbf{u}(\mathbf{k},r)=\hat{r}\gamma j_1\left(\frac{\omega_{\mathbf{k}}r}{V_l}\right)e^{-i\omega_{\mathbf{k}}t}, \tag{16}$$

where $\hat{r}$ is the unit vector in radial direction, γ is the normalization constant, V_l is the longitudinal sound speed, $V_l = \sqrt{(\lambda'+2\mu)/\rho}$, and j_1 is the spherical Bessel function of order one, $j_1(x)=\sin x/x^2-\cos x/x$, and the mode frequency $\omega_{\mathbf{k}}$ is determined by the condition that the traction force on the spherical surface T_{rr} vanishes at $r=a$. That is

$$T_{rr}=0 \quad \text{at } r=a, \tag{17}$$

or equivalently,

$$\left[(\lambda'+2\mu)\frac{d^2}{dr^2}j_0\left(\frac{\omega_{\mathbf{k}}r}{V_l}\right)+\frac{2\lambda'}{r}\frac{d}{dr}j_0\left(\frac{\omega_{\mathbf{k}}r}{V_l}\right)\right]_{r=a}=0, \tag{18}$$

in these results, j_0 is the spherical Bessel function of order zero, $j_0(x)=\sin x/x$. Equations (17) and (18) yield the dispersion relation

$$\tan\left(\frac{\omega_{\mathbf{k}}a}{V_l}\right)=\frac{\omega_{\mathbf{k}}a/V_l}{1-\dfrac{\lambda'+2\mu}{4\mu}(\omega_{\mathbf{k}}a/V_l)^2}. \tag{19}$$

For the breathing mode of Eq. (16), the normalization condition of Eq. (3) reduces to

$$\frac{3\gamma^2}{\bar{\omega}_l^3}\int_0^{\bar{\omega}_l}dr\,r^2j_1^2(r)=\frac{\hbar}{2M\omega_{\mathbf{k}}}, \tag{20}$$

where $\bar{\omega}_l = \omega_{\mathbf{k}}a/V_l$. Accordingly, the normalization constant γ for the longitudinal breathing mode is

$$\gamma=\frac{1}{\sqrt{j_1^2(\bar{\omega}_l)-j_0(\bar{\omega}_l)j_2(\bar{\omega}_l)}}\sqrt{\frac{\hbar}{3M\omega_{\mathbf{k}}}}, \tag{21}$$

where j_2 is the spherical Bessel function of order two, $j_2(x)=1/x(3/x^2-1)\sin x-3\cos x/x^2$. Hence, the normalization constant of the lowest-order breathing mode of a free-standing, isotropic sphere may be determined analytically.

In addition, the lowest-order pure shear mode, also known as the torsional mode, of a free-standing isotropic nanoscale sphere may be determined from the classical solution:[16]

$$\mathbf{u}(\mathbf{k},r,\theta)=\hat{\phi}\tau\cos\theta j_1\left(\frac{\omega_{\mathbf{k}}r}{V_s}\right)e^{-i\omega_{\mathbf{k}}t}, \tag{22}$$

where $\hat{\phi}$ is the unit vector in the ϕ direction, τ is the normalization constant, and V_s denotes the speed of propagation for shear modes, $V_s = \sqrt{\mu/\rho}$. In this case, the normalization condition of Eq. (3) reduces to

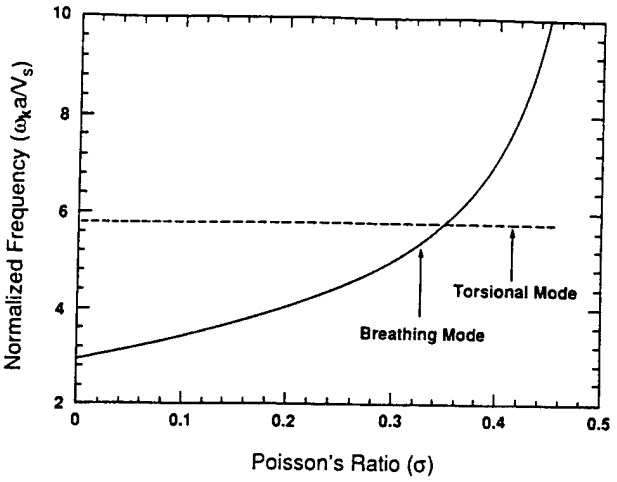

FIG. 3. Relation between mode frequencies and Poisson ratios for an isotropic sphere. The solid line denotes the lowest-order breathing mode and the dashed line is for the lowest-order torsional mode. V_s represents the shear sound speed.

$$\frac{\tau^2}{\bar{\omega}_s^3}\int_0^{\bar{\omega}_s}dr\,r^2j_1(r)=\frac{\hbar}{2M\omega_{\mathbf{k}}}, \tag{23}$$

where $\bar{\omega}_s = \omega_{\mathbf{k}}a/V_s$, and it follows that

$$\tau=\frac{1}{\sqrt{j_1^2(\bar{\omega}_s)-j_0(\bar{\omega}_s)j_2(\bar{\omega}_s)}}\sqrt{\frac{\hbar}{M\omega_{\mathbf{k}}}}. \tag{24}$$

Again, it is possible to specify the normalization constant analytically. For the torsional modes, the dispersion relation may be derived in a manner analogous to that used to derive Eq. (19); the result is

$$\tan\left(\frac{\omega_{\mathbf{k}}a}{V_s}\right)=\frac{\omega_{\mathbf{k}}a/V_s}{1-\frac{1}{3}(\omega_{\mathbf{k}}a/V_s)^2}. \tag{25}$$

Figure 2 shows the schematic drawing of the lowest-order longitudinal mode [Fig. 2(a)] and the lowest-order torsional mode [Fig. 2(b)]; the corresponding relationships between mode frequencies and Poisson ratios are depicted in Fig. 3.

As previously discussed for the case of a quantum wire with a rectangular cross section,[13] it is impossible to satisfy all boundary conditions for a quantum dot with rectangular faces. This difficulty in rigorously satisfying all boundary conditions results because the corner regions of the rectangular cross section represent singular points where, in general, the boundary conditions on adjacent faces require different fields at a given corner. Perhaps, the best-known case of this so-called corner problem is in electromagnetics where only approximate analytical solutions are obtainable for rectangular waveguides. However, an approximate solution, particularly in an analytical form, may prove to be useful to model confined phonons in nanoscale structures. To illustrate the procedure of quantizing the acoustic phonon modes in such quantum dots, this article considers the modes derived by McSkimin.[22] In particular, only the modes which correspond to flexural thickness modes of the quantum dot are

quantized as an example; there are, of course, similar width and length modes, as well as analogous compressional modes, as illustrated in Refs. 13 and 23 for the less complex case of a quantum wire. In McSkimin's approximate solution for the flexural thickness mode in a quantum dot with rectangular faces, the x-, y-, and z-directed displacements (denoted by u, v, and w, respectively) are written as

$$u(\mathbf{k},x,y,z)=A[\sin l_1 y+\alpha' \sin l_2 y + \beta' \sin l_2 y]\sin mx \cos nz, \tag{26}$$

$$v(\mathbf{k},x,y,z)=A\left[\frac{-l_1}{m}\cos l_1 y-\frac{\alpha' l_2}{m}\cos l_2 y + \frac{\beta'(m^2+n^2)}{l_2 m}\cos l_2 y\right]\cos mx \cos nz, \tag{27}$$

$$w(\mathbf{k},x,y,z)=A\left[\frac{n}{m}\sin l_1 y-\alpha' \frac{(m^2+l_2^2)}{nm}\sin l_2 y + \beta' \frac{n}{m}\sin l_2 y\right]\cos mx \sin nz, \tag{28}$$

where α' and β' are determined by applying desired boundary conditions on two sets of rectangular face. The discrete mode indices for the phonon in state $\mathbf{k}$ are presented by m and n for the x- and z-components, respectively. Two additional indices, l_1 and l_2, are required for the y-component where l_1 is the subject mode index for the irrotational contribution to the phonon displacement and l_2 is the subject mode index for the rotational contribution. This decomposition into rotational and irrotational components is discussed in standard texts on acoustics including those identified in Refs. 15 and 16. From Eq. (4), it follows that A is determined by

$$\frac{\hbar}{2M\omega_{\mathbf{k}}}=\frac{A}{abc}\Bigg\{f_2(m,a/2)f_1(n,c/2)[f_2(l_1,b/2)+2\alpha' g_1(l_1,l_2,b/2)+2\beta' g_1(l_1,l_2,b/2)+\alpha'^2 f_2(l_2,b/2) + 2\alpha'\beta' f_2(l_2,b/2)+\beta'^2 f_2(l_2,b/2)]+f_1(m,a/2)f_1(n,c/2)\Bigg[\frac{l_1^2}{m^2}f_1(l_1,b/2) + \frac{2\alpha' l_1 l_2}{m^2}g_2(l_1,l_2,b/2)-\frac{2\beta' l_1(m^2+n^2)}{l_2 m^2}g_2(l_1,l_2,b/2)+\frac{\alpha'^2 l_2^2}{m^2}f_1(l_2,b/2)-\frac{2\alpha'\beta' l_2(m^2+n^2)}{l_2 m^2}f_1(l_2,b/2) + \frac{\beta'^2(m^2+n^2)^2}{l_2^2 m^2}f_1(l_2,b/2)\Bigg]+f_1(m,a/2)f_2(n,c/2)\Bigg[\frac{n^2}{m^2}f_2(l_1,b/2)-\frac{2\alpha' n(n^2+l_2^2)}{nm^2}g_1(l_1,l_2,b/2) + \frac{2\beta' n^2}{m^2}g_1(l_1,l_2,b/2)+\frac{\alpha'^2(m^2+l_2^2)^2}{n^2 m^2}f_2(l_2,b/2)-\frac{2\alpha'\beta' n(m^2+l_2^2)}{nm^2}f_2(l_2,b/2)+\frac{\beta'^2 n^2}{m^2}f_2(l_2,b/2)\Bigg]\Bigg\}, \tag{29}$$

where

$$f_1(n,c/2)=\frac{c}{2}\left(1+\frac{\sin nc}{nc}\right), \tag{30}$$

$$f_2(n,c/2)=c-f_1(n,c/2), \tag{31}$$

$$g_1(l_i,l_j,b/2)=\frac{\sin(l_i-l_j)b/2}{l_i-l_j}-\frac{\sin(l_i+l_j)b/2}{l_i+l_j}, \tag{32}$$

$$g_2(l_i,l_j,b/2)=\frac{\sin(l_i-l_j)b/2}{l_i-l_j}+\frac{\sin(l_i+l_j)b/2}{l_i+l_j}. \tag{33}$$

The deformation potential H_{def} corresponding to the displacements of Eqs. (26)–(28) simplifies greatly for the case of spherically symmetric energy surfaces, and results in

$$H_{\text{def}}=E_a\Delta(\mathbf{r})=\frac{E_a}{\sqrt{N}}\sum_{\mathbf{k}}\left[\left(\frac{\partial u}{\partial x}+\frac{\partial v}{\partial y}+\frac{\partial w}{\partial z}\right)a_{\mathbf{k}}+\text{c.c.}\right] = \frac{1}{\sqrt{N}}\sum_{\mathbf{k}}\left[\frac{E_a A}{m}(m^2+l_1^2+n^2) \times\cos mx \sin l_1 y \cos nz\, a_{\mathbf{k}}+\text{c.c.}\right]. \tag{34}$$

In particular, the spatially dependent terms in H_{def} do not depend on α' and β'; thus, the α' and β' dependence of the deformation potential enters only in the normalization constant A.

V. SUMMARY

In this article, the normalized acoustic phonon modes have been derived for a number of potentially useful

quantum-wire and quantum-dot geometries. Specifically, the longitudinal, or compressional, acoustic mode in a free-standing cylindrical quantum wire has been normalized analytically. This result has special significance since quantum-wire components are widely envisioned for mesoscopic devices and since analytical solutions are not available for quantum wires with rectangular cross sections. Unlike the modes considered in Refs. 13 and 23, the modes presented in this article are not subject to the assumption of stress boundary conditions which are separable in the lateral coordinates of the quantum wire. Accordingly, the acoustic mode displacements as well as the deformation potential Hamiltonian discussed in this work are exact for a free-standing cylindrical quantum wire. Additional, new results presented in this article include the analytic normalization of the lowest-order breathing and lowest-order torsional modes in a spherical quantum dot. The fact that these modes can be normalized analytically is especially significant since the symmetries of these modes indicate clearly that it is essential to use confined acoustic modes in modeling acoustic-phonon-assisted processes in nanoscale spherical crystallites. In particular, it is clear from the depiction of the quantum-dot modes in Fig. 2 that bulk, or plane wave, acoustic phonons do not possess the correct spatial symmetries. Accordingly, the acoustic phonons modes for spherical quantum dots presented in this article provide the basis for properly calculating acoustic-phonon-assisted processes. Finally, the approximate flexural thickness modes of a quantum dot with rectangular faces have been normalized to illustrate the proper quantization procedure for the acoustic phonon modes in these nanostructures. It is expected that such quantum dot modes will be useful in modeling phonon bottleneck effects in quantum dots. In conclusion, this article provides quantized acoustic phonon modes and associated deformation potential Hamiltonians which are necessary for modeling carrier-acoustic-phonon interactions in a variety of mesoscopic devices.

ACKNOWLEDGMENTS

The authors gratefully acknowledge the many fruitful discussions with Dr. G. J. Iafrate, Dr. J. W. Mink, Professor M. A. Littlejohn, Dr. Mitra Dutta, Professor V. Mitin, N. Bannov, and Dr. H. Everitt. The authors would also like to thank Professor M. N. Wybourne for information on recent experimental evidence on acoustic-phonon confinement. The authors are also grateful to Patricia Lassiter for the excellent preparation of the manuscript. This research was supported, in part, by the U.S. Army Research Office and the Office of Naval Research.

[1] See, for example, M. A. Stroscio, G. J. Iafrate, K. W. Kim, M. A. Littlejohn, A. Bhatt, and M. Dutta, in *Integrated Optics and Optoelectronics*, edited by K.-K. Wong and M. Razeghi (SPIE, Bellingham, WA, 1993), Vol. CR-45, p. 341.
[2] J. Seyler and M. N. Wybourne, Phys. Rev. Lett. **69**, 1427 (1992); A. Tanaka, S. Onari, and T. Arai, Phys. Rev. B **47**, 1237 (1993).
[3] Z. V. Popovic, J. Spitzer, T. Ruf, M. Cardona, R. Notzel, and K. Ploog, Phys. Rev. B **48**, 1659 (1993).
[4] P. V. Santos, A. K. Sood, M. Cardona, K. Ploog, Y. Ohmori, and H. Okamoto, Phys. Rev. B **37**, 6381 (1988).
[5] Y. F. Chen, J. L. Shen, L. Y. Lin, and Y. S. Huang, J. Appl. Phys. **73**, 4555 (1993).
[6] A. Potts, M. J. Kelly, C. G. Smith, D. G. Hasko, J. R. A. Cleaver, H. Ahmed, D. C. Peacock, D. A. Ritchie, J. E. F. Frost, and G. A. C. Jones, J. Phys: Condens. Matter **2**, 1817 (1990).
[7] C. Colvard, T. A. Gant, M. V. Klein, R. Merlin, R. Fisher, H. Morkoç, and A. C. Gossard, Phys. Rev. B **31**, 2080 (1985).
[8] R. Bhadra, M. Grimsditch, I. K. Schuller, and F. Nizzoli, Phys. Rev. B **39**, 12456 (1989).
[9] M. Grimsditch, R. Bhadra, and I. K. Schuller, Phys. Rev. Lett. **58**, 1216 (1987).
[10] See, for example, S. Tamura and F. Nori, Phys. Rev. B **41**, 7941 (1990).
[11] N. Bannov, V. Mitin, and M. Stroscio, in *Proceedings of the 1993 International Semiconductor Device Research Symposium*, edited by M. Shur and E. Towe (University of Virginia Press, Charlottesville, VA, 1993), p. 659.
[12] M. A. Stroscio and K. W. Kim, Phys. Rev. B **48**, 1936 (1993); M. A. Stroscio, G. J. Iafrate, K. W. Kim, S. Yu, V. Mitin, and N. Bannov, in *Proceedings of the 1993 International Semiconductor Device Research Symposium*, edited by M. Shur and E. Towe (University of Virginia Press, Charlottesville, VA, 1993), p. 873.
[13] K. W. Kim, S. Yu, M. U. Erdoğan, M. A. Stroscio, and G. J. Iafrate, in *Ultrafast Phenomena in Semiconductors*, edited by D. K. Ferry and H. M. Van Driel (SPIE, Bellingham, WA, 1994), Vol. 2142, p. 77.
[14] T. Takagahara, Phys. Rev. Lett. **71**, 3577 (1993).
[15] A. E. H. Love, *A Treatise on the Mathematical Theory of Elasticity*, 4th ed. (Dover, New York, 1944), p. 288.
[16] B. A. Auld, *Acoustic Fields and Waves* (Wiley, New York, 1973).
[17] V. G. Grigoryan and D. G. Sedrakyan, Sov. Phys. Acoust. **29**, 281 (1983).
[18] H. Benistry, C. M. Sotomayor Torres, and C. Weisbuch, Phys. Rev. B **44**, 10945 (1991).
[19] R. de la Cruz, S. Teitsworth, and M. A. Stroscio, Superlatt. Microstruct. **13**, 481 (1993).
[20] H. Noguchi, J. P. Leburton, and H. Sakaki, Phys. Rev. B **47**, 15593 (1993).
[21] This form of the deformation potential was introduced originally by J. Bardeen and W. Shockley; numerous texts present the derivation of this deformation potential and an especially clear exposition of its derivation may be found in K. Hess, *Advanced Theory of Semiconductor Devices* (Prentice Hall, Englewood Cliffs, NJ, 1988), p. 90.
[22] H. J. McSkimin, Bell Syst. Tech. J. **23**, 151 (1944).
[23] R. W. Morse, J. Acoust. Soc. Am. **22**, 219 (1949).

PHYSICAL REVIEW B VOLUME 51, NUMBER 7 15 FEBRUARY 1995-I

Electron–acoustic-phonon scattering rates in cylindrical quantum wires

SeGi Yu* and K. W. Kim
Department of Electrical and Computer Engineering, North Carolina State University, Raleigh, North Carolina 27695-7911

Michael A. Stroscio and G. J. Iafrate
U.S. Army Research Office, P.O. Box 12211, Research Triangle Park, North Carolina 27709-2211
(Received 1 December 1994)

The electron–acoustic-phonon scattering rates in a cylindrical quantum wire are studied. Considering the quantum wire as an elastic continuum, the confined-phonon dispersion relation is calculated for two cardinal boundary conditions: free-surface and clamped-surface boundary conditions. The scattering rates due to the deformation-potential interaction are obtained for these two confined phonons and are compared with those of bulklike phonons. The results show that the inclusion of acoustic-phonon confinement effects may be crucial for calculating accurate low-energy-electron scattering rates in nanostructures. It is also demonstrated that the anisotropy should not be ignored for materials of cubic symmetry.

Proposed applications of mesoscopic electronic structures involve carrier transport at low temperatures and low carrier energies. In many cases, the regime of interest is one where dimensional confinement modifies the phase space substantially. In this low-temperature, low-energy regime,[1–7] acoustic phonons play an enhanced role in carrier scattering and may dominate over the scattering of carriers by optical phonons. Furthermore, in nanoscale structures it is possible that phase-space restrictions may weaken or forbid optical-phonon scattering processes that would normally dominate in bulk structures. In recent years, there has been an extensive literature on the role of dimensional confinement in modifying longitudinal-optical phonon modes and their interactions with charge carriers in nanoscale and mesoscopic semiconductor structures (see, for example, Refs. 8–10, and the numerous papers referenced therein); however, there are relatively few treatments dealing with the role of dimensional confinement in modifying acoustic-phonon modes and their interactions with charge carriers.[1–3,11,12] In particular, few efforts have been reported that formulate a theory of the electron–acoustic-phonon interaction in nanoscale structures where the treatment of acoustic-phonon confinement effects may be essential.[13–15] The need for such theoretical treatments has been demonstrated recently by experimental studies[1–5,7,11] providing both direct and indirect evidence of the importance of acoustic-phonon confinement in reduced-dimensional electronic structures. In this paper, we present golden-rule scattering rates for the electron interaction with confined acoustic phonons in a mesoscopic quantum wire with cylindrical geometry. A quantized description of acoustic-phonon modes (developed under the elastic-continuum model) is used to formulate the deformation-potential Hamiltonian. As for the case of rectangular quantum wires,[14] it is found that a proper treatment of confined acoustic phonons in cylindrical quantum wires may be crucial to correctly model electron-scattering rates at low energies in nanoscale structures.

In the limit of long-wavelength acoustic phonons, it is sufficient to treat the material as an elastic continuum. A number of experiments confirm the usefulness of the continuum model in nanostructures.[3–5,7] A cylindrical quantum wire of infinite length in the z direction with radius a is assumed for materials of isotropic symmetry. In this paper, we consider only the longitudinal modes of the confined acoustic phonons since the dominant contribution to the electron–acoustic-phonon interaction through the deformation potential comes from these modes. These longitudinal modes are well established in an isotropic medium of a cylinder,[16] and the normalization of confined phonons and the deformation Hamiltonian have been reported previously in Ref. 15. The acoustic waves move in radial planes without an azimuthal angle dependence, and the displacements are given by

$$u_r(r,z)=\left[\frac{d}{dr}\{BJ_0(k_d r)+AJ_0(k_t r)\}\right]e^{i(kz-\omega t)}, \quad (1a)$$

$$u_z(r,z)=i\left[kBJ_0(k_d r)+\frac{-k_t^2}{k}AJ_0(k_t r)\right]e^{i(kz-\omega t)}, \quad (1b)$$

where J_0 and J_1 are the ordinary Bessel functions, A and B are constants to be determined later, ω is an angular frequency, and k is the z-component wave vector. In addition, k_d and k_t are represented as

$$k_{d,t}^2=\frac{\omega^2}{v_{d,t}^2}-k^2, \quad (2)$$

where v_d (v_t) is the longitudinal (transverse) velocity. The longitudinal waves are coupled modes of axial and radial modes that have the quantized wave vectors k_t and k_d, respectively. In a cylinder, these two partial waves are coupled to satisfy the boundary condition (BC) at the surface in a manner similar to that for Lamb waves in a free isotropic plate.[16]

The general BC's for the confined acoustic phonons are that the displacement ($\vec{u}$) and the normal components of stress ($\vec{T}\cdot\hat{n}$), or the tractional force, are continuous across surfaces where the elastic properties change discontinuously. For simple cases, there are two cardinal BC's: the free-

0163-1829/95/51(7)/4695(4)/$06.00

surface BC (FSBC) and the clamped-surface BC (CSBC). The free surface is a boundary between an elastic material and vacuum where the normal components of the stress tensor are zero and the displacement is unrestricted. The clamped surface is a boundary between an elastic material and a perfectly rigid material where the displacement is zero and the normal components of the stress tensor are unrestricted. Although most quantum wires are not surrounded by vacuum or by an extraordinarily hard material, the use of these two cardinal BC's is employed frequently in classical acoustics for cases where analytical solutions are hard to find. Furthermore, the calculation for the FSBC case may be applied to free-standing quantum wires fabricated by lateral etching techniques. As a result, we have adopted these two BC's to investigate the electron–acoustic-phonon interaction in the present paper.

The dispersion relations of confined phonons and the constant ratios $\beta=B/A$ are obtained from the BC's. The dispersion relation for confined phonons with the FSBC is

$$(k^2-k_t^2)^2\frac{(k_da)J_0(k_da)}{J_1(k_da)}-2k_d^2(k^2+k_t^2)+4k^2k_d^2\frac{(k_ta)J_0(k_ta)}{J_1(k_ta)}=0, \quad (3)$$

and that for phonons with the CSBC is

$$k_d^2\frac{(k_ta)J_0(k_ta)}{J_1(k_ta)}+k^2\frac{(k_da)J_0(k_da)}{J_1(k_da)}=0. \quad (4)$$

(On the other hand, the bulklike phonons are dispersionless; i.e., phase velocity is constant with respect to the wave vector.) The constant ratios for β are given by

$$\beta=-\frac{k_t(k^2-k_t^2)}{2k^2k_d}\frac{J_1(k_ta)}{J_1(k_da)}$$

for FSBC and

$$\beta=\frac{k_t^2}{k^2}\frac{J_0(k_ta)}{J_0(k_da)}$$

for CSBC. The individual values of A and B are determined by phonon normalization.[15]

The Hamiltonian describing the deformation-potential interaction for the electron and the acoustic phonon is expressed such that $H_{\rm def}=-E_a\vec{\nabla}\cdot\vec{u}$, where E_a is the deformation-potential constant. Hence, in the confined phonon case the longitudinal modes are more important than torsional and flexural modes as discussed before. In the bulklike phonon case, only the modes vibrating parallel to the propagation direction contribute to the scattering rates, and accordingly the transverse velocity does not appear. The electrons confined in a cylindrical quantum wire are assumed to be the ground state in the extreme quantum limit. Finally, the scattering rates for the deformation potential are calculated using standard procedures and assuming the Fermi golden rule.

Although it is mathematically easy to treat acoustic waves in an isotropic material, there are few materials of isotropic symmetry. Furthermore, the symmetry of most semiconductor materials of interest is not isotropic but cubic. The acoustic waves in these materials may be determined directly for the case of the cubic symmetry or through proper analysis under the assumption that the material is isotropic. The acoustic-wave equation, or Christoffel equation, for the cylinder may be solved by the first approach, but there is great complexity due to the extra elastic constant that prevents one from extracting any information from the algebraic results. Accordingly, we follow the second method and analyze a range of solutions. Due to the potential technological importance of the GaAs quantum wire, calculations are confined to the case of GaAs that has cubic symmetry. This calculation can be extended to other materials of cubic symmetry without difficulty.

In isotropic materials, the slowness curve, or the inverse-velocity curve, which gives the magnitude of $\vec{k}/\omega$ as a function of its direction, consists of two concentric circles independent of the acoustic-wave-propagation characteristics.[16] On the other hand, the slowness curve for materials of cubic symmetry is more complicated than that for isotropic materials. But for the case of some special directions, the curve takes a simple form. For the propagation along any crystal axis, the curve is represented by two concentric circles that represent the pure shear wave and the pure longitudinal wave as for isotropic materials. As a result, it is possible to employ the isotropic assumption for GaAs as long as we consider propagation in the [001] direction; i.e., the case that one of the crystal axes coincides with the z direction. This is the condition we consider throughout the calculation.

Two different parameter sets are applied in order to determine the effect of the anisotropy of GaAs as well as to quantify the range of possible deformation-potential scattering rates for cylindrical quantum wires. The first set, denoted as PS1, is chosen such that the experimentally determined v_d and Poisson ratio σ fix the value of v_t from the isotropic assumption (PS1: $v_d=4.78\times10^5$ cm/sec, $v_t=2.56\times10^5$ cm/sec, $\sigma=0.33$).[17] The second set is obtained by taking v_d and v_t as the velocities of GaAs [001] propagating acoustic waves; these velocities yield a value for σ (PS2: $v_d=4.78\times10^5$ cm/sec, $v_t=3.35\times10^5$ cm/sec, $\sigma=0.018$). For both sets, the deformation-potential constant E_a and the lattice temperature are assumed to be 7.8 eV and 77 K, respectively, and five lowest modes are considered.

The scattering rates for the deformation-potential interaction of the electron with the FSBC (PS1, PS2) and the bulklike phonons are plotted in Fig. 1 as functions of electron energy. The important fact is that the FSBC scattering rates are very sensitive to the velocity of the confined phonon. The scattering rates corresponding to the PS1 and PS2 parameter sets differ substantially; indeed, the difference amounts to several orders of magnitude in the low-electron-energy region. This difference is due mainly to the different transverse velocities. To investigate the dependence of the scattering rate on velocity further, we have also considered other parameter sets that take the same values of PS1 except the value of v_t. The value of v_t is changed continuously from that of PS1 to that of PS2. In these cases, the scattering rates increase continuously with the increase in the value v_t. In particular, the enhancement is especially strong in the low-electron-energy region. The scattering rates with v_t having the value of PS2 are much higher than for PS1, and are very similar to those of the PS2 case. This finding is in striking

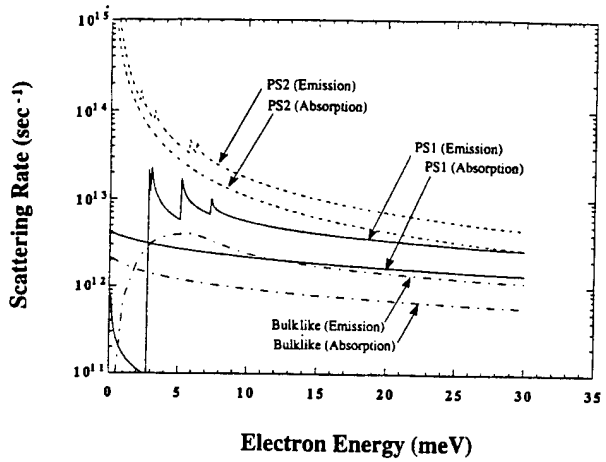

FIG. 1. Scattering rates for the deformation-potential interaction of electrons with the FSBC confined acoustic phonons (PS1, PS2) and bulklike phonons in a cylindrical GaAs quantum wire (radius of 22.6 Å) at 77 K as a function of electron energy. Solid (dashed) lines are for the PS1 (PS2), and dashed-dotted lines are for the bulklike phonons. The plotting resolution depicted is not fine enough to illustrate fully the importance of the density-of-states effects in the quantum wire.

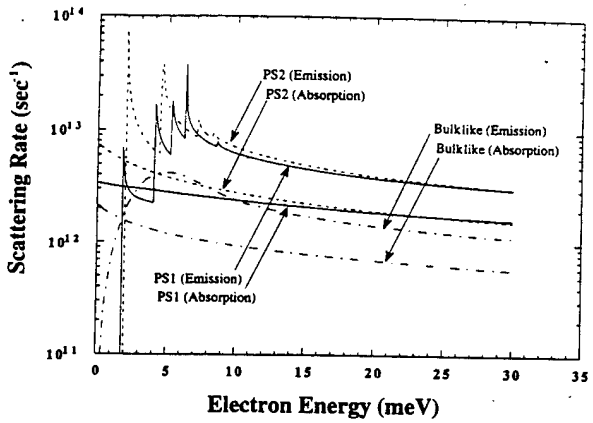

FIG. 3. Scattering rates for the deformation-potential interaction of electrons with the CSBC confined acoustic phonons (PS1, PS2) and bulklike phonons in a cylindrical quantum wire (radius of 22.6 Å) at 77 K as a function of electron energy. Solid (dashed) lines are for the PS1 (PS2), and dashed-dotted lines are for the bulklike phonons. As in Fig. 1, the plotting resolution is limited.

contrast to the case of PS1 considering that those two differ only in the value of v_t. A careful analysis reveals that the difference in the scattering rates (and, subsequently, the dependence on v_t) is associated with the lowest-phonon branch. As shown in Fig. 2, the lowest mode for the confined phonons with the FSBC has no cutoff frequency unlike the cases for the other higher modes. Hence the quantized wave vector k_t, defined in Eq. (2), of this lowest mode is very sensitive to the choice of v_t while the other are not. The magnitude of λ_t $(=2\pi/k_t)$, which corresponds to the characteristic wavelength of the axial partial wave, is a measure of the phonon amplitude. Since the deformation Hamiltonian is proportional to phonon amplitude, large values of λ_t, i.e., small k_t (or large v_t), imply large scattering rates for the deformation potential. Thus, the scattering rates are strongly affected by acoustic-phonon velocity; consequently, the electron-phonon scattering rate in a GaAs quantum wire is highly dependent on the direction of the phonon propagation due to the anisotropy of GaAs.

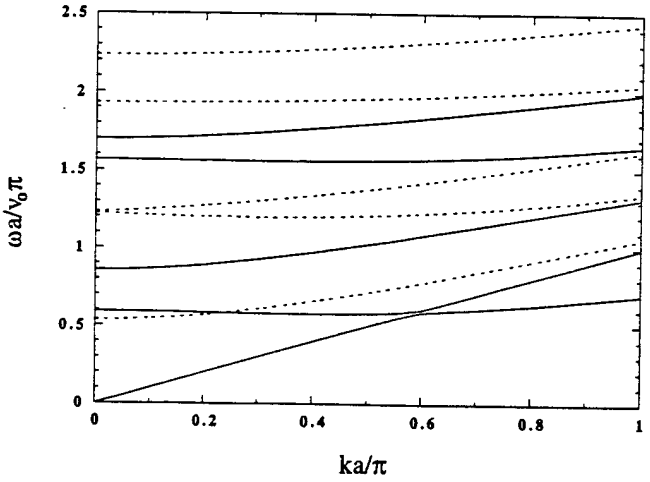

FIG. 2. Dispersion relation of the five lowest confined acoustic photons with the FSBC (solid lines) and the CSBC (dashed lines) in a cylindrical GaAs quantum wire. The value of the Poisson ratio σ is 0.018 and v_0 represents the sound velocity of Young's module mode.

Figure 3 depicts the scattering rate for the case of confined phonons with the CSBC; this plot exhibits smaller scattering rates in comparison with the case of the FSBC. The relatively small scattering rates are expected from the inspection in the functional form of the displacement. Since the CSBC requires the displacement at the boundary to be zero, the displacement of the lowest mode has maximum value at the center of the cylinder while its derivative (or divergence) is very small. This small divergence of the phonon displacement makes the electron-phonon coupling small since the electron's ground-state wave function has its maximum at the center. At the same time, the acoustic phonons with the CSBC generally have higher energies than those with the FSBC since every CSBC acoustic phonon has a cutoff frequency as shown in Fig. 2. It is difficult for the electron to emit or absorb phonons with higher energies. As a result, the relatively high energy characteristics of phonons and the small electron-phonon coupling make the scattering rate for the CSBC smaller than that for the FSBC. Another interesting point to note with the CSBC is a weak dependence on phonon velocity due to the existence of cutoff frequencies, as in the case of higher modes with the FSBC. From Figs. 1 and 3 it can be concluded that confined phonons (both with the FSBC and the CSBC) exhibit larger scattering rates than for the bulklike phonon case. Particularly in the low-electron-energy region, confined phonons exhibit much larger values as well as several peaks reflecting the characteristics of the one-dimensional density of state. Besides the large differences in values of scattering rates, the deformation-potential Hamiltonian for the bulklike phonon does not include the dependence on transverse velocity, which may have an important role in anisotropic materials.

Finally, in Fig. 4, we compare the scattering rates for a cylindrical and a rectangular wire. In the cylindrical wire

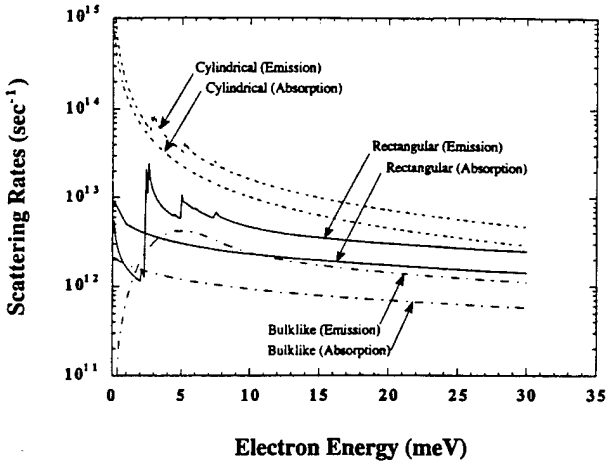

FIG. 4. Scattering rates for the deformation-potential interaction of electrons with the confined acoustic phonons in a cylindrical (dashed line) and a rectangular GaAs quantum wire (solid line). An identical cross section is chosen for the two wires (cylindrical wire of radius 22.6 Å, rectangular wire of 28.3×56.6 Å^2) and the values of parameters are the same as in Ref. 14. In the cylindrical wire confined phonons with FSBC are used, and the separable solutions for confined phonons are adopted for the rectangular wire as discussed in Ref. 14. For comparison, the rate with the bulklike phonons for the cylindrical wire is also plotted (dashed-dotted line). As in Figs. 1 and 3, the plotting resolution is limited.

confined phonons with FSBC are used, and an approximate solution as described in Ref. 14 is adopted for the rectangular geometry. The values of the parameters are taken to be those used in Ref. 14 ($v_d=4.78\times10^5$ cm/sec, $v_t=3.35\times10^5$ cm/sec, $\sigma=0.33$). When comparing two wires having a same cross-sectional area (cylindrical wire of radius 22.6 Å, rectangular wire of 28.3×56.6 Å^2), we find that there is a resemblance between the scattering rates for these two wires. Since the scattering rates for the rectangular and the cylindrical wires using bulklike phonons are very close, only the cylindrical-wire case is plotted to facilitate clear presentation of the results. The nearly identical scattering rates for the bulklike phonons can be easily understood, considering that the coupling between the electrons and the bulklike phonons are essentially the same in these two wires with the same cross-sectional area. For the confined acoustic phonons, the cylindrical wire exhibits considerably larger scattering rates than the corresponding rectangular wire. Aside from the difference in the functional form of the electron-phonon coupling (i.e., the difference in electron and phonon envelope functions), the gap in the magnitudes of the scattering rates between the cylindrical wire and the rectangular wire may be at least partly due to the incompleteness of the separable solutions used in the rectangular wire. However, the overall similarity between the rates obtained in two wires demonstrates the fact that the approximate theory developed previously for a rectangular wire[14] may be considered a valuable guideline for calculating the scattering rates in such a geometry, where an exact analytical solution does not exist.

In conclusion, we have calculated the scattering rates for the electron and several kinds of confined acoustic phonons through the deformation-potential interaction in a cylindrical quantum wire. It is found that confined phonons produce larger scattering rates than the bulklike phonons, and the scattering rates are highly dependent on the phonon propagation velocity. In addition to its relatively small scattering rates, the use of bulklike phonons in calculating electron–acoustic-phonon scattering rates may be flawed due to the neglect of anisotropic dependence on transverse velocity, which is of potential significance in many semiconductor materials and nanostructures.

The authors acknowledge many helpful discussions with Dr. A. Ballato and Professor V. Mitin. This work was supported, in part, by the Office of Naval Research and the U.S. Army Research Office.

*Also at Department of Physics, North Carolina State University, Raleigh, NC 27695-8202.

[1] B. Hillebrands, S. Lee, G. I. Stegeman, H. Cheng, J. E. Potts, and F. Nizzoli, Phys. Rev. Lett. **60**, 832 (1988).
[2] J. Seyler and M. N. Wybourne, Phys. Rev. Lett. **69**, 1427 (1992).
[3] Z. V. Popvic, J. Spitzer, T. Ruf, M. Cardona, R. Notzel, and K. Ploog, Phys. Rev. B **48**, 1659 (1993).
[4] R. Bhadra, M. Grimsditch, I. K. Schuller, and F. Nizzoli, Phys. Rev. B **39**, 12 456 (1989).
[5] M. Grimsditch, R. Bhadra, and I. K. Schuller, Phys. Rev. Lett. **58**, 1216 (1987).
[6] P. V. Santos, A. K. Sood, M. Cardona, K. Ploog, Y. Ohmori, and H. Okamoto, Phys. Rev. B **37**, 6381 (1988).
[7] A. Tanaka, S. Onari, and T. Arai, Phys. Rev. B **47**, 1237 (1993).
[8] N. Mori and T. Ando, Phys. Rev. B **40**, 6175 (1989).
[9] H. Rücker, E. Molinari, and P. Lugli, Phys. Rev. B **45**, 6747 (1992).
[10] M. A. Stroscio, G. J. Iafrate, K. W. Kim, M. A. Littlejohn, A. R. Bhatt, and M. Dutta, in *Integrated Optics and Optoelectronic*, edited by K.-K. Wong and M. Razeghi (SPIE, Bellingham, WA, 1993), Vol. CR45, p. 341.
[11] H. Benistry, C. M. Sotomayor-Torrés, and C. Weisbuch, Phys. Rev. B **44**, 10 945 (1991).
[12] N. Nishiguchi, Phys. Rev. B **50**, 10 970 (1994).
[13] N. Bannov, V. Mitin, and M. A. Stroscio, Phys. Status Solidi B **183**, 131 (1994).
[14] S. Yu, K. W. Kim, M. A. Stroscio, G. J. Iafrate, and A. Ballato, Phys. Rev. B **50**, 1733 (1994).
[15] M. A. Stroscio, K. W. Kim, S. Yu, and A. Ballato, J. Appl. Phys. **76**, 4670 (1994).
[16] B. A. Auld, *Acoustic Fields and Waves* (Wiley, New York, 1973).
[17] J. S. Blakemore, J. Appl. Phys. **53**, R123 (1982).

Electron–acoustic-phonon scattering rates in rectangular quantum wires

SeGi Yu* and K. W. Kim
Department of Electrical and Computer Engineering, North Carolina State University, Raleigh, North Carolina 27695-7911

Michael A. Stroscio and Gerald J. Iafrate
U.S. Army Research Office, P. O. Box 12211, Research Triangle Park, North Carolina 27709-2211

Arthur Ballato
Electronics and Power Sources Directorate, U.S. Army Research Laboratory, Ft. Monmouth, New Jersey 07703-5601
(Received 18 March 1994)

Electron–acoustic-phonon scattering in a rectangular quantum wire is studied. The Hamiltonian describing the deformation-potential interaction of confined acoustic phonons with carriers is derived by quantizing the appropriate, experimentally verified approximate compressional acoustic-phonon modes in a free-standing rectangular quantum wire. The scattering rate due to the deformation-potential interaction is obtained for GaAs quantum wires with a range of cross-sectional dimensions. The results demonstrate that a proper treatment of confined acoustic phonons may be essential to correctly model electron scattering rates at low energies in nanoscale structures.

I. INTRODUCTION

A number of proposed applications of mesoscopic electronic structures involve carrier transport at low temperatures and low carrier energies; frequently, the regime of interest is one where dimensional confinement modifies the phase space substantially. It is well known that in this low-temperature, low-energy regime,[1–6] acoustic phonons play an enhanced role in carrier scattering and may dominate over the scattering of carriers by optical phonons. In addition, in nanoscale structures it is possible that phase-space restrictions may weaken or forbid optical-phonon scattering processes that would normally dominate in bulk structures. Recently, there has been an extensive literature on the role of dimensional confinement in modifying longitudinal-optical (LO) phonon modes and their interactions with charge carriers in nanoscale and mesoscopic semiconductor structures (see, for example, Refs. 7–12 and the numerous papers referenced therein). On the other hand, there are relatively few treatments dealing with the role of dimensional confinement in modifying acoustic-phonon modes and their interactions with charge carriers.[2–4,13,14] In spite of the fact that there is an extensive literature on the theory of acoustic modes in conventional waveguides, resonators, and related structures, few efforts have been reported on formulating a theory of acoustic phonons in nanoscale structures, where both phonon confinement and a quantum-mechanical treatment of phonon normalization are essential. The necessity for such theoretical treatments has been demonstrated recently by experimental studies providing both direct and indirect[3,4] evidence of the importance of acoustic-phonon confinement in reduced dimensional electronic structures.

In this paper, we have obtained the normalized expressions for acoustic phonons confined in a free-standing rectangular quantum wire by appropriately quantizing the acoustic-phonon displacements. As is well known, there are no exact solutions for the complete set of phonon modes for a rectangular quantum wire; nevertheless, as for the case of LO phonon modes,[8] the approximate modes presented in this work provide simple and useful expressions, which are well suited for modeling the interaction of carriers with acoustic phonons. As a basis for investigating the role of reduced dimensionality on the coupling between acoustic phonons and carriers, we have formulated the interaction Hamiltonian for the deformation potential associated with confined acoustic-phonon modes in rectangular quantum wires. The resulting scattering rates (based on the golden rule approximation) are compared with those obtained from the bulk-phonon modes. For numerical calculations, GaAs is used as the material of choice throughout this study.

II. QUANTIZATION OF COMPRESSIONAL ACOUSTIC-PHONON MODES FOR A RECTANGULAR QUANTUM WIRE

The compressional, or dilatational, acoustic-phonon modes in free-standing rods of rectangular cross section have been examined both experimentally[15] and theoretically[16,17] by Morse in an extended study. Morse has derived an approximate set of hybrid compressional, or dilatational, acoustic-phonon modes,[16,17] which are found to accurately approximate the experimentally observed modes over a wide range of conditions.[15] Specifically, Morse has found that the approximate hybrid modes derived by assuming separable boundary conditions[16,17] have simple analytical representations and provide convenient approximations for the rectangular geometry when the cross-sectional dimensions have aspect ratios of approximately 2 or greater. For smaller aspect ratios (i.e., close to 1), Morse has argued correctly that it is necessary to turn to numerical solutions since exact

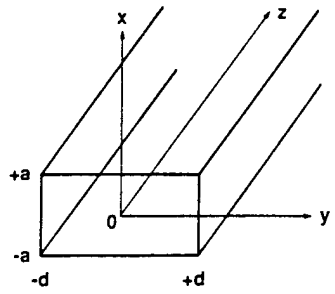

FIG. 1. Schematic drawing of a free-standing rectangular quantum wire considered in the analysis of electron–acoustic-phonon scattering.

analytical solutions for the compressional acoustic-phonon modes in a rectangular structure are not expressible analytically. In this paper, we shall restrict our analysis to rectangular quantum wires with aspect ratios of 2 or greater.

As depicted in Fig. 1, we consider a free-standing rectangular rod of infinite length in the z direction having an x-directed height (or thickness) $2a$, and a y-directed width $2d$; the origin of coordinates in the x-y plane is taken to be at the geometric center of the rectangular cross section, and the x-, y-, and z-directed acoustic-mode displacements are represented, respectively, by

$$u_1 = u(x,y)e^{i\gamma(z-ct)} , \tag{1}$$

$$v_1 = v(x,y)e^{i\gamma(z-ct)} , \tag{2}$$

$$w_1 = w(x,y)e^{i\gamma(z-ct)} , \tag{3}$$

where $\gamma = 2\pi/\lambda$, λ being the wavelength, γ is the z-directed free wave vector, and c is the phase velocity. Adopting Morse's form for the approximate separation-of-variables solution, the compressional waves for the "thickness" modes may be represented by

$$u = \{ A \sin k_1 x + B \sin k_2 x \} \cos(hy) , \tag{4}$$

$$v = \left\{ \frac{h}{k_1} A \cos k_1 x + C \cos k_2 x \right\} \sin(hy) , \tag{5}$$

$$w = i \left\{ -\frac{\gamma}{k_1} A \cos k_1 x + \frac{1}{\gamma}(k_2 B + hC) \cos k_2 x \right\} \cos(hy) , \tag{6}$$

where

$$k_1^2 + h^2 = \gamma^2[(c/c_d)^2 - 1] , \tag{7}$$

$$k_2^2 + h^2 = \gamma^2[(c/c_s)^2 - 1] , \tag{8}$$

and the compressional, or dilatational, sound speed c_d, as well as the transverse, or shear, sound speed c_s, are expressed in terms of the Lamé constants λ' and μ:

$$c_d^2 = (\lambda' + 2\mu)/\rho , \tag{9}$$

$$c_s^2 = \mu/\rho , \tag{10}$$

with ρ being the density of the medium. Substituting Eqs. (4)–(6) into the conditions that the T_{xx}, T_{yx}, and T_{zx} stress components vanish at $x = \pm a$, it follows that simultaneous equations for the amplitudes A, B, and C are given by

$$2Ah \sin k_1 a + Bh \sin k_2 a + Ck_2 \sin k_2 a = 0 , \tag{11}$$

$$-A(\gamma^2 + h^2 - k_2^2)\cos k_1 a + 2Bk_1 k_2 \cos k_2 a = 0 , \tag{12}$$

$$2A(h^2 + \gamma^2)\sin k_1 a + B(\gamma^2 + h^2 - k_2^2)\sin k_2 a = 0 . \tag{13}$$

When $k_2 \neq 0$, the condition that the determinant of coefficients vanishes requires that

$$\frac{\tan k_2 a}{\tan k_1 a} = -\frac{4k_1 k_2 (h^2 + \gamma^2)}{(h^2 + \gamma^2 - k_2^2)^2} , \tag{14}$$

which serves as the dispersion relation; this result is similar to the corresponding dispersion relation for the case of a slab.[18] Using Eq. (13) to solve for B in terms of A and applying the resultant expression in conjunction with Eq. (11) to solve for C in terms of A, Eqs. (3)–(6) may be written as

$$u_1 = A \{ \sin k_1 x + \alpha \sin k_2 x \} \cos(hy) e^{i\gamma(z-ct)} , \tag{15}$$

$$v_1 = A \left\{ \frac{h}{k_1} \cos k_1 x + \beta \cos k_2 x \right\} \sin(hy) e^{i\gamma(z-ct)} , \tag{16}$$

$$w_1 = iA \left\{ -\frac{\gamma}{k_1} \cos k_1 x + \frac{1}{\gamma}(k_2 \alpha + h\beta) \cos k_2 x \right\} \times \cos(hy) e^{i\gamma(z-ct)} , \tag{17}$$

where α and β are defined by

$$B = -\frac{\sin k_1 a}{\sin k_2 a} \frac{2(h^2 + \gamma^2)}{(\gamma^2 + h^2 - k_2^2)} A = \alpha A , \tag{18}$$

and

$$C = -\left[\frac{k_2 h}{h^2 + \gamma^2} \right] B = \frac{\sin k_1 a}{\sin k_2 a} \frac{2k_2 h}{(\gamma^2 + h^2 - k_2^2)} A = \beta A . \tag{19}$$

Following the quantization procedure of Ref. 14, the normalization constant may be determined by quantizing the phonon modes so that,

$$\frac{1}{4ad} \int_{-a}^{+a} dx \int_{-d}^{+d} dy \{ uu^* + vv^* + ww^* \} = \frac{\hbar}{2M\omega_\gamma} , \tag{20}$$

where ω_γ is the radial frequency of the mode with wave vector γ. Performing the indicated integration, Eq. (20) yields the amplitude A in terms of the following equations:

$$\frac{A^2}{4ad}\left\{f_1(h,d)[f_2(k_1,a)+2\alpha g_1(k_1,k_2,a)+\alpha^2 f_2(k_2,a)]-f_1(h,d)\left[\frac{h^2}{k_1^2}f_1(k_1,a)+\frac{2\beta h}{k_1}g_2(k_1,k_2,a)+\beta^2 f_1(k_2,a)\right]\right.$$
$$+f_1(h,d)\left[\frac{\gamma^2}{k_1^2}f_1(k_1,a)-\frac{2}{k_1}(k_2\alpha+h\beta)g_2(k_1,k_2,a)+\frac{(k_2\alpha+h\beta)^2}{\gamma^2}f_1(k_2,a)\right]$$
$$\left.+2d\left[\frac{h^2}{k_1^2}f_1(k_1,a)+\frac{2\beta h}{k_1}g_2(k_1,k_2,a)+\beta^2 f_1(k_2,a)\right]\right\}=\frac{\hbar}{2M\omega_\gamma}\ , \quad (21)$$

where

$$f_1(h,d)=d\left[1+\frac{\sin(2hd)}{(2hd)}\right]\ , \quad (22)$$

$$f_2(h,d)=2d-f_1(h,d)\ , \quad (23)$$

$$g_1(k_1,k_2,a)=\frac{\sin(k_1-k_2)a}{(k_1-k_2)}-\frac{\sin(k_1+k_2)a}{(k_1+k_2)}\ , \quad (24)$$

$$g_2(k_1,k_2,a)=\frac{\sin(k_1-k_2)a}{(k_1-k_2)}+\frac{\sin(k_1+k_2)a}{(k_1+k_2)}\ . \quad (25)$$

Henceforth, A^2 is written as

$$A^2=\frac{2\hbar}{M\omega_\gamma B_\gamma}\ , \quad (26)$$

where B_γ is defined straightforwardly by Eqs. (21) and (26).

In accordance with the solutions of Morse,[16] the boundary conditions at $y=\pm d$ determine the value of h; however, the adjustment of h alone is sufficient to make T_{yy}, T_{xy}, and T_{zy} vanish at $y=\pm d$. For aspect ratios where the width of the rectangular cross section ($2d$) is greater than or approximately equal to twice the height ($2a$), this problem can be circumvented since the two shear stresses T_{xy} and T_{zy} become negligible. Accordingly, Morse chooses h so that the extensional stress T_{yy} vanishes; this condition requires

$$hd=(n+\tfrac{1}{2})\pi\ , \quad n=0,1,2,\ldots . \quad (27)$$

The principal propagation mode (i.e., $n=0$ or $h=\pi/2d$) has no nodal surfaces parallel to the length. Motivated by the analysis in Sec. III, as well as by Morse's experimental observation that the principal mode is dominant,[15] the present paper considers the $n=0$ case for the thickness modes in numerical calculations. In addition to the thickness modes, another set of acoustic modes is observed experimentally.[15,16] These modes correspond to "width modes" and are determined in a manner similar to that used to determine the thickness modes. By satisfying the boundary conditions on the stress at $y=\pm d$, the solutions for the width modes show expressions analogous to Eqs. (15)–(17) with the roles of x and y as well as k and h interchanged, respectively. For these modes, k is then determined by approximate boundary conditions at $x=\pm a$.[16] The dispersion relation for the width mode is identical in form to Eq. (14), and the normalization procedure for proper quantization is as described in Eq. (20). As for the thickness modes, only the principal mode with $k=0$ is considered for the width modes.

We have calculated acoustic-phonon frequencies as a function of wave vector γ for the thickness and width modes in GaAs quantum wires. For this purpose, Eq. (14) may be written as

$$\frac{\tan(\pi\sqrt{\chi^2-\psi^2})}{\tan(\pi\sqrt{\epsilon\chi^2-\psi^2})}=-\frac{4\psi^2\sqrt{\chi^2-\psi^2}\sqrt{\epsilon\chi^2-\psi^2}}{(2\psi^2-\chi^2)^2}\ , \quad (28)$$

where

$$\chi^2=s^2(c/c_s)^2\ , \quad (29)$$

$$\psi^2=s^2+(ah/\pi)^2\ , \quad (30)$$

$$s=a\gamma/\pi\ , \quad (31)$$

$$\epsilon=(c_s/c_d)^2=(1-2\sigma)/2(1-\sigma)\ , \quad (32)$$

and σ is Poisson's ratio. Due to the periodic nature of trigonometric functions, the phonon frequency ω_γ ($=c\gamma$) has multiple solutions for a given γ and n (i.e., fixed h or k). Thus, an additional index m is needed to distinguish different modes. Figures 2 and 3 depict dispersion curves of the six lowest thickness modes ($h=\pi/2d$, $m=1,\ldots,6$) and the corresponding width modes ($k=0$, $m=1,\ldots,6$). The quantum wire cross-sectional dimensions are chosen to be 28.3×56.6 Å^2 for Fig. 2 and 50×200 Å^2 for Fig. 3, respectively. As expected, the width modes tend to have lower energies than the thick-

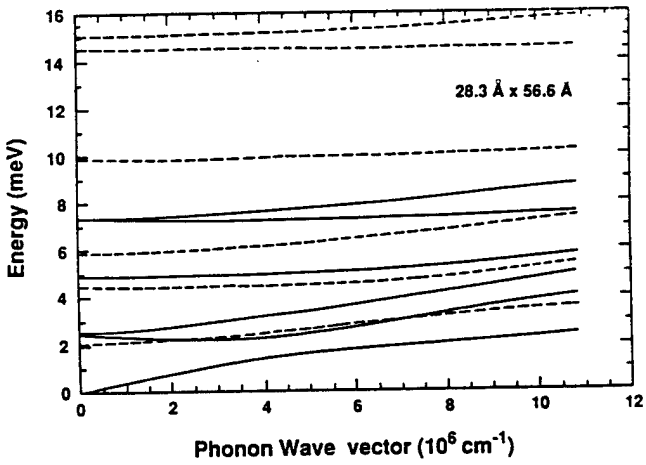

FIG. 2. Dispersion curves for the six lowest width and thickness modes ($m=1,\ldots,6$) of a 28.3×56.6-Å^2 GaAs quantum wire. The solid lines are for the width modes and the dashed lines are for the thickness modes.

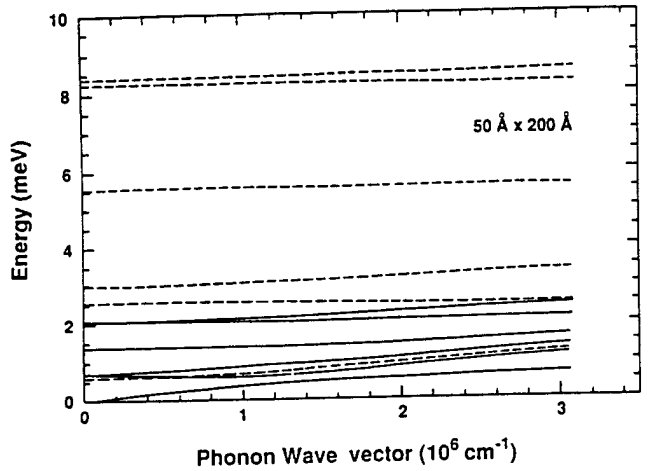

FIG. 3. Dispersion curves for the six lowest width and thickness modes ($m=1,\ldots,6$) of a 50×200-Å^2 GaAs quantum wire. The solid lines are for the width modes and the dashed lines are for the thickness modes.

ness modes, since the width is greater than the thickness for each of the cases represented in these figures.

III. ELECTRON–ACOUSTIC-PHONON SCATTERING RATES IN A RECTANGULAR QUANTUM WIRE

The deformation-potential interaction of the thickness mode is describable in terms of the Hamiltonian $H_{\rm def}$,

$$H_{\rm def}=E_a\nabla\cdot\mathbf{u}(\mathbf{r}) =E_a\sum_{\gamma,n,m}[c_{n,m}(\gamma)+c^{\dagger}_{n,m}(-\gamma)] \times\left[\frac{\partial u}{\partial x}+\frac{\partial v}{\partial y}+i\gamma w\right]e^{i\gamma z}, \tag{33}$$

where $c_{n,m}(\gamma)$ and $c^{\dagger}_{n,m}(-\gamma)$ are the usual annihilation and creation operators and

$$\mathbf{u}(\mathbf{r})=\sum_{\gamma,n,m}[c_{n,m}(\gamma)+c^{\dagger}_{n,m}(-\gamma)]\mathbf{u}(x,y,\gamma)e^{i\gamma z}. \tag{34}$$

The time-dependent factor $e^{-i\omega_\gamma t}$ is not included in Eqs. (33) and (34), since it will be included in the energy-conserving δ function in the golden rule. In Eqs. (33) and (34), the sum over γ represents the usual integration over wave vector, while the sums over n and m represent the addition of the various acoustic-phonon modes. For the normalized compressional, or dilatational, modes of Sec. II, it follows that

$$H_{\rm def}=\sum_{\gamma,n,m}E_a A\frac{\omega_\gamma^2}{c_d^2k_1}\cos(k_1x)\cos(hy) \times[c_{n,m}(\gamma)+c^{\dagger}_{n,m}(-\gamma)]e^{i\gamma z}, \tag{35}$$

where $\omega_\gamma^2=c^2\gamma^2$. Assuming the extreme quantum limit, the ground-state effective-mass electronic wave function is given by

$$\psi_q(x,y,z)=\frac{1}{\sqrt{ad}}\cos\left[\frac{\pi x}{2a}\right]\cos\left[\frac{\pi y}{2d}\right]e^{iqz}, \tag{36}$$

and the eigenenergy is

$$E=\frac{\hbar^2}{2m}\left[\left[\frac{\pi^2}{(2a)^2}+\frac{\pi^2}{(2d)^2}\right]+q^2\right]. \tag{37}$$

Hence, the matrix element $\langle q'|H_{\rm def}|q\rangle$ is given by

$$\langle q'|H_{\rm def}|q\rangle=\sum_{\gamma,n,m}E_a A\frac{\omega_\gamma^2}{c_d^2k_1}\frac{\pi^2\sin k_1a}{k_1a(\pi^2-k_1^2a^2)} \times\frac{\delta_{q-q'+\gamma}}{\{(n+\frac{1}{2})\pi[1-(n+\frac{1}{2})^2]\}} \times[c_{n,m}(\gamma)+c^{\dagger}_{n,m}(-\gamma)]. \tag{38}$$

An examination of the n-dependent terms in Eq. (38) makes it apparent that they contribute to the matrix element squared in such a way that these terms for $n=1$ are only $\frac{1}{25}$ of their magnitude for $n=0$; a similar reduction occurs in going from $n=1$ to $n=2$ and it is clear that only the principal mode contributes significantly to Eq. (38), which was derived on the assumption that the carriers remain in the ground state of the extreme quantum limit, x-y potential.

Hence, the Fermi golden rule scattering rate corresponding to the matrix element of Eq. (38) is given by

$$\frac{1}{\tau}=\sum_{n,m}\int_{-\infty}^{+\infty}d\gamma\frac{L}{2\pi}\frac{2\pi}{\hbar}\left[E_a A_\gamma\frac{\omega_\gamma^2}{c_d^2k_1}\right]^2 \times\left[\frac{\pi^2\sin k_1a}{k_1a(\pi^2-k_1^2a^2)}\right]^2\left[\frac{1}{(n+\frac{1}{2})\pi[1-(n+\frac{1}{2})^2]}\right]^2(N+\tfrac{1}{2}\pm\tfrac{1}{2})\delta\left[\frac{\hbar^2}{2m}(\gamma^2\mp2q\gamma)\pm\hbar\omega_\gamma\right], \tag{39}$$

where A has been written as A_γ to indicate the γ dependence of A_γ, L is the normalization length along the axis of the quantum wire, and N is the usual temperature-dependent Bose-Einstein occupation number for the acoustic phonons. Introducing B_γ through Eq. (26) and defining factors Z_1 and Z_2, Eq. (39) may be written as

$$\frac{1}{\tau}=\sum_{n,m}\int_{-\infty}^{+\infty}d\gamma\,E_a^2\left[\frac{1}{2\rho abB_\gamma}\right]\frac{\omega_\gamma^3}{(c_d^2k_1)^2}Z_1^2Z_2^2(N+\tfrac{1}{2}\pm\tfrac{1}{2}) \times\delta\left[\frac{\hbar^2}{2m}(\gamma^2\mp2q\gamma)\pm\hbar\omega_\gamma\right], \tag{40}$$

where

seen from Figs. 4–6, each of these modes makes a notable contribution to the density of states and to the scattering rate. In particular, the scattering rates at low energies show pronounced peaks and are strongly enhanced due to the dominance of selected compressional modes in the emission process. Thus, it is essential to retain a number of acoustic modes for an accurate estimation of scattering rates. The results shown in Figs. 4–6 have been obtained by including the six lowest-order thickness modes as well as the six lowest-order width modes. Due to the limited resolution in plotting, the details of one-dimensional nature (such as the number of peaks and their heights) are not illustrated fully in these figures. The second important feature of Figs. 4–6 is that the scattering rates for the case of the hybrid compressional modes are higher than the corresponding bulk scattering rates. These enhanced scattering rates provided an indication that conceptual designs for mesoscopic devices need to be based on an awareness of the fact that confined acoustic modes may play a significant role in carrier transport in these devices. As shown in Fig. 5, for the case of a 100×200-Å^2 cross section we find similar scaling of the scattering rates with energy as for the case of Fig. 4; however, the rates are approximately an order of magnitude lower than those for the 28.3×56.6-Å^2 quantum wire of Fig. 4.

The hybrid modes considered in this paper contain both longitudinal and transverse components as is evident from Eqs. (15)–(18); as expected, only the longitudinal components contribute to the deformation potential of Eq. (35). The appearance of a hybrid-mode dispersion relation, Eq. (14), similar to that for the dilatational modes of a slab[18] is entirely reasonable, since the flexural modes are similar to the shear modes.[19] Such modes have strong transverse components and they make little contribution to electron–acoustic-phonon interaction through the deformation potential.

V. CONCLUSION

The results in this analysis suggest that it may be important to consider carrier–acoustic-phonon scattering processes when designing mesoscopic devices containing quantum-wire elements. Based on what appears to be the most complete set of approximate compressional modes available for a free-standing rectangular quantum wire,[16] it is demonstrated that the details of the modal structure need to be taken into account if deformation-potential scattering is to be modeled accurately. Further analysis is necessary to rigorously show that deformation-potential scattering rates by confined acoustic phonons exceed the corresponding rates obtained from bulk phonons in quantum wires; however, these results provide an indication that acoustic-phonon scattering may be enhanced considerably in some nanoscale structures.

ACKNOWLEDGMENTS

The authors would like to thank Dr. James W. Mink for his support and Professor M. N. Wybourne for advance information on his recent experimental evidence for acoustic-phonon confinement. The authors are also grateful to Professor V. Mitin, Dr. R. Mickevičius, and N. Bannov for many interactions on related confined-phonon effects in nanostructures. This work was supported, in part, by the Office of Naval Research and the U.S. Army Research Office.

*Also with Department of Physics, North Carolina State University, Raleigh, NC 27695.

[1]T. Kawamura and S. Das Sarma, Phys. Rev. B **45**, 3612 (1992).
[2]B. Hillebrands, S. Lee, G. I. Stegeman, H. Cheng, J. E. Potts, and F. Nizzoli, Phys. Rev. Lett. **60**, 832 (1988).
[3]J. Seyler and M. N. Wybourne, Phys. Rev. Lett. **69**, 1427 (1992); Z. V. Popvic, J. Spitzer, T. Ruf, M. Cardona, R. Notzel, and K. Ploog, Phys. Rev. B **48**, 1659 (1993).
[4]H. Benistry, C. M. Sotomayor-Torrés, and C. Weisbuch, Phys. Rev. B **44**, 10 945 (1991).
[5]B. A. Auld, *Acoustic Fields and Waves* (Wiley, New York, 1973).
[6]P. J. Price, Ann. Phys. (N.Y.) **133**, 217 (1981).
[7]N. Mori and T. Ando, Phys. Rev. B **40**, 6175 (1989).
[8]M. A. Stroscio, Phys. Rev. B **40**, 6428 (1989); K. W. Kim, M. A. Stroscio, A. Bhatt, V. V. Mitin, and R. Mickevičius, J. Appl. Phys. **70**, 319 (1991).
[9]K. W. Kim and M. A. Stroscio, J. Appl. Phys. **68**, 6289 (1990).
[10]R. Rücker, E. Molinari, and P. Lugli, Phys. Rev. B **45**, 6747 (1992).
[11]K. J. Nash, Phys. Rev. B **46**, 7723 (1992).
[12]M. A. Stroscio, G. J. Iafrate, K. W. Kim, M. A. Littlejohn, A. R. Bhatt, and M. Dutta, in *Integrated Optics and Optoelectronics*, edited by K.-K. Wong and M. Razeghi (SPIE, Bellingham, WA, 1993), Vol. CR45, p. 341.
[13]N. C. Constantinou, *Proceedings of NATO Advanced Research Workshop on Phonons in Nanostructures* (Kluwer, Boston, 1993), pp. 113–119.
[14]M. A. Stroscio and K. W. Kim, Phys. Rev. B **48**, 1936 (1993).
[15]R. W. Morse, J. Acoust. Soc. Am. **20**, 833 (1948).
[16]R. W. Morse, J. Acoust. Soc. Am. **22**, 219 (1950).
[17]R. W. Morse, Ph.D. thesis, Brown University, 1949.
[18]M. Redwood, *Mechanical Waveguides* (Pergamon, Oxford, 1960).
[19]R. A. Sykes, in *Quartz Crystals for Electrical Circuits*, edited by R. A. Heising (Van Nostrand, Toronto, 1946), p. 205.

PROCEEDINGS

1995 INTERNATIONAL SEMICONDUCTOR DEVICE RESEARCH SYMPOSIUM

December 5 - 8, 1995 • Omni Charlottesville Hotel

IEEE MTT

URSI

The Russian Physical Society

UNITED STATES NAVY

EPS

VOLUME I of II

SCHOOL OF ENGINEERING & APPLIED SCIENCE

Academic Outreach

This work relates to Department of Navy Grant N00001-95-1-0972 issued by the Office of Naval Research and the U.S. Army Research Office Grant No. DAAH04-95-1-0502. The United States Government has a royalty-free license throughout the world in all copyrightable material contained herein.

Additional copies of this publication are available from

Engineering Academic Outreach
University of Virginia
Thornton Hall
Charlottesville, Virginia 22903-2442
(804) 924-3744

UVA/EAO Catalog Number: 95-CI066-3-004
ISBN Number: 1-880920-03-4

Tailoring Acoustic Modes in Mesoscopic Devices

Michael A. Stroscio, Gerald J. Iafrate and John Zavada
U.S. Army Research Office
Research Triangle Park, NC 27709-2211

K. W. Kim, Yuri Sirenko and SeGi Yu
Department of Electrical and Computer Engineering
North Carolina State University
Raleigh, NC 27695-7911

V. Mitin, N. Bannov and V. Mickevicius
Department of Electrical and Computer Engineering
Wayne State University
Detriot, Michigan 48202

Mitra Dutta and Arthur Ballato
Physical Sciences Directorate
U.S. Army Research Laboratory

In numerous publications of the last several years [1,8], acoustic phonons have been quantized for a variety of nanoscale and mesoscopic structures in order to assess to role of electron--acoustic-phonon scattering in limiting the performance of nanoscale and mesoscopic electronic devices. These structures include quantum wells, quantum wires with cylindrical and rectangular cross sections, and quantum dots with spherical, cylindrical and rectangular boundaries. These quantized phonons have been studies for the two cardinal boundary conditions of classical acoustics: free boundaries (open boundaries) where the phonon displacements are unrestricted and allowed to balance all normal traction forces to zero; and clamped boundaries (rigid boundaries) where phonon displacements are required to vanish at the boundaries. For quantum wells, scattering rates have been calculated for free-standing structures [4,8]. For the case of quantum wires, scattering rates have been calculated only for the case of infinitely long quantum wires and, as appropriate for this case, the acoustic phonons have been quantized in only the lateral dimensions. However, for realistic mesoscopic device designs, the quantum wire input and output "leads" as well as the active regions of the devices with quantum-wire geometries have finite lengths. Accordingly, deformation and piezoelectric scattering rates must be based on acoustic phonons that are quantized in all three spatial dimensions. The international community does not appear to have considered the role of three dimensional confinement of acoustic phonons in mesoscopic devices but it is clear from the solutions of classical acoustics that boundary conditions imposed at the ends of wire-like regions can have a profound effect on the properties of acoustic

modes. The results presented here are based, in part, on a consideration of the role of acoustic phonon confinement in mesoscopic devices containing finite wire-like regions. Based on our current understanding of such finite wire-like structures, we believe that it is possible to "engineer" mesoscopic structures so that electron--acoustic-phonon scattering is reduced. This reduction is likely to be most important in mesoscopic device which operate in the basis of "coherent" electron-wave interference effects.

In the domain of classical acoustics, especially revealing examples of the role of wire-like regions in modifying and tailoring selected acoustic mode patterns are those of the organ pipe and of the muffler. In the first example, the open boundary conditions at the ends of the organ pipe result in wave reflections with the reflected and transmitted waves having amplitudes with the same sign at the ends of the organ pipe. Subject to these boundary conditions, the acoustic modes in an organ pipe evolve so that standing wave amplitudes are maximized and anti-nodes are formed at the ends of the pipe; that is, the dominant modes are those having wavelengths such that the length of a half-integral number of wavelengths is equal to the length of the pipe. Thus, an organ pipe produces sounds at well defined and reproducible wavelengths. In the second example, a muffler suppresses sounds at exit ports through the use interfaces which produce modes with the required node and anti-node structures.

In the case of mesoscopic devices the situation is, perhaps, more complex than in the case of classical acoustic waveguides with open boundaries since, in general, the boundary conditions at the ends of the quantum wires require that both the mode displacements and the normal components of the stress be continuous. However, for the case of a quantum wire which couples to an "end" region composed of the same material as that in the interior of the quantum wire, the open boundary condition such be appropriate. Thus, for, example, in the case of a quantum wire with two "open" ends the ambient acoustic phonons in the wire will evolve so that the dominant modes are those having wavelengths such that the length of a half-integral number of wavelengths equals the length of the quantum wire. Just as in the organ pipe these modes will have their maximum amplitudes at the ends of the wires; that is, anti-nodes will be present at the ends of the quantum wire. Similar behavior may be expected for the case of free-standing quantum well structures. For the case of a quantum wire which couples to (or terminates on) a region composed of a material with acoustic properties different from those of the material in the interior of the wire, the exact boundary condition must, in general, be applied. From classical acoustics it is known that few analytical solutions are available for the cases where the complete boundary

conditions must be used. A useful simplification arises in the case where the material in the interior of the quantum wire and the material at the end of the quantum wire have such different properties that the phonon modes are damped abruptly at he interface between the two materials; in this case, the so-called "clamped" boundary condition is adequate and the modes amplitudes may be assumed to vanish at such interfaces. Such a case applies at some metal-semiconductor interfaces. In particular, for a mesoscopic device having wire-like regions which terminate on a variety of metal regions (regions used as contacts, gates, barriers, etc.) it is satisfactory to apply clamped boundary conditions. At these boundaries, the acoustic modes will have nodes instead of the anti-nodes that are established in the case of an open boundary.

With this set of simplified boundary conditions it is possible to design mesoscopic structures with the phonons "engineered" to produce desired standing wave patterns. As an example, consider a four-terminal generalization of the three-terminal "tee"-shaped de Broglie wave interference device [9]. More specifically, consider a mesoscopic structure with quantum wires intersecting each other at right angles such that the two wire "centers" are at the same point. For this structure the ends of one wire are taken to be open and the ends of the other wire are taken to be clamped. Hence, it is possible to select some acoustic modes such that nodes will occur in "center" of one wire and anti-nodes will occur at the "center" of the other wire. By selecting various wire lengths it is possible to define a standing wave pattern that either maximizes or minimizes the amplitudes of specific acoustic phonon modes in regions where the electronic wavefunctions are dominant. Furthermore, by "engineering" interfaces within a quantum wire which are perpendicular to the quantum-wire axis, it should be possible to control the acoustic modes in wire-like regions of mesoscopic devices just as the classical acoustic modes are controlled in a muffler. Thus, the deformation and piezoelectric scattering rates may be partially tuned by tailoring the ambient phonon standing wave patterns in such mesoscopic structures.

In this effort to "engineer" the ambient phonon modes, the quantum-wire phonon modes obtained previously [1,8] should correctly describe the lateral quantization of the phonon modes. Elementary examples of such effects are implicit in the results of Ref. [8]. The quantization along the lengths of the quantum wires will be treated approximately under the simplifying "open" and "clamped" boundary conditions to assess the extent to which mesoscopic device properties may be controlled through the "engineering" of the phonon modes in mesoscopic devices. It is emphasized once again that the major payoff from the "quantum engineering" of acoustic phonons in quantum wires is the

reduction of electron--acoustic-phonon scattering and the consequent preservation of "coherent" electron waves in mesoscopic devices. Achieving nearly-coherent electron waves may ultimately depend sensitively on reducing electron--acoustic-phonon scattering even though such processes may be considered to be weak by normal standards.

References

1. Michael A. Stroscio, K. W. Kim, SeGi Yu, and Arthur Ballato, "Quantized Acoustic Phonon Modes in Quantum Wires and Quantum Dots," J. Appl. Phys., 76, 4670 (1994).

2. SeGi Yu, K. W. Kim, Michael A. Stroscio, and G. J. Iafrate, "Electron--Acoustic-Phonon Scattering Rates in Cylindrical Quantum Wires," Phys. Rev. B, 51, 4695 (1994).

3. M. A. Stroscio and K. W. Kim, "Piezoelectric Scattering of Carriers in Confined Acoustic Modes in Cylindrical Quantum Wires," Phys. Rev. B, 48, 1936 (1993).

4. N. Bannov, V. Mitin, and M. Stroscio, "Confined Acoustic Phonons in a Free-Standing Quantum Well," in *Proceedings of the 1993 International Semiconductor Device Research Symposium*, edited by M. Shur an E. Towe (University of Virginia Press, Charlottesville, VA), p. 659.

5. V. Mitin, R. Mickevicius, N. Bannov, and Michael A. Stroscio, "Acoustic Phonon Scattering in Low Dimensional Structures," *in Proceedings of the 1993 International Semiconductor Device Research Symposium*, edited by M. Shur and E. Towe (U. of VA Press, Charlottesville, VA), p. 855.

6. M. A. Stroscio, G. J. Iafrate, K. W. Kim, SeGi Yu, V. Mitin, and N. Bannov, "Scattering of Carriers from Acoustic Modes in Nanostructures," *in Proceedings of the 1993 International Semiconductor Device Research Symposium*, edited by M. Shur and E. Towe (University of Virginia Press, Charlottesville, VA), p. 873.

7. N. Bannov, V. Mitin, and M. Stroscio, "Confined Acoustic Phonons in Semiconductor Slabs and Their Interactions with Electrons," Physica Status Solidi B, 183, 131 (1994).

8. N. Bannov, V. Aristov, V. Mitin, and M. A. Stroscio, "Electron Relaxation Times due to Deformation-Potential Interaction of Electrons with Confined Acoustic Phonons in a Free-Standing Quantum Well," Phys. Rev. B, 51, 9930 (1995).

9. F. Sols, M. Macucci, U. Ravaioli, and K. Hess, "On the Possibility of Transistor Action Based on Quantum Interference Phenomena," Appl. Phys. Lett., 54, 1067 (1989).

Theoretical calculation of longitudinal-optical-phonon lifetime in GaAs

A. R. Bhatt and K. W. Kim
Department of Electrical and Computer Engineering, North Carolina State University, Raleigh, North Carolina 27695-7911

M. A. Stroscio
U.S. Army Research Office, P.O. Box 12211, Research Triangle Park, North Carolina 27709-2211

(Received 5 May 1994; accepted for publication 31 May 1994)

The anharmonic decay of longitudinal-optical (LO) phonons in zinc-blende semiconductors has been studied. Based on an approach in which the anharmonic crystal potential is estimated using the theory of elasticity, the lifetime of LO phonons via emission of two acoustic phonons is calculated as a function of lattice temperature and phonon wave vector. Application of this model to bulk GaAs shows an excellent agreement with available experimental data. Since the parameters employed in the model can be obtained experimentally, the approach provides a useful tool to investigate LO-phonon lifetimes in semiconductors.

In polar semiconductors carrier energy and momentum relaxation processes are frequently dominated by the interaction of carriers with optical phonons, particularly the longitudinal-optical (LO) phonons. It is now well known that carrier relaxation rates underlie a range of phenomena other than simple carrier transport. For example, carrier relaxation processes in semiconductor lasers play a critical role in determining the intrinsic modulation limit for high-frequency operation of such devices.[1,2] Previous analyses of carrier relaxation in semiconductor microstructures have demonstrated that emission alone does not, in general, dominate the carrier energy-loss rates since subsequent optical-phonon absorption events slow the relaxation process.[3,4] Instead, it has been shown that the overall carrier relaxation rate is frequently dominated by the decay of the strongly interacting optical phonon into weakly interacting acoustic phonons. Thus, detailed knowledge of optical-phonon decay, which is characterized by lifetime, is of major importance in understanding carrier dynamics in semiconductors. The decay process of optical phonons arises primarily from the three-phonon interaction through the anharmonic terms of the crystal potential energy. This phenomenon has been scrutinized by a number of authors mostly in bulk materials.[5–12] The approaches taken by these authors can be classified broadly in two categories: highly complex and complete microscopic models[5–7,10,11] with parameters which are very difficult to measure, and simpler macroscopic treatments[8,9] where attempts have been made to approximate various anharmonic contributions by replacing them with a single parameter related to an average of third-order elastic constants or a Grüneisen constant. An approach similar to the latter treatments has been adopted recently to estimate optical-phonon lifetimes in heterostructures.[12] The difficulty associated with the simple approaches is to find a valid expression for this appropriately averaged single parameter from the experimentally measurable quantities.

In this communication the lifetime of LO phonons via emission of two acoustic phonons is studied in zinc-blende semiconductors as a function of lattice temperature and phonon wave vector; specific results are reported for wave vectors along the ⟨100⟩ direction as well as for the ⟨111⟩ direction. The interaction Hamiltonian for anharmonic decay is developed based on Keating's treatment[13] of anharmonic contributions in elastic strain energy of a crystal. By using second-order and third-order elastic constants available in the literature and atomic displacements estimated from a microscopic model,[14] this approach is applied to calculate LO-phonon lifetimes in bulk GaAs, and the results are compared with the experimental data.

When a crystal potential is expanded in powers of displacements of the atoms from their equilibrium positions, we obtain a quadratic term along with cubic, quartic, and other higher-order terms. For simple analysis of the dispersion relation, it is acceptable to consider only the quadratic term in what is known as the harmonic approximation. However, the harmonic approach cannot describe the decay of phonon modes caused by the cubic and other higher-order terms, also known as the anharmonic terms in the crystal potential. It is generally accepted that the cubic term dominates over all anharmonic terms in phonon decay. For this process involving three phonons, the interaction Hamiltonian may be written as

$$H'_{\mathbf{k},j;\mathbf{k}',j';\mathbf{k}'',j''} = \frac{1}{\sqrt{N}} P(\mathbf{k},j;\mathbf{k}',j';\mathbf{k}'',j'')\mathbf{u}_{\mathbf{k},j}\mathbf{u}_{\mathbf{k}',j'}\mathbf{u}_{\mathbf{k}'',j''}, \tag{1}$$

where k, k', and k'' (j, j', and j'') represent the phonon wave vectors (polarization modes), respectively, N is the number of unit cells, and P describes the cubic coupling. The displacement for the phonon mode in normal coordinates may be represented as

$$\mathbf{u}_{\mathbf{k},j} = \left(\frac{\hbar}{2m\omega_{\mathbf{k},j}}\right)^{1/2} \mathbf{e}'_{\mathbf{k},j}(a_{\mathbf{k},j}e^{i\mathbf{k}\cdot\mathbf{r}} + a^{\dagger}_{\mathbf{k},j}e^{-i\mathbf{k}\cdot\mathbf{r}}), \tag{2}$$

where $a_{\mathbf{k},j}$ and $a^{\dagger}_{\mathbf{k},j}$ are the annihilation and creation operators, $\mathbf{e}'_{\mathbf{k},j}$ is the polarization vector, m is the average mass of the lattice atoms, and $\omega_{\mathbf{k},j}$ is the frequency of the normal mode. For LO-phonon modes, the decay occurs mainly through the creation of two longitudinal-acoustic (LA) modes. At the same time, the normal process dominates over the umklapp process when the LO phonon wave vector is small. Retaining only this term, the decay Hamiltonian for LO phonons becomes

 0021-8979/94/76(6)/3905/3/$6.00

$$H'_{\mathbf{k};\mathbf{k}';\mathbf{k}''}=\frac{1}{\sqrt{N}}\left(\frac{\hbar}{2m}\right)^{3/2}\left(\frac{1}{\omega_{\mathbf{k}}\omega_{\mathbf{k}'}\omega_{\mathbf{k}''}}\right)^{1/2}$$
$$\times P(\mathbf{k};\mathbf{k}';\mathbf{k}'')a_{\mathbf{k}}a^{\dagger}_{\mathbf{k}'}a^{\dagger}_{\mathbf{k}''}e^{i(\mathbf{k}-\mathbf{k}'-\mathbf{k}'')\cdot r}. \quad (3)$$

The indices for mode polarization have been removed since only one decay path has been considered (i.e., $\mathbf{k}_{LO}\rightarrow\mathbf{k}'_{LA}+\mathbf{k}''_{LA}$). Contributions by other processes can be formulated easily from Eq. (2).

In the interaction Hamiltonian derived above, all the terms other than $P(\mathbf{k};\mathbf{k}';\mathbf{k}'')$ are known; however, it is quite difficult to properly measure the anharmonic potential term. To circumvent this problem, Keating[13] has used the theory of elasticity since there exists a relationship between the third-order elasticity coefficients and the anharmonic term in the crystal potential. Elasticity coefficients also are related closely to the Grünesien parameter. By using the Taylor-series expansion in terms of strain variables, Brugger[15] has represented the macroscopic elastic strain energy as

$$U=\frac{1}{2}\sum_{J}C_{JJ}\eta_J^2+\sum_{J<K}C_{JK}\eta_J\eta_K+\frac{1}{6}\sum_{J}C_{JJJ}\eta_J^3$$
$$+\frac{1}{2}\sum_{J\neq K}C_{JJK}\eta_J^2\eta_K+\sum_{J<K<L}C_{JKL}\eta_J\eta_K\eta_L, \quad (4)$$

where U is the internal energy per unit undeformed volume, and C_{JK} and C_{JKL} are the second- and third-order elasticity coefficients. The strain variable η_J as defined in Refs. 13 and 15 contains displacement gradient terms such as

$$u^{\alpha}_{\beta}=\frac{\partial u_{\alpha}}{\partial X_{\beta}}, \quad (5)$$

where X is the position in the undeformed solid. After proper substitutions for η_J, the strain energy density U_a associated with the third-order contributions in cubic crystals reduces to[13]

$$U_a=\tfrac{1}{6}C_{111}(e_1^3+e_2^3+e_3^3)+\tfrac{1}{2}C_{112}[e_1^2(e_2+e_3)+e_2^2(e_3+e_1)+e_3^2(e_1+e_2)]+C_{123}e_1e_2e_3+\tfrac{1}{2}C_{144}(e_1e_4^2+e_2e_5^2+e_3e_6^2)$$
$$+\tfrac{1}{2}C_{166}[e_1(e_5^2+e_6^2)+e_2(e_6^2+e_4^2)+e_3(e_4^2+e_5^2)]+C_{456}e_4e_5e_6+\tfrac{1}{2}C_{11}(e_1^3+e_2^3+e_3^3)+\tfrac{1}{2}C_{12}[e_1^2(e_2+e_3)+e_2^2(e_3+e_1)$$
$$+e_3^2(e_1+e_2)], \quad (6)$$

where e_J represents the linear part of η_J. A careful comparison of Keating's formulation[13] with that of Refs. 10 and 11 reveals that U_a corresponds to P as defined in Eq. (1); accordingly, a valid expression for the decay Hamiltonian can be developed once U_a is evaluated. In general, the values for the second- and third-order elastic constants can be obtained from the literature. At the same time, the magnitude of the strain variable e_J may be estimated based on numerical models for lattice dynamics such as that of Kunc and Nielson.[14]

Following Fermi's golden rule approximation, the LO phonon decay rate can be calculated readily. By defining the matrix element as

$$|M|^2=\frac{\hbar^3U_a^2}{8Nm^3}\left(\frac{1}{\omega_{\mathbf{k}}\omega_{\mathbf{k}'}\omega_{\mathbf{k}''}}\right)n_{\mathbf{k}}(n_{\mathbf{k}'}+1)(n_{\mathbf{k}''}+1)\delta_{\mathbf{k},\mathbf{k}'+\mathbf{k}''}, \quad (7)$$

the transition rate can be written as

$$\Gamma=\frac{2\pi}{\hbar}\sum_{\mathbf{k}',\mathbf{k}''}|M|^2\delta(\hbar\omega_{\mathbf{k}}-\hbar\omega_{\mathbf{k}'}-\hbar\omega_{\mathbf{k}''}), \quad (8)$$

where $n_{\mathbf{k}}=[\exp(\hbar\omega_{\mathbf{k}}/k_BT)-1]^{-1}$ is the normal Bose–Einstein occupation number. Then, following the analyses in Refs. 8 and 9, the lifetime for the LO phonon with wave vector $\mathbf{k}$ may be defined as

$$\frac{1}{\tau_p}=\sum\frac{\pi\hbar^2U_a^2}{4Nm^3}\left(\frac{1}{\omega_{\mathbf{k}}\omega_{\mathbf{k}'}\omega_{\mathbf{k}''}}\right)(1+n_{\mathbf{k}'}+n_{\mathbf{k}''})$$
$$\times\delta_{\mathbf{k},\mathbf{k}'+\mathbf{k}''}\delta(\hbar\omega_{\mathbf{k}}-\hbar\omega_{\mathbf{k}'}-\hbar\omega_{\mathbf{k}''}). \quad (9)$$

When more than one path exists for decay (i.e., paths other than LO→LA+LA), each contribution is added to obtain the LO-phonon lifetime. In this case, the sum in Eq. (9) is over both the phonon wave vector and mode polarization.

Using this formalism we have calculated the lifetime of bulk LO phonons in GaAs. In this calculations, the values for e_J have been estimated based on the valence shell model developed by Kunc and Nielson for lattice dynamics.[14] Since e_J depends only on the initial phonon wave vector $\mathbf{k}$, U_a for cubic coupling can be taken out of the sum in Eq. (9). For simplicity, a linear dispersion relation is assumed for acoustic phonons. At the same time, the occupation numbers for the $\mathbf{k}'$ and $\mathbf{k}''$ states are obtained by assuming that the energies for these two phonon modes are approximately $\hbar\omega_{LO}/2$. This is justifiable since only the near-zone-center LO phonons are of interest. Although elastic constants for GaAs are available in the literature, some of the measured third-order constants (C_{123} and C_{144}, in particular) show wide variations as can be seen in Ref. 16. To circumvent this uncertainty, we have used a relationship between the third-order elastic constants and the microscopic force constants developed by Keating.[13]

By varying microscopic force constant parameters, an optimum set of third-order elastic constants can be chosen systematically. The values adopted in this study are listed

TABLE I. Third-order elastic constants for GaAs in units of GPa.

C_{111}	C_{112}	C_{123}	C_{144}	C_{155}	C_{456}
−663	−391	−11	−41	−311	−41

in Table I. These values are well within the range of experimental variations. Although the relation given in Ref. 13 has been derived for crystals with diamond lattice structures, modifications for zinc-blende structures introduce only minor changes[17] and, thus, are not considered.

Figure 1 shows the LO-phonon lifetime as a function of temperature. Since the decay into two LA phonons is the dominant process, we have considered this mechanism only. The other processes are either not possible (when energy and momentum cannot be conserved) or provide a small contribution to the overall lifetime. As can be seen, the lifetime decreases with increasing temperature mainly due to the Bose–Einstein occupation number. The results obtained from our analysis agree well with the widely accepted experimental data (3.5 ps at 300 K and 7 ps at 77 K).[18–20] The agreement is better at room temperature than at low temperatures. This is reasonable since the third-order elastic constants used in our study are estimated at 300 K. Although elastic constants depend on temperature, their values are not provided over a wide range of temperature. Thus, it is likely that, if temperature-dependent elastic constants become available, the accuracy of calculation can be enhanced particularly at low temperatures. At the same time, inclusion of other decay mechanisms (i.e., other than an LO phonon decaying into two LA phonons) reduces the lifetime by approximately 0.5 ps and, thus, further improves the agreement. We have also studied the LO-phonon lifetime as a function of phonon wave vector, and the results are plotted along the ⟨100⟩ and

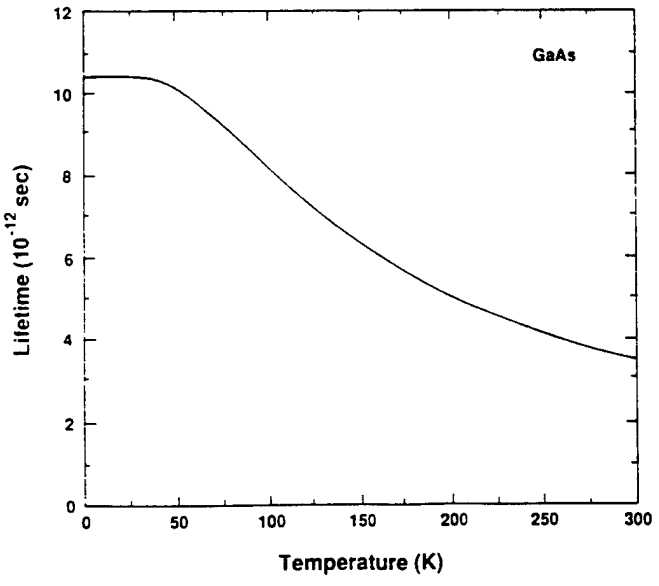

FIG. 1. Temperature dependence of LO-phonon lifetime in bulk GaAs. It has been assumed that elastic constants remain constant with temperature.

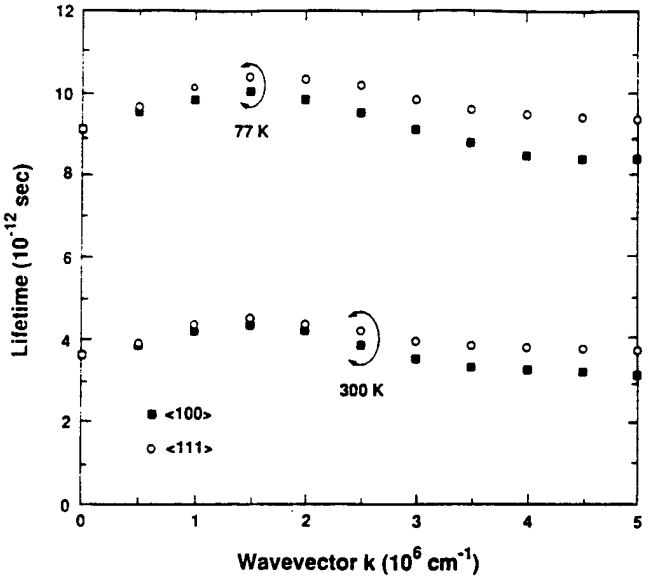

FIG. 2. LO-phonon lifetime as a function of wave vector in bulk GaAs along the ⟨100⟩ and ⟨111⟩ directions at 77 and 300 K.

⟨111⟩ directions in Fig. 2. It is found that the phonon lifetime does not depend strongly on the phonon wave vector. As a result, the $k=0$ value provides a good approximation for the LO-phonon lifetime in bulk materials.

The authors gratefully acknowledge helpful discussions with Dr. G. J. Iafrate, Dr. A. Ballato, and Professor M. A. Littlejohn. This work was supported, in part, by the Office of Naval Research and the U.S. Army Research Office.

[1] M. Yamada and Y. Suematsu, J. Appl. Phys. **52**, 2653 (1981).
[2] W. Rideout, W. F. Sharfin, E. S. Koteles, M. O. Vassell, and B. Elman, IEEE Photon. Technol. Lett. **PTL-3**, 784 (1991).
[3] S. Das Sarma, in *Hot Carriers in Semiconductor Nanostructures: Physics and Applications*, edited by J. Shah (Academic, Boston, 1992), pp. 53–85.
[4] S. Das Sarma, V. B. Campos, M. A. Stroscio, and K. W. Kim, Semicond. Sci. Technol. **7**, B60 (1992).
[5] M. Born and K. Huang, *Dynamical Theory of Crystal Lattices* (Oxford, London, 1954).
[6] P. G. Klemens, in *Solid State Physics*, edited by F. Seitz and D. Turnbull (Academic, New York, 1958), Vol. 7, p. 1.
[7] A. A. Maradudin and A. E. Fein, Phys. Rev. **128**, 2589 (1962).
[8] P. G. Klemens, Phys. Rev. **148**, 845 (1966).
[9] D. K. Ferry, Phys. Rev. B **9**, 4277 (1974).
[10] P. F. Tua, Ph.D. thesis, Indiana University, 1981.
[11] P. F. Tua and G. D. Mahan, Phys. Rev. B **26**, 2208 (1982).
[12] R. Gupta and B. K. Ridley, in *Proceedings of NATO Advanced Research Workshop on Phonons in Nanostructures*, edited by J.-P. Leburton, J. Pascual, and C. Sotomayor Torres (Kluwer, Boston, 1993), pp. 261–272.
[13] P. N. Keating, Phys. Rev. **149**, 674 (1966).
[14] K. Kunc and O. H. Nielson, Comput. Phys. Commun. **17**, 413 (1979); **16**, 181 (1979).
[15] K. Brugger, Phys. Rev. **133**, A1611 (1964).
[16] *Landolt-Börnstein Tables*, edited by K.-H. Kellwege and A. M. Kellwege (Springer, Berlin, 1979), Group III, Vol. 11.
[17] A. I. Gubanov and S. Yu. Davydov, Fiz. Tverd. Tela **14**, 1195 (1972) [Sov. Phys. Solid State **14**, 1020 (1972)].
[18] D. Von der Linde, J. Khul, and H. Klingerberg, Phys. Rev. Lett. **44**, 1505 (1980).
[19] J. A. Kash and J. C. Tsang, Solid-State Electron. **31**, 419 (1988).
[20] W. Pötz and P. Kocevar, in *Hot Carriers in Semiconductor Nanostructures: Physics and Applications*, edited by J. Shah (Academic, New York, 1992), p. 87.

Elastic vibrations of microtubules in a fluid

Yuri M. Sirenko
Department of Electrical and Computer Engineering, North Carolina State University, Raleigh, North Carolina 27695-7911

Michael A. Stroscio
U.S. Army Research Office, P.O. Box 12211, Research Triangle Park, North Carolina 27709-2211

K. W. Kim
Department of Electrical and Computer Engineering, North Carolina State University, Raleigh, North Carolina 27695-7911
(Received 13 April 1995)

We study theoretically vibrational properties of microtubules (MTs), which are long hollow cylindrical macromolecules with a diam. of the order of 25 nm and serve as a major component of cytoskeleton in eukariotic cells. Modeling MTs by thin elastic cylindrical shells, we derive the eigenfrequencies and eigenmodes of confined elastic vibrations in a shell-fluid system. Numerical calculations, based on recently obtained experimental data for Young's modulus of MT, show that MT-water system supports interface elastic waves with maximal frequencies in a gigahertz range. In a long-wavelength limit, there exist three axisymmetric acoustic waves with velocities of about 200 to 600 m/s, and an infinite set of helical waves with a parabolic dispersion law.

PACS number(s): 87.15.−v

I. INTRODUCTION

The increasing demand for miniaturization and enhancement of the operation speed has culminated in tremendous progress in nanostructure fabrication and the advent of the principally new microelectronic devices. Recently, much attention has been devoted to the problem of *confined* optical [1] and acoustic [2–5] vibrations in semiconductor heterostructures. Dispersion relations for acoustic waves and the effect of the phonon confinement on electron transport has been analyzed in such artificially grown objects as thin metal films [2], free-standing slabs [3] and whiskers [4], as well as buried cylindrical wires [5]. It has been suggested that such structures with confined lattice vibrations can provide an acoustic fiber for future acoustoelectronic devices [5].

On the other hand, the existence of the physical limitations for the miniaturization due to the atomic structure of matter brought about a new scientific direction, molecular electronics [6]. In contrast to the semiconductor technology that relies on artificially designed structures, molecular electronics explores the physical properties of existing organic macromolecules and their possible applications to information processing. In particular, elastic properties of biological membranes [7] and flagella [8] in an aqueous environment have been studied extensively.

From the point of view of nanophysics and molecular electronics, one of the most interesting biological objects is a cytoskeleton filamentous network existing in every eukariotic cell [9,10]. The various filaments have been classified according to their diameter and include microfilaments (5–7 nm), intermediate filaments (8–11 nm), and microtubules (24–28 nm). Though the cytoskeleton has an impact on some purely biological processes [11] (control of gene expression, protein synthesis, and cell cycle regulation), its main functions are based on the mechanical properties such as rigidity and elasticity. The cytoskeleton is responsible for supporting the cell shape and serves as a global framework for the mechanical and functional integration of the whole cell [12]. Recently, in a series of ingenious experiments, based on the change of filament shape due to thermal (Brownian) fluctuations, the flexural rigidity and Young's elastic modulus have been measured for the intermediate filaments [15] and microtubules [16–19].

Among three major filamentous components of the cytoskeleton, microtubules (MTs) have received the most attention and are subject to intensive research [9,20–22]. MTs are hollow cylinders [13] of approximately 25 nm outer diameter, 15 nm inner diameter, and indefinite length (see Fig. 1). The wall of a MT cylinder is made

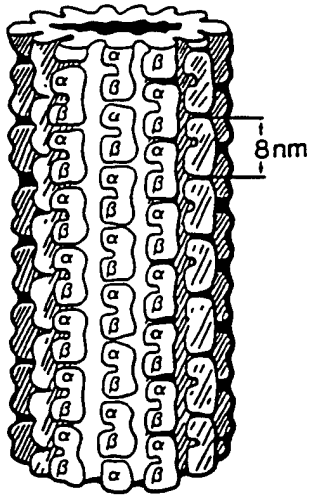

FIG. 1. Schematic drawing of a microtubule formed with protofilaments of tubulin dimers (from Ref. [14]).

up of (usually 13) linear elements termed protofilaments, which are formed of protein subunits known as tubulin dimers. Each 8-nm-long dimer consists of α and β tubulin monomers with a molecular weight of 55 kDa. Results of electron microscopy and x-ray fiber diffraction measurements demonstrate that tubulin dimers form a 120-Å pitch left-handed three-start helix set [23]. The thin-walled tubular shape of MT provides the maximal rigidity of the structure for given cross-sectional area and elastic constants of the constituent material [18].

The main directions of biophysical research on MTs include the study of their elastic properties [16–19] and the dynamical instability of assembling and disassembling [24,25]. The possibility of kinklike excitations in MTs has been investigated theoretically [26] and the experimental observation of MT disassembly due to a low-intensity ultrasound has been reported [27]. Incidentally, considerable attention in semiconductor physics has been focused on the study of electronic and vibrational properties of recently fabricated artificial counterparts of MT—graphene nanotubules [28].

In this paper, we study theoretically the confined acoustic vibrations of MT in a fluid using the formalism of the elasticity theory. The MT is modeled by a thin-walled hollow elastic cylinder immersed in liquid. This approach is similar to that used for the description of underwater acoustic scattering by thin metallic shells [29]. In Sec. II, we obtain the equations of motion for vibrations in a shell-fluid system and derive the dispersion relations for the elastic waves that are analyzed in Sec. III. The results of numerical calculations and discussion are provided in Sec. IV.

II. EQUATIONS OF MOTION

We model a microtubule with an infinitely long cylindrical shell of radius R and wall thickness h. In cylindrical coordinates (r,φ,z), the shell is chosen to be located in the region $R-h/2<r<R+h/2$; both the inner and outer parts of the shell are filled with a fluid. The equation of motion for the displacement vector $\mathbf{u}$ of the shell is given by the second Newton's law, which in cylindrical coordinates has the form [30]

$$\begin{aligned}\sigma_{rr,r}+\sigma_{rz,z}+(\sigma_{r\varphi,\varphi}+\sigma_{rr}-\sigma_{\varphi\varphi})/r&=\rho\ddot{u}_r\,,\\ \sigma_{r\varphi,r}+\sigma_{\varphi z,z}+(\sigma_{\varphi\varphi,\varphi}+2\sigma_{r\varphi})/r&=\rho\ddot{u}_\varphi\,,\\ \sigma_{rz,r}+\sigma_{zz,z}+(\sigma_{\varphi z,\varphi}+\sigma_{rz})/r&=\rho\ddot{u}_z\,,\end{aligned}\qquad(1)$$

where ρ is a volume density of the shell. The left-hand sides of these equations are equal to elastic forces per unit volume and are written in terms of the stress tensor σ. The subscripts after the commas denote partial derivatives over corresponding variables. Equation (1) is subject to conditions $P_i=\sigma_{ij}n_j$ at the inner and outer surfaces of the shell, where $\mathbf{P}$ is a surface force per unit area and $\mathbf{n}$ is a unit vector normal to the boundary. Since shear forces are absent in fluids, the boundary conditions take the form

$$\sigma_{r\varphi}|_{r=R\mp h/2}=\sigma_{rz}|_{r=R\mp h/2}=0\,,\qquad(2)$$

$$\sigma_{rr}|_{r=R+h/2}=p_o\,,\quad \sigma_{rr}|_{r=R-h/2}=p_i\,,\qquad(3)$$

where p_0 and p_i are the pressures of fluid at the outer and inner boundaries of the shell.

In order to obtain the equations of motion for a *thin* shell ($h\ll R$), Eq. (1) is integrated over r from $R-h/2$ to $R+h/2$. Assuming that all quantities (except σ_{rr}) are practically constant with respect to r, and taking into account the boundary conditions given in Eqs. (2) and (3), we find in the lowest order in small parameter h/R:

$$\begin{aligned}-\sigma_{\varphi\varphi}/R+(p_o-p_i)/h&=\rho\ddot{u}_r\,,\\ \sigma_{\varphi\varphi,\varphi}/R+\sigma_{\varphi z,z}&=\rho\ddot{u}_\varphi\,,\\ \sigma_{\varphi z,\varphi}/R+\sigma_{zz,z}&=\rho\ddot{u}_z\,.\end{aligned}\qquad(4)$$

The stress tensor σ can be expressed in terms of strain tensor ε with the help of the Hooke's law. In the assumption of isotropic material of the shell, it is given as

$$\sigma_{ij}=\frac{E}{1+\nu}\left[\frac{\nu}{1-2\nu}\,\delta_{ij}\sum_l\varepsilon_{ll}+\varepsilon_{ij}\right],\qquad(5)$$

where E and ν are Young's modulus and Poisson's ratio of the material. We substitute Eq. (5) into Eq. (4), eliminate the component ε_{rr} with the help of Eq. (2), and express the remaining components of strain tensor $\varepsilon_{\varphi\varphi}$, $\varepsilon_{\varphi z}$, and ε_{zz} in terms of derivatives of the displacement vector $\mathbf{u}$ [30]. Then, the equations of motion in the lowest order in h/R may be written as

$$\begin{aligned}-\frac{u_r+u_{\varphi,\varphi}}{R^2}-\frac{\nu\,u_{z,z}}{R}+\frac{p_i-p_o}{\rho hs^2}&=\frac{\ddot{u}_r}{s^2}\,,\\ \frac{u_{r,\varphi}+u_{\varphi,\varphi\varphi}}{R^2}+\nu_-u_{\varphi,zz}+\frac{\nu_+u_{z,\varphi z}}{R}&=\frac{\ddot{u}_\varphi}{s^2}\,,\\ \frac{\nu\,u_{r,z}+\nu_+u_{\varphi,\varphi z}}{R}+\frac{\nu_-u_{z,\varphi\varphi}}{R^2}+u_{z,zz}&=\frac{\ddot{u}_z}{s^2}\,.\end{aligned}\qquad(6)$$

Here $\nu_\pm=(1\pm\nu)/2$, and $s=\sqrt{E/\rho(1-\nu^2)}$ is the longitudinal "thin plate" sound speed of the shell.

To obtain the equation of motion of the fluid-shell system in a closed form, the pressure terms $p_{i,o}$ need to be related to the shell displacement vector $\mathbf{u}$. The displacement vector $\mathbf{u}_f$ of the fluid can be expressed in terms of the scalar potential Φ through the relationship

$$\mathbf{u}_f=\operatorname{grad}\Phi\,;\qquad(7)$$

Φ satisfies the wave equation [32]

$$\ddot{\Phi}-s_f^2\,\Delta\Phi=0\,,\qquad(8)$$

where s_f is a speed of sound in a fluid. Then, using the relation between the scalar potential and pressure

$$p=-\rho_f\ddot{\Phi}\,,$$

where ρ_f is a fluid density, the equation for the radial displacement u_r of the shell [given in Eq. (6)] can be rewritten as

$$-\frac{u_r + u_{\varphi,\varphi}}{R^2} - \frac{\nu u_{z,z}}{R} + \alpha \frac{\ddot{\Phi}_i - \ddot{\Phi}_o}{s^2 R} = \frac{\ddot{u}_r}{s^2} , \qquad (9)$$

where $\alpha = \rho_f R/\rho h$ is a dimensionless constant that characterizes the shell-fluid coupling.

We seek the solution of the equations of motion [i.e., Eqs. (6) and (9)] as a superposition of harmonic waves with longitudinal wave vector k_z and azimuthal number m,

$$\begin{bmatrix} u_r \\ u_\varphi \\ u_z \end{bmatrix} = \begin{bmatrix} -ic_r \\ c_\varphi \\ c_z \end{bmatrix} \exp(im\varphi + ik_z z - i\omega t) , \qquad (10)$$

and choose the solutions of Eq. (8) for scalar potentials of fluid corresponding to the evanescent *interface* vibrations localized in the vicinity of the shell:

$$\begin{bmatrix} \Phi_i \\ \Phi_o \end{bmatrix} = \begin{bmatrix} c_i I_m(\kappa r/R) \\ c_o K_m(\kappa r/R) \end{bmatrix} \exp(im\varphi + ik_z z - i\omega t) . \qquad (11)$$

Here the inverse confinement length κ (normalized by the radius R) is given by

$$\kappa^2 = R^2(k_z^2 - \omega^2/s_f^2) \equiv k^2 - \left(\frac{s}{s_f}\right)^2 \Omega^2 , \qquad (12)$$

where $\Omega = \omega R/s$ and $k = k_z R$ are the dimensionless frequency and wave vector, respectively. Interface vibrations of fluid, localized near the shell surface, correspond to region $\kappa^2 > 0$; in the opposite case of $\omega > s_f k_z$ the acoustic energy is radiated from the shell. The requirement of the continuity of the fluid and shell displacements at $r = R$ leads, after use of Eq. (7), to the following relation between $c_{i,o}$ and c_r:

$$\begin{bmatrix} c_i \\ c_o \end{bmatrix} = -ic_r R \begin{bmatrix} 1/\kappa I_m'(\kappa) \\ 1/\kappa K_m'(\kappa) \end{bmatrix} . \qquad (13)$$

Finally, substituting Eqs. (10)–(13) into (6) and (9), we obtain the eigenequation for the interface acoustic vibration in the a shell-fluid system:

$$\mathcal{D}\,[c_r,\, c_\varphi,\, c_z]^{\mathrm{T}} = 0 , \qquad (14)$$

where the dynamical matrix $\mathcal{D}$ is given by

$$\mathcal{D} = \begin{bmatrix} \Omega^2(1 + W_{m\kappa}) - 1 & m & \nu k \\ m & \Omega^2 - m^2 - \nu_- k^2 & -\nu_+ mk \\ \nu k & -\nu_+ mk & \Omega^2 - \nu_- m^2 - k^2 \end{bmatrix} , \qquad (15)$$

and the coupling term between the shell and fluid is equal to

$$W_{m\kappa} = \frac{\alpha}{\kappa}\left[\frac{I_m(\kappa)}{I_m'(\kappa)} + \frac{K_m(\kappa)}{-K_m'(\kappa)}\right] . \qquad (16)$$

III. ANALYSIS OF DISPERSION RELATION

From Eq. (14) we find the dispersion relation for confined waves in a shell-fluid system in a form

$$\det \mathcal{D} = 0 . \qquad (17)$$

As follows from Eqs. (15) and (16), $\mathcal{D}$ is a real symmetric 3×3 matrix depending on azimuthal number m. Therefore, for each given m the dispersion relation [Eq. (17)] specifies three positive vibrational modes $\Omega_m^{(j)}$, which are identified by j =I, II, and III in decreasing order:

$$\Omega_m^{\mathrm{I}}(k) > \Omega_m^{\mathrm{II}}(k) > \Omega_m^{\mathrm{III}}(k) . \qquad (18)$$

The only exclusion from inequality in Eq. (18) occurs for $m = 0$, where the pure *torsional* mode,

$$\Omega_0^{\mathrm{II}}(k) = \sqrt{\nu_-}\,k , \qquad (19)$$

is decoupled from other modes over the entire range of k, and can cross the mode with j =III; a graphical illustration is given in the next section.

A. Free cylindrical shell

Let us first analyze the vibration of a *free* cylindrical shell [31] by taking the coupling constant α equal to zero. In this case, the dispersion relation defined by Eqs. (15)–(17) is reduced to a *bicubic* equation with respect to the dimensionless frequency $\Omega \equiv \omega R/s$. It is more convenient, however, to calculate the inverse relation $k_{jm}(\Omega)$ as a solution of *bi-quadratic* equation in wave vector k. Since the explicit form of the dispersion relation can be readily obtained from Eqs. (15) and (17), we present only the asymptotic values of $\Omega_m^{(j)}(k)$. For a large wavelength ($k \equiv k_z R \ll 1$), we have

$$\Omega_m^{\mathrm{I}}(k) \simeq \sqrt{m^2 + 1}, \quad \Omega_m^{\mathrm{II}}(k) \simeq \sqrt{\nu_-}(m + k), \qquad (20)$$

$$\Omega_{m=0}^{\mathrm{III}}(k) \simeq \sqrt{1 - \nu^2}\,k, \quad \Omega_{m\neq 0}^{\mathrm{III}}(k) \simeq \sqrt{\frac{1-\nu^2}{m^2+1}}\,\frac{k^2}{m} .$$

In the axisymmetric case ($m = 0$) and a long-wavelength limit, the modes I, II, and III correspond to pure *radial*, *torsional*, and *longitudinal* motion; for $m \neq 0$ the radial and torsional motions are coupled. In the short-wavelength limit ($k \gg m + 1$), we obtain asymptotic expressions that are not dependent on the azimuthal number m:

$$\Omega_m^{\mathrm{I}}(k) \simeq k, \quad \Omega_m^{\mathrm{II}}(k) \simeq \sqrt{\nu_-}k, \quad \Omega_m^{\mathrm{III}}(k) \simeq \sqrt{1-\nu^2}. \quad (21)$$

Analysis of coefficients c_r, c_φ, and c_z in Eq. (14) shows that in the limit of large k the modes $\Omega_m^{\mathrm{I}}(k)$, $\Omega_m^{\mathrm{II}}(k)$, and $\Omega_m^{\mathrm{III}}(k)$ correspond to pure *longitudinal, torsional,* and *radial* vibrations. Note that for any m the minimal value of Ω_m^{I} is greater then the maximal value of Ω_m^{III}. Therefore, for given frequency Ω there exist no more than two positive wave vectors $k_m^{(j)}$, which is consistent with the availability of the *biquadratic* dispersion relation with respect to k.

B. Fluid-shell system

Let us return now to the analysis of Eq. (17) for vibrations in a *coupled* shell-fluid system ($\alpha \neq 0$). Existence of a fluid in the outer part of the shell can lead to a qualitative change in the dispersion relation. Now the (ω, k_z) plane is divided to two sectors by the line $\omega = s_f k_z$. The region $\omega < s_f k_z$ (or $\kappa^2 > 0$) corresponds to the *interface* vibrations, localized at distance R/κ from the shell according to Eq. (11). The opposite case of $\omega > s_f k_z$ (or $\kappa^2 < 0$) can be described by Eq. (11), after the substitution of [33]

$$I_m(-i|\kappa|) = i^{-m} J_m(|\kappa|),$$

$$K_m(-i|\kappa|) = \frac{\pi}{2} i^{m+1} H_m^{(1)}(|\kappa|),$$

as the radiation of an acoustic wave to the outer space since the Hankel function of the first kind, $H_m^{(1)}$, corresponds to an outgoing cylindrical wave. In this situation, the eigenfrequencies $\Omega(k)$ will be complex with negative imaginary parts and, according to Eqs. (10) and (11), the amplitudes of vibrations will decay exponentially in time due to an energy loss by the system. From the discussion above, it follows that the behavior of acoustic modes depends drastically on the relation between the sound speeds in a fluid and the shell, s_f and s. Since sound speed in water is approximately 2.5 times larger than that in the MT (as discussed in the next section), $s_f > s$ is assumed throughout the rest of this paper.

To describe the spectrum of vibrations in the shell-fluid system, we derive the asymptotical expressions for the coupling term $W_{m\kappa}$ in two limiting cases of phase velocities (i) close to s_f (small κ) and (ii) much smaller than s_f (large κ). Using the expression for the Wronskian of the modified Bessel equation [33], $I_m(\kappa)K_m'(\kappa) - K_m(\kappa)I_m'(\kappa) = 1/\kappa$, and asymptotics of functions I_m and K_m, we find from Eq. (16)

$$W_{m\kappa} \simeq \begin{cases} 2\alpha/\kappa^2, & \text{for } \kappa \ll 1 \text{ and } m = 0 \\ 2\alpha/m, & \text{for } \kappa \ll 1 \text{ and } m \neq 0 \\ 2\alpha/\kappa, & \text{for } \kappa \gg m+1 \text{ and any } m. \end{cases} \quad (22)$$

Since at large κ the coupling term $W_{m\kappa} \simeq 2\alpha/\kappa$ tends to zero, we deduce that in a *short-wavelength* limit ($k \gg m+1$), the vibration spectrum of the shell-fluid system tends to that of a free shell [Eq. (21)], and classification of modes I, II, III as pure *longitudinal, torsional,* and *radial,* is unchanged. The physical explanation for this result is that in the limit of large κ, only a fluid in the nearest vicinity, within R/κ from the shell, participates in vibration; therefore, the motion of the shell is essentially free.

In the *long-wavelength* limit, there exist two distinct cases: $m = 0$ and $m \neq 0$. For *axisymmetric* vibrations (m=0), the mode II with dispersion given by Eq. (19) corresponds to a pure torsional vibrations of the shell *only,* and is decoupled from the rest of the modes in the whole range of k. The frequencies of axisymmetric modes I and III should be found from the remaining 2×2 determinant involving the coupling term $W_{0\kappa}$. Since this term diverges at small κ [Eq. (22)], the frequencies $\Omega_0^{\mathrm{I}}(k)$ and $\Omega_0^{\mathrm{III}}(k)$ at small k should approach zero maintaining phase velocities less than s_f to avoid crossing the $\omega = s_f k_z$ line. Analysis shows that in the limiting case of small k the frequencies $\Omega_0^{\mathrm{I}}(k)$ and $\Omega_0^{\mathrm{III}}(k)$ are proportional to the wave vector:

$$\Omega_0^{\mathrm{I,III}}(k) \simeq \sqrt{c_{1,3}}k\,. \quad (23)$$

Substituting the expansion given in Eq. (23) into the dispersion equation, and collecting the terms of the lowest (second) order in k, the coefficients $c_{1,3}$ are found as solutions of the following quadratic equation:

$$(s^2 + 2\alpha s_f^2)c^2 - [s^2(1-\nu^2) + s_f^2(1+2\alpha)]c + s_f^2(1-\nu^2) = 0\,. \quad (24)$$

It can be shown that Eq. (24) always has two real positive roots, provided that $s_f > s$. In case of $2\alpha \gg (s/s_f)^2$ and $\nu^2 \ll 1$ the solutions of Eq. (24) are given by $c_1 \approx 1$ and $c_3 \approx 1/2\alpha$. For a coupled system (in contrast to a free shell), both modes I and III are of the mixed *radial-longitudinal* type even at $m = 0$ and small k. Note also that in the absence of fluid the frequency of the mode I would have a finite value at $k = 0$: in the case of $\alpha = 0$ we have $\Omega_0^{\mathrm{I}}(0) = 1$ in accordance with Eq. (20).

In the case of vibrations *without rotational symmetry* ($m \neq 0$), the coupling term $W_{m\kappa}$ reaches a finite value $W_{m0} = 2\alpha/m$ at $\kappa = 0$ [see Eq. (22)], and modes I and II touch the line $\omega = s_f k_z$ at finite frequencies, while the localization length R/κ will tend to infinity. However, in the case of $\mathrm{Re}\,(\omega) > s_f k_z$ the frequency ω will have a negative imaginary part, and the amplitudes of vibrations will decay as a result of the radiation of acoustic energy out of the shell. The frequency of the mode III will preserve its parabolic dependence on the wave vector in the limit of small k [Eq. (20)], though with a renormalized coefficient:

$$\Omega_{m\neq 0}^{\mathrm{III}}(k) \simeq \sqrt{\frac{1-\nu^2}{m^2+2\alpha m+1}}\frac{k^2}{m}\,. \quad (25)$$

Thus, in the long-wavelength limit ($k_z \ll 1/R$), the shell-fluid system supports three axisymmetric interface modes with a linear dispersion law, $\Omega_0^{(j)}(k) \propto k$, corresponding to conventional *acoustic waves* with linear dis-

persion. In addition, there exists an infinite set of interface modes with a parabolic dispersion law, $\Omega_m^{III}(k) \propto k^2$ and $m = 1, 2, \ldots$, as given by Eq. (25). Since the lines of constant phases for such waves,

$$m\varphi + k_z z - \omega t = \text{const} ,$$

have the form of helices according to Eqs. (10) and (11), this set of modes can be termed as *helical waves*. In contrast to acoustic waves with constant phase and group velocities, those for helical waves tend to zero at small wave vectors k_z.

IV. NUMERICAL RESULTS AND DISCUSSION

In order to find the vibrational spectrum of the shell-fluid system in the whole range of k, we have to solve the transcendental dispersion relation given by Eqs. (15)–(17) numerically. Among the parameters required for the numerical evaluation, the most difficult to obtain are the elastic constants, E and ν, for MT, since no direct measurement seems to be possible. However, the results depend only weakly on the Poisson's ratio ν, and reliable values for the Young's modulus E has been measured [16–19] using the elegant method based on thermal fluctuations of shape of MT.

The main physical idea for the measurement of a flexible rigidity (FR) of long macromolecules is that they are subject to the Brownian motion due to interaction with the surrounding molecules of water [34,35]. Since the macromolecules are relatively heavy, the fluctuation of their center of mass is negligible, but their shape can be changed notably, depending directly on the FR for the molecule. The latter is equal to EI, i.e., the product of Young's modulus E and the geometrical moment of inertia I of a molecule's cross section.

The first determination of the MT rigidity, performed by Yamazaki, Maeda, and Miki-Noumura [16] and Mizushima-Sugano, a Maeda, and Miki-Noumura [17], were based on measurement of the thermal fluctuations of the end-to-end distance of MT; knowledge of these fluctuations and the total length of MT allows the determination of the FR [35]. However, such measurements lack a test of internal consistency, which is desirable because of the difficulty in distinguishing fluctuations from measurement noise and nonthermal bending [18]. It is believed now that the values obtained in Refs. [16,17] are almost 2 orders of magnitude smaller than the actual ones because of measurement errors and intrinsic bend of MT [18].

The first reliable data on the rigidity of MT have been obtained by Gittes *et al.* [18] using dark-field and fluorescence video-enhanced microscopy to monitor the thermal fluctuations in shape of taxol-stabilized MT free in solution. In order to overcome the problems due to the measurement noise, the FR was deduced from the Fourier decomposition of the MT shape. Results of analysis of up to the three lowest Fourier modes of the shape of MT of different length were consistent with each other and gave the value of FR corresponding to the isotropic Young's modulus $E \sim 1.2$ GPa. Gittes *et al.* [18] have also measured the FR of actin filaments and obtained the value of the Young's modulus $E = 2.6$ GPa in good agreement with the earlier results [15]. More recently, Venier *et al.* [19] applied two independent methods to measure the FR of MT attached by one end to axonemal pieces fixed on the glass. In this study, the FR was obtained by analyzing the bending shape of MT in a hydrodynamic flow and the thermal fluctuations of the free end of MT. Both methods gave similar results for FR corresponding to an isotropic Young's modulus $E = 0.5 \pm 0.1$ GPa. The factor of 2 discrepancy with the results of Gittes *et al.* were interpreted as due to the stiffening action of taxol used in Ref. [18] to stabilize the MT.

In our numerical calculations, the most recent value of Young's modulus, $E = 0.5 \pm 0.1$ GPa from Ref. [19], is used. Another parameter needed in the calculation is Poisson's ratio ν. In general, the value for this parameter (of known materials) lies in the range $0 < \nu < 1/2$, with typical values of $\nu = 0.2$–0.3. Since our results depend only weakly on ν, we choose, for the sake of definiteness, the value $\nu = 0.3$.

Approximation of a microtubule by a hollow cylinder with ideal surfaces used in Refs. [18,19] to calculate the geometric moment of inertia, required the use of "contact" inner radius R_i of 11.5 nm (measured in Ref. [23]) and wall thickness h of 2.7 nm for 14-protofilament MT. Thus, the outer radius R_o of MT in our calculation is 14.2 nm and the mean radius $R \equiv (R_i + R_o)/2$ is approximately 12.8 nm. At the same time, by taking the mass of a tubulin dimer to be $M = 110$ kDa $= 1.83 \times 10^{-19}$ g, and the length $\ell = 8$ nm, we find the density $\rho = 14M/\pi(R_o^2 - R_i^2)\ell \approx 1.47$ g/cm^3 and the "thin-plate" sound speed $s = \sqrt{E/\rho(1-\nu^2)} \approx 610$ m/s. Using the density of water ($\rho_f = 1$ g/cm^3) and speed of sound in water ($s_f = 1.50$ km/s), the value of the dimensionless coupling constant $\alpha \equiv \rho_f R/\rho h$ is found to be approximately 3.22.

We note that the calculated sound speed in MT is 2.5 times lower than in water, in contrast to that in materials with cellulose-based cell walls (e.g., wood), where the propagation speed is substantially higher. The reason for such a difference lies in the large Young's modulus of cellulose, $E \sim 100$ GPa [36], and is because of the nature of chemical binding in this polymer. In fact, glucose monomers are linked to cellulose by strong β 1,4-glicosyde (covalent) bonds, while tubulin subunits assemble into MT due to much weaker hydrophobic interaction.

The results of numerical calculations of dispersion $\Omega_m^{(j)}(k)$ for azimuthal numbers m =1, 2, and 3 are presented in Figs. 2–4. Thick solid lines correspond to vibrations of MT interacting with water both *outside* and *inside* of MT. The eigenfrequencies of *free* MT are presented for comparison and are marked by thick dashed lines. The thin line is specified by $\omega = s_f k_z$ and it separates the region of interface vibrations in the MT-water system from that of radiative waves. Note that the dimensionless frequency $\Omega = 1$ corresponds to a cyclic frequency of $f_0 \approx 7.6$ GHz.

As can be seen from Figs. 2–4, the frequencies of vi-

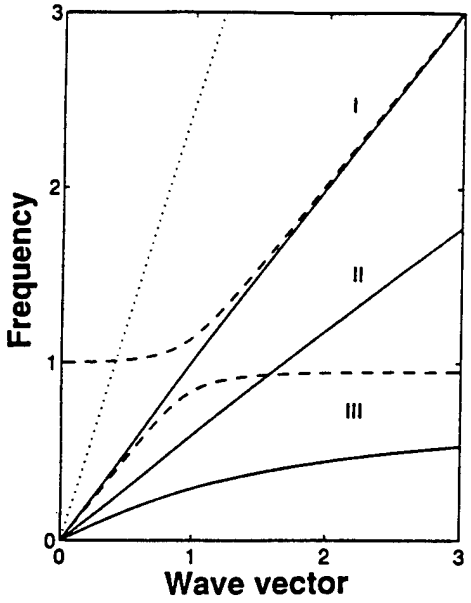

FIG. 2. Dimensionless frequency $\Omega = \omega R/s$ vs dimensionless wave vector $k = Rk_z$ for axisymmetric ($m = 0$) vibrations of MT. $\Omega = 1$ corresponds to a cyclic frequency 7.6 GHz. Solid and dashed lines correspond to vibrations in a MT with and without water, respectively. Thin dotted line at $\omega = s_f k_z$ separates regions of interface and radiative waves.

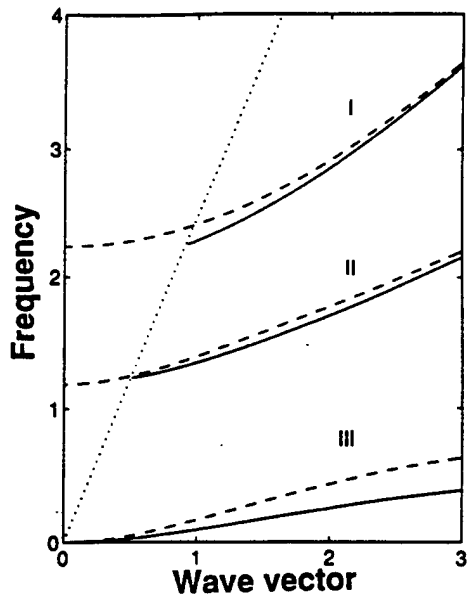

FIG. 4. Dispersion relations for vibration of MT with azimuthal number $m = 2$. Other notations coincide with those in Fig. 2.

brations for MT-water system tend to those of a *free* MT at large wave vectors ($k_z \gg m/R$) and do not depend on the azimuthal number m. In a short-wavelength limit, the modes I and II have a linear dispersion with velocities $s \approx 610$ m/s and $s\sqrt{(1-\nu)/2} \approx 360$ m/s, while the cyclic frequencies of the type-III modes tend to a constant value of 7.2 GHz [see Eq. (20)]. In the limit of large k, modes I, II, and III correspond to pure longitudinal, torsional, and radial vibrations. Note that because of our assumption of homogeneous MT walls, the results at $k \gtrsim 1$ are only of qualitative character (the length of the tubulin dimer, 8 nm, is comparable to the radius of MT, 13 nm). Moreover, since our derivation was based on the assumption of thin MT walls ($h \ll R$), the results are even qualitatively wrong for $k > R/h \approx 5$. The assumptions made do not modify the long-wavelength ($k \ll 1$) part of the spectrum, which is of prime importance for the study of conformational changes in proteins [37,38].

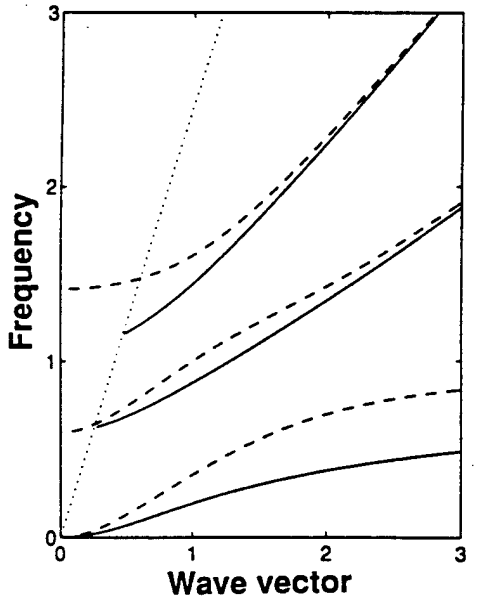

FIG. 3. Dispersion relations for vibration of MT with azimuthal number $m = 1$. Other notations coincide with those in Fig. 2.

The behavior of the eigenfrequencies at intermediate and small values of wave vector k depends essentially on whether the azimuthal number m is equal to zero.

For axisymmetric vibrations ($m = 0$), the mode $\Omega_0^{\mathrm{II}}(k) = \sqrt{(1-\nu)/2}k$ with the velocity 360 m/s (see Fig. 2) involves the pure torsional vibrations of the shell *only* and is decoupled from other modes [cf. Eq. (19)]. The other two modes in Fig. 2 (I and III) cannot touch the line $\omega = s_f k_z$, because the shell-fluid coupling term $W_{0\kappa}$ [given by Eq. (22)] diverges when phase velocity of a wave approaches sound speed in a fluid s_f. At large wavelength, the radial-longitudinal modes I and III depend linearly on k and are characterized by speeds of propagation 614 and 225 m/s according to Eqs. (23) and (24). The linear dependence of Ω_0^{I}, Ω_0^{II}, and Ω_0^{III} on k in the long-wavelength limit allows us to identify them with conventional *acoustic* modes, in contrast to other elastic modes that also could be called acoustical. For vibrations without rotational symmetry, two modes (Ω_m^{I} and Ω_m^{II}) for each given $m \neq 0$ cross the line $\omega = s_f k_z$ and become *radiative* modes at small k. Continuation of their dispersion curves is not shown at $k_z < \mathrm{Re}\,(\omega/s_f)$ in Figs. 3 and 4, since in this region the eigenfrequencies

are complex. The *helical* mode III remains real at all wavelengths, and $\Omega_m^{III} \propto k^2$ in agreement with Eq. (25).

V. CONCLUSION

We have investigated the existence of interface elastic vibrations of MT immersed in water. It is found that this system supports nonradiative elastic waves localized in the vicinity of the MT wall with maximal frequencies of order of tens of gigahertz. In the long-wavelength limit, there exist three axisymmetric *acoustic* waves with propagation speed of approximately 200–600 m/s and an infinite set of *helical* waves with a parabolic dispersion law.

Our results draw attention to a parallel existing between recent studies of acoustic phonon quantization in artificially grown semiconductor nanostructures [2–5,28] and vibrations of their biological counterparts, microtubules. On other hand we hope that our analysis of large-scale collective motions of MT based on elasticity formalism complements molucular dynamics simulations of vibrational spectra of globular proteins [37–39].

ACKNOWLEDGMENTS

This work was supported, in part, by the U.S. Army Research Office and the Office of Naval Research. We would like also to thank Jack Kohn of the U.S. Army Research Laboratory (formerly Electronics Technology and Devices Laboratory) for drawing our attention to this problem.

[1] L. Wendler, Phys. Status Solidi (b) **124**, 513 (1985); N. Mori and T. Ando, Phys. Rev. B **40**, 6175 (1989); M. A. Stroscio, *ibid.* **40**, 6428 (1989); K. W. Kim *et al.*, J. Appl. Phys. **72**, 2282 (1992).

[2] N. Perrin and M. N. Wybourne, Phys. Rev. B **43**, 9511 (1991); J. C. Nabity and M. N. Wybourne, *ibid.* **44**, 8990 (1991); K. Johnson, M. N. Wybourne, and N. Perrin, *ibid.* **50**, 2035 (1994).

[3] N. Bannov, V. Mitin, and M. Stroscio, Phys. Status Solidi (b) **183**, 131 (1994); N. Perrin, Phys. Rev. B **48**, 12 151 (1994); N. Bannov, V. Aristov, and V. Mitin, Solid State Commun. **93**, 483 (1995).

[4] A. K. Viswanath *et al.*, Microwave Optical Technol. Lett. **7**, 94 (1994); M. A. Stroscio and K. W. Kim, Phys. Rev. B **48**, 1936 (1993); S. Yu *et al.*, *ibid.* **50**, 1733 (1994); M. A. Stroscio *et al.*, J. Appl. Phys. **76**, 4670 (1994).

[5] N. Nishiguchi, Jpn. J. Appl. Phys. **33**, 2852 (1994); Phys. Rev. B **50**, 10 970 (1994).

[6] *Molecular Electronics — Science and Technology*, edited by A. Aviram (Engineering Foundation, New York, 1989); D. Koruga and J. Simić-Krstić, J. Mol. Electron. **6**, 167 (1990).

[7] R. Lipowsky, Festkörperprobleme **32**, 19 (1992); H. Bolterauer, J. A. Tuszyński, and M. V. Satarić, Phys. Rev. A **44**, 1366 (1991).

[8] R. Rikmenspoel, in *Dynamics in Fluids and Plasmas*, edited by S. I. Pai (Academic, New York, 1966), p. 9.

[9] M. Schliwa, *The Cytoskeleton. An Introductory Survey* (Springer, New York, 1986).

[10] P. Traub, *Intermediate filaments. A Review* (Springer, New York, 1985); K. C. Holmes *et al.*, Nature (London) **347**, 44 (1990).

[11] U. Z. Littauer and I. Ginsburg, in *Gene Expression in Brain*, edited by C. Zomzely-Neurath and W. A. Walker (Wiley, New York, 1985).

[12] K. Luby-Phelps, Current Opinion Cell Biol. **6**, 3 (1994).

[13] L. Beese, G. Stubbs, and C. Cohen, J. Mol. Biol. **194**, 257 (1987).

[14] S. Rasmussen *et al.*, Physica (Amsterdam) **42D**, 428 (1990).

[15] T. Takebayashi, Y. Morita, and F. Oosawa, Biochem. Biophys. Acta **492**, 357 (1977); H. Nagashima and S. Asakura, J. Mol. Biol. **136**, 169 (1980); T. Yanagida *et al.*, Nature (London) **307**, 58 (1984).

[16] S. Yamazaki, T. Maeda, and T. Miki-Noumura, in *Biological Functions of Microtubules and Related Structures*, edited by H. Sakai, H. Mohri, and G. G. Borisy (Academic, New York, 1982), p. 41.

[17] J. Mizushima-Sugano, T. Maeda, and T. Miki-Noumura, Biochem. Biophys. Acta **755**, 257 (1983).

[18] F. Gittes, B. Mickey, J. Nettleton, and J. Howard, J. Cell. Biol. **120**, 923 (1993).

[19] P. Venier, A. C. Maggs, M.-F. Carlier, and D. Pantaloni, J. Biol. Chem. **269**, 13 353 (1994).

[20] P. Dustin, *Microtubules* (Springer, Berlin, 1984).

[21] *Microtubules*, edited by K. Roberts and J. S. Hyams (Academic, New York, 1979).

[22] N. Hirokawa, Current Opinion Cell Biol. **6**, 71 (1994); H. C. Joshi, *ibid.* **6**, 55 (1994).

[23] D. Chrétien and R. H. Wade, Biol. Cell. **71**, 161 (1991).

[24] T. Mitchison and M. Kirschner, Nature (London) **312**, 232 (1984); D. K. Fygenson, E. Braun, and A. Libchaber, Phys. Rev. E **50**, 1579 (1994).

[25] P. M. Bayley, M. J. Schilstra, and S. R. Martin, J. Cell. Sci. **95**, 33 (1990); S. R. Martin, M. J. Schilstra, and P. M. Bayley, Biophys. J. **65**, 578 (1993).

[26] M. Satarić *et al.*, J. Mol. Electron. **6**, 63 (1990); M. V. Satarić, J. A. Tuszyński, and R. B. Žakula, Phys. Rev. E **48**, 589 (1993).

[27] J. Adler, O. Necas, and I. Hrazdira, Folia Biol. (Prague) **39**, 55 (1993).

[28] S. Iijima, Nature (London) **354**, 56 (1991); M. F. Lin and K. W.-K. Shung, Phys. Rev. B **47**, 6617 (1993); R. A. Jishi, M. S. Dresselhaus, and G. Dresselhaus, *ibid.* **48**, 11 385 (1993).

[29] R. D. Doolittle and H. Überall, J. Acoust. Soc. Am. **39**, 13 (1966); J. D. Murphy, E. D. Breitenbach, and H. Überall, *ibid.* **64**, 677 (1978); E. D. Breitenbach, H. Überall, and K.-B. Yoo, *ibid.* **74**, 1267 (1983); M. Talmant and G. Quentin, in *Progress in Underwater Acoustics*, edited by H. M. Merklinger (Plenum, New York, 1987), p. 137.

[30] K. F. Graff, *Wave Motion in Elastic Solids* (Clarendon, Oxford, 1975).

[31] S. Markuš, *The Mechanics of Vibrations of Cylindrical Shells* (Elsevier, Amsterdam, 1988).

[32] L. D. Landau and E. M. Lifshits, *Fluid Mechanics* (Pergamon, Oxford, 1987).

[33] I. S. Gradshtein and I. M. Ryzhik, *Tables of Integrals, Series, and Products* (Academic, Boston, 1994).

[34] R. A. Harris and J. E. Hearst, J. Chem. Phys. **44**, 2595 (1966).

[35] L. D. Landau and E. M. Lifshits, *Statistical Physics, Part 1* (Pergamon, Oxford, 1980).

[36] S. A. Wainwright, W. D. Biggs, J. D. Currey, and J. M. Gosline, *Mechanical Design in Organisms* (Princeton University Press, Princeton, 1982).

[37] M. M. Tirion, D. ben-Avraham, and K. C. Holmes, in *Actin: Biophysics, Biochemistry, and Cell Biology*, edited by J. E. Estes and P. J. Higgins (Plenum, New York, 1994), pp. 3–12.

[38] D. ben-Avraham, Phys. Rev. B **47**, 14 559 (1993); M. Tirion and D. ben-Avraham, J. Mol. Biol. **230**, 186 (1993).

[39] M. Levitt, J. Mol. Biol. **168**, 595 (1983); M. Levitt, C. Sander, and P. S. Stern, *ibid.* **181**, 423 (19985); B. Brooks and B. Karplus, Biophys. **80**, 6571 (1983); N. Go, T. Noguti, and T. Nishikawa, Proc. Natl. Acad. Sci. USA **80**, 3696 (1983).

Interface phonons in spherical GaAs/$Al_xGa_{1-x}As$ quantum dots

R. M. de la Cruz
Departamento de Ingeniería, Universidad Carlos III de Madrid, 28911 Leganés, Madrid, Spain

S. W. Teitsworth
Department of Physics, Box 90305, Duke University, Durham, North Carolina 27708-0305

M. A. Stroscio
U.S. Army Research Office, P.O. Box 12211, Research Triangle Park, North Carolina 27709-2211
(Received 23 February 1995)

Within the framework of the dielectric continuum model, the interface phonon frequencies for spherical GaAs/$Al_xGa_{1-x}As$ quantum dots are obtained as functions of the alloy composition in the range $x=0.2$–1.0. By imposing electrostatic boundary conditions, the two interface phonon frequencies are calculated for the first three modes. The frequency behavior of the different modes is found to be similar. However, for each mode one of the phonon frequencies is found to be strongly dependent on x. It is demonstrated that these phonon modes play an important role in determining resonant optical absorption of quantum dots.

I. INTRODUCTION

During the past few years there has been great interest in investigating microcrystals as small as a few nanometers, usually called quantum dots, because they exhibit optical properties very different from bulk crystals. Their distinct optical properties are largely a consequence of the three-dimensional confinement of electrons and holes[1–5] as well as phonons.[6–11] The interaction between the confined electrons (holes) and phonons is an important factor that determines the optical properties.[4,5,12] In fact, the photoluminescence degradation in small quantum dots has been ascribed recently to the decreasing relaxation rate of the carriers with decreasing dot size, a phenomenon referred to as the phonon bottleneck effect.[13,14] Thus, any realistic discussion of the light emission efficiency of low-dimensional semiconductor heterostructures should entail a discussion of the relaxation process via phonon emission.

The role of confined longitudinal-optical (LO) and interface (IF) phonon modes in the electron relaxation process, and consequently in the photoluminescence, has been investigated previously for cubical GaAs quantum dots which are free standing in vacuum.[15,16] On the other hand, the IF phonon modes are found to be especially important in optical absorption of semiconductor quantum dots fabricated by etching and grating techniques because these modes are very sensitive to the shape and size of the dots.[12,17–19] In optical experiments on inhomogeneous systems the frequency shifts from the bulk values are used to characterize the shapes and sizes as well as the constitutive materials of the dots. A general theoretical treatment for the IF frequencies and the corresponding optical properties as functions of the dot size and shape has been developed previously.[12] However, to our knowledge, the effect of the materials which constitute the dot and barrier on the optical properties has not been discussed.

The aim of this work is to investigate the effects of different barrier x values on interface phonon modes and associated resonant optical-absorption properties of spherical GaAs/$Al_xGa_{1-x}As$ quantum dots. For this, we estimate the IF phonon frequency shifts as a function of the Al mole fraction x in the material which surrounds the dot. The framework of these investigations is the dielectric continuum model neglecting retardation effects. This model has been applied extensively in the study of electron-phonon interactions of low-dimensional polar semiconductor heterostructures such as quantum wells, quantum wires, and quantum dots.[12,15,16,20–22] In the case of both LO and IF phonons, good agreement has been found between results obtained with the dielectric continuum model and those obtained with detailed lattice-dynamical calculations[23,24] and with more elaborate continuum approaches.[25] The dielectric continuum model has the advantage of giving relatively simple analytical results which are particularly useful for studying the interactions of electrons or light with the IF and LO modes. The region of validity of the continuum approach is limited to phonon wavelengths which are large compared with the lattice constant. The formalism of this model is described elsewhere.[12,20]

II. RESULTS AND DISCUSSION

The semiconductor heterostructures under investigation are spherical GaAs/$Al_xGa_{1-x}As$ quantum dots with GaAs as the dot material and $Al_xGa_{1-x}As$ as the barrier material. The subscript x is the Al mole fraction; values of x in the range 0.2–1.0 are considered. Each barrier material is characterized by a dielectric function $\epsilon_2(\omega)$ taken from Ref. 26. The Lyddane-Sach-Teller relation is assumed for the frequency dependences of $\epsilon_1(\omega)$ and $\epsilon_2(\omega)$. In polar semiconductors, such as GaAs and $Al_xGa_{1-x}As$, both confined LO and IF modes polarize the semiconductor generating an electric field and an as-

sociated electrostatic potential $\Phi(\mathbf{r})$. The confined LO and IF phonon modes for a cubical GaAs quantum dot which is free standing in vacuum have been given previously.[15,16]

Assuming there is no free charge in either dot or barrier materials (GaAs and $Al_xGa_{1-x}As$), the divergence of the displacement field $\mathbf{D}$ vanishes everywhere. Due to the relation between $\mathbf{D}$ and the electric field $\mathbf{E}$, $\mathbf{D}=\varepsilon(\omega)\mathbf{E}$, the above condition gives $\varepsilon_i(\omega)\nabla\cdot\mathbf{E}=0$ in each material. As the electric field derives from the scalar potential $\Phi(\mathbf{r})$, the last equation can be written as

$$\varepsilon_i(\omega)\nabla^2\Phi(\mathbf{r})=0, \quad i=1,2 . \tag{1}$$

For interface modes, $\varepsilon_i(\omega)\neq 0$; therefore, Eq. (1) is satisfied if $\nabla^2\Phi(\mathbf{r})=0$. We resolve the Laplace's equation with the standard electrostatic boundary conditions imposed at the interface between the two media, which are the continuity of tangential components of $\mathbf{E}$ and normal component of $\mathbf{D}$.

If the radius of the spherical $GaAs/Al_xGa_{1-x}As$ quantum dot is R, the solution of Laplace's equation for the electrostatic potential in spherical coordinates (r,θ,ϕ) can be expressed as

$$\Phi(r,\theta,\phi)=e^{im\phi}P_l^m(\cos\theta)\times\begin{cases}(r/R)^l, & r<R\\ (R/r)^{l+1}, & r>R,\end{cases} \tag{2}$$

where the integers $l(>0)$ and m ($|m|<l$) are IF mode quantum numbers, and P_l^m are associated Legendre polynomials of the first kind. From Eq. (2) it can be seen that the electrostatic potential is continuous and finite everywhere and tends to zero far away from the dot ($r\gg R$).

By imposing the continuity of the normal component of $\mathbf{D}$ at the dot boundary $r=R$, the following eigenfrequency condition is obtained:

$$\varepsilon_1(\omega_{IF})/\varepsilon_2(\omega_{IF})=-1-1/l . \tag{3}$$

By substituting the standard expressions for ε_1 and ε_2, one obtains a biquadratic equation in the frequency variable which gives two physical solutions for the IF frequency. These values depend only on the integer l, and they are independent of the integer m, as a consequence of the system symmetry. As the transversal-optical (TO) and LO branches of the dot and barrier materials (GaAs and $Al_xGa_{1-x}As$) are almost dispersionless, it is reasonable to assume that $\omega_{TO,i}$ and $\omega_{LO,i}$ ($i=1,2$) are nearly wave-vector independent and take the values that these parameters have for wave vectors equal to zero. This results in two dispersionless IF mode branches; the values for $\varepsilon_{\infty,i}$, $\omega_{LO,i}$, and $\omega_{TO,i}$ ($i=1,2$) used to evaluate Eq. (3) are taken from Ref. 26. One of the IF mode frequencies $\omega_{IF,1}$ satisfies the relation $\omega_{TO,1}<\omega_{IF,1}<\omega_{LO,1}$, and the other, $\omega_{IF,2}$, satisfies $\omega_{TO,2}<\omega_{IF,2}<\omega_{LO,2}$ depending on the composition of the surrounding medium. This is a consequence of the fact that the dot and the barrier materials have nonoverlapping reststrahl regions.

Figures 1–3 show the IF mode frequencies $\omega_{IF,1}$ and $\omega_{IF,2}$ as a function of x for the three first IF modes $l=1$, 2, and 3, respectively. The frequency $\omega_{IF,1}$ tends to decrease slightly with increasing x to get a nearly constant

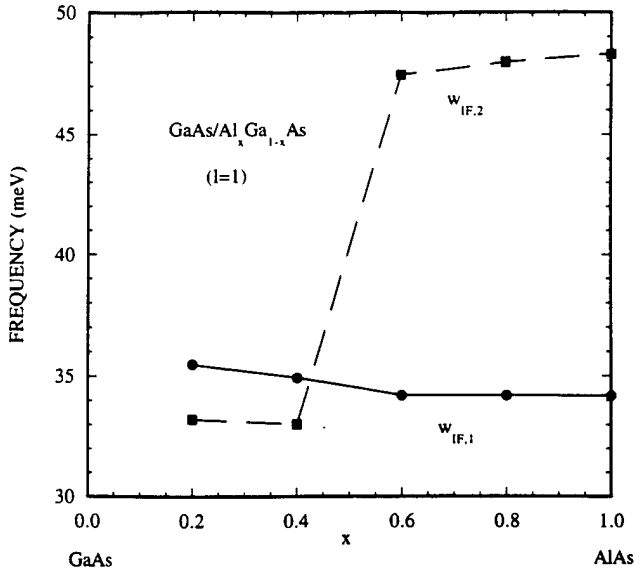

FIG. 1. Interface frequencies for the mode $l=1$ of a spherical $GaAs/Al_xGa_{1-x}As$ quantum dot as a function of the Al alloy concentration in the barrier material. The lines are a guide for the eyes.

value for $x\geq 0.6$. This behavior is similar for all IF modes investigated here ($l=1$, 2, and 3). Although $\omega_{IF,1}$ varies very slowly with the barrier material composition, this dependence can have important consequences on the resonant optical-absorption properties as will be discussed later.

Conversely, we obtain a much stronger dependence of the frequency $\omega_{IF,2}$ with the Al mole fraction x. First, the frequency $\omega_{IF,2}$ tends to decrease slightly for x values lesser than 0.4, but it increases steeply in the range $0.4\leq x\leq 0.6$. For $x>0.6$, the $\omega_{IF,2}$ value increases very slightly. This striking behavior is independent of the IF

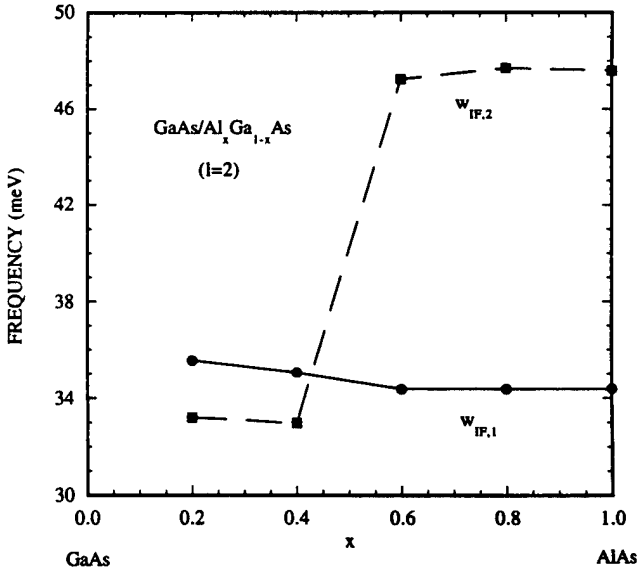

FIG. 2. Interface frequencies for the mode $l=2$ of a spherical $GaAs/Al_xGa_{1-x}As$ quantum dot as a function of the Al alloy concentration in the barrier material. The lines are a guide for the eyes.

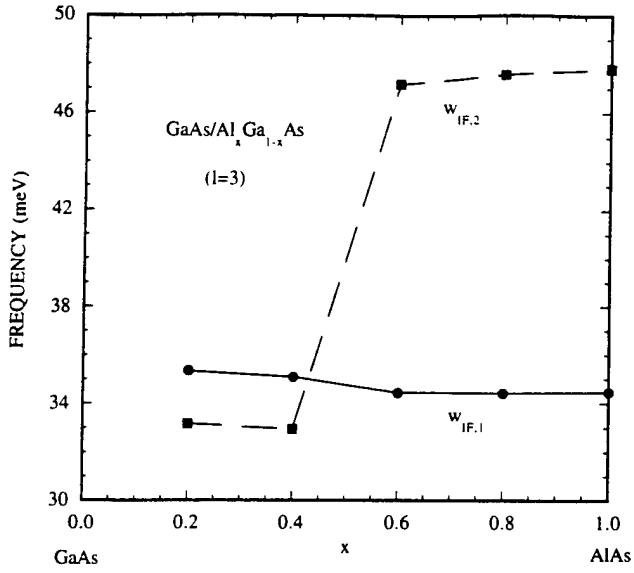

FIG. 3. Interface frequencies for the mode $l=3$ of a spherical GaAs/$Al_xGa_{1-x}As$ quantum dot as a function of the Al alloy concentration in the barrier material. The lines are a guide for the eyes.

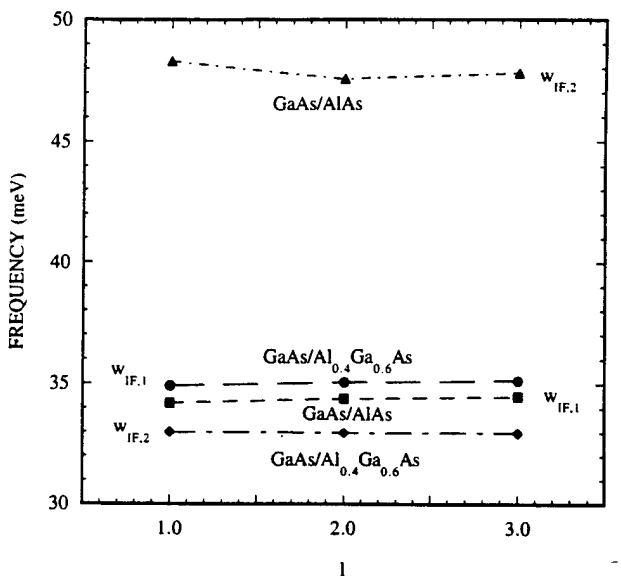

FIG. 4. Interface frequencies as a function of the interface mode l for spherical GaAs/$Al_{0.4}Ga_{0.6}As$ and GaAs/AlAs quantum dots. The lines are a guide for the eyes.

mode number l ($l=1$, 2, 3). The dependence of $\omega_{IF,2}$ with the Al mole fraction is completely reasonable because for $x \leq 0.4$, the barrier material is GaAs type and the IF mode frequency $\omega_{IF,2}$ must satisfy the relation ω_{TO} (GaAs) $< \omega_{IF,2} < \omega_{LO}$ (GaAs), whereas for $x > 0.5$, the barrier material is AlAs type and $\omega_{IF,2}$ must satisfy ω_{TO} (AlAs) $< \omega_{IF,2} < \omega_{LO}$ (AlAs). Therefore, the abrupt step observed in $\omega_{IF,2}$ should be interpreted as a result of the change in the barrier material composition.

Figure 4 shows the IF mode frequencies $\omega_{IF,1}$ and $\omega_{IF,2}$ as functions of the IF mode l for GaAs/$Al_{0.4}Ga_{0.6}As$ and GaAs/AlAs. The almost independence of $\omega_{IF,1}$ and $\omega_{IF,2}$ on the IF mode l can be clearly seen from Fig. 4 and it has been discussed above. For the case of the IF mode $l=0$, conservation of charge prohibits the existence of the dotlike mode and hence there exists only the barrier-like mode $\omega_{IF,2}$. This is the reason we are not interested in this mode and it will not be discussed herein.

The electric fields generated by these two different IF modes $\omega_{IF,1}$ and $\omega_{IF,2}$ are identical, but their polarizations $\mathbf{P}_i=[1-\varepsilon_i(\omega)]\mathbf{E}/4\pi$ ($i=1,2$) differ. The analytical expressions of these vectors for the mode $l=1$ appear in Table I. The subscript 1 (2) denotes the dot (barrier) materials whereas the superscript denotes the IF mode quantum number m. A distance dependencelike $1/R$ for $r \leq R$ and R^2/r^3 for $r \geq R$ is obtained. In general, for a given mode l, the polarization vector dependence with the distance scales as r^{l-1}/R^l for $r \leq R$ or R^{l+1}/r^{l+2} for $r \geq R$.

Now, we consider the optical absorption due to the IF modes of quantum dots. We assume that the illuminating source wavelength is larger than the dot radius R; therefore, retardation effects are not significant and the illuminating source field may be considered as homogeneous near the quantum dot. For the following discussion, we take the barrier material ($Al_xGa_{1-x}As$) to be nonabsorbing, which means that $\mathrm{Im}\varepsilon_2(\omega)=0$. We are interested in the effect of the barrier composition on the IF phonon frequency values. A variation of the IF frequencies as a result of a different composition in the surrounding medium could modify the position of the resonant optical-absorption peak if this variation is larger than the full width at half maximum (FWHM) of the peak. For a

TABLE I. Polarization vectors of a spherical GaAs/$Al_xGa_{1-x}As$ quantum dot for the mode $l=1$. The subscript 1 (2) denotes dot (barrier) materials and the superscript represents the interface quantum number m.

$$\mathbf{P}_1^{-1}=[\varepsilon_1(\omega)-1]e^{-i\theta}(8\pi R)^{-1}[(1-\cos^2\theta)^{1/2}\mathbf{u}_r + \sin\theta\cos\theta(1-\cos^2\theta)^{-1/2}\mathbf{u}_\theta - i(\sin\theta)^{-1}(1-\cos^2\theta)^{1/2}\mathbf{u}_\phi] .$$

$$\mathbf{P}_2^{-1}=[\varepsilon_2(\omega)-1]e^{-i\theta}r^2(8\pi R^3)^{-1}[-2(1-\cos^2\theta)^{1/2}\mathbf{u}_r + \sin\theta\cos\theta(1-\cos^2\theta)^{-1/2}\mathbf{u}_\theta - i(\sin\theta)^{-1}(1-\cos^2\theta)^{1/2}\mathbf{u}_\phi] .$$

$$\mathbf{P}_1^0=[1-\varepsilon_1(\omega)](4\pi R)^{-1}(\cos\theta\mathbf{u}_r-\sin\theta\mathbf{u}_\theta) .$$

$$\mathbf{P}_2^0=[\varepsilon_1(\omega)-1]R^2(4\pi r^3)^{-1}(2\cos\theta\mathbf{u}_r+\sin\theta\mathbf{u}_\theta) .$$

$$\mathbf{P}_1^1=[1-\varepsilon_1(\omega)]e^{i\theta}(4\pi R)^{-1}[(1-\cos^2\theta)^{1/2}\mathbf{u}_r + \sin\theta\cos\theta(1-\cos^2\theta)^{-1/2}\mathbf{u}_\theta + i(\sin\theta)^{-1}(1-\cos^2\theta)^{1/2}\mathbf{u}_\phi] .$$

$$\mathbf{P}_2^1=[1-\varepsilon_2(\omega)]e^{i\theta}R^2(4\pi r^3)^{-1}[(1-\cos^2\theta)^{1/2}\mathbf{u}_r + \sin\theta\cos\theta(1-\cos^2\theta)^{-1/2}\mathbf{u}_\theta + i(\sin\theta)^{-1}(1-\cos^2\theta)^{1/2}\mathbf{u}_\phi] .$$

TABLE II. Effect of the surrounding medium composition on the interface dotlike frequencies of spherical $GaAs/Al_xGa_{1-x}As$ quantum dots.

$\Delta x=0.2$				
	$0.2\rightarrow0.4$	$0.4\rightarrow0.6$	$0.6\rightarrow0.8$	$0.8\rightarrow1.0$
$\Delta\omega_{IF,l}$				
$l=1$	0.56 meV	0.72 meV	0.01 meV	0.01 meV
$l=2$	0.50 meV	0.68 meV	0.01 meV	0.02 meV
$l=3$	0.46 meV	0.67 meV	0.01 meV	0.02 meV

review of optical-absorption properties in quantum dots with different revolution geometries, see, for example, Ref. 12. A typical value for the FWHM in GaAs is 0.18 meV;[12] therefore, a variation of the barrier composition that yields a change in the IF frequencies higher than this value would cause a shift of the resonant optical absorption to another frequency. Table II shows the variation of IF dotlike frequencies for increments $\Delta x=0.2$ in the Al mole fraction of the surrounding material. Up to a value of x equal to 0.6, the variation of $\omega_{IF,1}$ causes significant shifts in the resonant peak; however, the same increase Δx for $x>0.6$ does not cause any shift in the peak. As a consequence of the high symmetry of the dot only the three modes with $l=1$ ($m=-1$, $m=0$, and $m=1$) make a nonzero contribution to the optical-absorption cross section and hence, these modes induce absorption. An analytical expression for the optical-absorption cross section has been given in Ref. 12.

III. CONCLUSION

We have investigated the IF phonon modes of spherical $GaAs/Al_xGa_{1-x}As$ quantum dots using the dielectric continuum approach with standard electrostatic boundary conditions. The dielectric continuum model is valid for phonon mode wavelengths larger than the lattice constant which is the region of greatest interest for the optical-absorption spectra. We have focused our interest on the IF phonon frequency dependences with the barrier alloy composition and its effect on the optical-absorption spectrum. For the case of spherical quantum dots, only the three modes with $l=1$ ($m=-1$, $m=0$, and $m=1$) are optically active and they are degenerate by symmetry. This means that the obtained eigenfrequency condition has no dependence on the IF mode quantum number m. Therefore, their optical-absorption spectra are characterized by a peak localized at the resonant frequency with the illuminating source. When the surrounding medium is GaAs type ($x\leq0.6$), we have found that for increases of $\Delta x=0.2$ in the percentage of Al, the dotlike resonant optical-absorption peak shifts to another frequency. However, when the surrounding medium is AlAs type ($x>0.6$), similar increases of Δx do not cause shifts of the resonant peak. Although we have assumed that the material surrounding the dot is nonabsorbing, a more general treatment of the problem would require to take into account the optical activity of the barrier medium and its effect on the resonant peak shift.

ACKNOWLEDGMENTS

R. M. de la Cruz would like to acknowledge the financial support of Ministerio de Educación y Ciencia, Spain through a postdoctoral grant. S. W. Teitsworth acknowledges support of the National Science Foundation through Grant No. DMR-9157539. The authors thank Professor R. Pareja for a critical reading of the manuscript.

[1]A. I. Ekimov, A. L. Efros, and A. A. Onoushchenko, Solid State Commun. **56**, 921 (1985).
[2]A. Nakamura, H. Yamada, and T. Tokizaki, Phys. Rev. B **40**, 8585 (1989).
[3]Y. Wang and A. Suna, J. Chem. Phys. **92**, 6927 (1990).
[4]T. Itoh and M. Furumiya, J. Lumin. **48 & 49**, 704 (1990).
[5]M. C. Klein, F. Hache, D. Ricard, and C. Flytzanis, Phys. Rev. B **42**, 11 123 (1990).
[6]S. Hayashi and H. Kanamori, Phys. Rev. B **26**, 7079 (1982).
[7]H. Richter, Z. P. Wang, and L. Ley, Solid State Commun. **39**, 625 (1981).
[8]Z. Iqbal and S. Veprek, J. Phys. C **15**, 377 (1982).
[9]I. H. Campbell and P. M. Fauchet, Solid State Commun. **58**, 739 (1990).
[10]M. Fujii, S. Hayashi, and K. Yamamoto, Appl. Phys. Lett. **57**, 2692 (1990).
[11]M. Fujii, S. Hayashi, and K. Yamamoto, Jpn. J. Appl. Phys. **30**, 687 (1991).
[12]P. A. Knipp and T. L. Reinecke, Phys. Rev. B **46**, 10 310 (1992).
[13]H. Benisty, C. M. Sotomayor-Torrès, and C. Weisbuch, Phys. Rev. B **44**, 10 945 (1991).
[14]T. Inoshita and H. Sakaki, Phys. Rev. B **46**, 7260 (1992).
[15]R. M. de la Cruz, S. W. Teitsworth, and M. A. Stroscio, Superlatt. Microstruct. **13**, 481 (1993).
[16]R. M. de la Cruz, Superlatt. Microstruct. **16**, 427 (1994).
[17]S. J. Allen, H. L. Störmer, and J. C. M. Hwang, Phys. Rev. B **28**, 4875 (1983).
[18]D. B. Mast, A. J. Dahm, and A. L. Fetter, Phys. Rev. Lett. **54**, 1706 (1985).
[19]Ch. Sikorski and U. Merkt, Phys. Rev. Lett. **62**, 2164 (1989).
[20]N. Mori and T. Ando, Phys. Rev. B **40**, 6175 (1989).
[21]P. J. Turley and S. W. Teitsworth, J. Appl. Phys. **72**, 2356 (1992).
[22]K. W. Kim, M. A. Stroscio, A. Bhatt, R. Mickevius, and V. V. Mitin, J. Appl. Phys. **70**, 319 (1991).
[23]H. Rücker, E. Molinari, and P. Lugli, Phys. Rev. B **44**, 3463 (1991).
[24]Ph. Lambin, P. Senet, and A. A. Lucas, Phys. Rev. B **44**, 6416 (1991).
[25]R. Enderlein, Phys. Rev. B **43**, 14 513 (1991).
[26]S. Adachi, J. Appl. Phys. **58**, R1 (1985).

J. Phys.: Condens. Matter 8 (1996) 2143–2151. Printed in the UK

Acoustic phonon quantization in buried waveguides and resonators

M A Stroscio†, Yu M Sirenko‡, S Yu‡ and K W Kim‡

† US Army Research Office, PO Box 12211, Research Triangle Park, NC 27709-2211, USA

‡ Department of Electrical and Computer Engineering, North Carolina State University, Raleigh, NC 27695-7911, USA

Received 17 November 1995, in final form 29 January 1996

Abstract. Starting from a classical Hamiltonian for nonhomogeneous elastic media, a procedure is developed for acoustic phonon quantization in resonators as well as linear and planar waveguides. The formalism is illustrated in an example of acoustic phonon modes in a buried cylindrical waveguide. The deformation potential Hamiltonian for electron–acoustic phonon interaction is also obtained.

1. Introduction

During the last decade much effort has been devoted to understanding of influence of spatial quantization on the vibrational properties of semiconductor heterostructures and superlattices. While optical phonon confinement has been analysed in great detail [1], it is only recently that much attention has been focused on the more subtle effects of acoustic phonon quantization in restricted geometries.

Early works on acoustic phonon properties in superlattices were devoted mainly to the study of acoustic mode folding [2]. More recently, Tamura and co-workers investigated the resonant transmission of acoustic wavepackets in superlattices and double-barrier systems [3]. Kochelap and Gülseren [4] have modelled the localization of acoustical modes due to electron–phonon interactions within a two-dimensional electron gas. Also, in a number of works the modification of acoustic modes in heterostructures has been studied [5–7] within the formalism of *classical* elasticity theory [8, 9].

Recent advances in material growth techniques have resulted in the fabrication of free-standing nanostructures [11] and have provided the possibility of observation of acoustic phonon confinement effects. Wybourne and co-workers [12] have presented experimental evidence of acoustic phonon confinement effects in self-supported thin films. Subsequently, these experimental findings motivated theoretical investigations on the role of acoustic phonon *quantization* in free-standing nanostructures [13–15]. Furthermore, acoustic phonon modes had been properly quantized in self-supported whiskers [13, 14], dots [13] and slabs [15], and electron–phonon interactions in such systems have been studied.

To the best of our knowledge, the quantum mechanical treatment of acoustic phonons has been provided only for free-boundary, homogeneous waveguides and resonators. On the other hand, semiconductor quantum wells, wires and dots are conventionally grown embedded in another material. It has been also proposed [7] that a buried quantum wire could serve as an acoustic fibre in semiconductor acoustoelectronic devices. Thus, proper

0953-8984/96/132143+09$19.50

quantization of acoustic phonon modes in buried structures is essential for an accurate treatment of mesoscopic and coherent phenomena in low-dimensional systems.

In this paper we develop a quantization procedure for acoustic vibrations confined in linear or planar waveguides as well as resonators. Expressions for the displacement operator are derived starting from the most general form of the Hamiltonian for an inhomogeneous elastic medium. The quantization formalism is illustrated by deriving the acoustic phonon spectrum for a buried cylindrical wire. We also present the resulting deformation potential Hamiltonian responsible for the electron–phonon interaction.

This paper is organized as follows. In section 2 we obtain general rules for acoustic phonon quantization in resonators and waveguides. Section 3 deals with application of the quantization procedure to a buried cylindrical fibre. Finally, we summarize the results obtained in section 4.

2. Quantization procedure

In section 2.1 we present the procedure for acoustic phonon quantization in resonators; section 2.2 contains the rule for quantization of phonons confined in one or two dimensions (acoustic waveguide), and section 2.3 presents the deformation potential Hamiltonian for acoustic phonons.

2.1. Acoustic phonon quantization in resonators

We consider the quantization of acoustic modes localized in a certain region of elastic material (resonator). The most general form of the Hamiltonian for an inhomogeneous elastic medium is given by [9, 10]

$$\mathcal{H} = \frac{1}{2}\int \mathrm{d}^3R \left[\rho(\boldsymbol{R})\dot{u}_i\dot{u}_i + \lambda_{ijkl}(\boldsymbol{R})\frac{\partial u_i}{\partial x_j}\frac{\partial u_k}{\partial x_l}\right] \tag{1}$$

where u_i are components of the displacement vector $\boldsymbol{u}(\boldsymbol{R}, t)$; also $\rho(\boldsymbol{R})$ is a mass density, and $\lambda_{ijkl}(\boldsymbol{R})$ is the elastic stiffness tensor of the medium.

The corresponding equations of motion take the following form:

$$\rho(\boldsymbol{R})\ddot{u}_i(\boldsymbol{R}, t) = \frac{\partial}{\partial x_j}\left[\lambda_{ijkl}(\boldsymbol{R})\frac{\partial u_k(\boldsymbol{R}, t)}{\partial x_l}\right]. \tag{2}$$

The general solution of equation (2) in the case of localized vibrations can be presented as a linear combination of normal modes $\boldsymbol{w}_n(\boldsymbol{R})$ which are labelled by a discrete number n. For the quantization of the elastic vibrations it is convenient to deal with a real (rather than complex) displacement vector $\boldsymbol{u}(\boldsymbol{R}, t)$; thus,

$$\boldsymbol{u}(\boldsymbol{R}, t) = \sum_n \left[c_n\boldsymbol{w}_n(\boldsymbol{R})\,\mathrm{e}^{-\mathrm{i}\omega_n t} + c_n^*\boldsymbol{w}_n^*(\boldsymbol{R})\,\mathrm{e}^{\mathrm{i}\omega_n t}\right]. \tag{3}$$

In order to define unambiguously the coefficients c_n and c_n^* in equation (3), the normalization rule for the modes $\boldsymbol{w}_n(\boldsymbol{R}, t)$ should be specified. Since the requirement of constant energy for confined vibrations implies their mutual orthogonality with the density $\rho(\boldsymbol{R})$ as a weight factor [10], the following orthonormality conditions can be imposed:

$$\int \mathrm{d}^3R\,\rho(\boldsymbol{R})\boldsymbol{w}_n^*(\boldsymbol{R})\cdot\boldsymbol{w}_{n'}(\boldsymbol{R}) = \delta_{n,n'}. \tag{4}$$

In order to obtain the quantization rules the Hamiltonian (1) must be expressed in terms of the amplitudes of the modes, c_n and c_n^*. Integrating by parts the second term in

equation (1), we find, with the help of equations (2)–(4), the following representation of the Hamiltonian:

$$\mathcal{H} = \sum_n \omega_n (c_n c_n^* + c_n^* c_n). \tag{5}$$

The classical form (5) for elastic vibrations corresponds to the free-phonon Hamiltonian $\hat{\mathcal{H}}$ in the second-quantization representation

$$\hat{\mathcal{H}} = \sum_n \hbar\omega_n \left[\hat{b}_n(t)\hat{b}_n^\dagger(t) + \frac{1}{2}\right] = \sum_n \frac{\hbar\omega_n}{2}\left[\hat{b}_n(t)\hat{b}_n^\dagger(t) + \hat{b}_n^\dagger(t)\hat{b}_n(t)\right] \tag{6}$$

where the time-dependent annihilation and creation operators satisfy standard commutation relations:

$$\hat{b}_n(t)\hat{b}_{n'}^\dagger(t) - \hat{b}_{n'}^\dagger(t)\hat{b}_n(t) = \delta_{n,n'}.$$

In essence, the quantization procedure amounts to (see, e.g., [16]) comparison of the classical Hamiltonian of equation (5) with the quantum mechanical Hamiltonian of equation (6). This comparison leads to the correspondence rule

$$c_n\, e^{-i\omega_n t} \to \sqrt{\frac{\hbar}{2\omega_n}}\hat{b}_n(t) \qquad c_n^*\, e^{i\omega_n t} \to \sqrt{\frac{\hbar}{2\omega_n}}\hat{b}_n^\dagger(t). \tag{7}$$

Finally, applying the rule (7) to the classical displacement vector in *resonators* given by equation (3), we find, in second-quantization representation,

$$\hat{\boldsymbol{u}}(\boldsymbol{R}, t) = \sum_n \sqrt{\frac{\hbar}{2\omega_n}}\left[\boldsymbol{w}_n(\boldsymbol{R})\,\hat{b}_n + \boldsymbol{w}_n^*(\boldsymbol{R})\,\hat{b}_n^\dagger\right]. \tag{8}$$

For simplicity we have suppressed the time dependence of the operators $\hat{b}(t)$ and $\hat{b}^\dagger(t)$. The phonon wavefunctions $\boldsymbol{w}_n(\boldsymbol{R})$ are normalized according to equation (4).

2.2. *Phonon quantization in acoustic waveguides*

The quantization rules for acoustic waveguides are easily obtained from comparison of equations (8), (4) for phonons confined in all dimensions with corresponding expressions, describing the homogeneous case [16]. Introducing the notation $\boldsymbol{R} = (\boldsymbol{r}, z)$ and $\boldsymbol{Q} = (\boldsymbol{q}, q_z)$, we consider (i) planar waveguides homogeneous in the plane with constant z and (ii) linear waveguides which are homogeneous along the z-direction.

Thus, for *linear* acoustic waveguides, the operator for the displacement vector is given by

$$\hat{\boldsymbol{u}}(\boldsymbol{R}, t) = \sum_{n,q_z} \sqrt{\frac{\hbar}{2\omega_{nq_z}}}\left[\boldsymbol{w}_{n,q_z}(\boldsymbol{r})\,\hat{b}_{n,q_z} + \boldsymbol{w}_{n,-q_z}^*(\boldsymbol{r})\,\hat{b}_{n,-q_z}^\dagger\right]\frac{e^{iq_z z}}{\sqrt{\mathcal{L}}}. \tag{9}$$

Here $\mathcal{L}$ is a normalization length; the phonon frequency ω_{nq_z} and eigenvectors $\boldsymbol{w}_{n,q_z}(\boldsymbol{r})$ should be found by solving of the equations of motion (2) with proper boundary condition. The normalization condition for the eigenvectors is

$$\int d^2r\ \rho(\boldsymbol{r})\boldsymbol{w}_{n,q_z}^*(\boldsymbol{r}) \cdot \boldsymbol{w}_{n',q_z}(\boldsymbol{r}) = \delta_{n,n'}. \tag{10}$$

In the same fashion, for a *planar* waveguide the displacement operator is equal to

$$\hat{\boldsymbol{u}}(\boldsymbol{R}, t) = \sum_{n,q} \sqrt{\frac{\hbar}{2\omega_{nq}}}\left[\boldsymbol{w}_{n,q}(z)\hat{b}_{n,q} + \boldsymbol{w}_{n,-q}^*(z)\hat{b}_{n,-q}^\dagger\right]\frac{e^{i\boldsymbol{q}\cdot\boldsymbol{r}}}{\sqrt{S}} \tag{11}$$

where S is a normalization area and the eigenvectors $w_{n,q}(z)$ must be normalized according to the prescription

$$\int dz\ \rho(z) w^*_{n,q}(z) \cdot w_{n',q}(z) = \delta_{n,n'}. \tag{12}$$

2.3. The deformation potential

Interaction via the deformation potential is usually a dominant mechanism for electron–acoustic phonon scattering in crystals. The deformation potential Hamiltonian can be written in a general form as

$$\hat{\mathcal{H}}_{\text{def}} = \Xi_{\text{ac}}\ \text{div}\ \hat{\boldsymbol{u}}(\boldsymbol{R}, t) \tag{13}$$

where Ξ_{ac} is an acoustic deformation potential constant, and an implicit form of the displacement operator $\hat{\boldsymbol{u}}$ is given by equations (8), (9), or (11).

3. The cylindrical waveguide

To illustrate the application of the acoustic phonon quantization procedure described in the previous section, we consider the example of a linear cylindrical waveguide in an isotropic medium. Section 3.1 provides the general solution for quantized acoustic modes in this system; in section 3.2, we investigate the particular case of axisymmetric modes in more detail. Section 3.3 contains the expression for the quantized deformational potential Hamiltonian.

3.1. Basic equations

We consider a buried cylindrical waveguide of radius a occupying the region $r < a$. The inner (outer) region of the waveguide is filled with an isotropic medium characterized by constant mass density ρ_1 (ρ_2) and Lamé coefficients λ_1, μ_1 (λ_2, μ_2) which specify the elastic stiffness tensor of each isotropic medium in equation (1) according to $\lambda_{ijkl} = \lambda\,\delta_{ij}\delta_{kl} + 2\mu\,\delta_{ik}\delta_{jl}$.

The general solution of the classical equations of motion (2) in each region can be written [9] in terms of three scalar potentials ϕ, ψ and χ:

$$\boldsymbol{u} = \nabla\phi + \nabla \times (\boldsymbol{e}_z\psi) + a\nabla \times \nabla \times (\boldsymbol{e}_z\chi). \tag{14}$$

Here $\boldsymbol{e}_z$ is a unit vector along the z-axis. Each potential ϕ (ψ, χ) satisfies a scalar wave equation with propagation speed equal to the longitudinal (transverse) sound speed s_l (s_t) given by

$$s_{l\nu} = \sqrt{(\lambda_\nu + 2\mu_\nu)/\rho_\nu} \qquad s_{t\nu} = \sqrt{\mu_\nu/\rho_\nu}.$$

In these expressions, $\nu = 1$ ($\nu = 2$) corresponds to the material constant of the inner (outer) region.

We seek the solutions of equation (2) as harmonic vibrations with frequency ω, wavevector $q_z \equiv q/a$, and azimuthal number m, confined in the vicinity of the waveguide. Using the cylindrical coordinate system, $\boldsymbol{R} = (r, \varphi, z)$, we take the scalar potentials in the inner region ($r < a$) as

$$\begin{bmatrix} \phi \\ \psi \\ \chi \end{bmatrix} = \frac{1}{a} \begin{bmatrix} ic_{l1} J_m(k_l r/a) \\ C_{t1} J_m(k_t r/a) \\ c_{t1} J_m(k_t r/a) \end{bmatrix} e^{im\varphi + iqz/a - i\omega t} \tag{15}$$

and for the outer region ($r > a$)

$$\begin{bmatrix} \phi \\ \psi \\ \chi \end{bmatrix} = \frac{1}{a} \begin{bmatrix} ic_{l2} K_m(\kappa_l r/a) \\ C_{t2} K_m(\kappa_t r/a) \\ c_{t2} K_m(\kappa_t r/a) \end{bmatrix} e^{im\varphi + iqz/a - i\omega t}. \tag{16}$$

Here the inverse wavelengths $k_{l,t}$ and localization length $\kappa_{l,t}$ in the radial direction are defined as

$$k_{l,t}^2 = q^2 - \omega^2 a^2 / s_{(l,t)1}^2 \qquad \kappa_{l,t}^2 = \omega^2 a^2 / s_{(l,t)2}^2 - q^2.$$

For definiteness, equations (15) and (16) are written under the assumption that $k_{l,t}^2, \kappa_{l,t}^2 > 0$ which corresponds to the case of confined acoustic vibrations. Other possible cases are treated formally in the same fashion using analytical properties of Bessel's functions, and are discussed in the appendix.

Substituting equations (15) and (16) into equation (14), we find the implicit form of the displacement vector:

$$u(r, \varphi, z, t) = u(r) e^{im\varphi + iqz/a - i\omega t} \tag{17}$$

where inside the waveguide ($r < a$)

$$\begin{aligned} -iu_r(r) &= c_{l1} k_l J_m'(k_l r/a) + C_{t1} m \frac{a}{r} J_m(k_t r/a) + c_{t1} q k_t J_m'(k_t r/a) \\ -u_\varphi(r) &= c_{l1} m \frac{a}{r} J_m(k_l r/a) + C_{t1} k_t J_m'(k_t r/a) + c_{t1} m q \frac{a}{r} J_m(k_t r/a) \\ -u_z(r) &= c_{l1} q J_m(k_l r/a) - c_{t1} k_t^2 J_m(k_t r/a) \end{aligned} \tag{18}$$

while for $r > a$ we have

$$\begin{aligned} -iu_r(r) &= c_{l2} \kappa_l K_m'(\kappa_l r/a) + C_{t2} m \frac{a}{r} K_m(\kappa_t r/a) + c_{t2} q \kappa_t K_m'(\kappa_t r/a) \\ -u_\varphi(r) &= c_{l2} m \frac{a}{r} K_m(\kappa_l r/a) + C_{t2} \kappa_t K_m'(\kappa_t r/a) + c_{t2} m q \frac{a}{r} K_m(\kappa_t r/a) \\ -u_z(r) &= c_{l2} q K_m(\kappa_l r/a) + c_{t2} \kappa_t^2 K_m(\kappa_t r/a). \end{aligned} \tag{19}$$

Applying standard boundary conditions (continuity of the displacement and normal components of the stress tensor at the boundary $r = a$) gives the following 6×6 characteristic equation for the acoustic vibrations of a buried cylindrical fibre:

$$\begin{bmatrix} \mathbf{U}_1 & -\mathbf{U}_2 \\ \mu_1 \mathbf{F}_1 & -\mu_2 \mathbf{F}_2 \end{bmatrix} \begin{bmatrix} C_1 \\ C_2 \end{bmatrix} = 0 \tag{20}$$

where $C_\nu = [c_{l\nu}, C_{t\nu}, c_{t\nu}]^T$; displacement matrices at $r = a$ are given by

$$\mathbf{U}_\nu = \begin{bmatrix} L_\nu & m t_\nu & q T_\nu \\ -m l_\nu & -T_\nu & -mq t_\nu \\ -q l_\nu & 0 & k_{\nu t}^2 t_\nu \end{bmatrix} \tag{21}$$

and matrices $\mathbf{F}_\nu$, related to the elastic forces at the interface, are equal to

$$\mathbf{F} = \begin{bmatrix} -2qL_\nu & -mqt_\nu & (k_{\nu t}^2 - q^2) T_\nu \\ 2m(l_\nu - L_\nu) & (k_{\nu t}^2 - 2m^2) t_\nu + 2T_\nu & 2mq(t_\nu - T_\nu) \\ (2m^2 + q^2 - k_{\nu l}^2) l_\nu - 2L_\nu & 2m(T_\nu - t_\nu) & 2q[(m^2 - k_{\nu t}^2) t_\nu - T_\nu] \end{bmatrix}. \tag{22}$$

Here $k^2_{1(l,t)} = k^2_{l,t}$, $k^2_{2(l,t)} = -\kappa^2_{l,t}$, and

$$l_1 = J_m(k_l) \qquad L_1 = k_l J'_m(k_l) \qquad t_1 = J_m(k_t) \qquad T_1 = k_t J'_m(k_t)$$
$$l_2 = K_m(\kappa_l) \qquad L_2 = \kappa_l K'_m(\kappa_l) \qquad t_2 = K_m(\kappa_t) \qquad T_2 = \kappa_t K'_m(\kappa_t).$$

Equations (20)–(22) define the dispersion law and eigenmodes of elastic vibrations in a buried cylindrical waveguide for arbitrary azimuthal number m.

Finally, taking into account the notation introduced above, we can rewrite equation (9) for the displacement operator as

$$\hat{u}(R,t) = \sum_{mn.q} \sqrt{\frac{\hbar}{2\omega_{mn.q}\mathcal{L}}} \left[w_{mn.q}(r)\hat{b}_{mn.q} + w^*_{mn.-q}(r)\hat{b}^\dagger_{mn.-q} \right] e^{im\varphi + iqz/a}. \tag{23}$$

Here, the discrete quantum number n enumerates phonon modes with the same m and q, and the normal modes w can be represented conveniently in the following form:

$$w_{mn.q}(r) \equiv w_{mn.q}(r)e^{im\varphi} = u(r)e^{im\varphi}/\sqrt{\pi a^2 \mathcal{N}} \tag{24}$$

where the normalization constant $\mathcal{N}$ must be determined from the condition of equation (10).

Below we consider in detail the important case of axisymmetric ($m = 0$) vibrations in a cylindrical waveguide.

3.2. Axisymmetric vibrations

In case of axisymmetric vibrations, $m = 0$, the 6×6 determinant corresponding to equation (20) decouples into 2×2 and 6×6 blocks, specifying axisymmetric *torsional* and *radial–axial* modes. Below we present the expressions for these two types of axisymmetric normal modes $w_q(r)$, which appear in equation (9) for the displacement operator of a cylindrical waveguide.

3.2.1. Torsional modes. According to equations (18)–(22), the dispersion relation for the torsional vibrations is specified by the following transcendental equation:

$$\mu_1 k_t J_2(k_t)/J_1(k_t) = \mu_2 \kappa_t K_2(\kappa_t)/K_1(\kappa_t) \tag{25}$$

while the envelope function is given by $w_r = w_z = 0$ and

$$w_\varphi = \frac{1}{\sqrt{\pi a^2 \mathcal{N}_\varphi}} \begin{cases} K_1(\kappa_t)J_1(k_t r/a) & r < a \\ J_1(k_t)K_1(\kappa_t r/a) & r > a. \end{cases} \tag{26}$$

Here $\mathcal{N}_\varphi$ is the dimensionless normalization constant. Using the notation that $J_{m(l,t)} \equiv J_m(k_{l,t})$ and $K_{m(l,t)} \equiv K_m(\kappa_{l,t})$, we find from the normalization condition (10)

$$\mathcal{N}_\varphi = \rho_1 K^2_{1t}(J^2_{1t} - J_{0t}J_{2t}) + \rho_2 J^2_{1t}(K_{0t}K_{2t} - K^2_{1t}). \tag{27}$$

3.2.2. Radial–axial modes. For radial–axial axisymmetric vibrations the normal modes are given by $w_\varphi = 0$ and

$$iw_r = \frac{1}{\sqrt{\pi a^2 \mathcal{N}_{rz}}} \begin{cases} c_{l1}k_l J_1(k_l r/a) + c_{t1} q k_t J_1(k_t r/a) & r < a \\ c_{l2}\kappa_l K_1(\kappa_l r/a) + c_{t2} q \kappa_t K_1(\kappa_t r/a) & r > a \end{cases} \tag{28}$$

$$-w_z = \frac{1}{\sqrt{\pi a^2 \mathcal{N}_{rz}}} \begin{cases} c_{l1} q J_0(k_l r/a) - c_{t1}k_t^2 J_0(k_t r/a) & r < a \\ c_{l2} q K_0(\kappa_l r/a) + c_{t2}\kappa_t^2 K_0(\kappa_t r/a) & r > a. \end{cases} \tag{29}$$

The dispersion relation and the relationship between coefficients c_{vl}, c_{vt} are specified by the following eigenequation (cf. equations (20)–(22)):

$$\begin{bmatrix} -k_l J_{1l} & -qk_t J_{1t} & \kappa_l K_{1l} & q\kappa_t K_{1t} \\ -q J_{0l} & k_t^2 J_{0t} & q K_{0l} & \kappa_t^2 K_{0t} \\ 2\mu_1 q k_l J_{1l} & \mu_2 k_t (q^2 - k_t^2) J_{1t} & -2\mu_2 q \kappa_l K_{1l} & -\mu_2 \kappa_t (\kappa_t^2 + q^2) K_{1t} \\ \mu_1 [A J_{0l} + 2k_l J_{1l}] & 2\mu_1 q k_t [J_{1t} - k_t J_{0t}] & -\mu_2 [B K_{0l} + 2\kappa_l K_{1l}] & -2\mu_2 q \kappa_t [J_{1t} + \kappa_t J_{0t}] \end{bmatrix} \times \begin{bmatrix} c_{1l} \\ c_{1t} \\ c_{2l} \\ c_{2t} \end{bmatrix} = 0. \tag{30}$$

where $A = q^2 - k_l^2$ and $B = q^2 + \kappa_l^2$.

The normalization constant $\mathcal{N}_{rz}$ in equations (28) and (29) may be determined from the condition (10). After some calculations, we find

$$\begin{aligned} \mathcal{N}_{rz} = \rho_1 \{ & c_{1l}^2 [q^2 (J_{0l}^2 + J_{1l}^2) + k_l^2 (J_{1l}^2 - J_{0l} J_{2l})] \\ & + c_{1t}^2 k_t^2 [k_t^2 (J_{0t}^2 + J_{1t}^2) + q^2 (J_{1t}^2 - J_{0t} J_{2t})] - 4 c_{1l} c_{1t} q k_t J_{0l} J_{1t} \} \\ & + \rho_2 \{ c_{2l}^2 [q^2 (K_{1l}^2 - K_{0l}^2) + \kappa_l^2 (K_{0l} K_{2l} - K_{1l}^2)] \\ & + c_{2t}^2 \kappa_t^2 [\kappa_t^2 (K_{1t}^2 - K_{0t}^2) + q^2 (K_{0t} K_{2t} - K_{1t}^2)] - 4 c_{2l} c_{2t} q \kappa_t K_{0l} K_{1t} \} \end{aligned}$$

where the notation used for $J_{m(l,t)}$ and $K_{m(l,t)}$ was introduced in section 3.2.1.

3.3. The deformation potential interaction

Substituting equations (23), (24), (15), and (16) into equation (13), and taking into account that $\nabla^2 \phi = -(\omega/s_l)^2 \phi$, we find

$$\hat{\mathcal{H}}_{\text{def}} = -\Xi_{\text{ac}} \sum_{mn.q} \left(\frac{\omega_{mn.q}}{a s_l} \right)^2 \sqrt{\frac{\hbar}{2\pi \omega_{mn.q} \mathcal{N} \mathcal{L}}} \left[\Phi_{mn.q} \hat{b}_{mn.q} + \Phi^*_{mn.-q} \hat{b}^\dagger_{mn.-q} \right] e^{im\varphi + iqz/a} \tag{31}$$

where the scalar potential Φ is given by

$$\Phi_{mn.q} = \begin{cases} i c_{l1} J_m(k_l r/a) & r < a \\ i c_{l2} K_m(\kappa_l r/a) & r > a. \end{cases} \tag{32}$$

As expected, only the longitudinal component of the vibration contributes to a deformation potential interaction.

4. Summary

In this paper we obtained the quantization rules for acoustic vibrations confined in one, two, or all spatial dimensions and presented a general form of the deformation potential Hamiltonian in a second-quantization representation. It should be noted that the quantization rules do not change the dispersion relations and displacement pattern of the classical acoustic waves in the waveguides. However, the procedure of second quantization performed

specifies uniquely the normalization constants for phonon fields and provides the operator representation for phonon variables. The formalism makes possible the consideration of processes with numbers of phonons of the order of one, and should be applied for analysis of electron–phonon interaction in mesoscopic devices.

As a specific example we considered the quantization of acoustic phonon modes in a buried cylindrical waveguide. The expressions obtained may be used for analysis of electron and phonon dynamics in buried quantum wires.

Acknowledgments

This work was supported by the US Army Research Office and the Office of Naval Research.

Appendix

All three scalar potentials in equation (15) for the inner region, $r < a$, are written in terms of Bessel's functions J_m, which describe *real* vibrations involving the whole cross-section of the waveguide, provided that $k_{l,t}^2 > 0$ (i.e. $\omega < s_{(l,t)1}q_z$). In the opposite case, where $\omega > s_{l,t}q_z$, the functions J_m should be replaced by the modified Bessel functions I_m according to the identity

$$J_m(-\mathrm{i}|z|) = \mathrm{i}^m I_m(|z|). \tag{A1}$$

This situation corresponds to (interface) evanescent vibrations, exponentially decreasing toward the centre of the waveguide.

As for the outer region, $r > a$, it is characterized by the evanescent solutions (16) in terms of MacDonald's functions K_m. Vibrations are confined in the vicinity of the waveguide, provided that $\omega < s_{t2}q_z < s_{l2}q_z$. The opposite case of $\omega > s_t q_z$ can be treated formally through the substitution

$$K_m(-\mathrm{i}|z|) = \frac{\pi}{2}\,\mathrm{i}^{m+1} H_m^{(1)}(|z|). \tag{A2}$$

Here the Hankel function describes the radiation of acoustic energy from the system, which is characterized by a complex frequency spectrum.

References

[1] Mori N and Ando T 1989 *Phys. Rev.* B **40** 6175
Stroscio M A 1989 *Phys. Rev.* B **40** 6428
Wendler L, Haupt R and Grigoryan V G 1990 *Physica* B **167** 101
Trallero-Giner C, Garcia-Moliner F, Velasco V R and Cardona M 1992 *Phys. Rev.* **45** 11 944
Chamberlain M P, Cardona M and Ridley B K 1993 *Phys. Rev.* B **48** 14 365
[2] Colvard C, Gant T A, Klein M V, Merlin R, Fischer R, Morkoç H and Gossard A C 1985 *Phys. Rev.* B **31** 2080
Klein M V 1986 *IEEE J. Quantum. Electron.* **22** 1760
Sapriel J and Djafari-Rouhani B 1989 *Surf. Sci. Rep.* **10** 189
Dharma-Wardana M W C, Zhang P X and Lockwood D J 1993 *Phys. Rev.* B **48** 11 960
[3] Tamura S I 1991 *Phys. Rev.* B **43** 12 646
Mizuno S and Tamura S I 1992 *Phys. Rev.* B **45** 13 423
Nishiguchi N, Tamura S I and Nori F 1993 *Phys. Rev.* **48** 2515
Mizuno S, Ito M and Tamura S I 1994 *Japan. J. Appl. Phys.* **33** 2280
Mizuno S and Tamura S I 1995 *Japan. J. Appl. Phys.* **34** 2556
[4] Kochelap V A and Gülseren 1993 *J. Phys.: Condens. Matter* **5** 94 589
[5] Wendler L and Grigoryan V G 1988 *Surf. Sci.* **206** 203

Grigoryan V G and Wendler L 1991 *Sov. Phys.–Solid State* **33** 1193
[6] Grigoryan V G and Sedrakyan D E 1984 *Sov. Phys.–Acoust.* **29** 281
[7] Nishiguchi N 1994 *Japan. J. Appl. Phys.* **33** 2852; 1994 *Phys. Rev.* B **50** 10 970
[8] Waldron R A 1969 *IEEE Trans. Microwave Theory Technol.* **17** 893
[9] Beltzer A I 1988 *Acoustics of Solids* (Berlin: Springer)
[10] Auld B A 1973 *Acoustic Fields and Waves* (New York: Wiley)
[11] Viswanath A K, Hiruma K, Yozawa M, Ogawa K and Katsuyama T 1994 *Microwave Optical Technol. Lett.* **7** 94
[12] Seyler J and Wybourne M N 1992 *J. Phys.: Condens. Matter* **4** L231
Perrin N and Wybourne M N 1991 *Phys. Rev.* B **43** 9511
Nabity J C and Wybourne M N 1991 *Phys. Rev.* B **44** 8990
Johnson K, Wybourne M N, and Perrin N 1994 *Phys. Rev.* B **50** 2035
[13] Stroscio M A, Kim K W, Yu S and Ballato A 1994 *J. Appl. Phys.* **76** 4670
[14] Stroscio M A and Kim K W 1993 *Phys. Rev.* B **48** 1936
Yu S, Kim K W, Stroscio M A, Iafrate G J, and Ballato A 1994 *Phys. Rev.* B **50** 1733
Yu S, Kim K W, Stroscio M A and Iafrate G J 1995 *Phys. Rev.* B **51** 4695
[15] Bannov N, Mitin V and Stroscio M A 1994 *Phys. Status Solidi* b **183** 131
Bannov N, Aristov V and Mitin V 1995 *Solid State Commun.* **93** 483
Bannov N, Aristov V, Mitin V and Stroscio M A 1995 *Phys. Rev.* B **51** 9930
[16] Anselm A I 1981 *Introduction to Semiconductor Theory* (New York: Prentice-Hall)